On the immune regulation of glioma angiogenesis

Immuunregulatie van angiogenese in gliomen

ISBN/EAN 9789462956001

© copyright Changbin Zhu, Rotterdam 2017

Printing - Lay-out: ProefschriftMaken.nl

ISBN

On the immune regulation of glioma angiogenesis

Immuunregulatie van angiogenese in gliomen

Proefschrift

Ter verkrijging van de graad van doctor aan de

Erasmus Universiteit Rotterdam

Op gezag van de

Rector magnificus

Prof. Dr. H.A.P. Pols

En volgens besluit van het College voor Promoties

De openbare verdediging zal plaatsvinden op

Dinsdag 16 mei 2017 om 13:30 uur

door

Changbin Zhu

Geboren te Shanghai, China

PROMOTIECOMMISSIE

Promotor:	Prof. Dr. J.M. Kros
Overige leden:	Prof. Dr. D.J.G.M. Duncker
	Prof. Dr. M.C. Verhaar
	Dr. P.J.M. Leenen
Copromotores:	Dr. C. Cheng
	Dr. D.A. Mustafa

Contents

Chapter 1	Introduction-Part I The contribution of Tumor-Associated Macrophages in tumor neo-angiogenesis and implications for anti-angiogenic strategies.	6
Chapter 2	Introduction-Part 2	29
Chapter 3	Activation of CECR1 in M2-like TAMs promotes paracrine stimulation mediated glial tumor progression.	38
Chapter 4	CECR1-mediated crosstalk between macrophages and vascular mural cells promotes neo-vascularization in malignant glioma.	70
Chapter 5	Periostin is expressed by pericytes and is crucial for angiogenesis in glioma.	99
Chapter 6	Proteome analysis of the CECR1 mediated response in tumor associated macrophages identifies key pathways and molecules in immune response regulation of glioma.	121
Chapter 7	Expression site of P2RY12 in residential microglial cells in astrocytomas correlates with M1 and M2 marker expression and tumor grade.	165
Chapter 8	General Discussion	188
Summary		200
Samenvatting		202
Acknowledgments		204
Curriculum Vitae		210
PhD Portfolio		212
Publication List		214

Chapter 1
Introduction-Part I

Chapter 1

Introduction-Part I

The contribution of Tumor-Associated Macrophages in tumor neo-angiogenesis and implications for anti-angiogenic strategies.

(accepted Neuro-oncology, 2017)

Changbin Zhu, M.D., M.Sc.; Johan M. Kros, M.D., Ph.D.; Caroline Cheng, Ph.D.[*]; Dana Mustafa, Ph.D.[*] (*these authors contributed equally to this work)

ABSTRACT

Tumor-associated macrophages (TAMs) form a significant cell population in malignant tumors and contribute to tumor growth, metastasis and neo-vascularization. Gliomas are characterized by extensive neo-angiogenesis and knowledge of the role of TAMs in neovascularization is important for future anti-angiogenic therapies. The phenotypes and functions of TAMs are heterogeneous and more complex than a classification into M1 and M2 inflammation response types would suggest. In this review, we provide an update on the current knowledge of the ontogeny of TAMs, focussing on diffuse gliomas. The role of TAMs in the regulation of the different processes in tumor angiogenesis is highlighted and the most recently discovered mechanisms by which TAMs mediate resistance against current anti-vascular therapies are mentioned. Novel compounds tested in clinical trials are discussed and brought in relation to different TAMs-related angiogenesis pathways. In addition, potential therapeutic targets used to intervene TAM-regulated tumor angiogenesis are summarized.

THE ORIGIN AND ACTION OF TUMOR-ASSOCIATED MACROPHAGES (TAMS).

The initiation of malignant tumors is associated with a sustained state of chronic inflammation [1]. In the initial stage of tumorigenesis, the first activated immune cells are usually the tissue resident macrophages. In glioma, these cells are mainly represented by microglial cells [2]. Activated microglial cells generate high levels of O^2 radicals that induce genomic mutations, and enhance IL-6 and TNFα production supporting tumor cell survival [3]. Recruitment of peripheral monocytes enhances this initial response. Various tumor cell-derived factors work together with hypoxia and trigger monocyte recruitment [4]. For example, glioma stem cells produce periostin, an extracellular matrix component that provides interactive binding sites to αVβ3 integrins on the cell surface of infiltrating M2-like TAMs (Figure 1a). Hypoxia can trigger activation of VEGFR1 and Neuropilin-1 (NRP1) in monocytes, leading to chemotaxis in e.g. glioma and breast cancer [5]. Neuropilin-1 (NRP1) and VEGFR1 bind with VEGFA secreted by cancer cells in glioma [6,7]. Tumor cell (including glioma[8])-derived Semaphorin 3a also serves to recruit monocytes [9]. Semaphorin 3A activation of NRP1 enhances VEGFR1 signalling in monocytes via the NRP-1/Plexin A1/PlexinA4 complex [10] (Figure 1b). In glioma, monocyte recruitment was also mediated by NG2-positive pericytes via macrophage inhibitory factor (MIF) secretion [11] (Figure 1c).

In mammary tumors, recruited VCAM1+ monocytes are triggered to undergo maturation via Notch upregulation of transcription factor RBP-J [12](Figure 1d). Similarly, sialic acid, which is abundantly available in e.g. breast cancer and melanoma, triggers monocyte differentiation via HIF-1α-mediated disruption of CD45 dimerization, causing decreased activation of STAT3 [13] (Figure 1e).

PHENOTYPES OF TAMS: BEYOND THE M1/M2 SPECTRUM.

The classification into M1/M2 profiles is a way to separate macrophage functions into pro- (Th1) and anti-inflammatory (Th2) responses of T lymphocytes [14]. M1 and M2 profiles represent the extremes of a continuum of phenotypical characteristics marked by sets of cytokines and surface markers. M1 macrophages regulate the acute inflammatory response and are induced by LPS and IFN-γ stimulation. M1 macrophages are characterized by expression of CD40, CD80, CD16/32, CD86, CCR7 and HLA-DR [15], and are capable of phagocytosis and antigen presentation to T cells. M2 macrophages reduce acute inflammation and promote tissue repair. The M2 profile is induced by IL-4 and IL-13, and macrophage-stimulating factor (M-CSF). Studies on Murine and human cancers, including glioblastomas, show that TAMs can express M1 and M2 markers, dependent on tumor stage and area [16,17],[18]. Glioma-associated macrophages may resemble naïve macrophages more than classic M1 or M2 macrophage subtypes [19] illustrative of the complex nature of TAMs in glioma.

Figure 1. Routes of TAM recruitment.

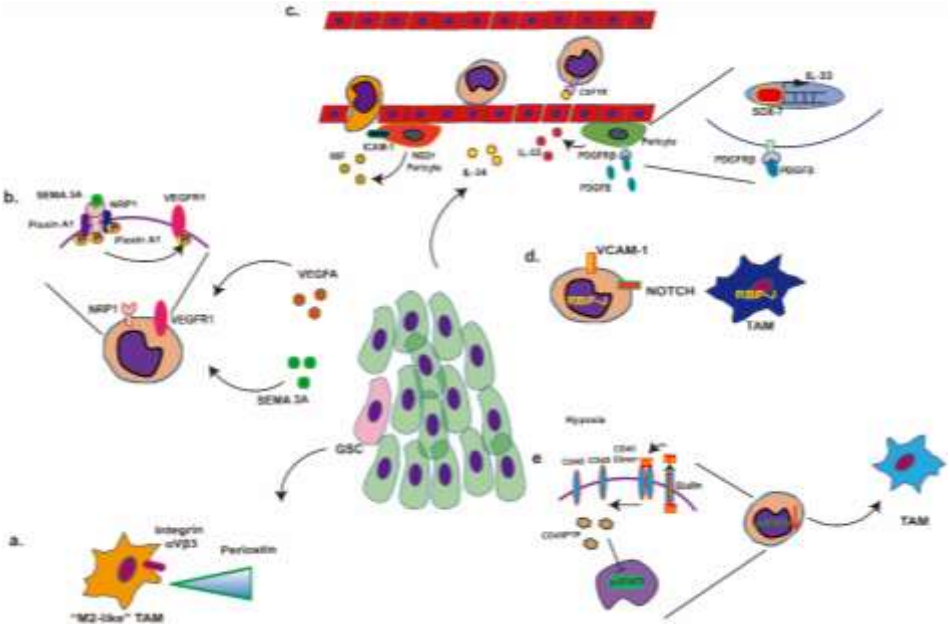

(a) Maturation of VCAM-1^{+} monocytes triggered by NOTCH signaling. **(b)** Glioma stem cells (pink) deposit periostin in the tumor stroma (green cells represent glioma cells), where it serves as a chemoattractant to infiltrating (M2-like) TAMs. **(c)** Under hypoxic stress in the tumor microenvironment levels of Silica acid (SA) increase leading to decreased CD45 dimer signaling, increase of CD45PTP (CD45 phosphatase) and a inhibition of STAT3 signaling in recruited monocytes, triggering differentiation of the TAM phenotype. **(d)** VEGFA and Semaphorin 3A (Sema 3A) released by the tumor cells activates Neuropilin-1 (NRP-1), triggering the activation of VEGFR1 and contribute to the recruitment of TAMs. **(f)** IL-34 derived from tumor cells stimulates M2 macrophages and mediates the attachment of monocytes to the endothelial layer of blood vessel through binding to CSF1R on the surface of peripheral monocytes. IL-33, released from perivascular pericytes via PDGF-BB-PDGFRβ-SOX7 signaling serves as chemoattractant to peripheral monocytes. Macrophage inhibitory factor (MIF) and NG2^{+} pericytes expressing ICAM-1 provide a guiding signal to monocytes during extravasation.

Analysis of TAMs in glioblastomas in our laboratory showed co-expression of the M1 surface markers HLA-DR and CD16 with M2 CD204 and CD163 (unpublished data), which is in line with previous findings demonstrating that the M2 marker CD204 colocalized with the M1 marker HLA-DR in perivascular macrophages in glioblastoma [20]. Similarly, in other malignant tumors like ovarian cancer, the M2 macrophage surface marker CD163 was co-expressed with classical Th1 cytokines as IL-6 and IL-8 [21]. Cytokines from the M1 profile like IL-6, CCL5, and CCL2 are typically tumor supportive and are associated with poor prognosis [22]. The mixed phenotypes of TAMs encountered in tumors may well result from simultaneous stimulation by both pro-inflammatory and anti-inflammatory factors in the tumor micro-environment.

TAMs and Tumor Neovascularization.

TAMs promote proliferation, invasion and metastasis of cancer cells, but also stimulate neo-angiogenesis [1]. Macrophages contribute to angiogenesis under a variety of conditions such as tissue regeneration/wound healing [23], immune-mediated diseases like rheumatoid arthritis [24], and neoplasia [25]. The number of macrophages present around blood vessels in healthy tissues is significantly increased in tumors such as glioblastoma [26,27], particularly during proliferative microvessels [28-30]. In glioblastoma, CD163+ TAMs are found in parenchymal and perivascular areas [31]. In addition, Tie-2+ TAMs are found at perivascular sites in various malignant cancers, including glioblastoma [32]. Perivascular TAMs in glioblastomas are positively correlated with microvascular density and higher expression of VEGFA, HO-1[33], and thymigen phosphorylase (TP)[34], which is not detected in anaplastic oligodendroglioma or ependymoma[35]. The secretion of inflammatory cytokines by TAMs promote neovascularization along various molecular pathways. For example, CCL18 secretion by (M2) type TAMs in breast cancer binds to PITPNM3, a membrane-associated phosphatidylinositol transfer domain-containing protein located on endothelial cells. This interaction triggers downstream ERK and Akt/GSK-3 β /Snail signalling, and promotes the Endothelial Mesenchymal Transition (EndoMT) process, increasing the migration ability of endothelial cells [36] (Figure 2a). Secretion of VEGFA by macrophages is regulated by macrophage-derived factors in an autocrine fashion in both non-cancerous and tumoral conditions: In macrophages, IL-10 activates STAT3 leading to VEGFA production [37,38]. Similarly, Il-1β secretion, induced by COX-2 activation in tumor cells and macrophages, is linked with the upregulation of IL-8, VEGFA, and HIF-1α [39,40]. TAM-derived WNT7b and M-CSF in breast cancer and glioma respectively, activate the canonical WNT/β catenin and IGFBP1 pathways in endothelial cells, thereby increasing the expression of VEGFA [41,42].

In glioblastoma, a link between inflammation-associated c-reactive protein (CRP) with IL-6 secretion, JAK-STAT activation, and production of IL-1 by TAMs, was discovered [43]. In this pathway, elevated CRP levels stimulate TAMs to secrete IL-1β that promotes the proliferation of endothelial cells, and causes IL-6 production of COX-2 positive TAMs. IL-6 promotes epithelial-mesenchymal transition (EMT) of cancer cells, which is typically operative in high-grade gliomas [36] (Figure 2b). In addition, YKL-40, a secreted protein member of the chitinase gene family, can act as a prognostic marker in various cancers including glioblastoma [44]. YKL-40 expression is regulated by IL-6 and was shown to be associated with angiogenesis [45]. Stimulation of macrophages by M-CSF or GM-CSF can induce 100-200 fold more YKL-40 [46]. YKL-40 activates the expression of VEGFR1 and VEGFR2 in endothelial cells through the FAK-MAPK signalling pathway, promoting vessel sprouting -the initial step in the formation of a new tubule structure from pre-existing vasculature [47]. YKL-40 also stimulates vascular smooth muscle cells (VSMCs) to secrete higher levels of IL-8 under the regulation of the MAPK and NF-κB pathways [48] (figure

2c). YKL-40 also promotes the contacts between glioma stem cell-derived pericvascular cells with endothelial cells, resulting in the stabilization of blood vessels in glioma [49].

Macrophages make contact with sprouting endothelial cells and actively contribute to new vessel formation[50]. Rymo et al. showed a VEGFA-independent involvement of microglial cells in the process of vessel sprouting and branching *in vivo* [51]. In a model of retinal vascular development, macrophages expressing Notch1 contact Jagged1-positive tip cells and mediate the elongation of vascular sprouts via this molecular interaction (Figure 2d) [52]. Tip cells are endothelial cells at the tip of newly formed blood vessels that determine the direction of growth. Tip cells are trailed by stalk cells, which are endothelial cells that form the new bloodvessel lining (creating an open lumen for blood flow).

Proangiogenic NRP-1 expressed by macrophages binds to VEGFR2 present on tip cells leading to vessel branching [53,54]. Macrophages also contribute to the maturation and remodelling of newly formed blood vessels in tumors: Macrophages act as cellular chaperons for tip cells to form anastomoses, which are fused junctions composed of two neighbouring vessel sprouts. Macrophages can secrete VEGF-C causing upregulation of DLL4 in endothelial cells through VEGFR3 signalling, followed by activation of transcription factor FoxC2. The VEGFC-VEGFR3-FoxC2 pathway mediates conversion of tip cells into stalk cells, contributing to the anastomose process (Figure 2e) [55].

Various *in vitro* and *in vivo* experiments have indicated that monocytes themselves are capable to transform into cord-like structures and can express endothelial markers like vWF, CD31, VE-Cadherin, and CD105, following exposure to proangiogenic factors such as VEGFA and IGF-1 [56,57]. In multiple myeloma, TAMs that expressed multiple endothelial markers cooperate with endothelial cells in the formation of the endothelial lining of tumor blood vessels [58]. The expression of endothelial lineage markers like VE-Cadherin, VEGFR2, FVIII-RA, and vWF is induced in macrophages/monocytes *in vitro* through VEGFA, bFGF [59] or pleiotrophin [60] stimulation. Exposure to these factors can induce the creation of capillary-like structures *in vitro* [60] (Figure 3f). In glioma, TAMs can enhance the vascular mimicry of glioma cells, a process mediated via COX-2 and IL-6 [61,62]. Macrophages are also involved in activation of IL-6 and JAK-STAT pathways in the recruitment of endothelial progenitor cells (EPC) that take part in *de novo* vascularization [63] (Figure 3g).

Newly formed blood vessels require the coverage of perivascular cells called “mural cells” for vascular stabilization and vasomotion control. These mural cells include pericytes in and VSMCs. PDGF-BB acts as one of the most potent chemoattractant of mural cells. Although PDGF-BB is produced by endothelial cells during angiogenesis, it is also secreted by TAMs. Perivascular TAMs aid in the recruitment of PDGFRβ+ mural cells, contributing to the coverage of newly formed blood vessels [64]. The recently discovered TAM-derived factor Semaphorin 4D (Sema 4D) is involved in the pericyte recruitment of neo-vessels as demonstrated in a murine breast cancer model (Figure 3h).

Taken together, these data suggest that TAMs participate in all stages of angiogenesis from early sprouting to late maturation, and the physical integration into vessel

endothelium under the direct (paracrine) influence of tumor cells. Since TAMs play such a critical role in the entire angiogenetic process in tumors, their role in the resistance to anti-angiogenic drug deserves to be scrutinized [65].

Figure 2. Various roles of macrophages in angiogenesis.

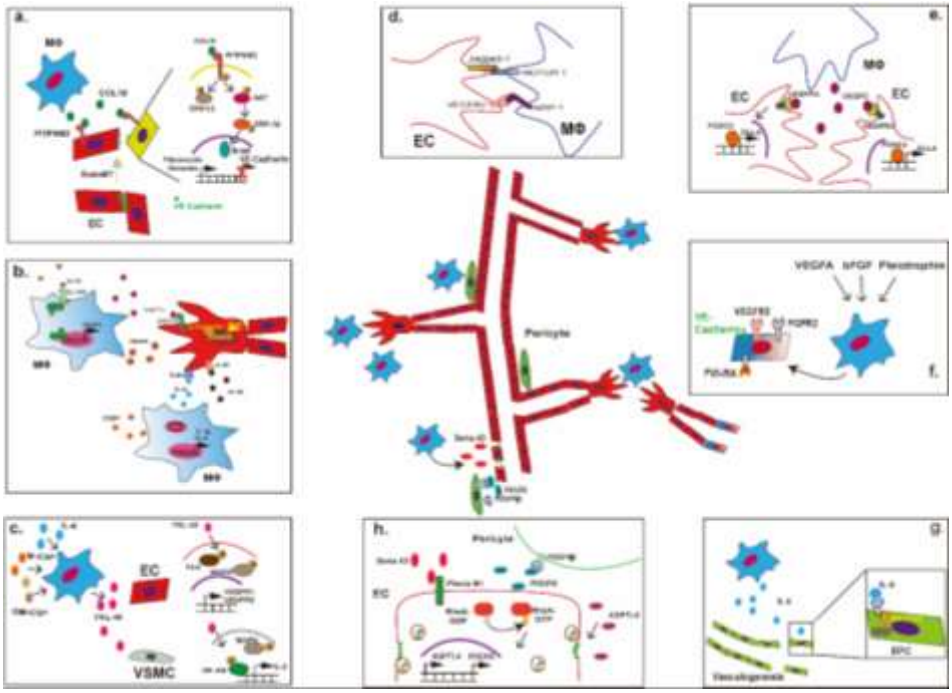

(a) CCL18 released by TAMs adding to the EndoMT process by interaction with the receptor PITPNM3, triggering activation of the ERK1/2 and AKT/GSK-3 signaling pathway. This results in decreased expression of VE-Cadherin and upregulation of Vimentin as well as Fibronectin. **(b)** IL-10 upregulates VEGFA expression in an autocrine fashion in order to activate STAT3 in TAMs. C-reactive protein (CRP) in glioma upregulates IL-6 and IL-1β expression in COX-2^{+} TAMs. As a result, IL-6 and IL-1β signal together with WNT-7b to increase the VEGFA expression in endothelial cells. **(c)** Putative interaction mechanisms between TAMs and Tip cells via ligand-receptor binding of Jagged-1(Tip cell) with NOTCH-1(MΦ) as well as VEGFR2(Tip cell) with NRP-1(MΦ). **(d)** Under the stimulation of GM/M-CSF and IL-6, TAM releases YKL-40 that triggers the signaling of FAK-MAPK in endothelial cells and of MAPK-NFκB in vascular smooth muscle cells (VSMCs), leading to overexpression of VEGFR1 and 2 in endothelial cells and IL-8 secretion by VSMCs. **(e)** VEGFC released by macrophages contributes to the expression of DLL4 in Tip cells via VEGFRC-FOXC3 signaling promoting fusion of sprouting anastomosis. **(f)** Stimulation via VEFGA, βFGF and Pleiotrophin triggers expression of the endothelial markers VEGFR2, FGFR2, FVIII-RA and VE-Cadherin by TAMs, and promotes the process of vasculogenesis. **(g)** IL-6 released by TAMs recruits endothelial progenitor cells (EPCs) from the peripheral circulation by activating JAK-STAT signaling to contribute to vasculogenesis. **(h)** Semaphorin-4D (Sema 4D) from TAMs stimulates the recruitment of pericytes via activating Plexin B1-RhoA signaling, increasing the expression of PDGFB and AGPTL4 in the endothelial cells. Increased expression of AGPTL4 leads to the endocytosis of VE-Cadherin in endothelial cells, enhancing the permeability of the blood vessels.

TAMS AND ANTI-ANGIOGENIC THERAPY.

Because neo-angiogenesis is an important component of tumorigenesis it was expected that anti-angiogenic agents would be effective in the treatment of solid tumors. Unfortunately, the results of trials in which anti-angiogenic therapies were tested have been disappointing so far. The agents were designed to interfere with target molecules from common angiogenic pathways. The lack of success of these agents may be partly due to overlooking the critical role of TAMs in tumor angiogenesis [66]. The main effect of anti-angiogenic therapy is reduction of the vascular bed, causing hypoxia and raised lactate levels. Subsequent elevation in intracellular HIF-1α levels leads to higher levels of pro-angiogenic factors secreted by the tumor cells that result in the paracrine activation of TAMs [67,68]. In experimental mammary tumors, the administration of combretastatin A4 phosphate (CA4P) caused narrowing of the tumor blood vessel diameters and tumor necrosis, but increased CXCL12 levels, leading to raised numbers of CXCR4+ Tie-2+ monocytes in the tumors, limiting treatment efficiency [69]. Over the last decennia, anti-angiogenic drugs targeting the receptor-ligand interactions by monoclonal antibodies like bevacizumab or tyrosine kinase inhibitors (TKIs) were widely applied in clinical practice. Both act as tumor suppressors by promoting TAMs with an anti-tumor phenotype [70-74] or by decreasing monocyte recruitment [75-79]. This beneficial effect is partially compromised by activation of hypoxia-induced HIF1α pathways that lead to an angiogenic counter response [80]. In pancreatic adenocarcinoma and murine breast cancers, activation of the Akt/PI3K pathway by prolonged exposure to Sorafenib triggers TAMs to adapt a tumor supportive and pro-angiogenic phenotype [81]. Similar effects are observed in glial tumors: bevacizumab and aflibercept reduce the effects of VEGFA, and increased CD206-positive and Tie-2-positive macrophages in human and murine gliomas by raising levels of endothelial cell-derived Angiopoietin-2. The inhibition of Angiopoietin-2 action together with the administration of bevacizumab or alibercept results in significant improvement of therapeutic efficiency [82]. Recent studies showed that treatment with the Ang-2/VEGF bispecific antibody shifted TAM into an anti-tumor phenotype, consequently resulting in vascular normalization and tumor regression in a mouse glioblastoma model[83,84]. Following treatment with bevacizumab and cetuximab, the numbers of TAMs in glioblastoma and colorectal cancer increased and the cells became activated respectively [80,85]. In biopsies of recurrent gliomas treated with bevacizumab, more Tie-2 expressing monocytes and macrophages were detected. Furthermore, in an orthotopic glioma mouse model an increase in Tie-2-positive TAMs in response to anti-VEGF agents was observed[86]; Recently, reduced MIF expression was observed in bevacizumab-resistant glioma cells, which in turn increased M2-like TAM recruitment, promoting tumor progression[87]. In experimentally induced primitive neuroectodermal tumors similar observations were made following drug-induced VEGFR2 blockade [88]. Contrasting with these data are the reported effects of the pan-VEGFR inhibitor cediranib that transiently decreases the intra-tumoral infiltration of macrophages. However,

Cediranib also increases the VEGFA levels in serum and the number of CXCR4 and CD45 positive circulatory cells in peripheral blood, boosting angiogenesis in murine models of pancreatic neuroendocrine and mammary tumors [81]. Cediranib induces JAK-STAT signaling in macrophages leading to the activation of STAT3 that triggers angiogenesis by VEGFA production. In murine xenograft glioma model, adverse effects of STAT3 activation in TAMs were counteracted by using the JAK-STAT-specific inhibitor AZD1480 [89]. Likewise, in a metastatic renal cell carcinoma model, the anti-angiogenic effects of sunitinib was enhanced by simultaneous treatment with STAT3 inhibitors [74]. Tyrosine kinase inhibitors (TKIs) have more effects on immune cells. Erlotinib reportedly induces apoptosis of monocytic cell lines *in vitro* [76]. The monoclonal antibodies cetuximab and SR1 enhance the phagocytic capability of macrophages, contributing to elimination of circulatory tumor cells [72,73]. Sunitinib and imatinib change the cytokine secretion profiles of macrophages from pro-inflammatory to anti-inflammatory (IL-12 versus IL-10) [71], and following the treatment with sorafnib, increased numbers of TAMs and levels of angiogenic factors including CXCL12 and IL-6 were detected [81]. Recruitment of M2-like TAMs or i*n situ* differentiation towards a tumor supportive TAM phenotype was reported after cediranib and axitinib treatment in glioma patients [90,91]. A summary of TAM-mediated effects of different tyrosine kinase inhibitors in various therapeutic regimes are provided in Table 1 and Table 2.

CURRENT PERSPECTIVES ON TARGETING PROANGIOGENIC TAMS.

1) Inhibition of tumor-related haematopoiesis and blocking of activating signals for TAMs.

Because the majority of TAMs are recruited from bone marrow-derived peripheral monocytes, the inhibition of tumor-related granulo-monocytopoiesis and interference with the monocyte recruitment signals will contribute to tumor suppression and inhibit tumor vascularization [92]. Inhibition of CSF-1R to deplete the TAM population increases survival time and decrease tumor microvascular density in animal cancer models [93,94]. Patients with tenosynovial giant cell tumors and glioblastomas treated with PLX3397 (CSF-1R blocker) showed a good tolerance to the drug, but only the patients with tenosynovial giant cell tumors showed a significant reduction in tumor size [95]. In recurrent GBM only a trend towards a decrease in the number of Iba-1 positive microglia/macrophages and a lower number of $CD14^{dim}$, CD16-positive monocytes in the glioma tissues was observed [96].

2) Inhibition of recruitment signals that guide circulatory monocytes into tumor tissue.

TAMs predominantly originate from recruited peripheral inflammatory monocytes. CCL2-CCR2 chemo-attractive signalling is the most studied mechanism in monocyte recruitment. The effectiveness of a CCR2 antagonist in decreasing macrophage infiltration and reducing tumor size was demonstrated in hepatocellular carcinoma [97] and AMD3100, an inhibitor of CXCR4, blocks the infiltration of Tie-2+ monocytes [98]. By responding to VEGFA gradients via cell surface expression of Flt-1, infiltrating monocytes are guided into cancer tissues. The agent IVR blocks the phosphorylation of VEGFR1 and decreases migration capacity of TAMs in experimental colonic cancer, resulting in reduced numbers of TAMs and reduction in tumor angiogenesis [99].

3) Targeting macrophage mediated/secreted angiogenic molecules.

Current studies in cancer therapy focus on the development of inhibitors and monoclonal antibodies against central regulatory molecules. Some of these interfere with TAM-mediated tumor angiogenesis and were tested in clinical trials. Monoclonal antibody-based therapy that targets VEGF-C has proven to inhibit vascularization and reduce carcinogenesis of skin squamous carcinoma [100]. Blocking of VEGF-C using the monoclonal antibody VGX-100 also inhibited infiltration of CD11b+ myeloid cells [101]. Monoclonal antibodies targeting Sema 4D showed promising results in inhibiting cancer growth and reduced tumor angiogenesis[102]. WNT7b activates the VEGFA-mediated angiogenic switch through stimulation of the Wnt/β-catenin canonical pathway. In contrast, Wnt5a, a Wnt ligand that mainly triggers non-canonical pathways, suppresses vessel sprouting by upregulation of soluble VEGFR1 [103]. The canonical and non-canonical Wnt signalling pathways may well mediate opposite angiogenic responses. Both inhibition of the Wnt canonical pathway by inhibitors, and agonist stimulation of the non-canonical Wnt pathways, may become future strategies for anti-angiogenesis. The presence of certain TAM subtypes, as well as circulatory TAM-secreted serum markers, could also be used as parameters to select receptive patients for anti-angiogenic therapy and predict therapeutic efficiency. For example, in a single arm phase II clinical trial, GBM patients who received the VEGF-trapper aflibercept showed elevated serum levels of PIGF and MMP-9, indicative of a poor prognosis. Patients with lower serum levels of PIGF and VEGFR1-positive monocytes and elevated levels of MIF, MCP-3, and CCL27, benefited from anti-VEGF treatment [104].

CONCLUSION.

Investigations of the recently identified roles of TAMs in angiogenesis may well lead to the development of biomarkers for assessing the anti-angiogenic therapy efficacy and receptiveness, and could help to identify therapeutic targets for novel anti-angiogenic treatments.

Table 1. Pro- and anti-tumor effects of multiple tyrosine kinase inhibitors mediated via TAMs				
Tyrosine kinase inhibitor	Molecular target(s)	Investigation Setting	TAM effect	Ref.
Sunitinib	VEGFR1-3, PDGFR-α/β, c-Kit, CSF-1R, Flt-3	Inflammatory Corneal Lymphangiogenesis	Decreases recruitment of F4/80+ macrophages and activity of their secreted factors such as VEGFA, VEGFC	77
		Human Renal Cell Carcinoma	Inhibits myeloid cell proliferation. However, GM-CSF induced resistance of Sunitinib was found in intratumor myeloid cells	105
		Human Recurrent Glioblastoma	More severe hypoxia was induced, which increased macrophage infiltration	80
		Gastrointestinal stroma tumor (GIST)	Promotes M1 macrophage secretion of IL-10 *in vitro*	106
		Human primary breast cancer	Synergizes with α-GITR to induce anti-tumor macrophages via inhibition of STAT3 activity	74
Sorafenib	VEGFR1-3, PDGFR-β, Raf-1, B-Raf, CSF-1R	Hepatocellular Carcinoma	Converts alternative TAMs to M1-like TAMs and increases secretion of pro-inflammatory cytokines	70
			Triggers macrophage-mediated cytotoxic NK cell activation	
		Murine breast cancer	Increases IL-12 and suppression of IL-10 levels in macrophage	71
		Human peripheral CD14+ monocyte derived macrophage	Induces apoptosis and autophagy in macrophages	108

		Mouse model for metastatic liver cancer model	Increases peripheral and F4/80+ and CD11b+ macrophages recruitment and infiltration in cancer tissues	109
		Mouse breast cancer model and pancreatic β-cell tumor model	Increases angiogenic and immunosuppressive molecules. Can be blocked by PI3K Inhibitor IPI145	81
		Classical Hodgekin's Lymphoma	Blocks CSF-1R activity	107
Imatinib	c-KIT	Murine GIST model; Human GIST	Shifts TAM into a more M2-like pro-tumor phenotype macrophage	110
			Promotes M1 macrophage secretion of IL-10 *in vitro*	106
Cediranib	VEGFR1-3	Alveolar Soft Part Sarcoma (ASPS)	Increases CD68+ and M2-like TAMs and increases CD163, Tie-2, and CCL2 mRNA levels	111
			Transiently decreases macrophage infiltration. Increases plasma VEGFA levels and CXCR4+ CD45+ immune cells.	
		Murine glioma xenograft model	Increase phosphorylation of STAT3 in macrophages. In combination with AZD1480 JAK2 inhibitor, decreases the phospho-STAT3 positive macrophages	89
Axitinib	VEGFR1-3, PDGFR-β and c-kit	Murine glioma xenograft model	Inhibits metronomic cyclophosphamide activated antitumor innate immunity and shifts TAM into a M2-like phenotype	91
Erlotinib	EGFR, ErbB1	Human U937 cell line induced macrophage	Inhibits monocyte-macrophage differentiation and proliferation	76

		Non Small Cell Lung Cancer	Administration of Erlotinib induces macrophage and other mononuclear cells infiltration into skin	112
Dasatinib	EGFR, ErbB1	Murine bone marrow-drived macrophage; RAW264.7 cell line	Induces macrophages with anti-inflammatory function by increasing IL-10 production and suppressing TNF-α and IL-12p40	113
Bosutinib				
PLX3397	c-kit ,c-fms inhibitor	Malignant Peripheral Nerve Sheath Tumor	Depleting Iba-1+ macrophages, combined with rapamycin lead to more severe depletion of tumor associated macrophages	78
		Recurrent glioblatoma	Depleting CD11b+ cells and potentiating the response of the intracranial tumors to irradiation	79

Table 2. Effects of monoclonal antibodies-based angiogenic therapies on TAMs

Monoclonal antibodies based therapeutic agent	Molecular target	Tumor Type	TAM effect	Ref.
Bevacizumab	VEGFA	Glioblastoma	Induces Tie-2+ monocyte infiltration and vast infiltration of M2-like macrophages	86
			Increases phosphorylation of STAT3 in macrophages, promoting a tumor supportive phenotype	89
Crossmab, A2V	Angiopoietin-2/VEGFA Bispecific		Transite TAM from M2-like phenotype to M1-like phenotype. Prolonging tumor-bearing mice survival time	84
MEDI3617	Angiopoietin-2		Promoting tumor vessel normalizaion and M1-like polarization of TAM when co-administration with cediranib	83
Cetuximab	EGFR	Colorectal Carcinoma	Increases phagocytosis by macrophages to eliminate circulating cancer cells	72
			Activation of M2-like macrophages	85
		Heck and neck cancer	Ameliorates suppressive phenotypes of FcγR bearing myeloid cells in cancer patients	112
Trastuzumab	HER2	HER2 positive breast cancers	Decreases CD68+ macrophages infiltration	75

SR1	c-KIT	Imatinib resistant GIST (Gastric Intestinal Stromal Tumor)	Increases phagocytosis in macrophages	73

REFERENCES

1. Qian BZ, Pollard JW. Macrophage diversity enhances tumor progression and metastasis. *Cell.* 2010; 141(1):39-51.
2. Bajenaru ML, Garbow JR, Perry A, Hernandez MR, Gutmann DH. Natural history of neurofibromatosis 1-associated optic nerve glioma in mice. *Ann Neurol.* 2005; 57(1):119-127.
3. Biswas S, Allavena P, Mantovani A. Tumor-associated macrophages: functional diversity, clinical significance, and open questions. *Semin Immunopathol.* 2013; 35(5):585-600.
4. Hambardzumyan D, Gutmann DH, Kettenmann H. The role of microglia and macrophages in glioma maintenance and progression. *Nature Neuroscience.* 2016; 19(1):20-27.
5. Murakami M, Zheng Y, Hirashima M, et al. VEGFR1 Tyrosine Kinase Signaling Promotes Lymphangiogenesis as Well as Angiogenesis Indirectly via Macrophage Recruitment. *Arteriosclerosis, Thrombosis, and Vascular Biology.* 2008; 28(4):658-664.
6. Schuch G, Machluf M, Bartsch G, Jr., et al. In vivo administration of vascular endothelial growth factor (VEGF) and its antagonist, soluble neuropilin-1, predicts a role of VEGF in the progression of acute myeloid leukemia in vivo. *Blood.* 2002; 100(13):4622-4628.
7. Kerber M, Reiss Y, Wickersheim A, et al. Flt-1 signaling in macrophages promotes glioma growth in vivo. *Cancer Res.* 2008; 68(18):7342-7351.
8. Sabag AD, Bode J, Fink D, Kigel B, Kugler W, Neufeld G. Semaphorin-3D and semaphorin-3E inhibit the development of tumors from glioblastoma cells implanted in the cortex of the brain. *PLoS One.* 2012; 7(8):e42912.
9. Ji JD, Park-Min KH, Ivashkiv LB. Expression and function of semaphorin 3A and its receptors in human monocyte-derived macrophages. *Hum Immunol.* 2009; 70(4):211-217.
10. Casazza A, Laoui D, Wenes M, et al. Impeding Macrophage Entry into Hypoxic Tumor Areas by Sema3A/Nrp1 Signaling Blockade Inhibits Angiogenesis and Restores Antitumor Immunity. *Cancer cell.* 2013; 24(6):695-709.
11. Yotsumoto F, You W-K, Cejudo-Martin P, Kucharova K, Sakimura K, Stallcup WB. NG2 proteoglycan-dependent recruitment of tumor macrophages promotes pericyte-endothelial cell interactions required for brain tumor vascularization. *OncoImmunology.* 2015; 4(4):e1001204.
12. Franklin RA, Liao W, Sarkar A, et al. The cellular and molecular origin of tumor-associated macrophages. *Science.* 2014; 344(6186):921-925.
13. Kumar V, Cheng P, Condamine T, et al. CD45 Phosphatase Inhibits STAT3 Transcription Factor Activity in Myeloid Cells and Promotes Tumor-Associated Macrophage Differentiation. *Immunity.* 2016; 44(2):303-315.
14. Mills CD. Anatomy of a discovery: m1 and m2 macrophages. *Frontiers in Immunology.* 2015; 6:212.
15. Martinez FO, Gordon S, Locati M, Mantovani A. Transcriptional profiling of the human monocyte-to-macrophage differentiation and polarization: new molecules and patterns of gene expression. *J Immunol.* 2006; 177(10):7303-7311.
16. Movahedi K, Laoui D, Gysemans C, et al. Different tumor microenvironments contain functionally distinct subsets of macrophages derived from Ly6C(high) monocytes. *Cancer Res.* 2010; 70(14):5728-5739.
17. Laoui D, Van Overmeire E, Movahedi K, et al. Mononuclear phagocyte heterogeneity in cancer: different subsets and activation states reaching out at the tumor site. *Immunobiology.* 2011; 216(11):1192-1202.
18. Szulzewsky F, Pelz A, Feng X, et al. Glioma-associated microglia/macrophages display an expression profile different from M1 and M2 polarization and highly express Gpnmb and Spp1. *PLoS One.* 2015; 10(2):e0116644.
19. Gabrusiewicz K, Rodriguez B, Wei J, et al. Glioblastoma-infiltrated innate immune cells resemble M0 macrophage phenotype. *JCI Insight.* 2016; 1(2).
20. Sasaki A. Microglia and brain macrophages: An update. *Neuropathology.* 2016:n/a-n/a.

21. Reinartz S, Schumann T, Finkernagel F, et al. Mixed-polarization phenotype of ascites-associated macrophages in human ovarian carcinoma: Correlation of CD163 expression, cytokine levels and early relapse. *International Journal of Cancer.* 2014; 134(1):32-42.
22. Cai J, Zhang W, Yang P, et al. Identification of a 6-cytokine prognostic signature in patients with primary glioblastoma harboring M2 microglia/macrophage phenotype relevance. *PLoS One.* 2015; 10(5):e0126022.
23. Zhang S, Dehn S, DeBerge M, Rhee KJ, Hudson B, Thorp EB. Phagocyte-myocyte interactions and consequences during hypoxic wound healing. *Cell Immunol.* 2014; 291(1-2):65-73.
24. Elshabrawy HA, Chen Z, Volin MV, Ravella S, Virupannavar S, Shahrara S. The pathogenic role of angiogenesis in rheumatoid arthritis. *Angiogenesis.* 2015; 18(4):433-448.
25. Murdoch C, Muthana M, Coffelt SB, Lewis CE. The role of myeloid cells in the promotion of tumour angiogenesis. *Nat Rev Cancer.* 2008; 8(8):618-631.
26. Karasawa K, Asano K, Moriyama S, et al. Vascular-resident CD169-positive monocytes and macrophages control neutrophil accumulation in the kidney with ischemia-reperfusion injury. *J Am Soc Nephrol.* 2015; 26(4):896-906.
27. Hughes R, Qian BZ, Rowan C, et al. Perivascular M2 Macrophages Stimulate Tumor Relapse after Chemotherapy. *Cancer Res.* 2015; 75(17):3479-3491.
28. Valverde LF, Pereira TA, Dias RB, et al. Macrophages and endothelial cells orchestrate tumor-associated angiogenesis in oral cancer via hedgehog pathway activation. *Tumour Biol.* 2016.
29. Park JY, Sung JY, Lee J, et al. Polarized CD163+ tumor-associated macrophages are associated with increased angiogenesis and CXCL12 expression in gastric cancer. *Clinics and research in hepatology and gastroenterology.* 2015.
30. Marinaccio C, Ingravallo G, Gaudio F, et al. Microvascular density, CD68 and tryptase expression in human diffuse large B-cell lymphoma. *Leuk Res.* 2014; 38(11):1374-1377.
31. Mignogna C, Signorelli F, Vismara MFM, et al. A reappraisal of macrophage polarization in glioblastoma: Histopathological and immunohistochemical findings and review of the literature. *Pathology - Research and Practice.* 2016; 212(6):491-499.
32. Lewis CE, De Palma M, Naldini L. Tie2-expressing monocytes and tumor angiogenesis: regulation by hypoxia and angiopoietin-2. *Cancer Res.* 2007; 67(18):8429-8432.
33. Nishie A, Ono M, Shono T, et al. Macrophage infiltration and heme oxygenase-1 expression correlate with angiogenesis in human gliomas. *Clin Cancer Res.* 1999; 5(5):1107-1113.
34. Angiogenic effect of thymidine phosphorylase on macrophages in glioblastoma multiforme. *Journal of Neurosurgery.* 2001; 95(1):89-95.
35. Deininger MH, Meyermann R, Trautmann K, et al. Heme oxygenase (HO)-1 expressing macrophages/microglial cells accumulate during oligodendroglioma progression. *Brain Res.* 2000; 882(1-2):1-8.
36. Lin L, Chen YS, Yao YD, et al. CCL18 from tumor-associated macrophages promotes angiogenesis in breast cancer. *Oncotarget.* 2015; 6(33):34758-34773.
37. Nakamura R, Sene A, Santeford A, et al. IL10-driven STAT3 signalling in senescent macrophages promotes pathological eye angiogenesis. *Nature Communications.* 2015; 6.
38. Wu W-K, Llewellyn OPC, Bates DO, Nicholson LB, Dick AD. IL-10 regulation of macrophage VEGF production is dependent on macrophage polarisation and hypoxia. *Immunobiology.* 2010; 215(9–10):796-803.
39. Hou Z, Falcone DJ, Subbaramaiah K, Dannenberg AJ. Macrophages induce COX-2 expression in breast cancer cells: role of IL-1 beta autoamplification. *Carcinogenesis.* 2011; 32(5):695-702.
40. Carmi Y, Dotan S, Rider P, et al. The role of IL-1beta in the early tumor cell-induced angiogenic response. *J Immunol.* 2013; 190(7):3500-3509.
41. Yeo EJ, Cassetta L, Qian BZ, et al. Myeloid WNT7b mediates the angiogenic switch and metastasis in breast cancer. *Cancer Res.* 2014; 74(11):2962-2973.
42. Nijaguna MB, Patil V, Urbach S, et al. Glioblastoma-derived Macrophage Colony-stimulating Factor (MCSF) Induces Microglial Release of Insulin-like Growth Factor-binding Protein 1 (IGFBP1) to Promote Angiogenesis. *Journal of Biological Chemistry.* 2015; 290(38):23401-23415.

43. Nijaguna MB, Schroder C, Patil V, et al. Definition of a serum marker panel for glioblastoma discrimination and identification of Interleukin 1beta in the microglial secretome as a novel mediator of endothelial cell survival induced by C-reactive protein. *J Proteomics.* 2015; 128:251-261.
44. Johansen JS, Jensen BV, Roslind A, Nielsen D, Price PA. Serum YKL-40, a new prognostic biomarker in cancer patients? *Cancer Epidemiol Biomarkers Prev.* 2006; 15(2):194-202.
45. De Ceuninck F, Pastoureau P, Bouet F, Bonnet J, Vanhoutte PM. Purification of guinea pig YKL40 and modulation of its secretion by cultured articular chondrocytes. *J Cell Biochem.* 1998; 69(4):414-424.
46. Junker N, Johansen JS, Andersen CB, Kristjansen PE. Expression of YKL-40 by peritumoral macrophages in human small cell lung cancer. *Lung Cancer.* 2005; 48(2):223-231.
47. Shao R. YKL-40 acts as an angiogenic factor to promote tumor angiogenesis. *Frontiers in Physiology.* 2013; 4.
48. Tang H, Shi ZQ, Xiu QY, Li B, Sun Y. YKL-40 mediated Interleukin 8 Production May Be Closely Associated with Remodeling of Bronchial Smooth Muscle Cells. *Am J Resp Crit Care.* 2012; 186(4):386-386.
49. Francescone R, Ngernyuang N, Yan W, Bentley B, Shao R. Tumor-derived mural-like cells coordinate with endothelial cells: role of YKL-40 in mural cell-mediated angiogenesis. *Oncogene.* 2014; 33(16):2110-2122.
50. Clear AJ, Lee AM, Calaminici M, et al. Increased angiogenic sprouting in poor prognosis FL is associated with elevated numbers of CD163(+) macrophages within the immediate sprouting microenvironment. *Blood.* 2010; 115(24):5053-5056.
51. Rymo SF, Gerhardt H, Sand FW, Lang R, Uv A, Betsholtz C. A Two-Way Communication between Microglial Cells and Angiogenic Sprouts Regulates Angiogenesis in Aortic Ring Cultures. *PLoS One.* 2011; 6(1).
52. Outtz HH, Tattersall IW, Kofler NM, Steinbach N, Kitajewski J. Notch1 controls macrophage recruitment and Notch signaling is activated at sites of endothelial cell anastomosis during retinal angiogenesis in mice. *Blood.* 2011; 118(12):3436-3439.
53. Fantin A, Vieira JM, Plein A, et al. NRP1 acts cell autonomously in endothelium to promote tip cell function during sprouting angiogenesis. *Blood.* 2013; 121(12):2352-2362.
54. Fantin A, Vieira JM, Gestri G, et al. Tissue macrophages act as cellular chaperones for vascular anastomosis downstream of VEGF-mediated endothelial tip cell induction. *Blood.* 2010; 116(5):829-840.
55. Tammela T, Zarkada G, Nurmi H, et al. VEGFR-3 controls tip to stalk conversion at vessel fusion sites by reinforcing Notch signalling. *Nature Cell Biology.* 2011; 13(10):1202-1213.
56. Schmeisser A, Garlichs CD, Zhang H, et al. Monocytes coexpress endothelial and macrophagocytic lineage markers and form cord-like structures in Matrigel under angiogenic conditions. *Cardiovasc Res.* 2001; 49(3):671-680.
57. Yan D, Wang XY, Li DJ, Qu ZL, Ruan QR. Macrophages overexpressing VEGF, transdifferentiate into endothelial-like cells in vitro and in vivo. *Biotechnol Lett.* 2011; 33(9):1751-1758.
58. Ribatti D, Vacca A. The role of monocytes-macrophages in vasculogenesis in multiple myeloma. *Leukemia.* 2009; 23(9):1535-1536.
59. Scavelli C, Nico B, Cirulli T, et al. Vasculogenic mimicry by bone marrow macrophages in patients with multiple myeloma. *Oncogene.* 2008; 27(5):663-674.
60. Chen HM, Campbell RA, Chang YC, et al. Pleiotrophin produced by multiple myeloma induces transdifferentiation of monocytes into vascular endothelial cells: a novel mechanism of tumor-induced vasculogenesis. *Blood.* 2009; 113(9):1992-2002.
61. Zhang L, Xu Y, Sun J, et al. M2-like tumor-associated macrophages drive vasculogenic mimicry through amplification of IL-6 expression in glioma cells. *Oncotarget.* 2016; 8(1).
62. Rong X, Huang B, Qiu S, Li X, He L, Peng Y. Tumor-associated macrophages induce vasculogenic mimicry of glioblastoma multiforme through cyclooxygenase-2 activation. *Oncotarget.* 2016; 7(51).
63. Fan Y, Ye J, Shen F, et al. Interleukin-6 stimulates circulating blood-derived endothelial progenitor cell angiogenesis in vitro. *J Cereb Blood Flow Metab.* 2008; 28(1):90-98.
64. Spiller KL, Anfang RR, Spiller KJ, et al. The role of macrophage phenotype in vascularization of tissue engineering scaffolds. *Biomaterials.* 2014; 35(15):4477-4488.

65. Li JL, Sainson RC, Oon CE, et al. DLL4-Notch signaling mediates tumor resistance to anti-VEGF therapy in vivo. *Cancer Res.* 2011; 71(18):6073-6083.
66. van Beijnum JR, Nowak-Sliwinska P, Huijbers EJ, Thijssen VL, Griffioen AW. The great escape; the hallmarks of resistance to antiangiogenic therapy. *Pharmacological reviews.* 2015; 67(2):441-461.
67. Van Overmeire E, Laoui D, Keirsse J, Van Ginderachter JA. Hypoxia and tumor-associated macrophages A deadly alliance in support of tumor progression. *Oncoimmunology.* 2014; 3(1).
68. Laoui D, Van Overmeire E, Di Conza G, et al. Tumor Hypoxia Does Not Drive Differentiation of Tumor-Associated Macrophages but Rather Fine-Tunes the M2-like Macrophage Population. *Cancer Research.* 2014; 74(1):24-30.
69. Welford AF, Biziato D, Coffelt SB, et al. TIE2-expressing macrophages limit the therapeutic efficacy of the vascular-disrupting agent combretastatin A4 phosphate in mice. *The Journal of clinical investigation.* 2011; 121(5):1969.
70. Sprinzl MF, Reisinger F, Puschnik A, et al. Sorafenib perpetuates cellular anticancer effector functions by modulating the crosstalk between macrophages and natural killer cells. *Hepatology.* 2013; 57(6):2358-2368.
71. Edwards JP, Emens L. The Multikinase Inhibitor Sorafenib Reverses the Suppression of IL-12 and Enhancement of IL-10 by PGE2 in Murine Macrophages. *J Immunother.* 2010; 33(8):869-869.
72. Gul N, Babes L, Siegmund K, et al. Macrophages eliminate circulating tumor cells after monoclonal antibody therapy. *Journal of Clinical Investigation.* 2014; 124(2):812-823.
73. Edris B, Willingham SB, Weiskopf K, et al. Anti-KIT monoclonal antibody inhibits imatinib-resistant gastrointestinal stromal tumor growth. *P Natl Acad Sci USA.* 2013; 110(9):3501-3506.
74. Yu N, Fu S, Xu Z, et al. Synergistic antitumor responses by combined GITR activation and sunitinib in metastatic renal cell carcinoma. *Int J Cancer.* 2015.
75. Arnould L, Gelly M, Penault-Llorca F, et al. Trastuzumab-based treatment of HER2-positive breast cancer: an antibody-dependent cellular cytotoxicity mechanism? *British Journal of Cancer.* 2006; 94(2):259-267.
76. Savikko J, Rintala JM, Rintala S, Koskinen P. Epidermal growth factor receptor inhibition by erlotinib prevents vascular smooth muscle cell and monocyte-macrophage function in vitro. *Transpl Immunol.* 2015; 32(3):175-178.
77. Detry B, Blacher S, Erpicum C, et al. Sunitinib Inhibits Inflammatory Corneal Lymphangiogenesis. *Invest Ophth Vis Sci.* 2013; 54(5):3082-3093.
78. Patwardhan PP, Surriga O, Beckman MJ, et al. Sustained Inhibition of Receptor Tyrosine Kinases and Macrophage Depletion by PLX3397 and Rapamycin as a Potential New Approach for the Treatment of MPNSTs. *Clinical Cancer Research.* 2014; 20(12):3146-3158.
79. Stafford JH, Hirai T, Deng L, et al. Colony stimulating factor 1 receptor inhibition delays recurrence of glioblastoma after radiation by altering myeloid cell recruitment and polarization. *Neuro Oncol.* 2015.
80. Piao YJ, Liang J, Holmes L, et al. Glioblastoma resistance to anti-VEGF therapy is associated with myeloid cell infiltration, stem cell accumulation, and a mesenchymal phenotype. *Neuro-Oncology.* 2012; 14(11):1379-1392.
81. Rivera LB, Meyronet D, Hervieu V, Frederick MJ, Bergsland E, Bergers G. Intratumoral myeloid cells regulate responsiveness and resistance to antiangiogenic therapy. *Cell Rep.* 2015; 11(4):577-591.
82. Scholz A, Harter PN, Cremer S, et al. Endothelial cell-derived angiopoietin-2 is a therapeutic target in treatment-naive and bevacizumab-resistant glioblastoma. *Embo Mol Med.* 2015:1503 - 1594.
83. Peterson TE, Kirkpatrick ND, Huang Y, et al. Dual inhibition of Ang-2 and VEGF receptors normalizes tumor vasculature and prolongs survival in glioblastoma by altering macrophages. *Proc Natl Acad Sci U S A.* 2016; 113(16):4470-4475.
84. Kloepper J, Riedemann L, Amoozgar Z, et al. Ang-2/VEGF bispecific antibody reprograms macrophages and resident microglia to anti-tumor phenotype and prolongs glioblastoma survival. *Proc Natl Acad Sci U S A.* 2016; 113(16):4476-4481.
85. Pander J, Heusinkveld M, van der Straaten T, et al. Activation of Tumor-Promoting Type 2 Macrophages by EGFR-Targeting Antibody Cetuximab. *Clinical Cancer Research.* 2011; 17(17):5668-5673.

86. Gabrusiewicz K, Liu D, Cortes-Santiago N, et al. Anti-vascular endothelial growth factor therapy-induced glioma invasion is associated with accumulation of Tie2-expressing monocytes. *Oncotarget.* 2014; 5(8):2208-2220.
87. Castro BA, Flanigan P, Jahangiri A, et al. Macrophage migration inhibitory factor downregulation: a novel mechanism of resistance to anti-angiogenic therapy. *Oncogene.* 2017.
88. Rigamonti N, Kadioglu E, Keklikoglou I, Wyser Rmili C, Leow Ching C, De Palma M. Role of Angiopoietin-2 in Adaptive Tumor Resistance to VEGF Signaling Blockade. *Cell Reports.* 2014; 8(3):696-706.
89. de Groot J, Liang J, Kong LY, et al. Modulating Antiangiogenic Resistance by Inhibiting the Signal Transducer and Activator of Transcription 3 Pathway in Glioblastoma. *Oncotarget.* 2012; 3(9):1036-1048.
90. Lu-Emerson C, Snuderl M, Kirkpatrick ND, et al. Increase in tumor-associated macrophages after antiangiogenic therapy is associated with poor survival among patients with recurrent glioblastoma. *Neuro-Oncology.* 2013; 15(8):1079-1087.
91. Doloff JC, Waxman DJ. VEGF Receptor Inhibitors Block the Ability of Metronomically Dosed Cyclophosphamide to Activate Innate Immunity-Induced Tumor Regression. *Cancer Research.* 2012; 72(5):1103-1115.
92. Strauss L, Sangaletti S, Consonni FM, et al. RORC1 Regulates Tumor-Promoting "Emergency" Granulo-Monocytopoiesis. *Cancer Cell.* 2015; 28(2):253-269.
93. Mitchem JB, Brennan DJ, Knolhoff BL, et al. Targeting tumor-infiltrating macrophages decreases tumor-initiating cells, relieves immunosuppression, and improves chemotherapeutic responses. *Cancer Res.* 2013; 73(3):1128-1141.
94. Strachan DC, Ruffell B, Oei Y, et al. CSF1R inhibition delays cervical and mammary tumor growth in murine models by attenuating the turnover of tumor-associated macrophages and enhancing infiltration by CD8+ T cells. *OncoImmunology.* 2013; 2(12):e26968.
95. Tap WD, Wainberg ZA, Anthony SP, et al. Structure-Guided Blockade of CSF1R Kinase in Tenosynovial Giant-Cell Tumor. *New England Journal of Medicine.* 2015; 373(5):428-437.
96. Butowski N, Colman H, De Groot JF, et al. Orally administered colony stimulating factor 1 receptor inhibitor PLX3397 in recurrent glioblastoma: an Ivy Foundation Early Phase Clinical Trials Consortium phase II study. *Neuro-Oncology.* 2015.
97. Li X, Yao W, Yuan Y, et al. Targeting of tumour-infiltrating macrophages via CCL2/CCR2 signalling as a therapeutic strategy against hepatocellular carcinoma. *Gut.* 2015.
98. De Palma M, Lewis CE. Macrophage regulation of tumor responses to anticancer therapies. *Cancer cell.* 2013; 23(3):277-286.
99. Cicatiello V, Apicella I, Tudisco L, et al. Powerful anti-tumor and anti-angiogenic activity of a new anti-vascular endothelial growth factor receptor 1 peptide in colorectal cancer models. *Oncotarget.* 2015; 6(12):10563-10576.
100. Alitalo AK, Proulx ST, Karaman S, et al. VEGF-C and VEGF-D Blockade Inhibits Inflammatory Skin Carcinogenesis. *Cancer Research.* 2013; 73(14):4212-4221.
101. Hajrasouliha AR, Funaki T, Sadrai Z, Hattori T, Chauhan SK, Dana R. Vascular Endothelial Growth Factor-C Promotes Alloimmunity by Amplifying Antigen-Presenting Cell Maturation and Lymphangiogenesis. *Invest Ophth Vis Sci.* 2012; 53(3):1244-1250.
102. Sierra JR, Corso S, Caione L, et al. Tumor angiogenesis and progression are enhanced by Sema4D produced by tumor-associated macrophages. *J Exp Med.* 2008; 205(7):1673-1685.
103. Stefater JA, Lewkowich I, Rao S, et al. Regulation of angiogenesis by a non-canonical Wnt-Flt1 pathway in myeloid cells. *Nature.* 2011; 474(7352):511-515.
104. de Groot JF, Piao Y, Tran H, et al. Myeloid biomarkers associated with glioblastoma response to anti-VEGF therapy with aflibercept. *Clin Cancer Res.* 2011; 17(14):4872-4881.
105. Ko JS, Rayman P, Ireland J, et al. Direct and Differential Suppression of Myeloid-Derived Suppressor Cell Subsets by Sunitinib Is Compartmentally Constrained. *Cancer Research.* 2010; 70(9):3526-3536.
106. van Dongen M, Savage NDL, Jordanova ES, et al. Anti-inflammatory M2 type macrophages characterize metastasized and tyrosine kinase inhibitor-treated gastrointestinal stromal tumors. *International Journal of Cancer.* 2010; 127(4):899-909.

107. Ullrich K, Wurster KD, Lamprecht B, et al. BAY 43-9006/Sorafenib blocks CSF1R activity and induces apoptosis in various classical Hodgkin lymphoma cell lines. *Brit J Haematol.* 2011; 155(3):398-402.

108. Lin JC, Liu CL, Lee JJ, et al. Sorafenib induces autophagy and suppresses activation of human macrophage (vol 15, pg 333, 2013). *International Immunopharmacology.* 2013; 16(1):123-123.

109. Zhang W, Zhu XD, Sun HC, et al. Depletion of Tumor-Associated Macrophages Enhances the Effect of Sorafenib in Metastatic Liver Cancer Models by Antimetastatic and Antiangiogenic Effects. *Clinical Cancer Research.* 2010; 16(13):3420-3430.

110. Cavnar MJ, Zeng S, Kim TS, et al. KIT oncogene inhibition drives intratumoral macrophage M2 polarization. *J Exp Med.* 2013; 210(13):2873-2886.

111. Kummar S, Allen D, Monks A, et al. Cediranib for Metastatic Alveolar Soft Part Sarcoma. *Journal of Clinical Oncology.* 2013; 31(18):2296-U2106.

112. Guttman-Yassky E, Mita A, De Jonge M, et al. Characterisation of the cutaneous pathology in non-small cell lung cancer (NSCLC) patients treated with the EGFR tyrosine kinase inhibitor erlotinib. *Eur J Cancer.* 2010; 46(11):2010-2019.

113. Ozanne J, Prescott AR, Clark K. The clinically approved drugs dasatinib and bosutinib induce anti-inflammatory macrophages by inhibiting the salt-inducible kinases. *Biochem J.* 2015; 465:271-279.

114. Li J, Srivastava RM, Ettyreddy A, Ferris RL. Cetuximab ameliorates suppressive phenotypes of myeloid antigen presenting cells in head and neck cancer patients. *J Immunother Cancer.* 2015; 3:54.

Chapter 2
Introduction-Part 2

Chapter 2

Introduction-Part 2

CECR1

CECR1 [1] is a secreted member of the adenyl-deaminase growth factor family. Members of this family share similar functions with ADA (Adenosine Deaminase), which enables CECR1 to degrade adenosine to inosine in purine metabolism [2]. Homologs of CECR1 in other species like IDGF in flesh fly or MDGF in sea slug has been shown to also act as growth factors whose function requires their adenosine deaminase (AD) activity [3, 4]. Although little is known about the function of CECR1 in both invertebrates and vertebrates, it was shown to regulate immune function, maintaining hematopoietic stem cell pluripotency in Drosophila and regulate Xenopus embryogenesis via interacting with Adenosine P1 receptor [5].

In humans, CECR1 was found to be expressed by the monocyte/macrophage system[6]. CECR1 is activated in the context of hypoxia under a variety of pathologic circumstances in response to excessive extracellular adenosine [7]. Reportedly, higher production of CECR1 is detected in the serum and pleural fluid in patients with tuberculosis[8]. Similarly, in the serum of patients with breast carcinoma [9] and systemic erythroid lupus [10], CECR1 levels are higher than the physiological levels. CECR1 promotes the differentiation of monocytes into macrophages and stimulates the proliferation of lymphocytes and macrophages [11]. Further, CECR1 was proven to bind with adenosine receptors serving as a mechanism in regulating macrophage differentiation and proliferation [12]. CECR1 anchors on the surface of monocytes / macrophages and lymphocytes via binding to adenosine receptors and HPSG [5]. Unlike ADA-1 that binds to CD26, CECR1 binds to CD39 on the surface of regulatory T cells, indicative of a role in mediating ATP hydrolysis and Adenosine biosynthesis [13]. In addition, CECR1 functions in the immune regulation by influencing the subpopulation of CD4+ T cells. In diabetic retinopathy CECR1 is highly expressed in macrophages, activated monocytes and in retinal microglia [14]. Elevated levels of CECR1 adenosine deaminase activity was found in several neoplasm [9, 15-17] and considered as a marker for regression of cancer after chemotherapy [18].

Recent studies strengthen the link of CECR1 with immune functions. Several somatic mutations in exons of CECR1 were found in patients with auto-immune diseases characterized by early-onset lacunar stroke, severe peripheral vasculitis and systemic inflammation [19-21]. Overproduction of pro-inflammatory factors like TNF-α, iNOS, IL-1β were detected in either patient serum or skin biopsies. Coincidently, in peripheral blood mononuclear cell (PBMC) of patients with CECR1 mutations, neutrophil gene signatures pointing to an altered immune response were recorded. In monocytes of these patients, CECR1 mutations caused IFN-γ responses featured by the expression of genes like ISG15, IFI27, IFI44L [22]. Data from *in vitro* experiments showed loss of CECR1 or CECR1 mutations in monocytic cell lines or patient derived monocytes causing blockage of the differentiation of monocytes into M2 macrophages in response to M-CSF, the main growth factor regulating the survival of macrophages [21]. Very little is known

about CECR1 expression in the microglia cells of the CNS and the contribution of CECR1 in the development of glioma remains to be investigated. In this thesis, in **Chapter 3**, we investigated the contribution of CECR1 in the differentiation of specific tumor-associated-macrophages (TAM) subtypes in glial tumors. Furthermore, we investigated in **Chapter 4** the role of CECR1-mediated crosstalk between macrophages and vascular mural cells in angiogenesis in glioma. Proteosome adaptation of TAMS in response to CECR1 is also investigated in **Chapter 6**.

PERIOSTIN

Periostin is a member of the TGF family of which the expression is induced by TGF-β as well as BMP-2 [23]. Periostin is an adhesion-related protein containing 4 repetitive conservative fasciclin domains that are similar in sequence to the insect protein fasciclin-1. As a matricellular protein, periostin is a multifunctional protein that regulates formation of the peridontal ligaments and the cardiac valves. It also contributes to bone morphogenesis[24]. Additionally, recent studies revealed that periostin is involved in various neoplasms including gastric cancer [25], colorectal cancer [26], pancreatic cancer [27] and cerebral tumors [28]. Periostin plays a role among extracellular matrix proteins in regulating the proliferation, migration and epithelial-mesenchymal transition of cancer cells [29]. Structurally, Periostin interacts with other ECM components like Tenascin-C [30] and bone morphogenic proteins 1/2 (BMP1/2) [31] which promote the remodeling of extracellular matrix by promoting the secretion of fibronectin [32] and collagen [31]. A wide spectrum of molecules can interact with periostin. The N-terminal region binds to the integrins αVβ+3,αVβ5,α6β4 through its FAS domain [29] thereby promoting the migration of tumor associated endothelial cells and cancer cells via the activation of Akt/PKB and Focal Adhesion Kinase(FAK)-mediated signaling pathways [33]. The intracellular domain of pre-NOTCH1 is recognized by periostin causing the activation of the Notch pathway [34]. Loss of Postn in the ErbB2/Neu-driven mouse breast tumor models results in a reduced Notch signaling pathway and deceleration of tumor growth [35].

Periostin was shown to be expressed by the stromal cells like fibroblast in the microenvironment of breast cancer and enhances the metastatic potential of breast cancer cells [36]. Canonical Wnt signaling is activated by periostin by its interaction with Wnt3/4 and LRP5/6. The signal of periostin, secreted by tumor stroma, particularly by tumor associated fibroblasts, is vital in maintaining the breast cancer stem cells. In addition, during breast cancer-associated angiogenesis the so-called tip cells (endothelial cells that navigate the branching of newly formed vessels), transiently express periostin as well. As a consequence, periostin promotes the resuscitation and proliferation of perivascular located metastatic breast cancer cells [37]. In GBM, periostin is overexpressed and deposited in the neuropil. The expression of periostin in GBM is reversely

related to clinical outcome (Disease free survival and overall survival) [38]. Glioma stem cells defined by SOX-2 and Oligo-2 also produce periostin. Through interaction with Integrin αVβ3 on the surface of monocytes, peripheral monocytes are recruited by glioma stem cells that express periostin and subsequently differentiate into M2-like macrophages [39]. In GBM samples periostin expression is foremost perivascular and it appears that cells with the phenotype of pericytes express this protein [40]. In mice, cell types that express periostin have been reported to include pericytes and glioma stem cells (GSCs). Periostin interaction between GSCs, pericytes, TAMs and perhaps other cells of the perivascular niche, may contribute to glioma growth and tumor angiogenesis.

In **Chapter 5** the expression of periostin in human gliomas is detailed and its contribution to neo-angiogenesis is studied in an *in vitro* model of angiogenesis.

P2RY12

The receptor P2RY12 was proposed as a specific marker for healthy rodent CNS microglial cells, rather than any other type of tissue resident macrophages or blood-derived monocytes [41]. P2RY12 belongs to the family of P2 purinergic receptors, consisting of seven transmembrane G protein coupled receptors (GPCRs) that have been implicated to contribute to ATP-and ADP-mediated cell migration *in vitro* [42]. Except for expression in activated platelets [43], P2RY12 was found to be mainly expressed by microglial cells. P2RY12 deficiency in P2RY12 knockdown mice significantly compromised microglial chemotaxis and extension of microglial foot processes in response to CNS injury [44, 45]. In **Chapter 7**, we aimed to label glioma samples with P2RY12 to distinguish the expression of CECR1 by either resident microglia, or recruited/infiltrated macrophages. We found that P2RY12 is a consistent marker for resident microglial cells in low grade glioma. However, the P2RY12 signal tends to translocate from cell surface to the nucleus in high grade glioma. We also investigated the relation between the expression of the marker and the M1/M2 profiles of the microglial cells, and the relation with malignant behavior of the gliomas.

OBJECTIVES AND OUTLINE OF THIS THESIS

The scope of this thesis is to elucidate the role of the CECR1 molecule on angiogenesis, and specifically, glioma neo-angiogenesis. In **Chapter 3 and 4**, the expression, distribution, localization and function of CECR1 in glioma-associated macrophages is described. The influence of CECR1 through macrophage-mediated paracrine effects on glial cell proliferation and migration, and on glioma angiogenesis is demonstrated. In **Chapter 6**, proteomic analysis revealed the CECR1 mediated intracellular pathways that contributed to the observed M2-like TAM phenotype associated with CECR1 expression. In addition, the cell types that express CECR1 are pin-pointed and their position among other immune-regulating cells and the cells engaged in the formation of blood vessels (endo-

thelial cells, pericytes and other mural cells) is studied in detail. In Chapter 5 the expression of periostin in human gliomas is detailed and its contribution to neo-angiogenesis is studied in an *in vitro* model of angiogenesis. In Chapter 7, we investigated the subpopulation of microglial cells in glioma using the P2RY12 marker.

REFERENCES

1. Riazi, M.A., et al., *The human homolog of insect-derived growth factor, CECR1, is a candidate gene for features of cat eye syndrome.* Genomics, 2000. **64**(3): p. 277-85.
2. Zavialov, A.V. and A. Engstrom, *Human ADA2 belongs to a new family of growth factors with adenosine deaminase activity.* Biochem J, 2005. **391**(Pt 1): p. 51-7.
3. Akalal, D., C. Schein, and G. Nagle, *Mollusk-derived growth factor and the new subfamily of adenosine deaminase-related growth factors.* Current pharmaceutical design, 2004. **10**(31): p. 3893-3900.
4. Charlab, R., et al., *The invertebrate growth factor/CECR1 subfamily of adenosine deaminase proteins.* Gene, 2001. **267**(1): p. 13-22.
5. Iijima, R., et al., *The extracellular adenosine deaminase growth factor, ADGF/CECR1, plays a role in Xenopus embryogenesis via the adenosine/P1 receptor.* J Biol Chem, 2008. **283**(4): p. 2255-64.
6. Conlon, B.A. and W.R. Law, *Macrophages are a source of extracellular adenosine deaminase-2 during inflammatory responses.* Clin Exp Immunol, 2004. **138**(1): p. 14-20.
7. Caorsi, R., et al., *Monogenic polyarteritis: the lesson of ADA2 deficiency.* Pediatr Rheumatol Online J, 2016. **14**(1): p. 51.
8. Li, M., et al., *Diagnostic accuracy of tumor necrosis factor-alpha, interferon-gamma, interlukine-10 and adenosine deaminase 2 in differential diagnosis between tuberculous pleural effusion and malignant pleural effusion.* Journal of Cardiothoracic Surgery, 2014. **9**(1): p. 118.
9. Aghaei, M., et al., *Adenosine deaminase activity in the serum and malignant tumors of breast cancer: the assessment of isoenzyme ADA1 and ADA2 activities.* Clin Biochem, 2005. **38**(10): p. 887-91.
10. Hitoglou, S., et al., *Adenosine deaminase activity and its isoenzyme pattern in patients with juvenile rheumatoid arthritis and systemic lupus erythematosus.* Clin Rheumatol, 2001. **20**(6): p. 411-6.
11. Zavialov, A.V., et al., *Human adenosine deaminase 2 induces differentiation of monocytes into macrophages and stimulates proliferation of T helper cells and macrophages.* Journal of Leukocyte Biology, 2010. **88**(2): p. 279-290.
12. Zavialov, A.V., et al., *Human adenosine deaminase 2 induces differentiation of monocytes into macrophages and stimulates proliferation of T helper cells and macrophages.* J Leukoc Biol, 2010. **88**(2): p. 279-90.
13. Kaljas, Y., et al., *Human adenosine deaminases ADA1 and ADA2 bind to different subsets of immune cells.* Cell Mol Life Sci, 2016.
14. Elsherbiny, N.M., et al., *Potential roles of adenosine deaminase-2 in diabetic retinopathy.* Biochem Biophys Res Commun, 2013. **436**(3): p. 355-61.
15. Aghaei, M., et al., *Diagnostic value of adenosine deaminase activity in benign and malignant breast tumors.* Arch Med Res, 2010. **41**(1): p. 14-8.
16. Maldonado, P.A., et al., *Role of the purinergic system in patients with cervical intraepithelial neoplasia and uterine cancer.* Biomed Pharmacother, 2012. **66**(1): p. 6-11.
17. Nikkhoo, B., et al., *Diagnostic Utility of Adenosine Deaminase in Serum and Bronchoalveolar Lavage Fluid for Screening Lung Cancer in Western Iran.* Journal of Medical Biochemistry, 2013. **32**(2): p. 109-115.

18. Roberts, E.L. and O.T. Roberts, *Plasma adenosine deaminase isoform 2 in cancer patients undergoing chemotherapy.* Br J Biomed Sci, 2012. **69**(1): p. 11-3.
19. Elkan, P.N., et al., *Mutant Adenosine Deaminase 2 in a Polyarteritis Nodosa Vasculopathy.* New England Journal of Medicine, 2014. **370**(10): p. 921-931.
20. Garg, N., et al., *Novel adenosine deaminase 2 mutations in a child with a fatal vasculopathy.* Eur J Pediatr, 2014. **173**(6): p. 827-30.
21. Zhou, Q., et al., *Early-onset stroke and vasculopathy associated with mutations in ADA2.* N Engl J Med, 2014. **370**(10): p. 911-20.
22. Uettwiller, F., et al., *ADA2 deficiency: case report of a new phenotype and novel mutation in two sisters.* RMD Open, 2016. **2**(1): p. e000236.
23. Horiuchi, K., et al., *Identification and characterization of a novel protein, periostin, with restricted expression to periosteum and periodontal ligament and increased expression by transforming growth factor beta.* J Bone Miner Res, 1999. **14**(7): p. 1239-49.
24. Conway, S.J., et al., *The role of periostin in tissue remodeling across health and disease.* Cell Mol Life Sci, 2013.
25. Moniuszko, T., et al., *Role of periostin in esophageal, gastric and colon cancer.* Oncol Lett, 2016. **12**(2): p. 783-787.
26. Xu, X., et al., *Periostin expression in intra-tumoral stromal cells is prognostic and predictive for colorectal carcinoma via creating a cancer-supportive niche*. 2015. 2015.
27. Sato-Matsubara, M. and N. Kawada, *New player in tumor-stromal interaction: Granulin as a novel therapeutic target for pancreatic ductal adenocarcinoma liver metastasis.* Hepatology, 2016: p. n/a-n/a.
28. Park, S.Y., et al., *Periostin (POSTN) Regulates Tumor Resistance to Antiangiogenic Therapy in Glioma Models.* Mol Cancer Ther, 2016. **15**(9): p. 2187-97.
29. Morra, L. and H. Moch, *Periostin expression and epithelial-mesenchymal transition in cancer: a review and an update.* Virchows Arch, 2011. **459**(5): p. 465-75.
30. Kii, I., et al., *Incorporation of Tenascin-C into the Extracellular Matrix by Periostin Underlies an Extracellular Meshwork Architecture.* Journal of Biological Chemistry, 2010. **285**(3): p. 2028-2039.
31. Hwang, E.Y., et al., *Structural characterization and interaction of periostin and bone morphogenetic protein for regulation of collagen cross-linking.* Biochem Biophys Res Commun, 2014. **449**(4): p. 425-31.
32. Kii, I., T. Nishiyama, and A. Kudo, *Periostin promotes secretion of fibronectin from the endoplasmic reticulum.* Biochem Biophys Res Commun, 2016. **470**(4): p. 888-93.
33. Ruan, K., S. Bao, and G. Ouyang, *The multifaceted role of periostin in tumorigenesis.* Cell Mol Life Sci, 2009. **66**(14): p. 2219-30.
34. Tanabe, H., et al., *Periostin associates with Notch1 precursor to maintain Notch1 expression under a stress condition in mouse cells.* PLoS One, 2010. **5**(8): p. e12234.
35. Sriram, R., et al., *Loss of periostin/OSF-2 in ErbB2/Neu-driven tumors results in androgen receptor-positive molecular apocrine-like tumors with reduced Notch1 activity.* Breast Cancer Res, 2015. **17**: p. 7.
36. Malanchi, I., et al., *Interactions between cancer stem cells and their niche govern metastatic colonization.* Nature, 2012. **481**(7379): p. 85-U95.
37. Ghajar, C.M., et al., *The perivascular niche regulates breast tumour dormancy.* Nat Cell Biol, 2013. **15**(7): p. 807-17.
38. Mikheev, A.M., et al., *Periostin is a novel therapeutic target that predicts and regulates glioma malignancy.* Neuro-Oncology, 2015. **17**(3): p. 372-382.
39. Zhou, W., et al., *Periostin secreted by glioblastoma stem cells recruits M2 tumour-associated macrophages and promotes malignant growth.* Nat Cell Biol, 2015. **17**(2): p. 170-82.
40. Mustafa, D.A.M., et al., *A Proteome Comparison Between Physiological Angiogenesis and Angiogenesis in Glioblastoma.* Molecular & Cellular Proteomics, 2012. **11**(6).
41. Butovsky, O., et al., *Identification of a unique TGF-beta-dependent molecular and functional signature in microglia.* Nat Neurosci, 2014. **17**(1): p. 131-43.
42. Cattaneo, M., *P2Y12 receptors: structure and function.* J Thromb Haemost, 2015. **13 Suppl 1**: p. S10-6.

43. Lecchi, A., et al., *Identification of a new dysfunctional platelet P2Y12 receptor variant associated with bleeding diathesis.* Blood, 2015. **125**(6): p. 1006-13.
44. Haynes, S.E., et al., *The P2Y12 receptor regulates microglial activation by extracellular nucleotides.* Nat Neurosci, 2006. **9**(12): p. 1512-9.
45. Ohsawa, K., et al., *P2Y12 receptor-mediated integrin-β1 activation regulates microglial process extension induced by ATP*. Glia, 2010. **58**(7): p. 790-801.

Chapter 3

Activation of CECR1 in M2-like TAMs promotes paracrine stimulation mediated glial tumor progression

Changbin Zhu M.D. M.Sc., Dana Mustafa Ph.D., Ping-pin Zheng M.D. Ph.D., Marcel van der Weiden, Andrea Sacchetti Ph.D., Maarten Brandt B.A.Sc., Ihsan Chrifi B.A.Sc., Dennie.Tempel Ph.D., Pieter.J.M. Leenen Ph.D., Dirk Jan Duncker M.D. Ph.D., Caroline Cheng Ph.D.*, Johan M Kros M.D. Ph.D*. (*these authors contributed equally to this work)

(Neuro-oncology 2017, jan. 3, (ahead of print) PMID: 27738887)

ABSTRACT

Background: The majority of glioma associated microglia/macrophages have been identified as M2-type macrophages with immune suppressive and tumor supportive action. Recently, the extracellular adenosine deaminase protein Cat Eye Syndrome Critical Region Protein 1(CECR1) was shown to regulate macrophage maturation. In this study, we investigate the role of CECR1 in the regulation of the glioma-associated macrophage response.

Methods: Expression of CECR1 was assessed in human glioma samples. CECR1 mediated macrophage response was studied *in vitro*, using donor derived CD14+ monocytes and THP-1 monocytic cell line. The response of human glioma cell line U87 to conditioned medium of macrophages preconditioned with recombinant human (rh)CECR1 or CECR1 silencing was also assessed.

Results: CECR1 was strongly expressed in high-grade gliomas ($P<0.001$) and correlated positively with that of the M2 phenotype markers in tumor associated microglia/macrophages (TAMs) (overall, $P<0.05$). *In vitro* studies confirmed the presence of a significant higher level of CECR1 expression in M2-like macrophages exposed to U87 conditioned medium ($P<0.001$). CECR1 knockdown or stimulation of macrophages affected differentiation towards the M2-like phenotype. Stimulation of U87 cells with conditioned medium of CECR1 knockdown or stimulated macrophages affected tumor cell proliferation and migration, coinciding with altered intracellular MAPK signaling. In glioma tissue samples. CECR1 expression correlated with Ki67 and MAPK signaling protein.

Conclusions: CECR1 is a potent regulator of TAM polarization, and is consistently highly expressed by M2-type TAMs, particularly in high-grade glioma. Paracrine effects induced by CECR1 in M2-like TAMs activate MAPK signaling and stimulate the proliferation and migration of glioma cells.

INTRODUCTION

The heterogeneity of glial tumor cells and the immune privileged environment of the central nervous system hamper the development of effective treatment strategies. The immune system plays a complex and largely undiscovered role in the development of gliomas. Infiltrating myeloid cells including monocytes and macrophages are key players in promoting tumor progression and recurrences[1,2], as their robust presence with the accumulation of microglial cells in GBM facilitate an immune suppressive and oncogenic micro-environment. Macrophages in GBM are heterogeneous and display considerable plasticity, complicating their characterization and analysis[2]. To ease data interpretation, tumor associated macrophages (TAMs) are divided in M1- and M2-like cells. M1-like cells express high levels of CD80, CD86, MHC II molecules and secrete higher levels of TNF-α, IL1β and IL-12. M1-like TAMs are reportedly anti-tumoral and associated with better prognosis[3,4]. However, it has been reported that (paracrine) stimulation of glial tumor cells and the hypoxic microenvironment trigger resident microglial cells and infiltrating macrophages to adopt the M2-like phenotype[5]. Indeed, M2-like TAMs outnumber their M1 counterparts in GBM. M2-like TAMs are defined by high cell surface levels of CD163, CD204, CD14; lower levels of CD80 and MHC II, and mediate the immunosuppressive response by secreting cytokines like IL-10, CCL20, CCL22, and PGE2[5]. M2-like glioma associated microglia/macrophages are also known to mediate tumor angiogenesis by producing pro-angiogenic factors such as VEGFA, and uPA and are associated with high-grade tumors and poor clinical outcomes[6,7]. Thus, microglial/macrophages are relevant to glial tumorigenesis and could become targets of therapeutic intervention.

In humans, the Cat Eye Syndrome Critical Region Protein 1 (CECR1) is highly expressed by monocyte/macrophage[8]. Recent reports indicate that in patients with genetic loss of function of CECR1, monocyte maturation and polarization into M2 macrophage subtype are reduced, coinciding with loss of vessel integrity[9,10]. CECR1 is an evolutionary highly conserved member of the adenyl-deaminase growth factor family, known for its immune modulatory function[11]. To date, the role of CECR1 in TAMs regulation in gliomas has not been explored. In this study, we investigated the role of CECR1, specifically with respect to TAMs, in glial tumors.

MATERIAL AND METHODS

Patient samples

Patient samples as listed in Supplementary table 1 and 2 and were obtained from the Biobank of the Department of Pathology, Erasmus MC, Rotterdam. The use of these samples was approved by the medical ethical committee of the Erasmus Medical Center.

siRNA transfection

SiRNA targeting CECR1 and scrambled non-targeting siRNAs were obtained from Dharmacon (GE health care, Netherland). THP-1 derived macrophage cultures were transfected after 48 hours of PMA treatment, following the manufacture's protocol (using Dharmafect transfection reagent). Efficiency of CECR1 knockdown was assessed after 24 and 48 hours at transcriptional level and protein level (see supplements). For functional assays or to obtain Macrophage-derived conditioned medium, siRNA transfected cells were used 24 hours post transfection.

Cell Cultures

CD14+ monocytes were obtained according to manufacturer's protocols. Cells were induced with 10 ng/ml GM-CSF (R&D, United States) or 10 ng/ml M-CSF (Immunotools, Germany) as previously reported[12].

THP-1 cells were cultured in RPMI-1640 supplemented with antibiotics and 10% FCS and matured by PMA (sigma, Sweden). IFN-γ/LPS, IL-4 and IL-10 were applied to generate M1, and M2a/M2c phenotypes *in vitro*. rhCECR1 was used for macrophage treatment for 96 hours.

Human glioblastoma cell lines U87, U373, and U251 were cultured in DMEM medium supplemented with 10%FCS and antibiotics. U87-derived conditioned medium (U87-CM) was used to stimulate macrophages for 48 hours.

MTT Assay

U87, U373, and U251 cells were seeded in 96-well setup followed by treatment with macrophage-conditioned medium. The growth of U87 cells was monitored by MTT (Sigma, Sweden) for five days. One plate without macrophage conditional medium was measured at the same day for reference (see Supplements).

Migration Assay

The Oris cell migration assay kit (Platypus Technologies, United States) was used to measure migration of PKH-67 labeled U87, U373, and U251 cells according to manufacturer's protocols in 96-well plate setup. Macrophage conditional medium was added and after 24 hours of incubation, pictures were taken at 0 and 24 h and quantified using image J. (see Supplements).

RNA isolation and Quantitative real-time PCR

Total RNA was isolated and reversely transcripted to cDNA from cryo-materials and macrophages. For the cryo-samples, transcripts of CECR1, CD68, CD86, CD16, CD204, CD206, NOS-2, IL-10, IL-12p35 and β-actin (reference gene) were measured. For *in vitro* experiments, transcripts of CECR1, IL-10, IL-12p35, IL-6, CXCL12, CCL18 and CCL22 were measured and normalized to β-actin level. Primers are listed in supplemental Table 3 (see Supplements).

Western blot analysis

Total protein was loaded onto SDS-PAGE gel and blotted to Nitro cellulose membranes followed by blocking and immunoblotting using specific antibodies. Incubation of secondary antibodies and detection of signals was followed using the Odyssey imaging system (Licor Bioscience, USA) (See Supplements).

Flow cytometry analysis

Macrophages were harvested and incubated with primary antibody against CD163 (Abd Serotec, 1:400) followed by Alexa Fluor-555 conjugated secondary antibody. Cells were counterstained with Hoechst 33258 and analyzed with a BD FACS Aria III. (See Supplements).

Immunostaining

Adjacent (cryo)sections were used for immunohistochemical and immunofluorescence analysis. Immunostaining and slide scanning were performed according to the protocol described previously[13].

Macrophages and U87 cells were fixed using 4% PFA/PBS, followed by antibody incubation. Signal areas were quantified using Image J (See Supplements and Supplemental Table 4).

Statistics

Data from clinical samples were analyzed by Mann-Whitney U test and Spearman Correlation using SPSS 21.0. All *in vitro* data were tested using unpaired two-tailed student's T test (Significance levels $P<0.05$). All data are presented in Mean ± S.E.M. unless otherwise stated.

RESULTS

Expression of CECR1 is skewed to high-grade astrocytoma and associated with the M2-like macrophage phenotype

Transcription of CECR1 was assessed in astrocytomas of various malignancy grades, using 2 different online GEO database (GDS 4467, GDS1813). CECR1 was mainly expressed in GBMs (Supplementary Figure 1a). QPCR analysis of astrocytoma samples from our biobank (19 astrocytomas grade II, 5 astrocytomas grade III, and 19 GBMs) shows that expression of the M2-microglia/macrophage specific markers CD16, CD204 and IL-10 was significantly higher in the astrocytomas grade III and GBM than in the grade II astrocytomas (Supplementary Figure 1b). The microglia/macrophage markers CD68 (pan macrophage marker), CD86 (M1 marker), CD206 (M2 marker), iNOS (M1 marker), and IL-12p35 (M1 marker) were equally expressed in the low and high grade tumors (Supplementary Figure 1c, d). Seven autopsy brains, 6 astrocytomas grade II, and 8 astrocytomas grade IV (GBM) were immunostained for CECR1, CD204, CD206 and CD16. CECR1 overlapped with CD204+, CD206+, and CD16+ perivascular cells in autopsy brain and low grade glioma (Figure 1a, Supplementary Figure 2a). In GBM, the CECR1 signal mainly overlapped with CD204+ and CD16+ cells at both perivascular and in the tumor parenchymal locations. Areas where CECR1 negative cell with features of M2-like macrophages located were also detected (Supplementary 3a,b). Overlap between CECR1 and CD206+ cells was only detected at the peripheral perivascular locations. Quantitation of the sections revealed significant higher numbers of CECR1, CD204, CD206, CD16+ cells in GBM versus the autopsy brains and astrocytomas grade II (Figure 1b, Supplementary Figure 2b).

qPCR dataset showed in astrocytomas grade III and IV (GBM) positive correlations of CECR1 expression with CD68, CD86, CD16, CD204, and IL-10. In astrocytomas grade III, CECR1 expression showed a negative correlation with IL-12p35. In contrast, no significant correlations between the markers iNOS, IL-12p35, CD206 and CECR1 was detected in high grade GBM samples (Figure 1c).

In GBM, CECR1 co-localized with the pan macrophage markers CD68 and Iba-1 (Figure 1d). CECR1 co-localized with CD68 in both perivascular areas and sites remote from the vasculature in autopsy brains (Supplemental Figure 4a-d), but only at perivascular locations in grade II astrocytoma (Supplemental Figure 4e, f). No CECR1 signal was detected in CD68+ macrophages remote from blood vessels (data not shown). In addition, CECR1 co-localized with markers of M2-like TAMs (CD204, CD163, CD16) in GBM (Figure 1e and f , Supplementary Figure 2c and d). CECR1+/CD163+ cells were only detected in the perivascular areas in autopsy brains and in astrocytomas grade II (Supplemental Figure 5a-d).

Figure 1 CECR1 is highly expressed by M2-like macrophage in GBM

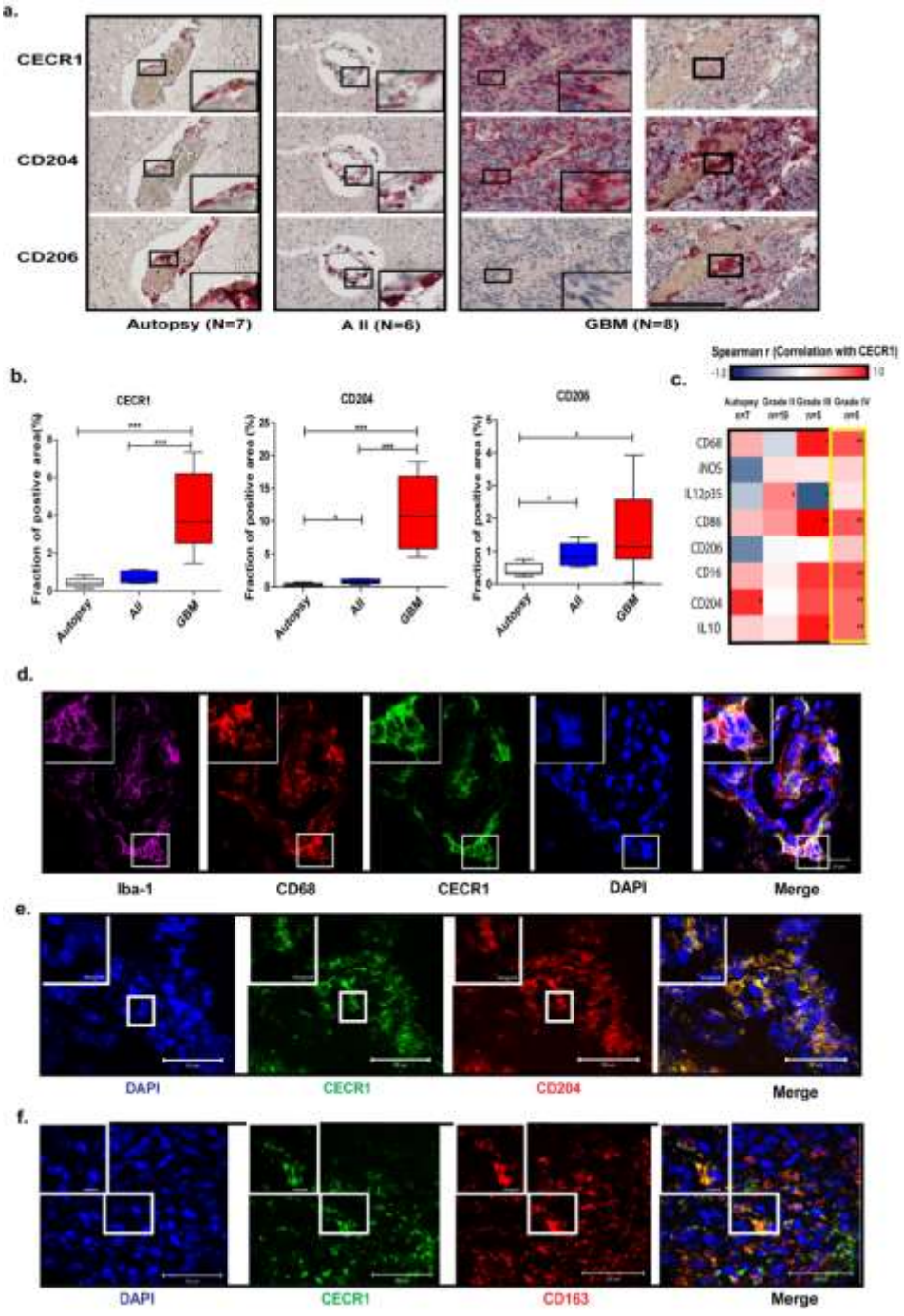

(a) Immunohistochemistry for CECR1, CD204, and CD206 in autopsy brain, astrocytoma grade II (AII) and grade IV (GBM) (scale bar: 200 μm). **(b)** Box plots displaying the mean percentages of CECR1, CD204, CD206 positive areas per image view in autopsy brains, AII and GBM. * P<0.05, ***P<0.005. **(c)** Heat map summarizing the Spearman correlation coefficients between CECR1 and CD68, IL-12p35, iNOS, CD86, CD206, CD16, CD204, IL-10 in autopsy, astrocytoma grade II and III and GBMs. * P<0.05, ** P<0.01. **(d)** Confocal images showing the co-localization of CECR1 with CD68 and Iba-1 in GBM (scale bar: 20 μm). **(e) (f)** Confocal images showing the co-localization of CECR1 with CD204, CD163 in GBM (scale bar: 50 μm for the low magnification field; 10 μm for high magnification inlet).

CECR1 is preferentially expressed in M2-like U87 stimulated macrophages in vitro

M-CSF induced (M2-like) macrophages showed a higher protein level of CECR1 than GM-CSF induced (M1-like) macrophages (figure 2a). This was coincided by higher protein levels of M2 phenotype markers (CD204, CD163) and higher mRNA levels of M2 cytokines (IL10, CXCL12) (supplementary figures 6 a-d).

CECR1 protein levels in both types of macrophages were further up-regulated in response to stimulation with U87 conditioned medium (U87-CM)(1.4 and 2.4 fold increase in GM/M-CSF induced macrophage respectively, figure 2a). Similarly, expression of CECR1 was detected in THP-1 derived macrophages (figure 2b). Elevated levels of CECR1 protein were detected in M2a and M2c macrophages (1.2 and 1.6 fold increase in IL4 and IL-10 stimulated groups respectively) and U87-CM stimulated macrophages (1.8 fold increase) compared to control (RPMI) group. In contrast, in M1 macrophages (LPS+INFγ group), a lower level of CECR1 (0.8 fold change) was detected (figure 2b).

CECR1 protein levels were further assessed in GM/M-CSF induced macrophages (Figure 2c and d). CECR1 protein detected by immunostaining was significantly higher in M-CSF induced (M2-like) macrophages than in GM-CSF induced (M1-like) counterparts. Furthermore, stimulation of U87-CM increased CECR1 protein levels in both M-CSF and GM-CSF induced macrophages and enhanced protein signal of M2 marker CD163 (Figure 2c, d).

CECR1 expression induces the M2-like macrophage phenotype in vitro

Effective siRNA mediated silencing of CECR1 was validated by qPCR, Western blotting and immunofluorescent staining (Figures 2e and f, and Supplementary Figure 7a and b) as compared to non-targeting siRNA treated controls (siSham).

In THP-1 macrophage with siCECR1 condition, lower protein levels of M2 marker CD163 compared to siSham conditions was detected, as observed by qPCR, Western blot analysis and cell immunostaining (Supplementary Figure 7c and Figure 2g, h, i), and mRNA level of M2 marker IL-10 and M1 marker CD86 were significantly decreased and increased upon CECR1 silencing, respectively (Figure 2i). Stimulation with rhCECR1 raised CD163 transcript and protein levels in THP-1 macrophages in a dose responsive

manner (Figure 3a and b). Similar observations were made at the protein level using the M-CSF induced

Figure 2. CECR1 is highly expressed in M2-like, U87 stimulated macrophage

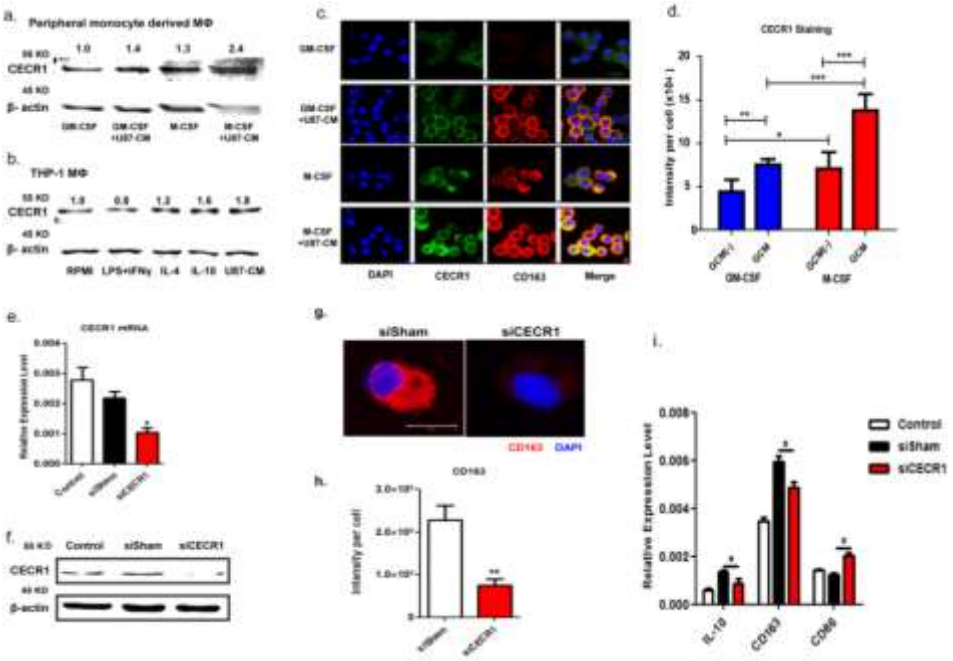

(a) Western blot of CECR1 protein in GM/M-CSF induced macrophages (MΦ) with/without U87-CM from three experiments. Numbers above bands indicate quantified levels normalized to β-actin. **(b)** Western blot of CECR1 protein in THP-1 derived macrophages (MΦ) in response to RPMI-1640, LPS-INFγ (M1), IL-4 (M2a), IL-10 (M2b), and U87-CM from three experiments. Numbers above bands indicate quantified levels normalized to β-actin. **(c)** Representative staining of CECR1 and CD163 in GM-CSF and M-CSF induced macrophages with/without U87 stimulation for 96 hours. (scale bar: 20 μm). **(d)** Quantification of fluorescent signal of CECR1 per cell in different groups. Data are presented as mean ± S.E.M. and were obtained of three independent experiments. *P<0.05, **P<0.01, *** P<0.005. **(e)** qPCR of CECR1 in macrophages with CECR1 knockdown and control were obtained from three experiments and presented as mean ± S.E.M. *P<0.05. **(f)** Western blot of CECR1 protein in THP-1 macrophages with siCECR1, siSham, and non-transfected control. **(g)** CD163 immunostaining in siCECR1 and sisham transfected THP-1 macrophages. (scale bar: 20 μm). **(h)** Quantified CD163 signal per cell in siCECR1 and siSham control groups are presented as mean ± S.E.M. and were obtained of three independent experiments. ** P<0.01. **(i)** IL-10, CD163, and CD86 expression in siCECR1, siSham, and non-transfected THP-1 macrophages as measured by RT-qPCR. Data are presented as mean ±S.E.M. and obtained from three experiments. *P<0.05.

(M2-like) macrophages (Figure 3c-e). FACs further confirmed that cell surface expression of CD163 increased in M-CSF induced macrophages following treatment with rhCECR1 during M2 macrophage differentiation (Supplementary Figure 7d). Enrichment of CD163+ cells was observed in the GBM samples with high CECR1 signal (>5% CECR1+

area per image view), as compared to those with low CECR1 signal (<5% CECR1+ area per image view) (Supplementary Figure 7e and f). More CD204+ (M2-like) cells were detected in the samples with high CECR1 signal (Supplemental Figure 8a, b).

Figure 3 CECR1 promotes macrophage towards a M2-like phenotype

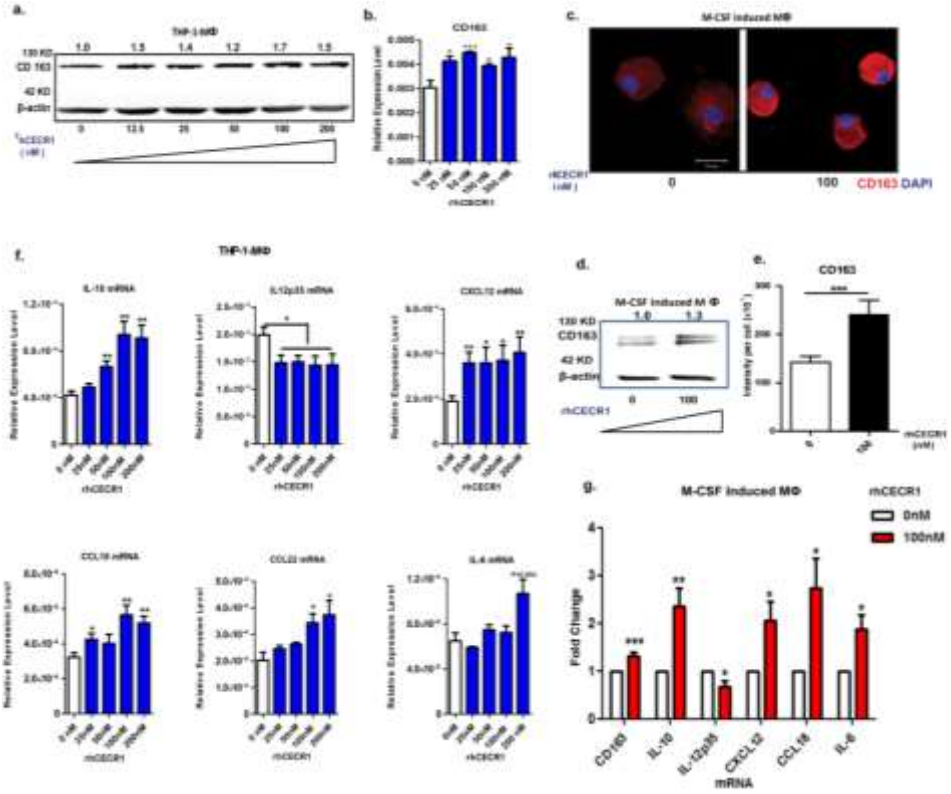

(a) Western blot of CD163 in THP-1 derived macrophages treated with rhCECR1 for 96 hours. Numbers above bands indicate quantified protein levels normalized to β-actin. **(b)** QPCR analysis of CD163 expression in THP-1 macrophages treated with rhCECR1. Data are from three experiments, normalized to β-actin, presented as mean ± S.E.M. *P<0.05, ***P<0.005. **(c)** Representative CD163 immunostaining of M-CSF induced macrophages with or without stimulation with CECR1 (100 nM), for 96 hours. Experiments were repeated three times independently. (scale bar: 100 μm) **(d)** Representative western blot of CD163 in M-CSF induced macrophages with or without CECR1 stimulation for 96 hours from three experiments. Numbers above bands indicate quantified protein normalized to β-actin. **(e)** Quantified CD163 intensity in M-CSF induced macrophages with or without CECR1 (100nM) stimulation is shown in mean ± S.E.M. ***P<0.005. **(f)** QPCR analysis of M2-macrophage associated genes; IL-10, CXCL12, CCL18, CCL22, IL-6 and inflammatory gene IL-12p35 in THP-1 derived macrophages treated with CECR1 for 96 hours. Data normalized to β-actin are of three independent experiments and shown as mean ± S.E.M. *P<0.05 **P<0.01. **(g)** QPCR analysis of IL-10, CXCL12, CCL18, IL-6, IL-12p35 in M-CSF induced macrophages treated by CECR1(100nM) for 96 hours. Data are of three experiments and shown as mean ± S.E.M. in fold change compared to the CECR1 free condition. *P<0.05 **P<0.01.

Cytokines specifically expressed by M2-like TAMs or M1-like macrophage were selected for qPCR analysis. In response to rhCECR1, THP-1 macrophages demonstrated a dose responsive up-regulation of CD163, IL-10, CXCL12, CCL18, and CCL22. Increased IL-6 was only observed in response to the highest concentration of rhCECR1 (Figure 3f). RhCECR1 stimulation of M-CSF induced macrophages also induced expression of CD163, IL-10, CXCL12, CCL18 and IL-6 (Figure 3g), but suppressed expression of CCL22 (Figure 3g). The difference in CCL22 may be the result of intrinsic differences between THP-1 derived macrophages and M-CSF induced macrophages[14]. In contrast, rhCECR1 lowered expression of M1 cytokine IL-12p35 in both THP-1 and peripheral M2 macrophages (Figure 3f, g).

CECR1 regulates proliferation and migration of glioma cells via M2-like macrophages

In malignant tumors, macrophage leads to tumor progression[15]. We first confirmed the effects of conditioned medium derived from THP-1 macrophages on the proliferation rate of three commonly used GBM cell lines[16-18], U87, U373, and U251 cells. These cell lines have been previously used in macrophage studies[19,20]. GBM cells that received conditioned medium from rhCECR1 treated THP-1 macrophages presented higher proliferation rates (Supplementary Figure 9a and b and Supplementary Figure 10a and b). GBM cells treated by MΦ-CM from THP-1 macrophage with CECR1 silencing (siCECR1 CM) showed a significant lower proliferation rate than cells stimulated with MΦ-CM from THP-1 macrophage with siSham treatment (siSham CM) (Figure 4b, Supplementary Figure 10a and b). A significant reduction in Ki67 was observed in U87 and U251 exposed to siCECR1 CM in comparison to those exposed to siSham CM (Figure 4d and f; Supplementary Figure 10c and d). U87 and U251 cells treated with medium from THP-1 macrophages exposed to rhCECR1 resulted in rising levels of Ki67 (Figure 4d and f; Supplementary Figure 10c and f). Direct stimulation with rhCECR1 without macrophages did not affect the proliferation rate of U87 cells (Supplementary figure 13a).

Next, all three GBM cell lines were exposed to siCECR1 CM to assess the effects on cell migration. SiCECR1 CM induced a weaker migration response than exposure to siSham CM (figure 4c). Medium derived from rhCECR1 treated THP-1 macrophages enhanced migration of GBM cells (Supplementary Figure 9c and d; Supplementary Figure 11 and 12).

Figure 4 CECR1 in macrophages regulates proliferation and migration of U87 cells

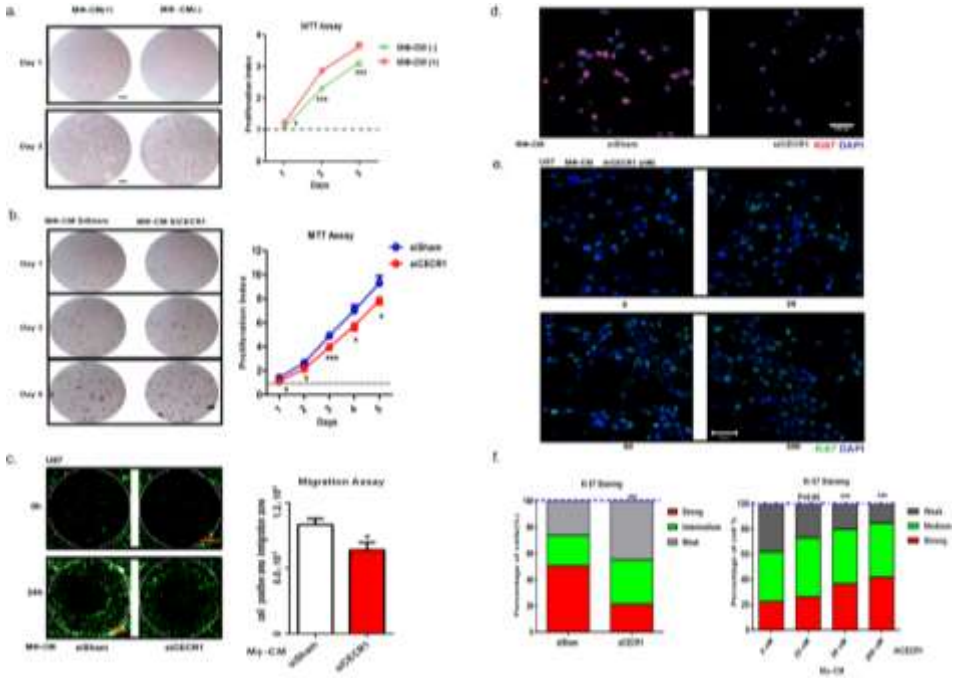

(a) Representative images of U87 cells with/without treatment of macrophage conditioned medium (MΦ-CM) at day 1,3 post stimulation of three experiments. (scale bar: 200 μm). Data are obtained from three experiments (n=6 each) and presented as mean ± S.E.M. in fold change compared to MΦ-CM free condition. *P<0.05 ***P<0.005. **(b)** Representative figures of U87 cells with treatment of MΦ-CM from non-targeting sisham or siCECR1 transfected macrophages. Pictures were taken at day 1, 3, 5 post stimulation (scale bar: 200 μm). Data are represented of three experiments (n=6 for each), and presented as mean ± S.E.M. in fold change compared to U87 cells exposed to MΦ-CM of siSham treated macrophages. *P<0.05 ***P<0.005. **(c)** Left panel: representative pictures of U87 migration into the detection zone (indicated by the white circle) after stimulation with MΦ-CM from macrophage with sisham and siCECR1 (scale bar: 200 μm). Right panel: Quantification of fluorescent cells in the migration zones in sisham and siCECR1 MΦ-CM conditions. Data are represented of three experiments and presented as mean ± S.E.M. *P<0.05. **(d)** Representative images of Ki67 staining in U87 cells, which were treated with MΦ-CM from siSham and siCECR1 transfected macrophages for 48 hours (scale bar: 100 μm). **(e)** Representative pictures of Ki67 staining in U87 cells, which were treated with MΦ-CM for 48 hours from macrophages treated with rhCECR1 for 96 hours (scale bar: 100 μm). **(f)** Quantification of Ki67 staining in U87 cells treated with different MΦ-CM for 48 hours. Left graph: Ki67 signal distribution of U87 cells treated with MΦ-CMs of sisham and siCECR1 macrophages. Right graph: Ki67 signal distribution of U87 cells treated with MΦ-CMs of macrophages that were stimulated by CECR1. Data are of three experiments. Chi-square test was for analysis. ***P<0.005.

CECR1 expression in macrophages mediates paracrine activation of the MAPK signaling in U87 and U373 glioma cells

The mitogen activated protein kinase (MAPK) pathway, consisting of ERK 1/2, JNK/SAPK and P38 signaling, are the most recognized and important signaling pathways for the modulation of key cancer cell responses[21]. It plays crucial roles in tumor cell survival and motility[22].

Serum-free medium starved glioma cells (U87 and U373) were stimulated for 10 and 20 minutes by siCECR1 CM or siSham CM. Phospho-ERK1/2/ total ERK1/2 and phospho-JNK/SAPK /total JNK/SAPK ratios decreased in U87 and U373 cells exposed to THP-1 siCECR1 CM (Figure 5a-d and Supplementary 14 a-d). The transcription factor c-Jun is a potential downstream target of JNK/SAPK. Phospho-c-Jun (Ser73)/total c-Jun ratio was reduced in the U87 and U373 cells exposed to THP-1 siCECR1 CM (Figure 5e-f, and Supplementary Figure 14e-f). Immunostaining for phospho-c-Jun showed a reduced signal in U87 with THP-1 siCECR1 CM treatment (Figure 5g and h).

In contrast, medium derived from THP-1 macrophages treated with rhCECR1 increased phospho-protein/total protein ratios of both ERK1/2 and JNK/SAPK (Supplemental Figure 15c and d) in U87 cells. Direct rhCECR1 treatment of U87 cells without macrophage mediation did not increase phospho-ERK1/2 and phospho-JNK/SAPK ratios (Supplementary Figure 13b). These data indicate that the MAPK signaling pathways in U87 and U373 cells are activated by CECR1-mediated paracrine effect from macrophages.

Expression of CECR1 correlates with increased levels of Ki67 positive cells and phosphorylation of ERK1/2 and JNK/SAPK in patient GBM samples

Thirty-three GBM surgical samples were selected for immunohistochemical evaluation and divided into two groups based on the median of the percentage of CECR1+ area per image view in all samples (Figure 6a-c). The number of Ki67 positive cells and percentage of positive areas for phospho-ERK1/2, phospho-JNK/SAPK, and phospho-c-Jun(ser73) proteins were analyzed and compared between the two groups (Figure 6a-c). A significant higher number of Ki67+ cells were counted in the samples with high CECR1 signal (Figure 6c). The number of Ki67 positive cells is positively correlated with the percentage of CECR1+ area (Figure 6d). In addition, phospho-ERK1/2, phospho-JNK/SAPK, and phospho-c-Jun signals were significantly higher in the CECR1 high group. The ratios of the phospho-ERK1/2/total ERK1/2, phospho-JNK/SAPK/total JNK/SAPK and phospho-c-Jun/total c-Jun signals correlated positively with the percentage of CECR1+ area in GBM samples (Figure 6d). In addition, phospho-ERK1/2/total ERK1/2, phospho-JNK/SAPK/total JNK/SAPK, and phospho-c-Jun/total c-Jun signals were positively correlated with the number of Ki67 positive cells in GBM specimens (Supplementary Figure 16).

Figure 5 CECR1 function in macrophages activates the MAPK pathway in U87 cells

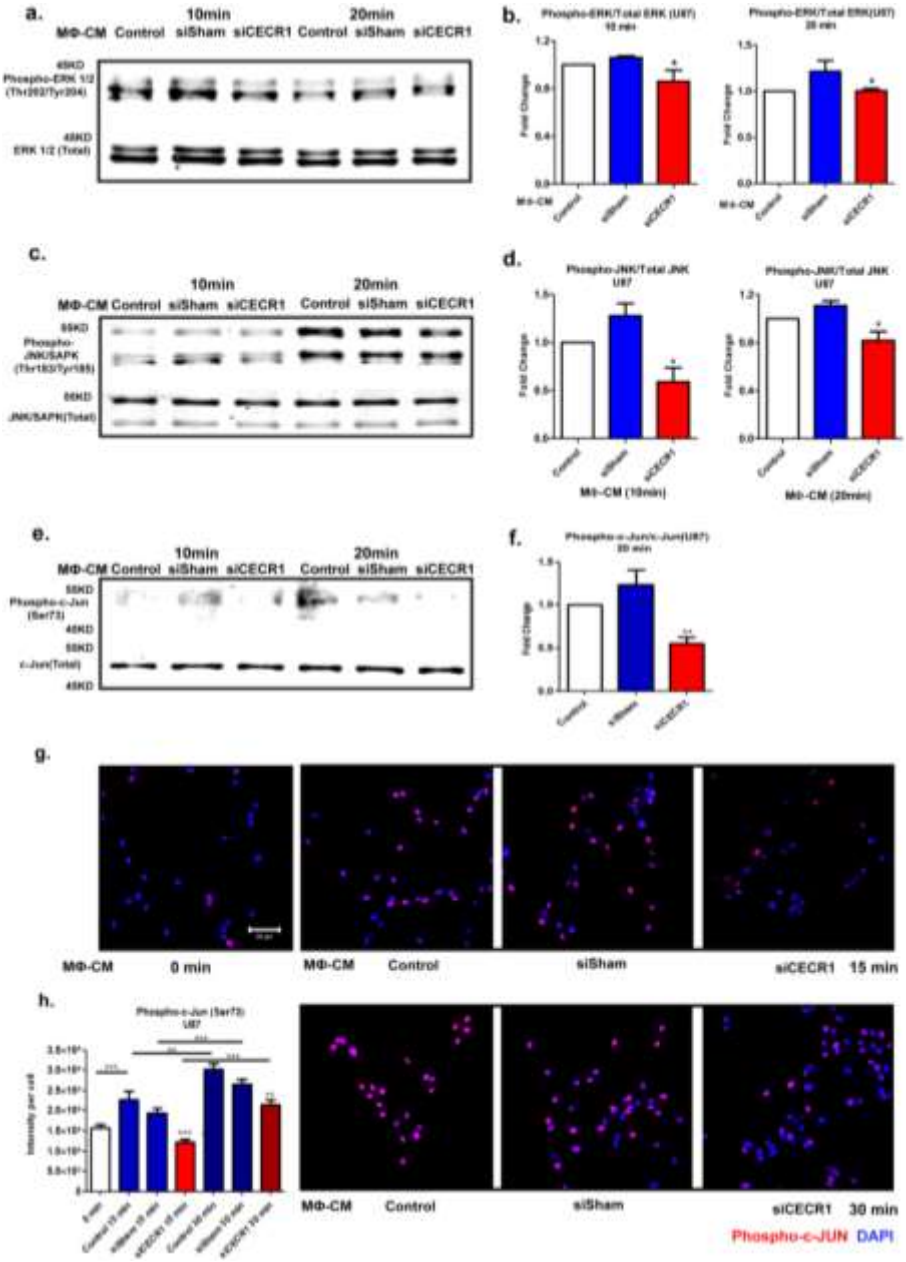

(a) Western blot of phospho-ERK1/2 and total ERK1/2 in U87 cells at 10 and 20 minutes after stimulation with MΦ-CM from siSham and siCECR1 transfected macrophages. **(b)** Phospho-ERK/Total ERK ratios are presented as mean ± S.E.M. in fold change compared to MΦ-CM derived of macrophages with non-targeted siRNA (siSham) and siRNA targeting CECR1 (siCECR1) from five experiments. *P<0.05. **(c)** Western blot of phospho-

JNK/SAPK and total JNK/SAPK protein in U87 cells at 10 and 20 minutes after stimulation with MΦ-CM derived from siSham and siCECR1 transfected macrophages. **(d)** Phospho-JNK/Total JNK ratios are presented as mean ± S.E.M. in fold change compared to MΦ-CM derived of macrophages with non-targeted siRNA (siSham) and siRNA targeting CECR1 (siCECR1) from three experiments. *P<0.05. **(e)** Western blot of phospho-/total c-Jun in U87 cells at 10 and 20 minutes after stimulation with MΦ-CM derived from siSham and siCECR1 siRNA transfected macrophages. **(f)** Phospho-c-Jun/Total c-Jun ratios are presented as mean ± S.E.M. in fold change compared to MΦ-CM derived of macrophages with non-targeted siRNA (siSham) and siRNA targeting CECR1 (siCECR1) from three experiments. *P<0.05. **(g)** Representative immunostainings of phosphor-c-Jun in U87 cells of two experiments. U87 were stimulated with MΦ-CM derived from siSham and siCECR1 transfected macrophages for 15 and 30 minutes (scale bar: 100 µm). **(h)** Quantified phosphor-c-Jun in U87 cells were obtained from 200 randomly selected cells and presented as mean ± S.E.M in each condition. **P<0.01, ***P<0.005.

Figure 6 CECR1 correlates with Ki67, MAPK signals in GBM samples

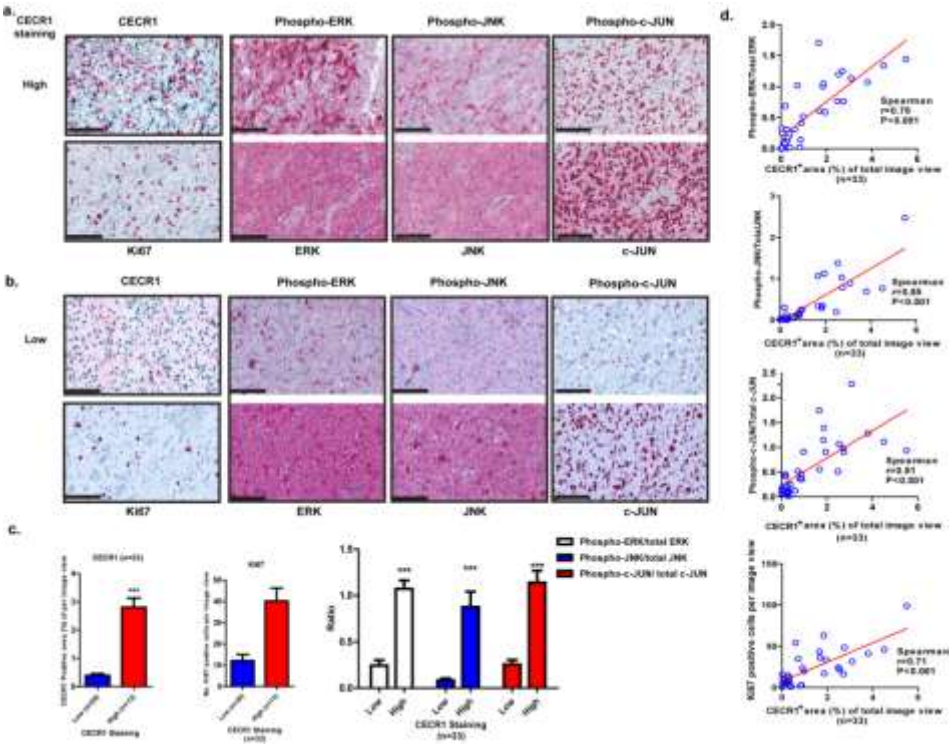

(a) (b) Representative figures of GBM samples immunostained for CECR1, Ki67, phospho-/total ERK1/2, phospho-/ total JNK, phospho-/ total c-Jun are shown (scale bar: 100 µm). **(c)** Left graph: Quantificatified CECR1 staining level (%CECR1+ area per image view) in CECR1 high and low groups are presented as mean ± S.E.M. ***P<0.005. Middle graph: Quantificatified Ki67 in CECR1 high and low group are presented as mean ± S.E.M. ***P<0.005. Right panel: Ratios of phospho-ERK/total ERK, phospho-JNK/total JNK and phospho-c-Jun/total c-Jun. Data are presented as mean ± S.E.M. ***P<0.005. **(d)** Correlation between %CECR1+ area with ratios of phospho-ERK/total ERK, phospho-JNK/total JNK, phospho-c-Jun/total c-Jun and numbers of Ki67+ cells. Spearman correlation co-efficient and P value are shown.

DISCUSSION

The main findings of the current study are: (a) CECR1 is highly expressed in GBM. (b) CECR1 expression is enhanced in M2-like TAMs compared to M1-like TAMs. (c) CECR1 induces macrophage differentiation towards a M2-like phenotype. (d) CECR1 activity in TAMs mediates tumor glioma cell proliferation and migration, possibly by activating the MAPK pathway in tumor cells.

The main function of CECR1 is the conversion of extracellular adenosine to inosine by removing an amino-group and replacing it with a hydroxyl group[23]. CECR1 was reported to bind to and activate adenosine receptors $A_{2A}R$ and $A_{2B}R$[24]. Adenosine is well known for its anti-inflammatory effect on classical M1 activation, limiting the production of pro-inflammatory factors as TNFα, and IL12, and increasing the production of anti-inflammatory cytokines including IL10[25,26]. LPS stimulation of Macrophage upregulates adenosine receptor $A_{2A}R$, which probably increases the sensitivity of M1 macrophages to adenosine. This further amplifies the anti-inflammatory effect of adenosine and mediates a switch towards a more "mild" M2 phenotype[27]. In addition, in line with the present findings, monocytes from patients with CECR1 deficiency were able to differentiate into M1-, but not M2 macrophages. Therefore, the intrinsic (genetic or epigenetic) ability of monocyte/macrophages to produce high or low levels of CECR1, could be an important determinant for M2 or M1 polarization capacity. Especially, in GBM. we hypothesized that low levels of CECR1 produced by M1-like macrophages are not able to reduce local GBM extracellular adenosine levels, thus a predominant M2-like phenotype would be induced by adenosine. Alternatively, higher level of CECR1 produced by M2-like macrophages could amplify the signaling of $A_{2A}R$ and $A_{2B}R$[28] in both M1/M2-like macrophages, further promoting a predominant M2-like macrophage population.

The effects of CECR1 knockdown *in vitro* were modest, contrasting to the strong correlation between CECR1 protein expression levels and phospho-JNK and phospho-ERK1/2 levels found in the tumor samples. This discrepancy could be explained by the isolated conditions in our experimental set-up *in vitro*. We designed the study to investigate the direct paracrine effects of CECR1 modulation in macrophages on GBM cells response, and chose to use conditioned medium derived from the siCECR1 treated macrophages to stimulate GBM cells. *In vivo*, direct interaction with $CECR1^{high}$ expressing macrophages with the surrounding tumor environment, including tumor cells and other (inflammatory) cells such as subsets of CD3+ T cells[29], microglia[2], and neutrophils[30], could further enhance JNK and ERK signaling.

The immune modulating function of CECR1 discovered in the study is underscored by other data on CECR1. Schep at al. demonstrated that a CECR1 heterozygous mutation is associated with respiratory infections and common variable immunodeficiency (CVID) in an index patient with immune dysregulation[31]. Recessively inherited CECR1 mutations that were deleterious for protein function have also been shown to cause systemic vasculopathy and early-onset of lacunar strokes in affected patients[9,10]. This

phenotype was further validated in zebrafish models in which knockdown of the zebrafish homologue of CECR1 caused intracranial hemorrhages and neutropenia. The link between immune modulation and the vasculopathy phenotype was further strengthened by a report on two patients with biallelic CECR1 mutations and histories of vasculitis and intracranial hemorrhages[32]. In the present study CECR1 expressing immune cells were observed at the perivascular areas of the lower-graded gliomas, while in the GBMs CECR1 expressing cells were also found further away from the vasculature in the tumor parenchyma. These findings possibly reflect the modulation of immune cells by CECR1 leading to a progressive defect of the endothelial barrier function in glioma vasculature. Taken together, the influence of CECR1 on immune cells, and on macrophage polarization in particular, seems to impact the cerebral vasculature of normal brain and brain tumors.

The fraction of resident microglia and TAMs reportedly constitute up to 30% of the total cell population of GBM[33]. The glioma cells are capable of actively reprogram the TAMs in order to support tumor progression[5]. Based on expression profiling of mouse gliomas, subtyping beyond the classic M1 and M2 poles has been introduced and M2a (Th2, anti-pathogens response), M2b (Th2, immune regulatory), and M2c (immune modulatory and tissue remodeling) TAMs are now being recognized[34]. Expression analysis of typical M2a, b, and c subtype markers validated the presence of the TAM subtypes in human gliomas, with in particular enrichment of M2b and M2c cells in GBM.

It remains unclear if the glioma TAMs constitute a unique phenotype that is not found in macrophage populations in non-neoplastic tissues – which would make them a potential therapeutic target. Investigations of the influence of CECR1 on the expression of the M1, M2a, b, and c markers may further reveal its regulatory function TAM polarization.

In conclusion, the current study has demonstrated a new CECR1-mediated cross-talk mechanism between macrophages and glioma cells. Continuous CECR1 autocrine stimulation of macrophages enables M2-like TAMs to stimulate MAPK and c-Jun signaling in glioma cells via paracrine activation, leading to higher proliferation and motility rates in tumor glioma cells. Based on our findings, CECR1 could become a suitable drug target for selective modulation of the M2-like TAMs in glioma.

REFERENCES

1. Qian BZ, Pollard JW. Macrophage diversity enhances tumor progression and metastasis. *Cell.* 2010; 141(1):39-51.
2. Hambardzumyan D, Gutmann DH, Kettenmann H. The role of microglia and macrophages in glioma maintenance and progression. *Nature Neuroscience.* 2016; 19(1):20-27.
3. Alvaro T, Lejeune M, Camacho FI, et al. The presence of STAT1-positive tumor-associated macrophages and their relation to outcome in patients with follicular lymphoma. *Haematologica.* 2006; 91(12):1605-1612.
4. Kinouchi M, Miura K, Mizoi T, et al. Infiltration of CD40-positive tumor-associated macrophages indicates a favorable prognosis in colorectal cancer patients. *Hepato-Gastroenterology.* 2013; 60(121):83-88.
5. Li W, Graeber MB. The molecular profile of microglia under the influence of glioma. *Neuro Oncol.* 2012; 14(8):958-978.
6. Prosniak M, Harshyne LA, Andrews DW, et al. Glioma grade is associated with the accumulation and activity of cells bearing M2 monocyte markers. *Clin Cancer Res.* 2013; 19(14):3776-3786.
7. Komohara Y, Ohnishi K, Kuratsu J, Takeya M. Possible involvement of the M2 anti-inflammatory macrophage phenotype in growth of human gliomas. *J Pathol.* 2008; 216(1):15-24.
8. Conlon BA, Law WR. Macrophages are a source of extracellular adenosine deaminase-2 during inflammatory responses. *Clin Exp Immunol.* 2004; 138(1):14-20.
9. Navon Elkan P, Pierce SB, Segel R, et al. Mutant adenosine deaminase 2 in a polyarteritis nodosa vasculopathy. *New England Journal of Medicine.* 2014; 370(10):921-931.
10. Zhou Q, Yang D, Ombrello AK, et al. Early-onset stroke and vasculopathy associated with mutations in ADA2. *New England Journal of Medicine.* 2014; 370(10):911-920.
11. Footz TK, Brinkman-Mills P, Banting GS, et al. Analysis of the cat eye syndrome critical region in humans and the region of conserved synteny in mice: a search for candidate genes at or near the human chromosome 22 pericentromere. *Genome Research.* 2001; 11(6):1053-1070.
12. Lacey DC, Achuthan A, Fleetwood AJ, et al. Defining GM-CSF- and macrophage-CSF-dependent macrophage responses by in vitro models. *J Immunol.* 2012; 188(11):5752-5765.
13. Zheng PP, van der Weiden M, Kros JM. Fast tracking of co-localization of multiple markers by using the nanozoomer slide scanner and NDPViewer. *Journal of Cellular Physiology.* 2014; 229(8):967-973.
14. Schildberger A, Rossmanith E, Eichhorn T, Strassl K, Weber V. Monocytes, peripheral blood mononuclear cells, and THP-1 cells exhibit different cytokine expression patterns following stimulation with lipopolysaccharide. *Mediators Inflamm.* 2013; 2013:697972.
15. Ugel S, De Sanctis F, Mandruzzato S, Bronte V. Tumor-induced myeloid deviation: when myeloid-derived suppressor cells meet tumor-associated macrophages. *The Journal of clinical investigation.* 2015; 125(9):3365-3376.
16. Clark MJ, Homer N, O'Connor BD, et al. U87MG decoded: the genomic sequence of a cytogenetically aberrant human cancer cell line. *PLoS Genet.* 2010; 6(1):e1000832.
17. Siegelin MD, Reuss DE, Habel A, Rami A, von Deimling A. Quercetin promotes degradation of survivin and thereby enhances death-receptor-mediated apoptosis in glioma cells. *Neuro Oncol.* 2009; 11(2):122-131.
18. Fukumura D, Xavier R, Sugiura T, et al. Tumor induction of VEGF promoter activity in stromal cells. *Cell.* 1998; 94(6):715-725.
19. Leblond MM, Gerault AN, Corroyer-Dulmont A, et al. Hypoxia induces macrophage polarization and re-education toward an M2 phenotype in U87 and U251 glioblastoma models. *Oncoimmunology.* 2016; 5(1):e1056442.
20. Fujiwara Y, Komohara Y, Kudo R, et al. Oleanolic acid inhibits macrophage differentiation into the M2 phenotype and glioblastoma cell proliferation by suppressing the activation of STAT3. *Oncology Reports.* 2011; 26(6):1533-1537.
21. Johnson GL, Lapadat R. Mitogen-activated protein kinase pathways mediated by ERK, JNK, and p38 protein kinases. *Science.* 2002; 298(5600):1911-1912.

22. Dhillon AS, Hagan S, Rath O, Kolch W. MAP kinase signalling pathways in cancer. *Oncogene.* 2007; 26(22):3279-3290.
23. Zavialov AV, Engstrom A. Human ADA2 belongs to a new family of growth factors with adenosine deaminase activity. *Biochem J.* 2005; 391(Pt 1):51-57.
24. Zavialov AV, Gracia E, Glaichenhaus N, Franco R, Zavialov AV, Lauvau G. Human adenosine deaminase 2 induces differentiation of monocytes into macrophages and stimulates proliferation of T helper cells and macrophages. *J Leukoc Biol.* 2010; 88(2):279-290.
25. Hasko G, Cronstein B. Regulation of inflammation by adenosine. *Front Immunol.* 2013; 4:85.
26. Linden J. New insights into the regulation of inflammation by adenosine. *J Clin Invest.* 2006; 116(7):1835-1837.
27. Ferrante CJ, Pinhal-Enfield G, Elson G, et al. The Adenosine-Dependent Angiogenic Switch of Macrophages to an M2-Like Phenotype is Independent of Interleukin-4 Receptor Alpha (IL-4R alpha) Signaling. *Inflammation.* 2013; 36(4):921-931.
28. Csoka B, Selmeczy Z, Koscso B, et al. Adenosine promotes alternative macrophage activation via A2A and A2B receptors. *FASEB J.* 2012; 26(1):376-386.
29. Sims JS, Grinshpun B, Feng Y, et al. Diversity and divergence of the glioma-infiltrating T-cell receptor repertoire. *Proc Natl Acad Sci U S A.* 2016; 113(25):E3529-3537.
30. Liang J, Piao Y, Holmes L, et al. Neutrophils Promote the Malignant Glioma Phenotype through S100A4. *Clinical Cancer Research.* 2014; 20(1):187-198.
31. Schepp J, Bulashevska A, Mannhardt-Laakmann W, et al. Deficiency of Adenosine Deaminase 2 Causes Antibody Deficiency. *J Clin Immunol.* 2016; 36(3):179-186.
32. Belot A, Wassmer E, Twilt M, et al. Mutations in CECR1 associated with a neutrophil signature in peripheral blood. *Pediatr Rheumatol Online J.* 2014; 12:44.
33. Kerber M, Reiss Y, Wickersheim A, et al. Flt-1 signaling in macrophages promotes glioma growth in vivo. *Cancer Res.* 2008; 68(18):7342-7351.
34. Szulzewsky F, Pelz A, Feng X, et al. Glioma-associated microglia/macrophages display an expression profile different from M1 and M2 polarization and highly express Gpnmb and Spp1. *PLoS One.* 2015; 10(2):e0116644.

SUPPLEMENTARY DATA

Supplemental Figure 1 CECR1 is highly enriched in GBM.

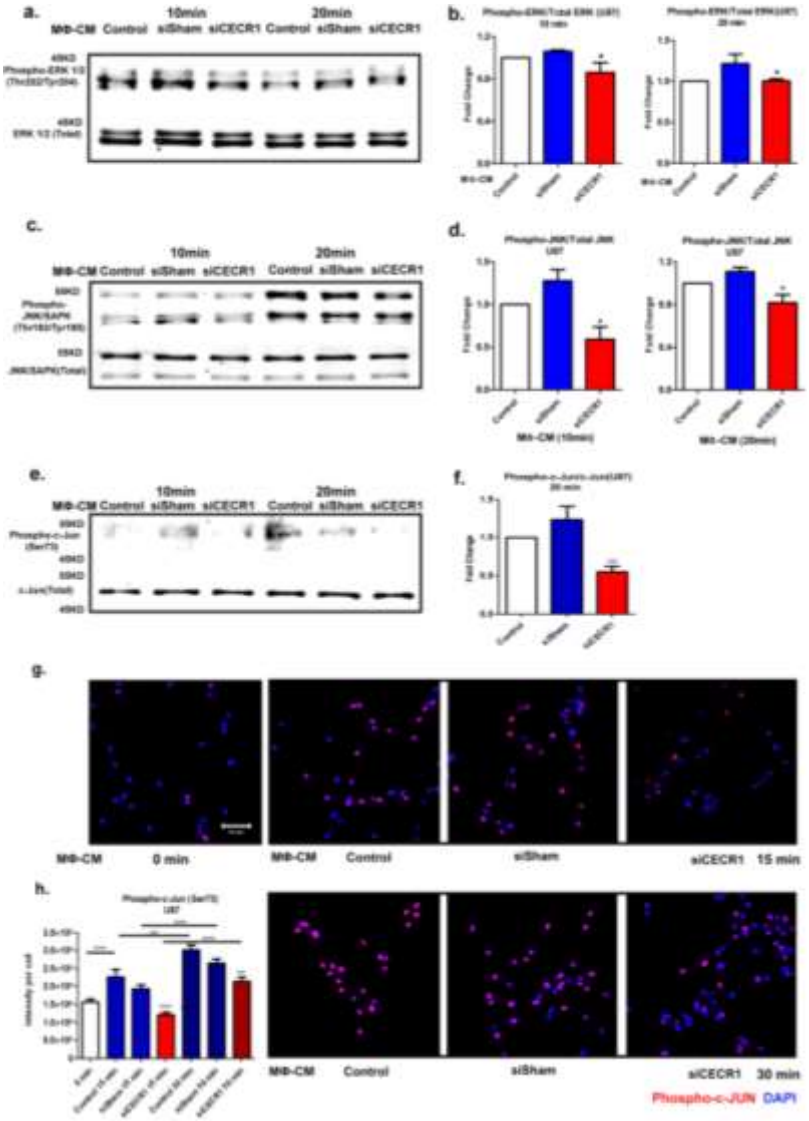

(a) Analysis of two different GEO datasets shows CECR1 transcript level in glioblastoma. Shown are median values of CECR1 levels. * P<0.05; ** P<0.01. Left panel: AII: Astrocytoma grade II, AIII: Astrocytoma grade III. Right panel: OG II: Oligodentroglioma grade II, AO: Anaplastic Oligodentroglioma, AOA: Anaplastic Oligoastrocytoma. **(b)** QPCR analysis of macrophage markers CD16, CD204, and IL-10 in grade II, III and IV human gliomas. Results are shown in mean ± S.E.M.; * P<0.05; ** P<0.01. Grade II, N=19; Grade III, N=5; Grade IV, N=19. QPCR results of human glioma lysates showing **(c)** the mRNA expression levels of iNOS and IL-12p35 in glioma grades II, III and IV (Mean ± S.E.M), **(d)** the mRNA expression levels of CD68, CD86, and CD206 between the different grades (mean ± S.E.M). Displayed values were normalized with the β actin housekeeping gene.

Supplemental Figure 2 CECR1 co-localized with CD16 expression in autopsy brain, astrocytoma grade II and GBM

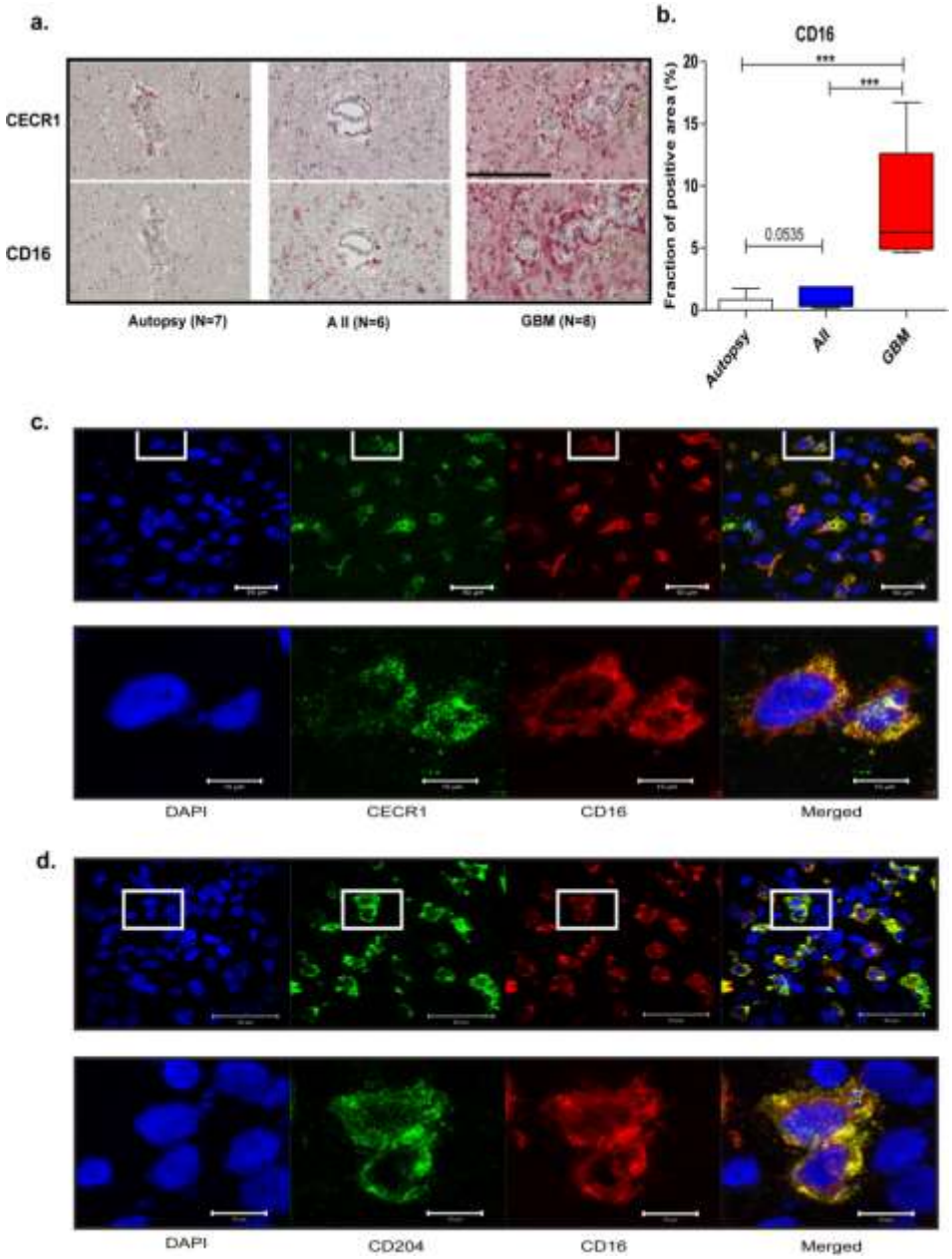

(a) Immunohistochemistry for CECR1 and CD16 in autopsy brain, astrocytoma grade II and GBM (scale bar: 200 µm). **(b)** Percentages of CD16 positive areas in autopsy brains, AII and GBM. Mean values of CD16 are shown. * P<0.05, ***P<0.005. **(c)** Confocal microscope images showing co-localization of CECR1 with CD16 in GBMs (scale bar: 50 µm for upper panel; 10 µm for lower panel). **(d)** Confocal microscope images showing co-localization of CD204 with CD16 in GBMs (scale bar: 50 µm for upper panel; 10 µm for lower panel).

Supplemental Figure 3 CECR1 is expressed by microglia and perivascular macrophages in autopsy brain samples and low-grade astrocytomas

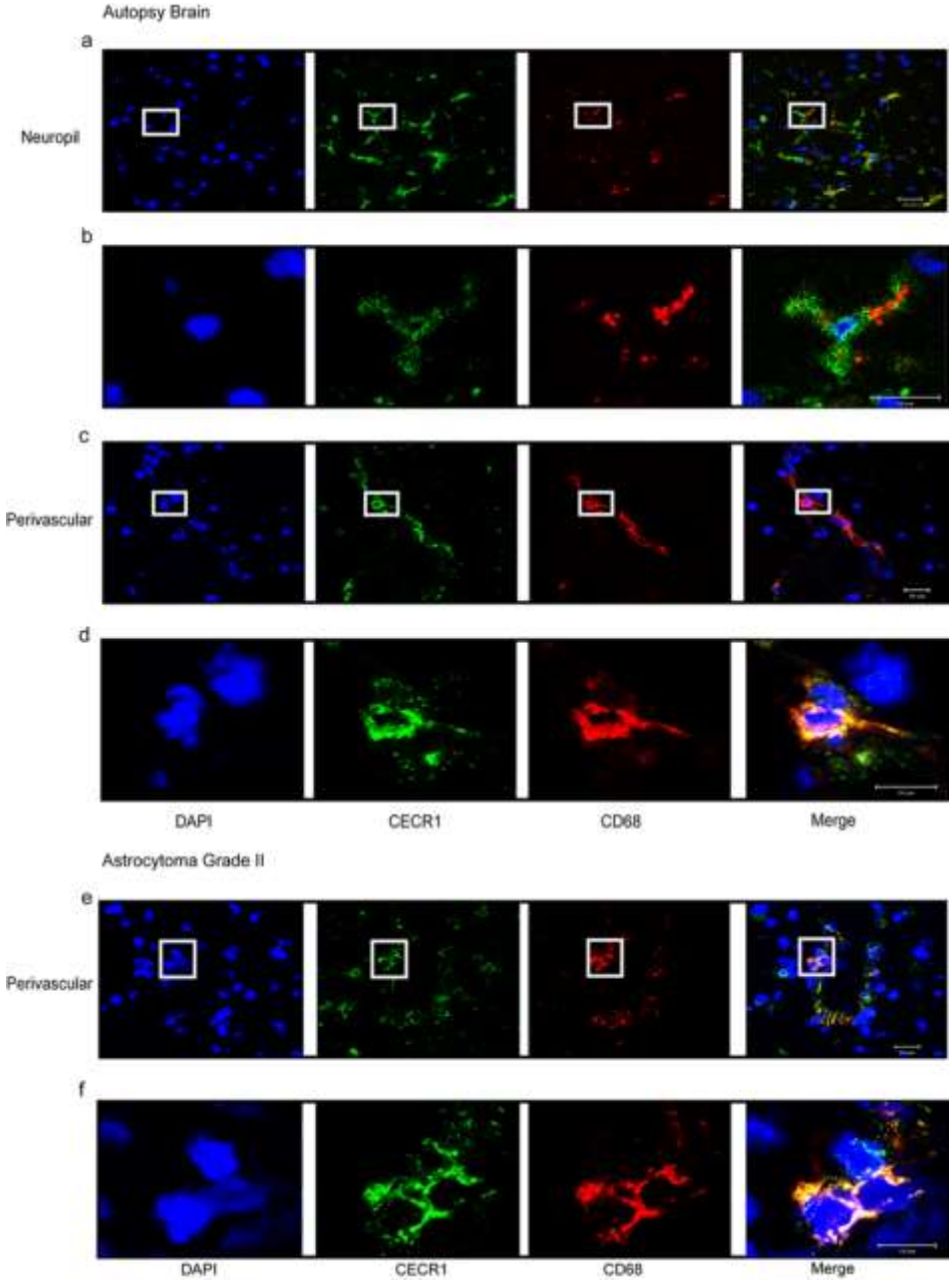

Representative pictures of CD68 and CECR1 double immunostaining from four cases of autopsy brain samples and three low-grade astrocytomas. In autopsy brain tissue, showing **(a)** CECR1 co-localization with CD68 in parenchyma (scale bar: 20 µm), **(b)** co-localization of CECR1 and CD68 in a single cell structure (scale bar: 10

µm), **(c)** CECR1 co-localization with CD68 in perivascular macrophages (scale bar: 20 µm). **(d)** Co-localization of CD68 and CECR1 in a single perivascular macrophage(scale bar: 10 µm). **(e)** In low-grade astrocytomas, CECR1 co-localized with CD68 in macrophages at perivascular sites (scale bar: 20 µm). **(f)** High magnification of the selected area (scale bar: 10 µm).

Supplemental Figure 4 Co-localization of CECR1 with CD163 in perivascular macrophages in autopsy brain tissue and low-grade astrocytomas

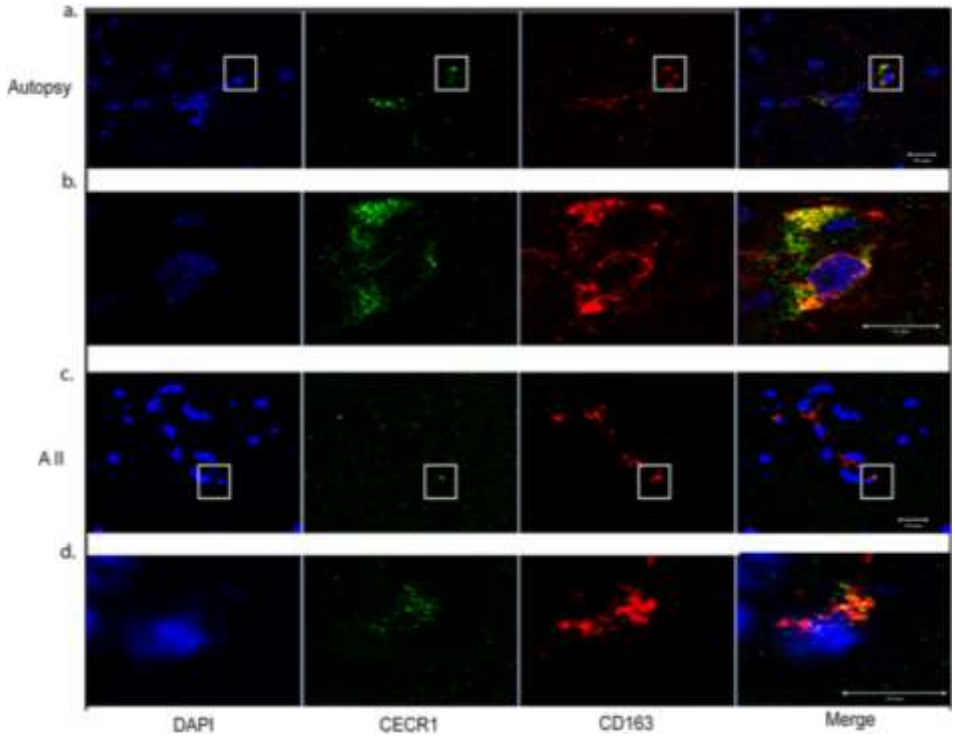

Representative pictures of CD163 and CECR1 double immunostaining from four autopsy brain samples and three low-grade astrocytomas. Co-localization of CECR1 with CD163 in **(a)** perivascular macrophages in autopsy brains (scale bar: 20 µm); **(b)** high magnification view of select area (scale bar: 10 µm). Co-localization of CECR1 with CD163 in **(c)** astrocytomas grade II (scale bar: 20 µm); **(d)** high magnification view of select area (scale bar: 10 µm).

Supplemental Figure 5 M-CSF induced macrophages from peripheral monocytes express higher levels of M2-like macrophage markers

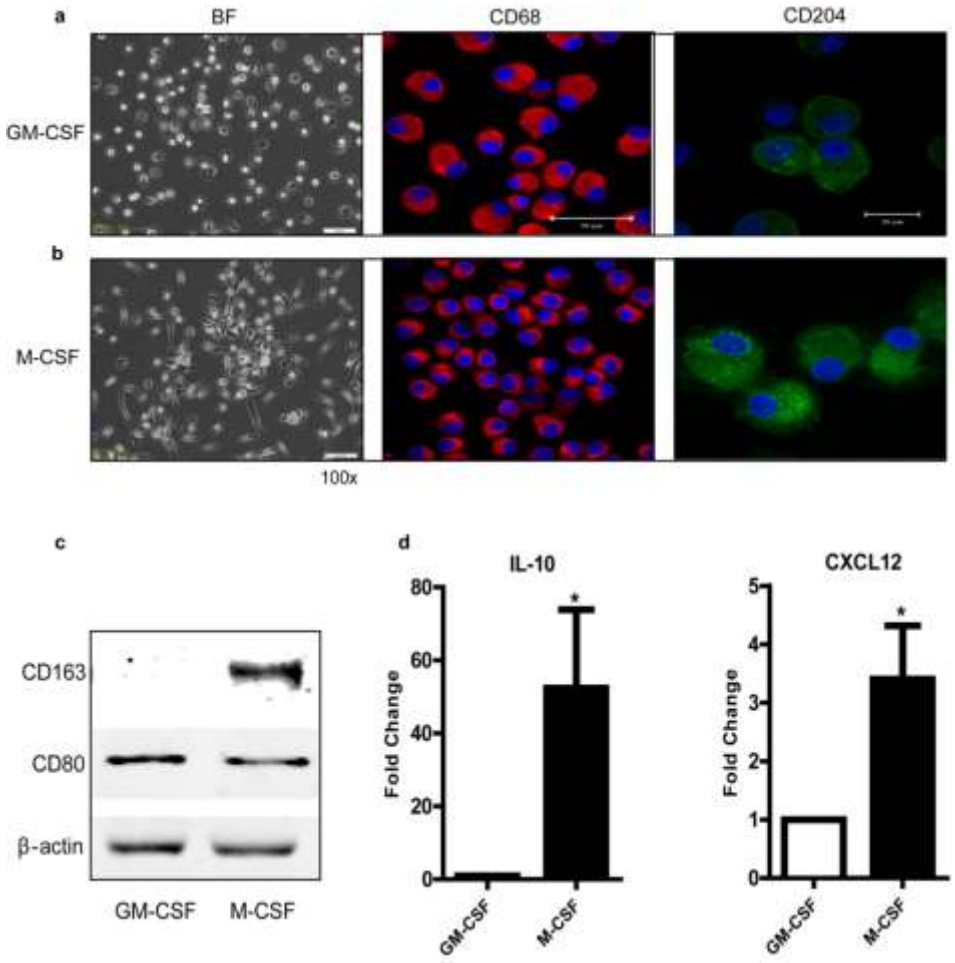

Peripheral monocytes were differentiated into M1 and M2-like macrophages by GM-CSF (10 ng/ml) and M-CSF (10 ng/ml) stimulation respectively for 7 days.
(a, b left panel) Bright field examination show typical morphological features for M1 and M2-like macrophages as a result of GM-CSF and M-CSF induced differentiation respectively**. (a, b middle panel)** Immunofluorescent signal of CD68 of GM-CSF and M-CSF induced macrophages (scale bar: 50 µm). **(a, b right panel)** Immunofluorescent signal of CD204 (scale bar: 20 µm). **(c)** Representative Western blot of three independent experiments showing typical CD163 and CD80 protein expression levels for GM-CSF and M-CSF induced macrophages. **(d)** IL-10 and CXCL12 transcript levels as measured by qPCR. Mean ± S.E.M, *P<0.05, N=3.

Supplemental Figure 6

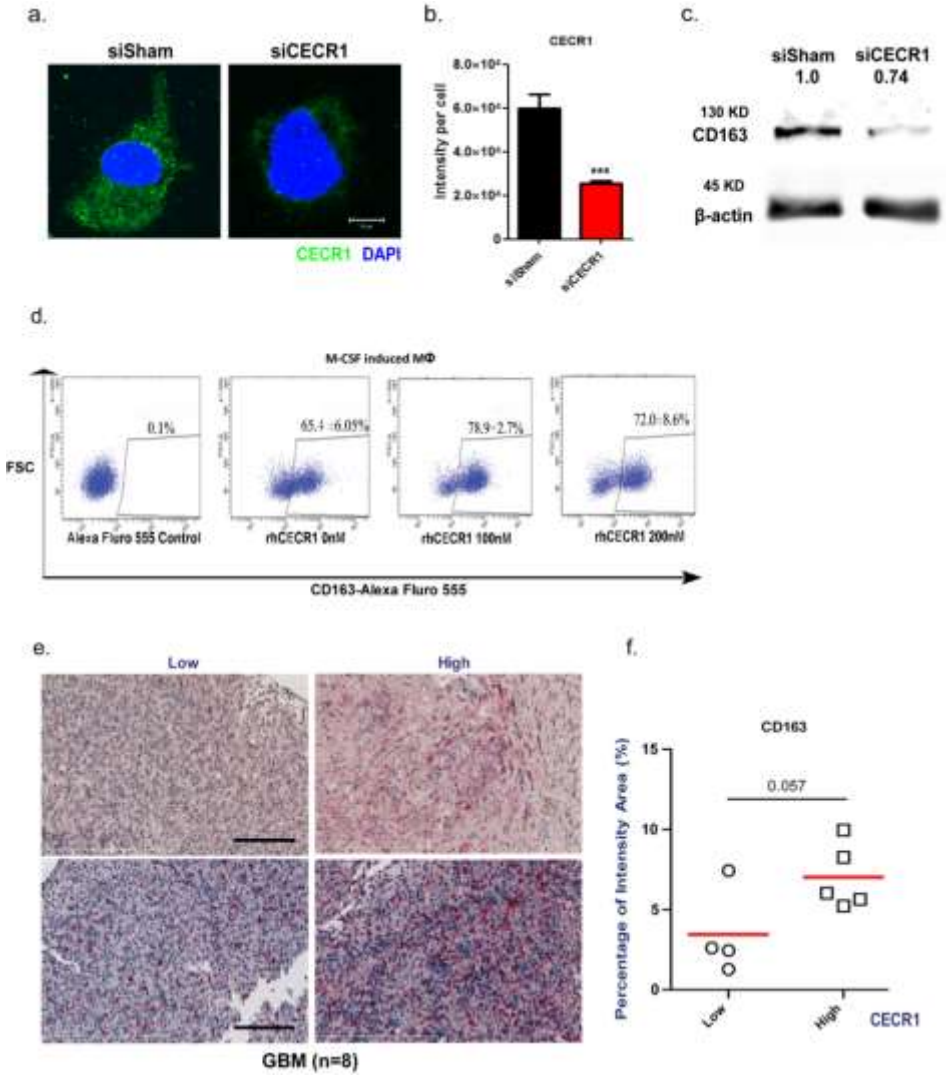

(a) Representative cell immunostaining of CECR1 staining in THP-1 macrophages with CECR1 knockdown versus sisham transfected controls of three experiments. (scale bar: 10 µm). **(b)** Quantification of the fluorescent intensity of CECR1 signal per cell in CECR1 knockdown and sisham. Data are presented as mean ± S.E.M., of 3 independent experiments. Five image fields were randomly selected for quantification of each experiment group. *** P<0.005. **(c)** Western blot of CD163 in siCECR1 and sisham transfected THP-1 macrophages. Numbers above bands indicate quantified protein normalized to β-actin control. Represented figures are of three experiments. **(d)** Flow cytometry shows percentage of CD163+ cells in M-CSF induced macrophages with and without rhCECR1 for 96 hours. Most left graph: Negative control only stained with the secondary antibody conjugated with Alexa Fluor 555. Data are of three experiments; data are in mean values ± S.D. **(e)** GBM immunostained for CECR1 and CD163. Tumors were divided in a CECR1-low and high group based on %CECR1+ area per image view (scale bar: 100 µm). **(f)** Comparison of %CD163+ areas in CECR1 expression low and high GBM samples. Each scatter dot represents one individual sample. Medians are indicated

(P=0.057).

Supplemental Figure 7 GBM with higher CECR1 levels show higher numbers of CD204 positive macrophages

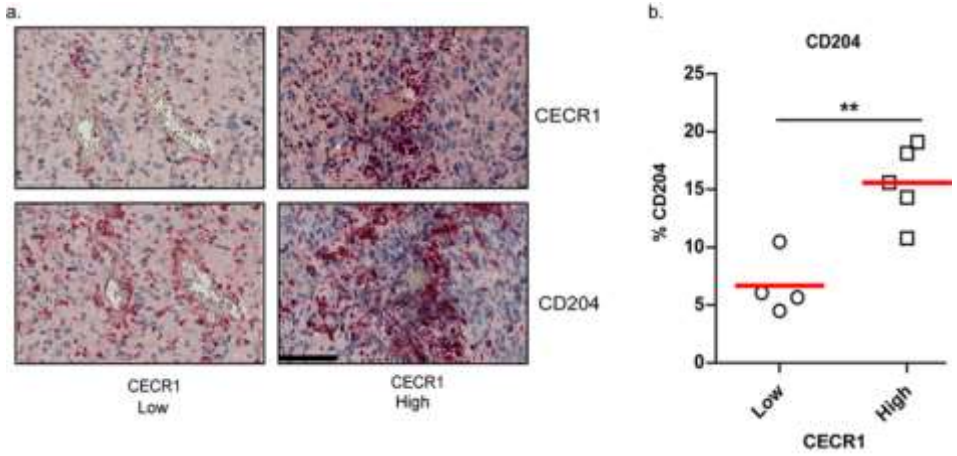

GBM samples were divided into two groups based on CECR1 level. **(a)** Representative figures of immunostaining for CD204 in GBM cross-sections of CECR1 high and low groups. (scale bar: 100 μm). **(b)** Quantification of the CECR1 and CD204 signal in CECR1 high group compared to samples with lower CECR1 levels. **P<0.01.

Supplemental Figure 8 RhCECR1 stimulation of macrophages regulates proliferation and migration of U87 cells

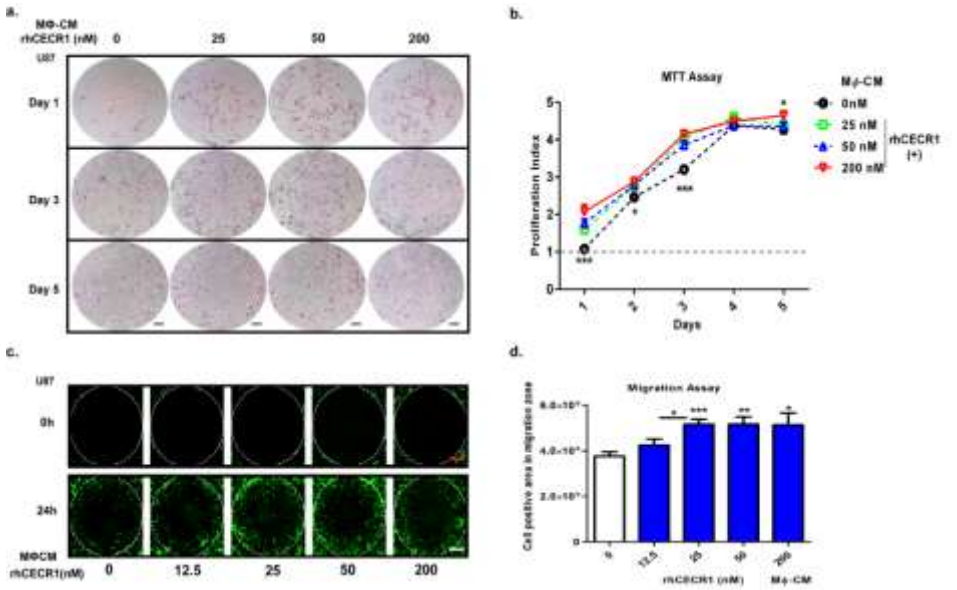

(a) Representative figures of U87 cells with treatment of MΦ-CM derived from macrophages treated with a range of rhCECR1 concentrations for 96 hours. Pictures were taken at day 1, day 3 and day 5 post MΦ-CM stimulation. (scale bar: 200 μm). **(b)** Quantification of MTT reaction. Data are represented of three experiments. Six replicated wells of each condition were used. Data are in mean ± S.E.M. in fold change compared to MΦ-CM derived of macrophages without rhCECR1 treatment. *P<0.05 ***P<0.005. **(c)** Representative pic-

tures of U87 migration into the detection zone after stimulation with MΦ-CM of macrophages treated with different concentrations of rhCECR1 for 96 hours. Pictures were taken at 0 hour and 24 hours after start of migration experiment (scale bar: 200 µm). Detection zone is indicated by a white circle. **(d)** Quantification of fluorescent cells in migration zones in MΦ-CM conditions in which macrophages were stimulated with different rhCECR1 concentrations for 96 hours. Data are represented of three experiments and presented as mean ± S.E.M. *P<0.05, **P<0.01, ***P<0.005.

Supplemental Figure 9 CECR1 activation in macrophages regulates parachrine-mediated proliferation in U373 and U251 cells

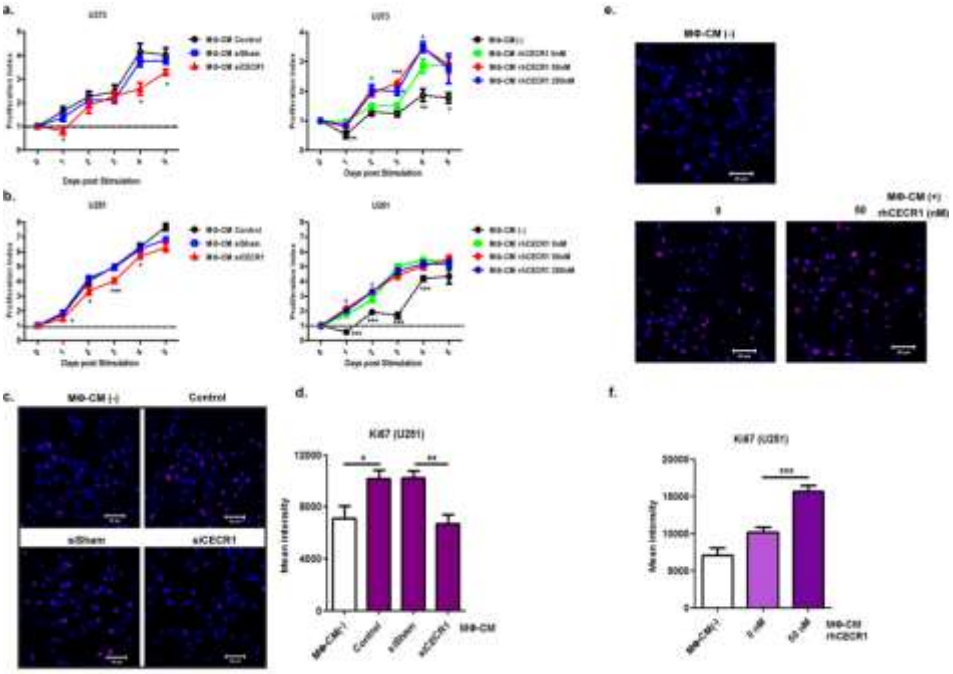

(a) Left panel: Quantification of MTT reaction of U373 with treatment of MΦ-CM from siCECR1, siSham and non-transfected THP-1 macrophages. Right panel: Quantification of MTT assay of U373 with/without treatment of MΦ-CM from THP-1 macrophages with rhCECR1 treatment for 96 hours. **(b)** Left panel: Quantification of MTT reaction of U251 with treatment of MΦ-CM from siCECR1, siSham and non-transfected THP-1 macrophages. Right panel: Quantification of MTT assay of U251 with/without treatment of MΦ-CM from THP-1 macrophages with rhCECR1 treatment for 96 hours. Data are represented of three experiments. Six replicated wells of each condition were used. Data are in mean ± S.E.M. in fold change compared to MΦ-CM derived of macrophages without rhCECR1 treatment. *P<0.05, **P<0.01, ***P<0.005. **(c)** Representative pictures of Ki67 staining in U251 cells treated with/without MΦ-CM from non-transfected, siSham, and siCECR1 transfected macrophages (scale bar: 50 µm). **(d)** Quantification of Ki67 in U251 cells treated with different MΦ-CMs for 48 hours. Data are obtained from three experiments. * P<0.05, **P<0.01. **(e)** Representative pictures of Ki67 staining in U251 cells treated with/without MΦ-CM and MΦ-CM with treatment of RhCECR1 50nM for 48 hours. (scale bar: 50 µm). **(f)** Quantification of Ki67 in U251 cells treated with different MΦ-CMs for 48 hours. Data are obtained from three experiments. ***P<0.005.

Supplemental Figure 10 CECR1 activation in macrophages regulates parachrine-mediated migration in U373 cells

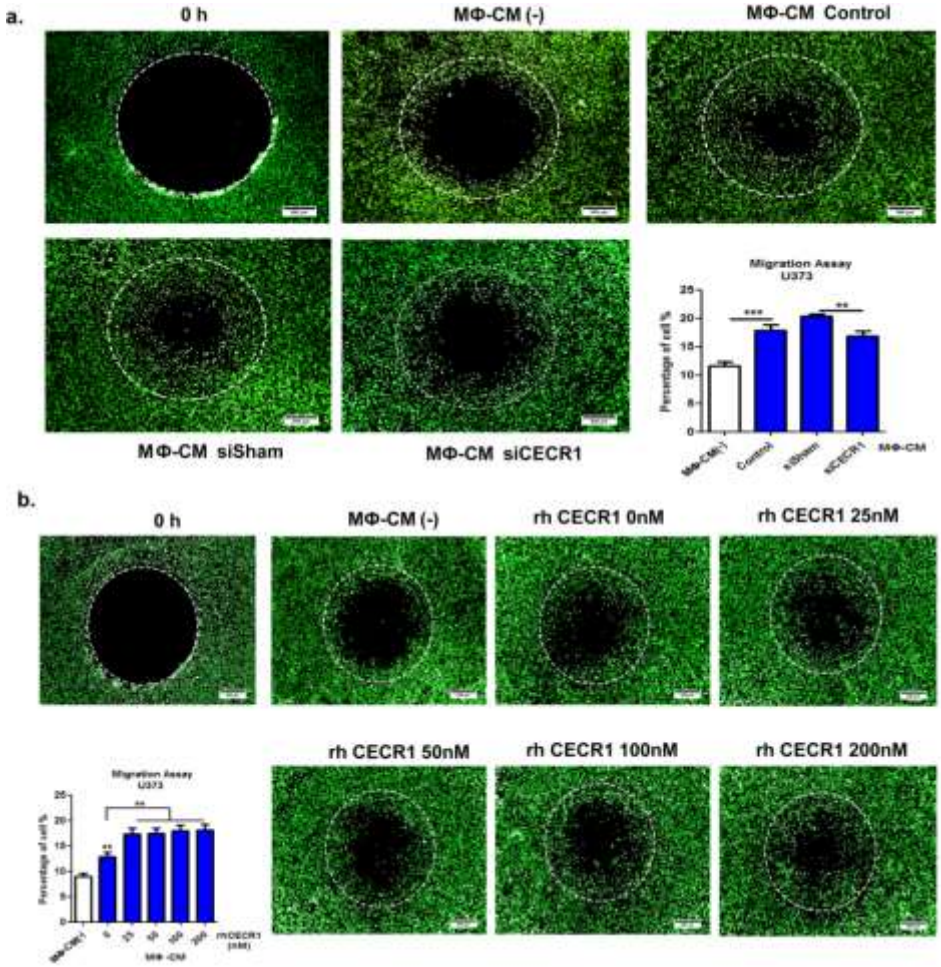

(a) Representative pictures of U373 migration into the detection zone after stimulation with MΦ-CM of macrophages with non-transfection, sisham and siCECR1 transfection (Scale bar: 200 µm). Right lower panel: Quantification of fluorescent cells in migration zones in different MΦ-CM conditions. Data are represented of three experiments and presented as mean ± S.E.M. **P<0.01, ***P<0.005. **(b)** Representative pictures of U373 migration into the detection zone after stimulation with MΦ-CM of macrophages treated with different concentrations of rhCECR1 for 96 hours (scale bar: 200 µm). Right lower panel: Quantification of fluorescent cells in migration zones in different MΦ-CM conditions. Data are represented of three experiments and presented as mean ± S.E.M. **P<0.01.

Supplemental Figure 11 CECR1 activation in macrophages regulates parachrine-mediated migration in U251 cells

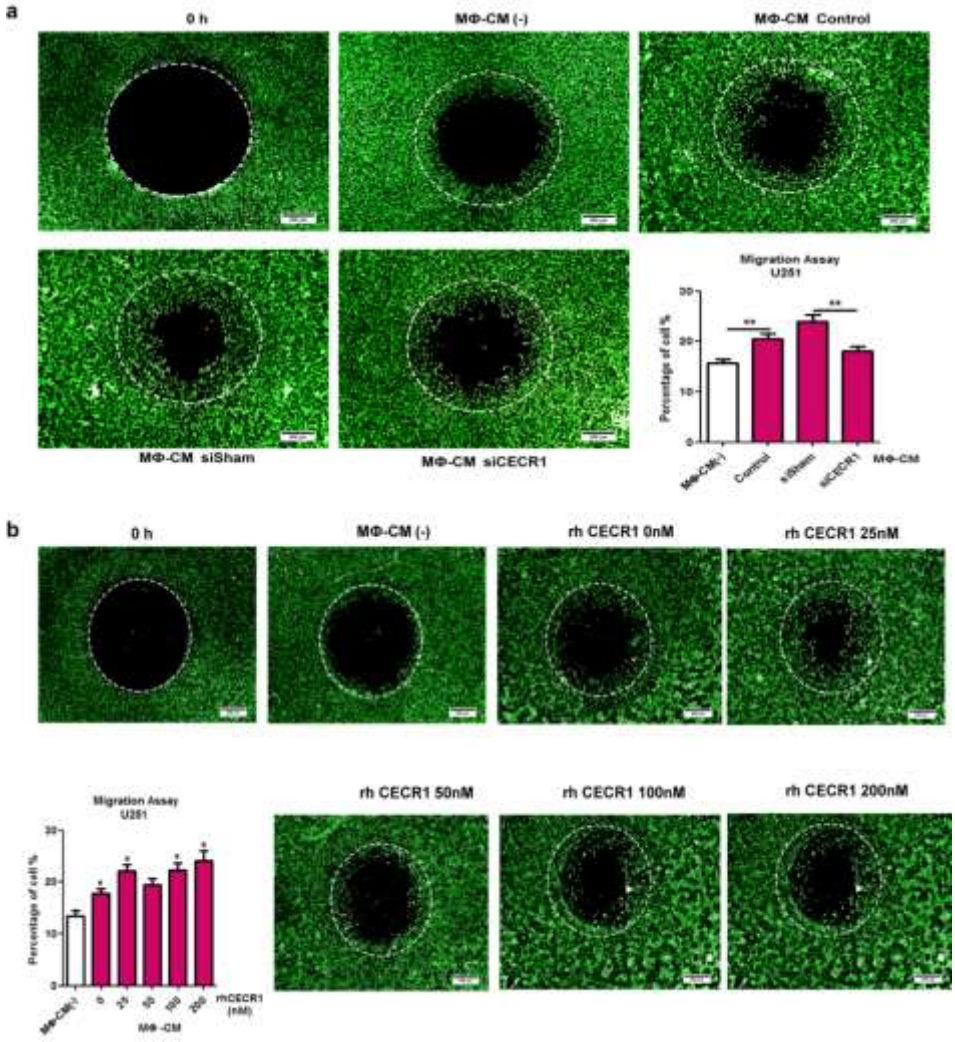

(a) Representative pictures of U251 migration into the detection zone after stimulation with MΦ-CM of macrophages with non-transfection, sisham and siCECR1 transfection (Scale bar: 200 µm). Right lower panel: Quantification of fluorescent cells in migration zones in different MΦ-CM conditions. Data are represented of three experiments and presented as mean ± S.E.M. **P<0.01. **(b)** Representative pictures of U251 migration into the detection zone after stimulation with MΦ-CM of macrophages treated with different concentrations of rhCECR1 for 96 hours (scale bar: 200 µm). Right lower panel: Quantification of fluorescent cells in migration zones in different MΦ-CM conditions. Data are represented of three experiments and presented as mean ± S.E.M. *P<0.05.

Supplemental Figure 12 Direct stimulation with rhCECR1 does not influence proliferation of U87 cells and activation of MAPK in U87 cells.

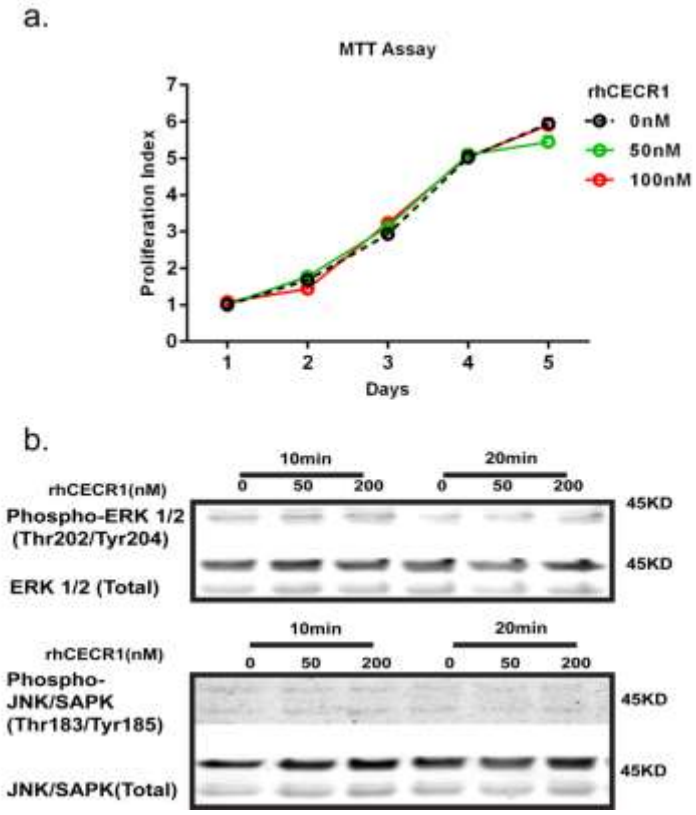

(a) Quantification of the absorbance of the end product of the MTT assay, measured in U87 cells stimulated with different concentrations of rhCECR1. **(b)** Upper panel: Representative pictures of Western blots measuring phosphor-ERK1/2 and total ERK1/2 in U87 directly treated with rhCECR1 for 10 and 20 minutes. Lower panel: Representative pictures of Western blots measuring phosphor-JNK and total JNK in U87 directly treated with rhCECR1 for 10 and 20 minutes.

Supplemental Figure 13 CECR1 function in macrophages activates the MAPK pathway in U373 cells

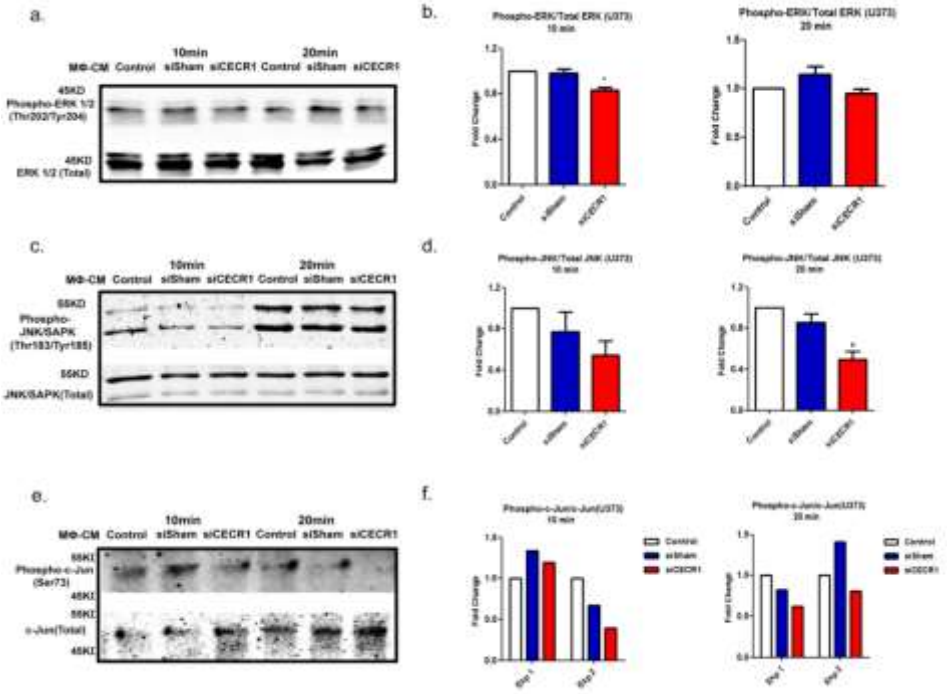

(a) Western blot of phospho-ERK1/2 and total ERK1/2 protein in U373 cells at 10 and 20 minutes after stimulation with MΦ-CM from siSham and siCECR1 transfected macrophages. Representative figures are shown of three experiments. **(b)** Western blot quantification shows phospho-ERK1/2/total ERK1/2 ratio. Data are of three observations at different time points. Phospho-ERK/Total ERK ratios are presented as mean ± S.E.M. in fold change compared to MΦ-CM derived of macrophages with non-targeted siRNA (siSham) and siRNA targeting CECR1 (siCECR1). **(c)** Western blot of phospho-JNK/SAPK and total JNK/SAPK protein in U373 cells at 10 and 20 minutes after stimulation with MΦ-CM derived from siSham and siCECR1 transfected macrophages. Representative figures are shown from three experiments. **(d)** Quantified Western blot results showing phospho-JNK/SAPK/total JNK/SAPK ratios. Data was obtained from three experiments at different time points. Quantified Phospho-JNK/Total JNK ratios are presented as mean ± S.E.M. in fold change compared to MΦ-CM derived of macrophages with non-targeted siRNA (siSham) and siRNA targeting CECR1 (siCECR1). *P<0.05. **(e)** Western blot of phospho-c-Jun and total c-Jun in U373 cells at 10 and 20 minutes after stimulation with MΦ-CM derived from siSham and siCECR1 siRNA transfected macrophages. **(f)** Quantified Western blot results showing phospho-c-Jun/total c-Jun ratios. Data was obtained from two experiments, shown individually. Quantified Phospho-c-Jun/Total c-Jun ratios are presented as mean ± S.E.M. in fold change compared to MΦ-CM derived of macrophages with non-targeted siRNA (siSham) and siRNA targeting CECR1 (siCECR1).

Supplemental Figure 14 RhCECR1 stimulation of macrophages activate MAPK pathways in U87 cells

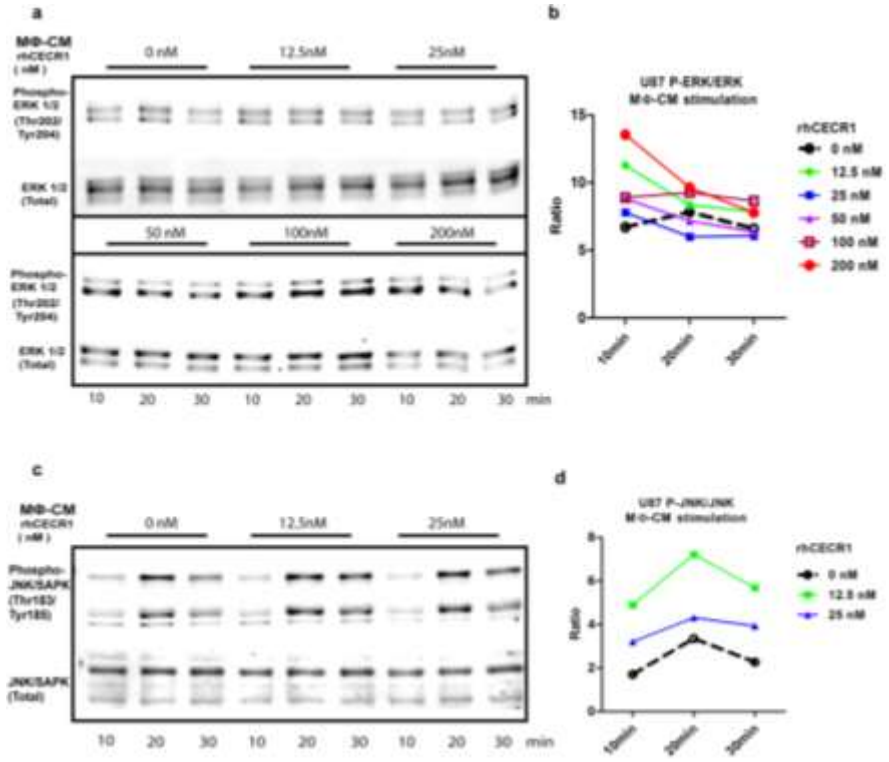

(a) Representative Western blot of two independent experiments, showing phospho-ERK1/2 and ERK1/2 in U87 cells at 10, 20, and 30 minutes after stimulation with mediums derived from macrophages treated with different concentration of rhCECR1 (MΦ-CM). **(b)** Graph showing quantified Western blot results of phospho-ERK1/2/total ERK1/2 ratios in response to conditioned mediums derived from macrophages treated with different concentration of rhCECR1. (c) Representative Western blot of two independent experiments, showing phospho-JNK/SAPK and total JNK/SAPK in U87 cells at 10, 20, 30 minutes after stimulation with mediums derived from macrophages treated with different concentration of rhCECR1 (MΦ-CM). (D) Graph showing quantified Western blot results of phospho-JNK/SAPK/total JNK/SAPK ratios in response to conditioned mediums derived from macrophages treated with different concentration of rhCECR1.

Supplemental Figure 15 Ki67 correlated positively with phosphor-ERK,JNK and c-Jun in GBM samples

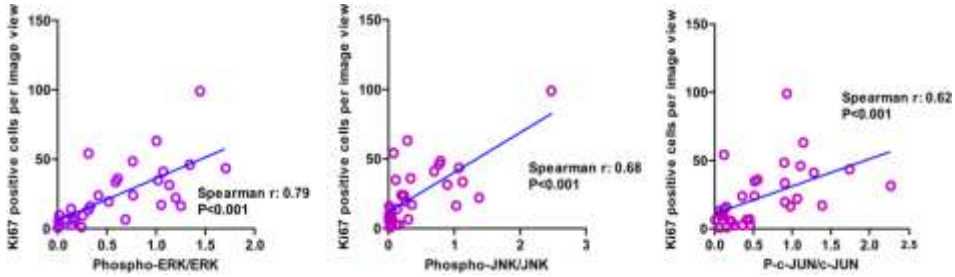

Correlation between numbers of Ki67+ cells with ratios of phospho-ERK/total ERK, phospho-JNK/total JNK, and phospho-c-Jun/total c-Jun. Spearman correlation co-efficient and P value are shown.

Chapter 4
CECR1-mediated cellular crosstalk promotes glioma vascularization

Chapter 4

CECR1-mediated crosstalk between macrophages and vascular mural cells promotes neo-vascularization in malignant glioma

Changbin Zhu, M.D. M.Sc [#]; Ihsan Chrifi, B.A.Sc. [#]; Dana Mustafa, Ph.D.; Marcel van der Weiden, M.Sc.; Pieter J.M. Leenen, Ph.D.; Dirk J. Duncker, M.D., Ph.D.; Johan M. Kros, M.D., Ph.D. [*]; Caroline Cheng Ph.D. [*] (# equal contribution of first authors; * these authors contributed equally to this work)

(in press, Oncogene, 2017)

ABSTRACT:

Introduction: Glioblastomas (GBM) are most malignant brain tumors characterized by profound vascularization. Activation of macrophages strongly contributes to tumor angiogenesis during GBM development. Previously, we showed that extracellular adenosine deaminase protein Cat Eye Syndrome Critical Region Protein 1(CECR1) is highly expressed by M2-like macrophages in GBM where it defines macrophage M2 polarization and contributes to tumor expansion. In this study, the effect of CECR1 in macrophages on tumor angiogenesis was investigated.

Methods and Results: Immunohistochemical evaluation of GBM tissue samples showed that the expression of CECR1 correlates with microvascular density in the tumors, confirming data from the TCGA set. In a 3D co-culture system consisting of human pericytes, HUVECs and THP1-derived macrophages, CECR1 knockdown by siRNA and CECR1 stimulation of macrophages inhibited and promoted new vessel formation respectively. Loss and gain of function studies demonstrated that PDGFB mRNA and protein levels in macrophages are modulated by CECR1. The pro-angiogenic properties of CECR1 in macrophages were partially mediated via paracrine activation of pericytes by PDGFB-PDGFRβ signaling. CECR1-PDGFB-PDGFRβ crosstalk between macrophages and pericytes promoted pericyte migration, shown by transwell migration assay, and enhanced expression of periostin, a matrix component with pro-angiogenic properties.

Conclusions: CECR1 function in (M2-like) macrophages mediates crosstalk between macrophages and pericytes in GBM via paracrine PDGFB-PDGFRβ signaling, promoting pericyte recruitment and migration, and tumor angiogenesis. Therefore, CECR1 offers a new target for anti-angiogenic therapy in GBM.

INTRODUCTION

Glioblastoma multiform (GBM) represents the highest grade of glioma and carries a dismal prognosis of merely 12-15 months, even after current standard chemo-radiotherapy and tumor resection regimes (1). Presently, our understanding of the exact mechanisms driving GBM pathogenesis remains limited and further research is essential for the design of more effective therapies. GBMs are highly vascularized tumors that are hall marked by vascular hyper-proliferative capacity (2) and vast myeloid infiltration (3).

So far, the therapeutic effects of anti-angiogenic regimes targeting VEGF were shown to be limited, due to rapid acquirement of resistance by the tumor cells (4). It has been proposed that the drug-resistance may be related to the activation of alternative angiogenic pathways such as FGF2-mediated and HIF1-independent mechanisms that bypass the need for VEGFA regulation of tumor angiogenesis (5). In addition, the recruitment and activation of bone marrow derived circulatory cells, including macrophages, could rescue tumor angiogenesis by secretion of these alternative pro-angiogenic factors (6).

Previous studies have well established the involvement of resident macrophages (microglia) and infiltrated macrophages, also called glioma-associated macrophages (GAMs), in tumor angiogenesis of GBM (7, 8). Although GAMs can produce VEGFA, alternative mechanisms including GAMs-induced RAGE (9), CXCL2 (10), and IGFBP1 (11) mediated regulation of tumor angiogenesis, have also been demonstrated. In addition to regulating angiogenesis, GAMs actively promote glioma growth, migration and invasion (12), and help maintain a glioma stem cell niche (13). Furthermore, findings of clinical studies imply an important functional contribution of GAMs to prognosis or recurrence of GBM (3, 8, 14, 15). Macrophages are classically distinguished into M1 and M2 phenotypes. M1 macrophages are primarily associated with a pro-inflammatory state, whereas M2 macrophages are associated with immune modulation and wound healing. Compared to M1 macrophages, M2 macrophages have been shown to act pro-angiogenic, both *in vitro* and *in vivo* (16-18). In line with these observations, recent studies have indicated that mainly tumor-associated macrophages with a M2-like phenotype can act as pro-angiogenic modulators, stimulating expansion of disorganized neovessels by e.g. paracrine release of PIGF (19) and CCL18 (20). In GBM, M2-like GAMs have been mainly described for their immune suppressive and tumor supportive function. As the majority of GAMs in GMB are known to have a M2-like phenotype, specific drug-targeting of M2 macrophages could become a viable alternative therapy for the inhibition of tumor angiogenesis in GBM (6).

Recently, the extracellular adenosine deaminase protein Cat Eye Syndrome Critical Region Protein 1(CECR1) has been shown to regulate macrophage maturation. In previous studies we demonstrated that CECR1 is consistently highly expressed by M2-type GAMs, particularly in high-grade glioma. In line with the findings presented by Zhou et

al (21), we could validate that CECR1 is an important promoter of GAM polarization towards M2-like macrophages. Our previous study also demonstrated that CECR1-mediated paracrine activation of M2-like GAMs directly affected the GBM cells, promoting tumor cell proliferation and migration. However, the effect of CECR1 regulation of GAMs on tumor angiogenesis remains to be investigated. Considering the important role that CECR1 plays in M2-like macrophage polarization, and the general pro-angiogenic function of GAMs, we hypothesize that CECR1 contributes to the paracrine pro-angiogenic function of (M2-like) GAMs.

In the present study we demonstrated that CECR1 expression correlated with microvascular density in GBM samples based analysis. Using a well-validated 3D co-culture system consisting of human pericytes, HUVECs and THP1-derived macrophages, we further demonstrated that gain and loss of function of CECR1 activity in macrophages inhibited and promoted new vessel formation respectively. Further investigation revealed that CECR1 modulated pericyte function (mainly migration), a process that was mediated by CECR1-PDGFB-PDGFRβ paracrine crosstalk between macrophages and pericytes.

RESULTS

CECR1 levels correlate with microvascular density in human GBM

Immuno-histochemisty analysis of human GBM samples indicated strong CECR1 intensity in GBM samples with high microvascular density, as shown by CD31+ staining of vascular endothelium (Figure 1a). The high level of CECR1 coincided with a strong signal of CD204+ M2 macrophages. In contrast, regions in GBM samples with weak CECR1 immunostaining showed limited numbers of CD204+ cells, and low microvascular density (Figure 1a). Quantitative analysis using ImageJ software confirmed the conclusions of the initial visual evaluation, with the mean percentage of CD31+ area per image field per GBM sample being significantly higher in the group of samples with high versus low CECR1 levels (Figure 1b). Further analysis revealed a significant positive correlation between the CD31 and CECR1 in the collection of GBM samples (Figure 1b). These data were in line with the findings obtained by data mining in the TCGA data set: significant positive correlations were identified between PECAM1 (endothelial cell marker), Endoglin (endothelial (progenitor) cell marker) and CECR1 expression in a set of 166 samples (Figure 1c, d). The findings were validated in a second TCGA GBM set (22) of 154 GBM samples (Figure 1c, d). Taken together, these observations indicate that high CECR1 levels in GBM relate to high microvascular density and the presence of CD204+ M2 macrophages.

Figure 1 CECR1 levels correlates with microvascular density in human GBM

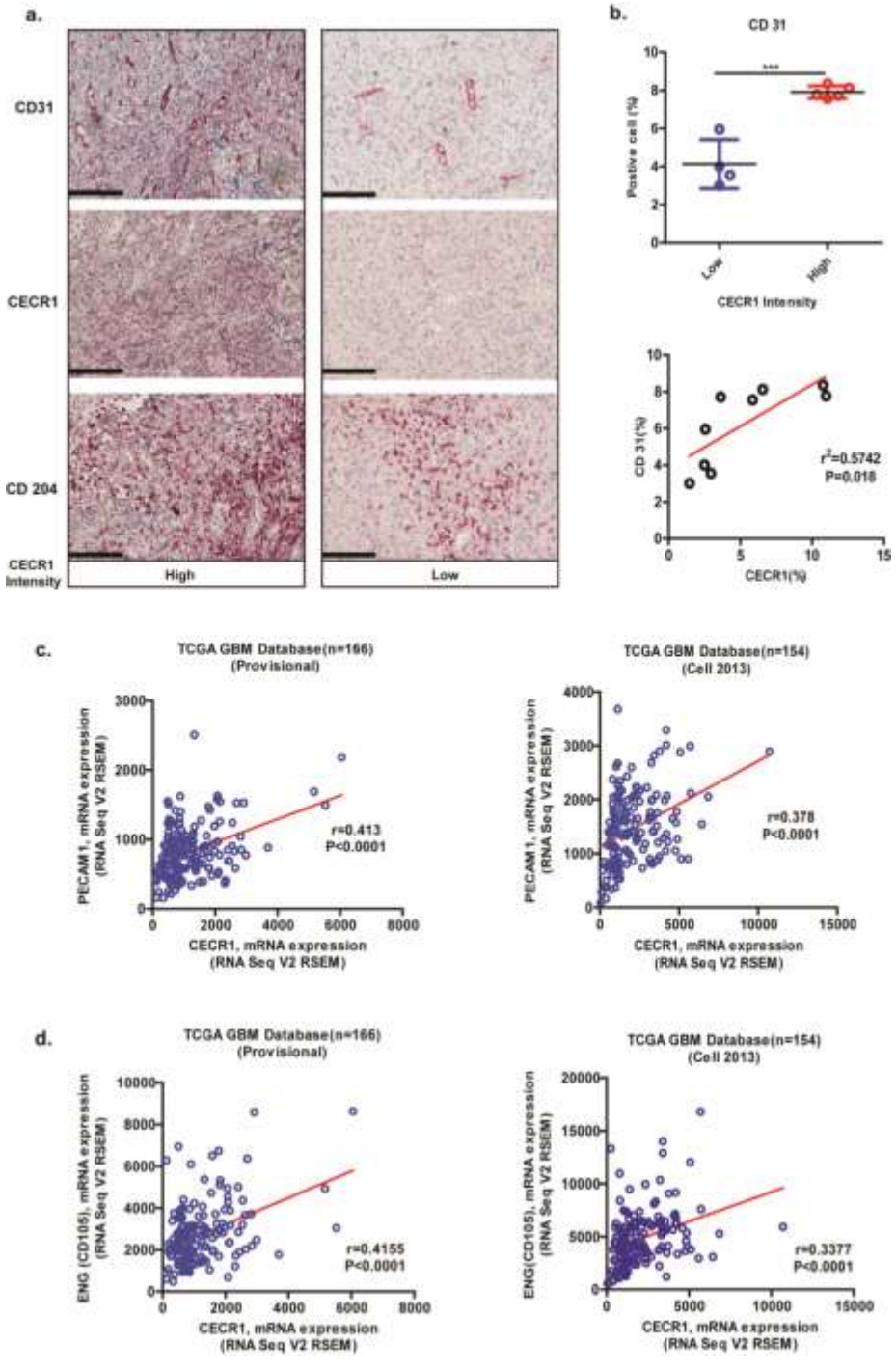

(a) Immuno-histological staining of human GBM cross-sections for CD31, CECR1 and CD204, in samples with high CECR1 signal (column High) and low CECR1 signal (column Low) (Scale bar: 200 µm). **(b)** Upper graph shows the results of a quantitative analysis using ImageJ software of the mean percentage of CD31+ cells per image field per GBM patient in CECR1 low and high signal groups. Lower graph shows the correlation between mean %CD31+ cells and %CECR1+ cells per image field per GBM patient. **(c)** Left graph: Correlation between PECAM1 and CECR1 mRNA levels in a set of 166 TCGA-dataset derived GBM samples. Right graph: Correlation between PECAM1 and CECR1 mRNA levels in a second set of 154 TCGA-dataset derived GBM samples. **(d)** Left graph: Correlation between Endoglin and CECR1 mRNA levels in a set of 166 TCGA-dataset derived GBM samples. Right graph: Correlation between Endoglin and CECR1 mRNA levels in a second set of 154 TCGA-dataset derived GBM samples. ***P<0.01.

CECR1 promotes the pro-angiogenic paracrine action of M2 macrophages

Previously we have identified M2-like macrophages as the main cell type in GBM to produce high levels of CECR1. We also showed that CECR1 promotes M0 to M2 macrophage polarization and determined M2 paracrine activity. Here we investigated the function of CECR1 in macrophage-mediated angiogenesis in a GBM-like environment. Angiogenesis was assessed in a 3D co-culture assay consisting of a collagen matrix in which GFP labeled HUVECs directly interact with dsRed labeled human-derived pericytes. This complex system mimics the complete sequence of events in microvasculature formation, allowing us to study vessel sprouting, vascular cell migration through a 3D matrix environment, multicellular vessel formation, lumenization, pericyte recruitment, perivascular coverage, and microvascular stabilization, all within a 5-day time range. To assess CECR1 function in GAMs in a GBM environment, THP1 monocytic cells were maturated by stimulation with PMA for 48 hours, before transfection with CECR1 targeting siRNA to obtain CECR1 silenced macrophages. These siCECR1 macrophages were further stimulated for 48 hours with or without U87 derived medium to assess the effect of a GBM paracrine environment. To assess the paracrine effect of the modified macrophages on angiogenesis, the THP1-derived macrophages were harvested and seeded on top of the co-culture system (Figure 2a). Stimulation of the co-cultures with THP1 macrophages significantly increased microvascular density, as observed by quantitative analysis of the number of tubules, total tubule length and number of junctions at day 5 (Figure 2b, c, f). Successful siRNA mediated knockdown CECR1 in THP1 macrophages, as validated by western blot and qPCR (Figure 2e), significantly reduced the response of the co-culture to the macrophages, as shown by a reduction in total tubule length compared to treatment with sisham and control macrophages. These effects were further amplified when the co-cultures were treated with THP1 macrophages stimulated with U87 supernatant during maturation, with CECR1-silenced + U87 supernatant-treated THP1 cells reducing the number of tubules and junctions and decreasing the total tubule length in the exposed co-cultures compared to the control groups (Figure 2d, f). In contrast, stimulation of co-cultures with the supernatant of THP1 macrophages that were stimulated with human recombinant CECR1 during maturation, showed a significant increase in all assessed vascular parameters (Supplementary figure 1a, b), demonstrating a dose-response relation.

Figure 2 CECR1 promotes the pro-angiogenic paracrine action of M2 macrophages

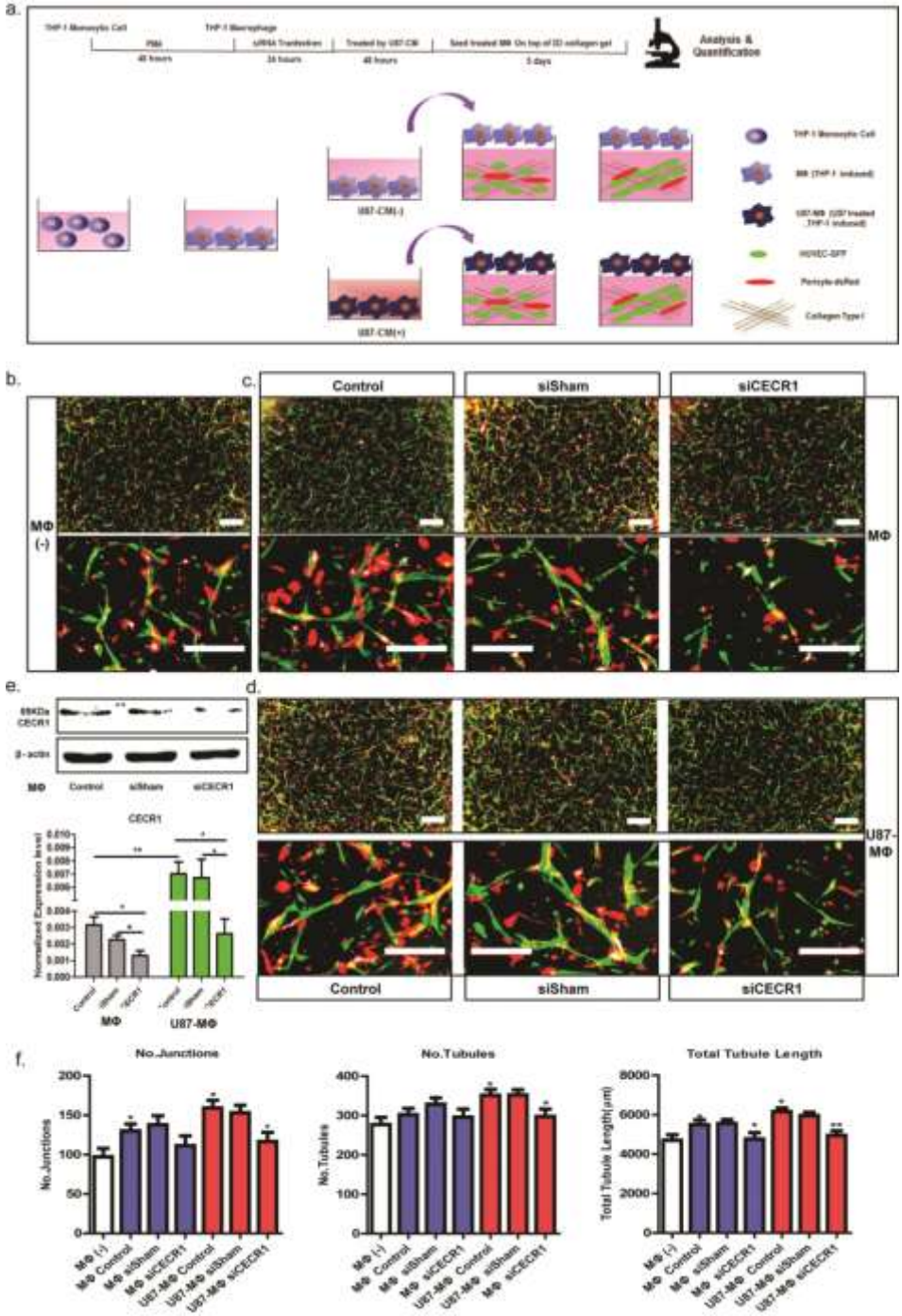

(a) Diagram showing the experimental setup of testing paracrine angiogenic activation of vascular cells in 3D co-cultures by THP1 macrophages. **(b)** Low and high magnification fluorescent images of neo-vessel formation by HUVECs (GFP-marked) and human derived pericytes (dsRed-marked) without THP1 marcrophage stimulation. (c) Low and high magnification fluorescent images of neo-vessel formation by HUVECs (GFP-marked) and human derived pericytes (dsRed-marked) with stimulation of non-treated (control), and sisham or siCECR1 treated THP1 macrophages. **(d)** Low and high magnification fluorescent images of neo-vessel formation by HUVECs (GFP-marked) and human derived pericytes (dsRed-marked) with stimulation of non-treated (control), and sisham or siCECR1 treated THP1 macrophages with U87 stimulation. (Scale bar: 100 μm for b, c, and d). **(e)** Upper image: Western blot of CECR1 protein and β actin loading control in THP1 macrophages. Blot represents results from three observations. Lower graph: QPCR results of CECR1 mRNA levels normalized to housekeeping genes in non-treated (control), and sisham or siCECR1 treated THP1 macrophages, without and with U87 stimulation. *P<0.05; **P<0.01. **(f)** Quantified results of the co-culture experiment. No. of junctions, tubules, and total tubule length data are shown. *P<0.05; **P<0.01. Representative graphs were taken from at least three experiments. Six wells were analyzed in each experiment.

Our previous studies demonstrated that M2 macrophages were the main producers of CECR1 in GBM. Here we investigated if the paracrine pro-angiogenic effects could be partially mediated by direct stimulation of vascular cells by CECR1. Indeed, stimulation of the co-cultures with recombinant CECR1 increased the number of junctions, tubules, and total tubule length, demonstrating that vascular cells can be directly stimulated by CECR1
(Supplemental figure 2a,b). Combined these data indicate that CECR1 plays an important role in regulating the pro-angiogenic function of macrophages.

PDGFB expression correlates with M2 GAMs and is enhanced by CECR1

In order to identify which particular known pro-angiogenic molecules are related to the expression of CECR1, qPCR was carried out on 6 common pro-angiogenic genes (VEGFA, TIE1, TIE2, ANGPT1, ANGPT2, PDGFB). QPCR analysis of macrophages silenced for CECR1 showed a significant decrease in PDGFB levels (Figure 3a), while expression levels of other pro-angiogenic genes were not affected (VEGFA, TIE1, TIE2, ANGPT1, ANGPT2, data not shown). Visa versa, stimulation of macrophages with recombinant human (rh)CECR1 significantly increased PDGFB in a dose-responsive manner (Figure 3b). These data were further validated by immuno-fluorescent staining of cytospin THP1 macrophages, showing a reduction in PDGFB signal that coincided with a reduction in CD163 (M2) marker signal in the CECR1 silenced versus control macrophages and sisham treated macrophages (Figure 3c). This effect was CECR1 knockdown specific, as knockdown of PDGFB in THP1 macrophages did not reduce the CD163 M2 marker signal, while the PDGFB signal was clearly decreased (Figure 3c). In contrast, treatment of macrophages with rhCECR1 increased both CD163 and PDGFB mean intensity signals (Figure 3e). Quantification of the mean intensity levels of PDGFB of the different groups confirmed

Figure 3 PDGFB expression correlates with M2 GAMs and is enhanced by CECR1

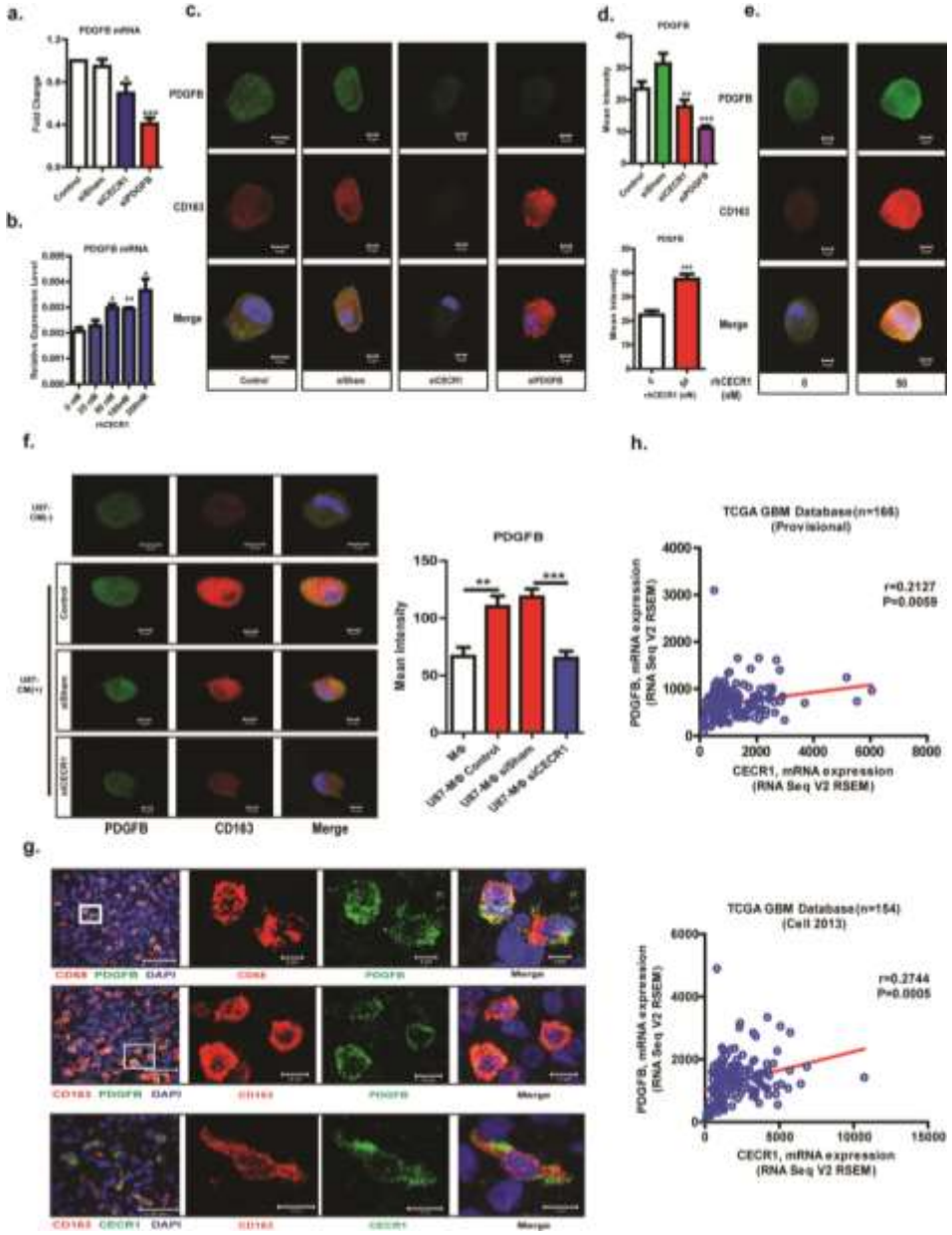

(a) QPCR analysis of PDGFβ mRNA levels normalized to housekeeping genes in non-treated (control), and sisham or siCECR1 or siPDGFB treated THP1 macrophages. *P<0.05; ***P<0.005. Experiments were repeated at least three times. **(b)** QPCR analysis of PDGFB mRNA levels normalized to housekeeping genes in THP1 macrophages treated with different concentrations of rhCECR1 from three experiments. *P<0.05; ***P<0.005. **(c)** Image panel shows immuno-fluorescent staining of PDGFB and CD163, and merged images of

cytospin non-treated (control), and sisham or siCECR1 or siPDGFB treated THP1 macrophages (Scale bar: 10 µm). **(d)** Graph shows mean PDGFβ intensity of each treatment group. **P<0.01; ***P<0.005. Experiments were repeated at least three times. **(e)** Image panel shows immuno-fluorescent staining of PDGFB and CD163, and merged images of cytospun non-treated (control), and rhCECR1 treated THP1 macrophages (Scale bar: 10 µm) **(f)** Image panel shows immuno-fluorescent staining of PDGFB (green) and CD163 (red), and merged images of cytospin non-treated controls with exposure to U87 supernatant U87 conditioned medium (CM), and THP1 macrophages treated with sisham + U87 supernatant or siCECR1 + U87 supernatant. Graph shows mean PDGFB intensity of each treatment group from at least three experiments. **P<0.01; ***P<0.005. **(g)** Low and high magnification confocal images of double immuno-fluorescent staining of CD68, CD163 and PDGFB, CECR1 in human GBM sections (scale bar: Left panel, 50 µm, Right upper panel, 5 µm, right lower panel 10 µm). **(h)** Upper graph: Correlation between PDGFB and CECR1 mRNA levels in a set of 166 TCGA-dataset derived GBM samples. Right graph: Correlation between PDGFB and CECR1 mRNA levels in a second set of 154 TCGA-dataset derived GBM samples.

that PDGFB was decreased and increased by CECR1 silencing, and rhCECR1 stimulation, respectively (Figure 3d). Stimulation of THP1 macrophages with U87 derived supernatant showed upregulation of PDGFβ signal in cytospin samples. This effect was significantly reduced in siCECR1 versus sisham treated THP1 macrophages (Figure 3f). A correlation between CECR1 and PDGFB levels was also found by analysis of TCGA datasets, which showed a positive correlation between PDGFB and CECR1 expression levels in a provisional set of 166 GBM samples, and was subsequently validated in a second set of 154 GBM samples (Figure 3h). Similar to CECR1, immunostaining of GBM samples revealed that PDGFB+ cells were mainly GAMs that express pan macrophage and M2 markers such as CD68 and CD163 (Figure 3g).

CECR1-mediated paracrine activation of macrophages promotes pericyte recruitment via PDGFB/PDGFβR signaling in GBM

To assess the role of PDGFB in CECR1 regulation of macrophages in angiogenesis, we conducted co-culture experiments with macrophages silenced for PDGFB. Co-cultures with PDGFB silenced macrophages seeded on top mimicked the phenotype of co-cultures that were treated by CECR1 silenced macrophages, demonstrating a general decrease of all parameters of active angiogenesis (Figure 4a b). Co-culture analysis of siPDGFB macrophages that differentiated with exposure to U87 supernatant showed a similar negative effect on angiogenic parameters (Supplemental data Figure 3a, b). This reduction was partially rescued by treating siPDGFβ macrophages with rhCECR1 (siPDGFB versus siPDGFB + rhCECR1, total tubule length), indicating that the paracrine pro-angiogenic effect of CECR1 in macrophages is partially mediated via PDGFB (Figure 4a, b). PDGFB mediates its activity via PDGFβ receptor (PDGFβR) signaling. In GBM samples, immuno-staining revealed that PDGFβR+ cells are mainly perivascular mural cells that are closely located near CD163+ M2 macrophages (Figure 5a, b). QPCR analysis of different *in vitro* human cell types that have equivalents in GBM *in vivo*, including HUVECs, pericytes, U87, U251, and THP1 macrophages, demonstrated that PDGFβR was

Figure 4 CECR1-mediated macrophage paracrine activation of angiogenesis is partially regulated via PDGFB

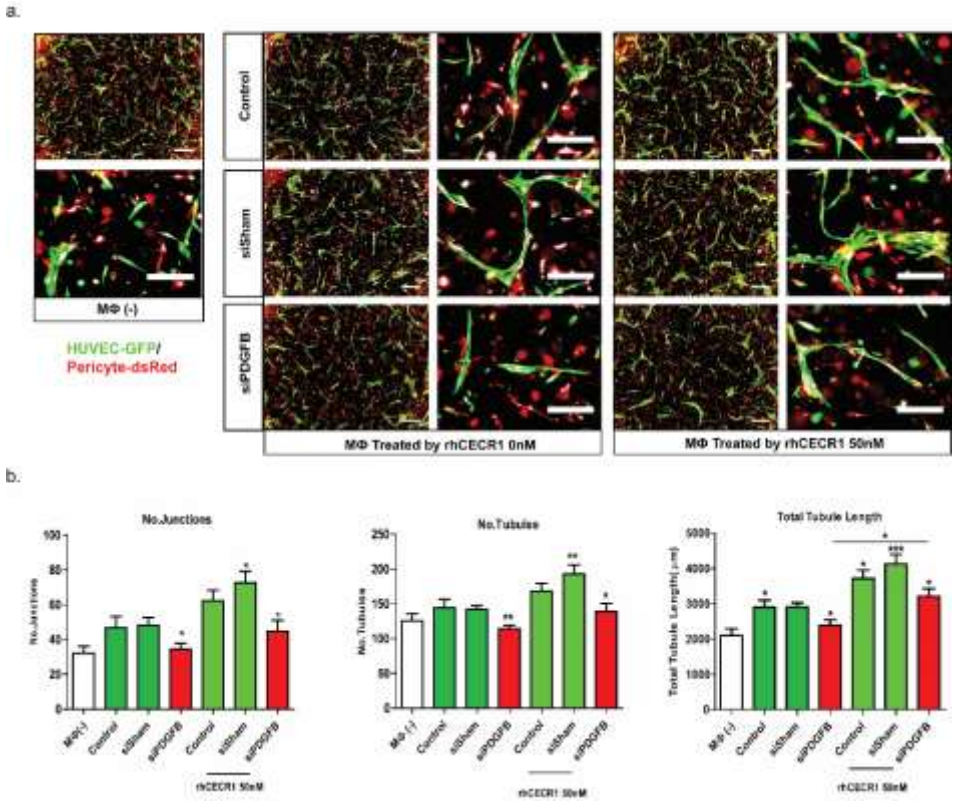

(a) Low and high magnification fluorescent images of neovessel formation by HUVECs (GFP-marked) and human derived pericytes (dsRed-marked) without THP1 marcrophage stimulation, and with stimulation of non-treated (control), and sisham or siPDGFB treated THP1 macrophages, without or with rhCECR1 rescue. **(b)** Quantified results of the co-culture experiment. No. of junctions, tubules, and total tubule length data are shown. *P<0.05; **P<0.01 ***P<0.005. Scale bar: 100 µm. N>10 cocultures in total.

mainly expressed by pericytes (Figure 5c). Confocal imaging combined with double immuno-staining further confirms mural cell expression of PDGFβR and the close localization of CD163+ GAMs in human GBMs (Figure 5d). The PDGFB/PDGFRβ ligand/receptor signaling mechanism is well-known to promote mural cell proliferation and is critical for mural cell recruitment to newly formed vessels to ensure vascular coverage and stabilization. Next, we investigated the CECR1-mediated effects of THP1 macrophages on pericyte recruitment. Pericytes were evaluated for their migratory capacity in a transwell migration assay in response to paracrine factors that are present in macrophage-derived supernatants of the different groups (Figure 5e). Pericyte migration increased upon stimulation by supernatant of THP1 macrophages (Figure 5f, g). Pericyte migration significantly decreased in response to supernatant derived from

CECR1 silenced THP1 macrophages (Figure 5e-g). This effect was mimicked by PDGFB silencing in THP1 macrophages in normal medium (Figure 5f, g). The data imply that CECR1-enhanced release of PDGFB by M2-like GAMs promotes pericyte recruitment to inflammatory pro-angiogenic sites via PDGFRβ signaling in GBM.

Figure 5 CECR1-mediated paracrine activation of macrophages may promote pericyte recruitment via PDGFB/PDGFRβ signaling in GBM

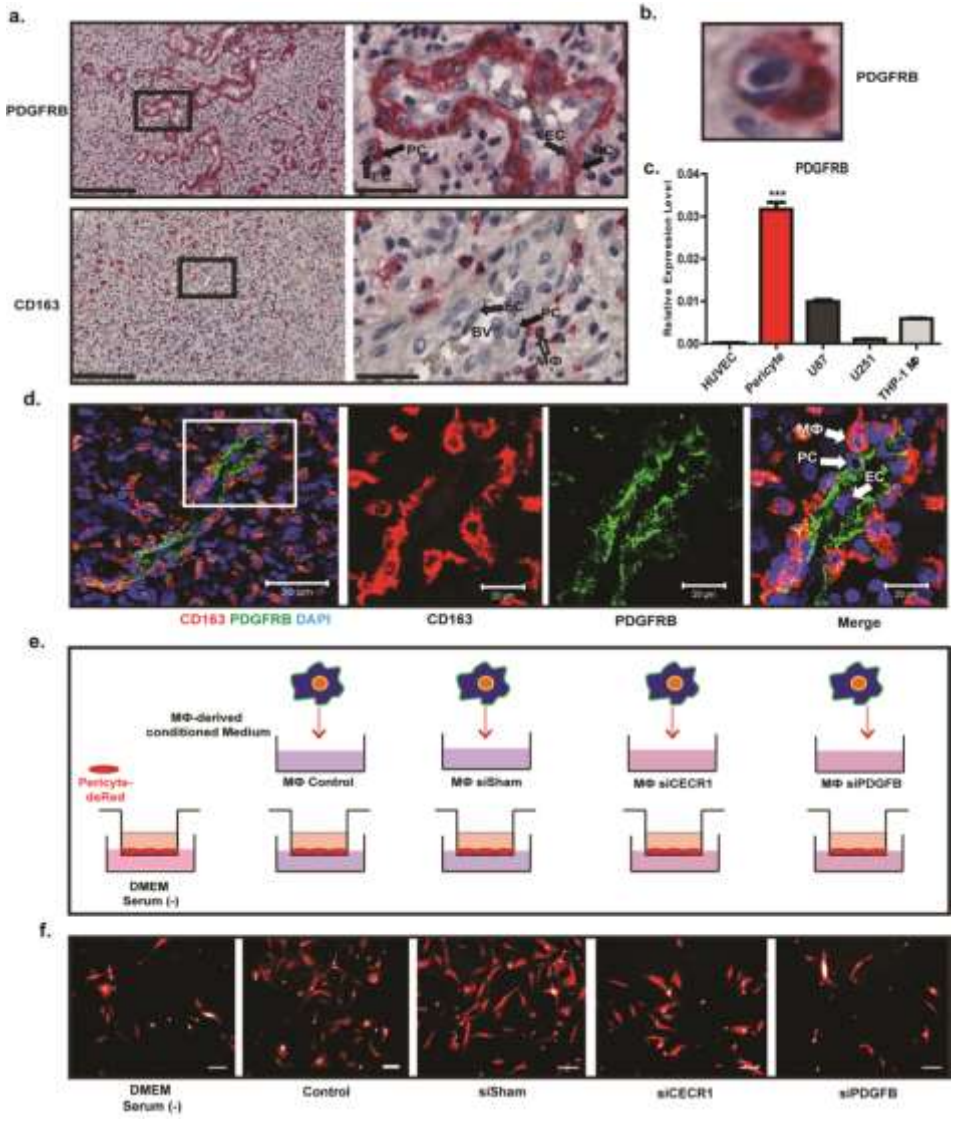

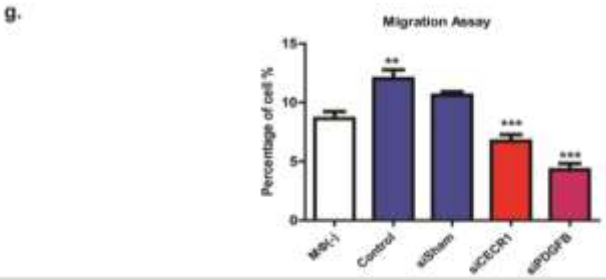

(a) Low (right panel) and high (left panel) immunohistological staining of PDGFRβ and CD163 in human GBM sections. Black arrows indicate pericytes and endothelial cells (EC) forming blood vessels (BV). White arrow indicates macrophages (Mφ) (Scale bar: Left panel, 200 μm, right panel, 40 μm). **(b)** High magnification image of PDGFRβ immunohistological staining in human GBM sections. **(c)** QPCR analysis of PDGFRβ mRNA expression levels normalized to housekeeping genes in HUVECs, pericytes, U87, U251, and THP1 macrophages from three experiments. *** P<0.001 (Pericyte versus other cell types). **(d)** Confocal images of CD163 and PDGFRβ double immuno-fluorescent staining in human GBM sections. White arrows indicate pericytes, endothelial cells (EC), and macrophages (Mφ). Scale bars: left panel, 50μm; right panel, 20 μm. **(e)** Diagram of the experimental setup of the transwell migration assay of pericytes (dsRed marked) seeded on top of the transwell. Cell migration aws towards a lower chamber with DMEM medium only, or with supernatant derived from non-treated (control) macrophages, and sisham or siCECR1 treated macrophages. **(f)** Panel of fluorescent images of dsRed marked pericytes that have migrated through the transwell setting in response to the different conditions (DMEM only, or in response to supernatant of non-treated macrophages (control), or sisham, siCECR1, or siPDGFRβ treated macrophages). **(g)** Quantified results of the transwell migration assay. **P<0.01; ***P<0.005, N>6 migration assays per condition.

CECR1 activation in THP1 macrophages promotes paracrine activation of periostin protein production in pericytes

Further confocal immuno-histochemical analysis of human GBM samples revealed colocalization of PDGFRβ+ perivascular mural cells with the extra cellular matrix component periostin (Figure 6a). Previously, we have detected enrichment of periostin in the microvasculature of GBMs using a proteomics screen (23). Work by others revealed an important role for periostin in recruitment of M2-like tumor associated macrophages and subsequent support of malignant growth (13). In line with these reports, periostin deposition was detected in close proximity of CD163+ M2 GAMs (Figure 6b). A significant positive correlation was also identified between CD163 and periostin expression in a set of 154 samples using the TCGA GBM database (Figure 6c). Similarly to PDGFRβ, qPCR analysis of different *in vitro* human cell types that can be found in GBM, including HUVECs, pericytes, U87, U251, and macrophages, demonstrated that periostin was mainly expressed by pericytes (Figure 6d). Paracrine stimulation of pericytes by THP1 macrophages enhanced periostin protein levels in the co-culture setup (Figure 6e, f). THP1 macrophages stimulated with U87 supernatant during maturation further enhanced periostin protein levels (Figure 6e, f), indicating that GAMs can significantly promote periostin protein production in pericytes.

Figure 6 CECR1 activation in THP1 macrophages promotes paracrine activation of periostin protein production in pericytes

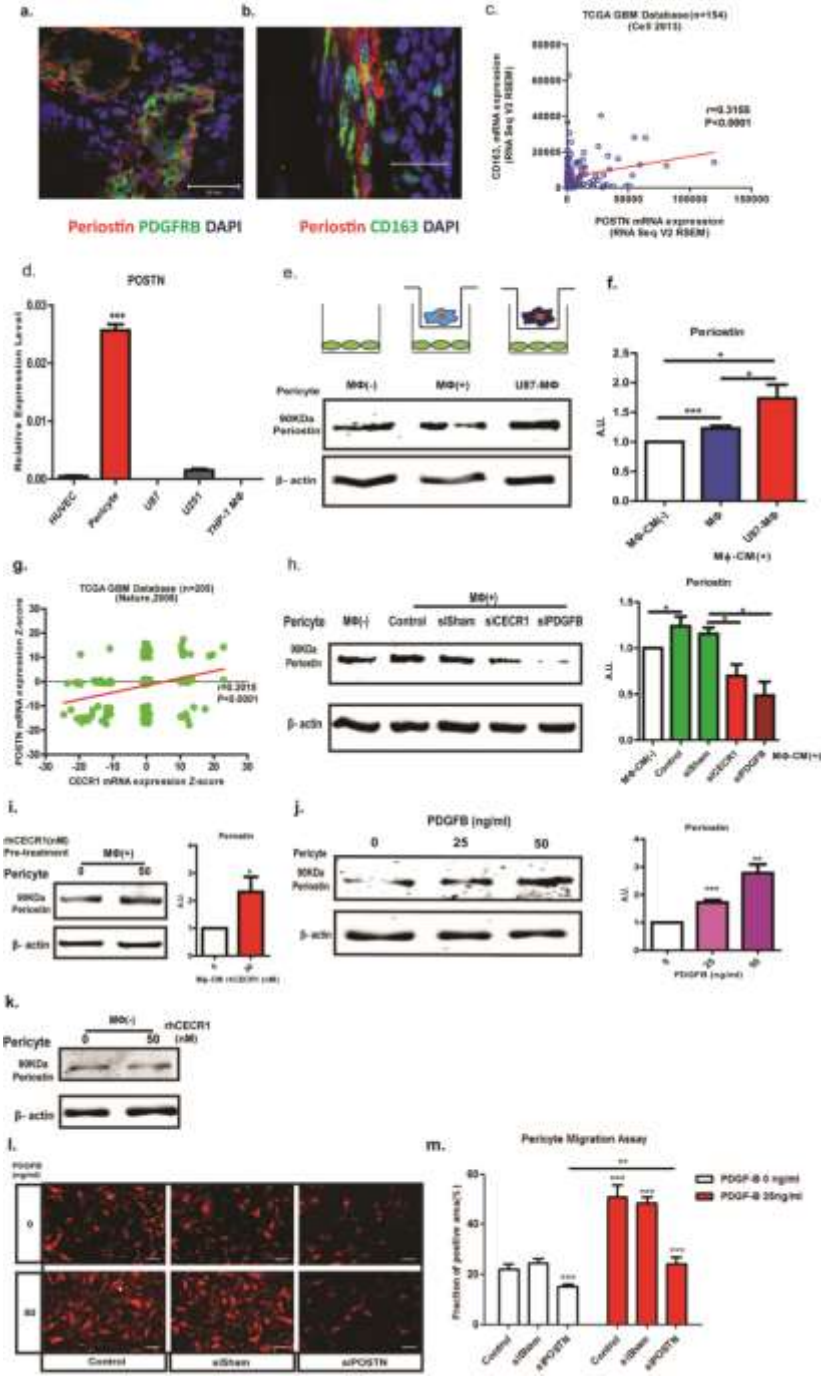

(a, b) Confocal images of imunohistological stainings of periostin, PDGFRβ, and CD163 in human GBM sections. Scale bar: 50 µm. **(c)** Correlation between CD163 and periostin mRNA levels in a set of 154 TCGA-dataset derived GBM samples. **(d)** QPCR analysis of periostin mRNA expression levels normalized to housekeeping genes in HUVECs, pericytes, U87, U251, and THP1 macrophages from three experiments. *** P<0.001 (Pericyte versus other cell types). **(e)** Diagram showing experimental setup with pericytes (green) cocultured with macrophages without (light blue) and with U87 pre-stimulation (dark blue) seeded in filter insert. Western blot shows periostin and β actin protein levels in pericytes of the different treatment groups. **(f)** Quantitative results of Western blot analysis normalized to β actin loading control from four experiments. *P<0.05; ***P<0.005. **(g)** Correlation between periostin and CECR1 mRNA levels in a set of 205 TCGA-dataset derived GBM samples. **(h)** Western blot shows periostin and β actin protein levels in pericytes treated with no macrophages, with non-transfected macrophages (control), and macrophages transfected with sisham, siCECR1, or siPDGFRβ. Graph shows quantitative results of Western blot analysis normalized to β actin loading control from four experiments. *P<0.05. **(i)** Western blot shows periostin and β actin protein levels in pericytes treated with macrophages with and without pre-treatment with rhCECR1. Graph shows quantitative results of Western blot analysis normalized to β actin loading control of at least four experiments. *P<0.05. **(j)** Western blot shows periostin and β actin protein levels in pericytes treated with different concentrations of PDGFB. Graph shows quantitative results of Western blot analysis normalized to β actin loading control from at least three experiments. ** P<0.01; ***P<0.005. **(k)** Representative western blot of three independent experiments, showing periostin and β actin protein levels in pericytes treated with rhCECR1. **(l)** Panel of fluorescent images of dsRed marked pericytes that have migrated through the transwell setting in response to the different conditions (in response to supernatant of non-treated macrophages (control), or sisham, or siperiostin treated macrophages), with and without PDGFB stimulation (Scale bar: 50 µm). **(m)** Quantified results of the transwell migration assay from three experiements. **P<0.01; ***P<0.005.

Periostin expression correlates (r=0.3015; p<0.0001) with CECR1 expression levels in a set of 205 samples derived from the TCGA GBM database (Figure 6g). The periostin protein levels of pericytes exposed to the paracrine activity of THP1 macrophages dropped significantly following silencing the macrophages for CECR1 (Figure 6h). Similarly, silencing of PDGFB in the THP1 macrophages resulted in decreased periostin production by pericytes (Figure 6h). In support of these findings, THP1 macrophages that were treated with rhCECR1 during maturation, increased periostin protein levels produced by pericytes (Figure 6i). Similarly, periostin production by pericytes that were directly stimulated with physiological levels of PDGFB was significantly increased (Figure 6j). However, direct stimulation of pericytes with rhCECR1 did not enhance their periostin production (Figure 6k), indicating that the CECR1-mediated macrophage activation of periostin expression in pericytes is indirect and requires an intermediate paracrine factor, such PDGFB. In line with these findings, direct stimulation of pericytes with PDGFB promoted their migration, and silencing of periostin in pericytes inhibited this response (Figure 6l, m). Further evidence for the involvement of periostin in angiogenesis and cell migration is provided by correlation analysis of periostin expression in three different TCGA derived human GBM data sets (Supplementary Figure 4a). Overlap analysis identified a set of 139 genes that was significantly correlated with periostin expression in the three GBM gene sets (Supplemental Figure 4b). Functional annotation of the 139 genes identified the top 20 of the significant biological processes including angiogenesis related GO terms such as "*blood vessel morphology*", "*angiogenesis*", "*blood*

vessel development", and "*cardiovascular system development*" (Supplemental Figure 4c). Furthermore, GO terms associated with cell migration such as; "*cell adhesion*", and "*extracellular matrix disassembly*" were also identified (Supplemental Figure 4c). Taken together, the data reveal a link between periostin expression by pericytes and CECR1-mediated macrophage paracrine activity.

DISCUSSION

The main findings of this study are: a) Expression of CECR1 is positively correlated with microvascular density in glioblastoma. b) CECR1 expression by GAMs promotes angiogenesis in a 3D co-culture assay. c) The level of CECR1 regulates PDGFB production in GAMs. d) The CECR1-PDGFB mediated cross-talk between macrophages and pericytes promotes migration of pericytes and contributes to new vessel formation. e) Macrophage-pericyte CECR1-PDGFB-PDGFRβ signaling upregulates the expression of the pro-angiogenic extracellular matrix component periostin in pericytes.

Current knowledge of the proangiogenic capacities of GAMs mainly concerns the effects of these cells on vascular endothelial cells (24). The regulation of perivascular cells, such as pericytes, by GAMs, is rarely studied. In this study we describe the proangiogenic role of CECR1 that is mediated via an autocrine feedback loop in which CECR1 production in (M2) GAMs enhances PDGFB expression and secretion. PDGFB/PDGFRβ signaling is crucial for the vascular maturation process in angiogenesis, during which newly formed microvessels secrete PDGFB to guide perivasular coverage by pericytes. PDGFB secreted by (M2) GAMs promote both pericyte migration and angiogenesis, as shown by our migration and 3D co-culture data respectively. Periostin is an extracellular matrix protein that is specifically present in the basal membrane of the microvasculature of GBMs [19]. In the present study we identified periostin as a potent down-stream target of the macrophage CECR1-PDGFB paracrine signaling cascade (See Supplemental data Figure 5). Pericytes are defined by their singular perivascular position, their remarkable dendrite-like morphology and their expression of PDGFRβ and NG-2 (25), Pericytes are multifunctional cells (26), being vital cells for vessel construction, maintenance, and the regulation of the vascular physiology (27). Pericyte dysfunction could lead to delay in blood vessel maturation, and contributes to vascular instability and leakage (28). Pericytes also contribute to recruitment of immune cells, including monocytes, during inflammation (29). A process of mutual activation between GAMs and pericytes during tumorangiogenesis has been previously identified. In tumors the paracrine influence of GAMs leads to activation of the PDGFB-SOX17 axis, which is initiated by tumor cells and leads to pericyte production of IL-33 (30). In addition, tumor associated macrophages secrete MMP-9, which has been shown to enhance the recruitment of pericyte precursor cells into the tumor microenvironment (31). The present data demonstrate the pro-angiogenic function of CECR1 in macrophages, mediated via paracrine regulation of PDGFB. The relation be-

tween CECR1 and angiogenesis and vascular density is reflected by the hyper-inflammatory response in patients with a CECR1 loss of function mutation (32). One of the most prominent symptoms displayed by these patients was early-onset stroke and profound vasculopathy. Similarly, vascular instability was observed in zebrafish with CECR1 knockdown. In previous studies we pointed out that CECR1 in GBM is mainly expressed by M2-like GAMs. We also discovered that CECR1 acts as a potent polarizing factor in GAMs differentiation towards the M2-like phenotype. CECR1 activity also increased the pro-tumoral function of M2 macrophages in a paracrine fashion(33). In the current study, we have shown that CECR1 activity in GAMs enhances PDGFB mRNA and protein production levels. In line with these findings, PDGFB was previously reported not only to be expressed by activated endothelial cells, but also by M2-like GAMs (34). Elevated levels of PDGFB produced in malignant cancers upregulate erythropoietin expression in stromal cells via activation of PDGRB that accelerates tumor angiogenesis (35). The CECR1-PDGFB-PDGFRβ axis that is revealed in this study points to a putative CECR1-mediated functional cross-talk between macrophages and pericytes, guiding the process of vascular maturation and development. This process may be involved in the vascular symptoms observed in patients with CECR1 mutations (21).

Aberrant vessel morphology with abnormal pericyte coverage is considered as one of the classical hallmarks of tumor vasculature in malignant tumors including GBM. Recent studies in pericytes have revealed hyperplasia of this cell type in GBM (36). The function of pericytes in malignant tumors is not only restricted to support vascular growth. As a potent producer of VEGFA, perivascular pericytes protect the tumor microvasculature against disintegration during anti-VEGFA therapy by elevating local VEGFA levels (26). Furthermore, pericytes in glioma were shown to produce other angiogenic molecules like HGF, TGFβ1 and Prostaglandins. Pericytes also inhibit the activation of T cells and thereby induce immunosuppression in glioma (37), while expressing plasminogen urokinase in support of the self-renewal and invasion of glioma initiating cells (38). Based on these reports, we can conclude that pericytes play many significant roles in promoting angiogenesis and tumor progression in glial tumors.

In this study we have identified periostin as a down-stream target of PDGFB signaling in pericytes. Periostin was identified as a pro-angiogenic extracellular matrix component in glioma (23). As a multifunctional protein it is involved in various carcinogenic processes such as the regulation of cell migration and the epithelial-mesenchymal transition in cancer cells, mainly via activation of cell focal adhesion kinases through cell binding to integrins (39). Recently, periostin was shown to play a role in the recruitment of M2-like GAMs in GBM (13) and to mediate the resistance to anti-VEGFA therapy by increasing expression of caveolin-1, HIF-1α, and VEGFA (40). In addition, periostin is expressed by mammary stromal cells in breast cancer where it is involved in actively maintaining a breast cancer stem cell niche via the canonical WNT signaling pathway (41). In pancreatic carcinoma the expression of periostin was found upregulated in response to PDGFB stimulation (42). Our data provides evidence that the modulation of

CECR1 in macrophages influences the expression of periostin in pericytes via PDGFB-mediated paracrine signaling.

In conclusion, this study demonstrates that in glioblastoma CECR1 produced by M2-like GAMs regulates the cross-talk between macrophages and pericytes via paracrine PDGFB-PDGFRβ signaling, promoting pericyte recruitment and migration, and tumor angiogenesis. The pro-angiogenic function of the CECR1-PDGFB-PDGFRβ signaling cascade is related to the expression of periostin by pericytes. This new knowledge on complex interaction between immuno cells and vascular cells, in the process of tumor neo-angiogenesis could lead to better immune-modulatory and anti-angiogenic strategies for treatment of GBM in the future.

MATERIAL AND METHODS

Patient samples

Patient samples of glioblastoma were collected from the Department of Pathology, Erasmus Medical Center with the approval of committee of research ethics. All the samples were diagnosed as glioblastoma by a board certificated pathologist (J.M.K).

Cell culture

Human monocytic cell line THP-1, obtained from Department of Hematology, Erasmus Medical Center, was maintained in culture in RPMI-1640 (Lonza, Breda) supplemented with 10%FBS and 1% Penicillin/Streptomycin. THP-1 cells were differentiated into macrophage-like cells by PMA (Sigma, Sweden) at concentration of 100ng/ml for 48 hours. Recombinant human CECR1 protein (rhCECR1) was added to the macrophage cultures at a concentration gradient of 0, 12.5, 25, 50, 100, 200 nM for 96 hours.

Human umbilical vein endothelial cells (HUVECs) (Lonza, Breda) and HUVECs transfected with a lentiviral vector encoding GFP were cultured in EGM-2 endothelial medium (Lonza, Breda) with 1% Penicillin/Streptomycin.

Human brain vascular pericytes (HBVP) with and without lentiviral transfection of a vector encoding for dsRed, and GBM cell lines; U87, and U251 were maintained in DMEM (Lonza, Breda) with 10% FBS and 1% Penicillin/Streptomycin. Pericytes were treated with recombinant human PDGFB (Sigma, Sweden) at different concentrations according to the specifications of the different assays.

siRNA transfection

siCECR1(5'-GUGCCAAAGGCUUGUCCUA-3',5-CUUCCACGCCGGAGAAACA-3',5'-GCCCAA AGCUAGUUAGUAC-3';5'-UCGCAGAAUCCAUCCGAAU-3'); siPDGFB(5'-CCGAGGAGCUU

UAUGAGAU-3', 5'-GAAGAAGGAGCCUGGGUUC-3',5'-GCAAGCACCGGAAAUUCAA-3', 5'-GGGCCGAGUUGGACCUGAA-3'), siPOSTN(5'-CCGAAGCUCUUAUGAAGUA-3'), and scrambled siRNA (5'-UGGUUUACAUGUCGACUAA-3',5'-UGGUUUACAUGUUGUGUGA-3',5'-UGGUUUACAUGUUUUCUGA-3', UGGUUUACAUGUUUUCCUA-3') (siSham) were purchased from Dharmacon (GE health care, the Netherlands). Macrophages were transfected with SiCECR1 and siPDGFB using transfection buffer 2 (Dharmacon, GE, The Netherlands); pericytes or pericytes-dsRed were transfected with siPOSTN using transfection buffer 1 (Dharmacon, GE, the Netherlands) according to manufactural instructions (See supplementary material and methods for details).

RNA isolation and RT-qPCR

Total RNA was isolated from macrophages and pericytes using RNA isolation kit (Bioline, UK) and cDNA was synthesized by sensi-fast cDNA synthesis kit (bio-line, UK). Transcripts of CECR1, PDGFB, and POSTN were measured and normalized to β-actin in macrophages and pericytes (For primers sequences see supplementary Table 1).

Trans-well co-culture

Macrophages were seeded in 0.4µm trans-well insert (Fisher scientific, USA) and were treated with U87-derived conditioned medium or recombinant human (rh)CECR1 protein for 48 hours followed by co-culture with pericytes for extra 72 hours. Pericytes were harvested afterwards for performing downstream assays.

Western blot

20 µg of total protein lysate derived from macrophages and pericytes was loaded onto 10% SDS-PAGE gel and blotted to Nitro cellulous membranes followed by blocking and incubation of primary antibody. Protein levels were assessed by immunoblotting using specific antibodies against CECR1 (Sigma, 1:200), Periostin (R&D, 1:200), PDGFRβ (Abcam, 1:10000), and β-actin (Abcam, 1:500) as a loading control, followed by incubation with secondary antibodies (IRdye 680 CW, IRDye 800 CW, Licor Bioscience, USA) and detection of signals using the Odyssey imaging system (Licor Bioscience, USA).

Immunostaining

4 µm of adjacent sections were used for immunohistochemical and immunofluorescence analysis. Immunostaining and slide scanning were performed according to the protocol described previously (43). Macrophages were fixed using 4% PFA/PBS, followed by antibody incubation. All fluorescence labeled samples was analyzed under the confocal microscope LSM 700 (Zeiss, The Netherlands). Five areas in high magnification

field were randomly selected from each slide and quantified using Image J (Antibodies applied were listed in supplementary table2).

Transwell migration assay

7,000 Pericytes-dsRed with transfected with siPOSTN, siSham and non-transfected controls were seeded into the top compartment of the Fluor block 8 μm transwell inserts (Fisher Scientific, USA). Recombinant PDGFB protein was added in the lower chamber with serum free DMEM medium. Serum free macrophage conditioned medium from sisham, siCECR1, siPDGFB, and non-transfected control macrophages was added into the lower chamber. After 24 hours of migration, pictures from five randomly selected areas under 10x view were taken under a fluorescent microscope for image quantification by image J.

3D collagen tubule formation assay

HUVEC-GFP and Pericyte-dsRed were co-cultured in 96-well plate at 5:1 ratio within a 3D culture environment of bovine collagen type I (Gibco, USA) supplemented with SCF-1, SDF-1α, and IL-3, as described previously (44). 300 macrophages with different conditions were seeded on top of collagen gel and maintained for 5 days. At the 5^{th} day, tubule formation was captured by fluorescent microscope and quantified by Angiosys 1.0.

TCGA Database

Three GBM datasets were obtained from TCGA via the c-Bioportal provided by the Memorial Sloan Kettering Cancer Center. Genes that positively correlated with POSTN expression (cut off point: spearman r>0.4) in all three GBM database were selected for pathway analysis by String.

Statistics

Data from clinical samples were analyzed by Mann-Whitney U test and Spearman Correlation using SPSS 21.0. All *in vitro* data were tested using unpaired two-tailed student's T test (Significance levels $P<0.05$). All data are presented in Mean ± S.E.M. unless otherwise stated.

REFERENCES

1. Wen PY, Kesari S. Malignant gliomas in adults. New England Journal of Medicine. 2008;359(5):492-507.
2. Das S, Marsden PA. Angiogenesis in glioblastoma. New England Journal of Medicine. 2013;369(16):1561-3.
3. Prosniak M, Harshyne LA, Andrews DW, Kenyon LC, Bedelbaeva K, Apanasovich TV, et al. Glioma grade is associated with the accumulation and activity of cells bearing M2 monocyte markers. Clin Cancer Res. 2013;19(14):3776-86.
4. Gilbert MR. Antiangiogenic Therapy for Glioblastoma: Complex Biology and Complicated Results. J Clin Oncol. 2016;34(14):1567-9.
5. Takano S. Glioblastoma angiogenesis: VEGF resistance solutions and new strategies based on molecular mechanisms of tumor vessel formation. Brain Tumor Pathol. 2012;29(2):73-86.
6. Ferrara N. Pathways mediating VEGF-independent tumor angiogenesis. Cytokine Growth Factor Rev. 2010;21(1):21-6.
7. Hambardzumyan D, Gutmann DH, Kettenmann H. The role of microglia and macrophages in glioma maintenance and progression. Nature Neuroscience. 2016;19(1):20-7.
8. Lu-Emerson C, Snuderl M, Kirkpatrick ND, Goveia J, Davidson C, Huang YH, et al. Increase in tumor-associated macrophages after antiangiogenic therapy is associated with poor survival among patients with recurrent glioblastoma. Neuro-Oncology. 2013;15(8):1079-87.
9. Chen X, Zhang L, Zhang IY, Liang J, Wang H, Ouyang M, et al. RAGE expression in tumor-associated macrophages promotes angiogenesis in glioma. Cancer Res. 2014;74(24):7285-97.
10. Brandenburg S, Müller A, Turkowski K, Radev Y, Rot S, Schmidt C, et al. Resident microglia rather than peripheral macrophages promote vascularization in brain tumors and are source of alternative pro-angiogenic factors. Acta Neuropathol. 2015:1-14.
11. Nijaguna MB, Patil V, Urbach S, Shwetha SD, Sravani K, Hegde AS, et al. Glioblastoma-derived Macrophage Colony-stimulating Factor (MCSF) Induces Microglial Release of Insulin-like Growth Factor-binding Protein 1 (IGFBP1) to Promote Angiogenesis. J Biol Chem. 2015;290(38):23401-15.
12. Li W, Graeber MB. The molecular profile of microglia under the influence of glioma. Neuro Oncol. 2012;14(8):958-78.
13. Squadrito ML, De Palma M. A niche role for periostin and macrophages in glioblastoma. Nat Cell Biol. 2015;17(2):107-9.
14. Pong WW, Walker J, Wylie T, Magrini V, Luo JQ, Emnett RJ, et al. F11R Is a Novel Monocyte Prognostic Biomarker for Malignant Glioma. Plos One. 2013;8(10).
15. Komohara Y, Ohnishi K, Kuratsu J, Takeya M. Possible involvement of the M2 anti-inflammatory macrophage phenotype in growth of human gliomas. J Pathol. 2008;216(1):15-24.
16. Roma-Lavisse C, Tagzirt M, Zawadzki C, Lorenzi R, Vincentelli A, Haulon S, et al. M1 and M2 macrophage proteolytic and angiogenic profile analysis in atherosclerotic patients reveals a distinctive profile in type 2 diabetes. Diab Vasc Dis Res. 2015;12(4):279-89.
17. Nakamura R, Sene A, Santeford A, Gdoura A, Kubota S, Zapata N, et al. IL10-driven STAT3 signalling in senescent macrophages promotes pathological eye angiogenesis. Nat Commun. 2015;6:7847.
18. Jetten N, Verbruggen S, Gijbels MJ, Post MJ, De Winther MP, Donners MM. Anti-inflammatory M2, but not pro-inflammatory M1 macrophages promote angiogenesis in vivo. Angiogenesis. 2014;17(1):109-18.
19. Potente M, Gerhardt H, Carmeliet P. Basic and Therapeutic Aspects of Angiogenesis. Cell.146(6):873-87.
20. Lin L, Chen YS, Yao YD, Chen JQ, Chen JN, Huang SY, et al. CCL18 from tumor-associated macrophages promotes angiogenesis in breast cancer. Oncotarget. 2015;6(33):34758-73.
21. Navon Elkan P, Pierce SB, Segel R, Walsh T, Barash J, Padeh S, et al. Mutant adenosine deaminase 2 in a polyarteritis nodosa vasculopathy. New England Journal of Medicine. 2014;370(10):921-31.
22. Brennan CW, Verhaak RG, McKenna A, Campos B, Noushmehr H, Salama SR, et al. The somatic genomic landscape of glioblastoma. Cell. 2013;155(2):462-77.
23. Mustafa DAM, Dekker LJ, Stingl C, Kremer A, Stoop M, Smitt PAES, et al. A Proteome Comparison Between Physiological Angiogenesis and Angiogenesis in Glioblastoma. Mol Cell Proteomics. 2012;11(6).

24. Riabov V, Gudima A, Wang N, Mickley A, Orekhov A, Kzhyshkowska J. Role of tumor associated macrophages in tumor angiogenesis and lymphangiogenesis. Front Physiol. 2014;5:75.
25. Armulik A, Genove G, Betsholtz C. Pericytes: developmental, physiological, and pathological perspectives, problems, and promises. Dev Cell. 2011;21(2):193-215.
26. Sweeney MD, Ayyadurai S, Zlokovic BV. Pericytes of the neurovascular unit: key functions and signaling pathways. Nat Neurosci. 2016;19(6):771-83.
27. Bergers G, Song S. The role of pericytes in blood-vessel formation and maintenance. Neuro Oncol. 2005;7(4):452-64.
28. Garcia-Quintans N, Sanchez-Ramos C, Prieto I, Tierrez A, Arza E, Alfranca A, et al. Oxidative stress induces loss of pericyte coverage and vascular instability in PGC-1 alpha-deficient mice. Angiogenesis. 2016;19(2):217-28.
29. Stark K, Eckart A, Haidari S, Tirniceriu A, Lorenz M, von Bruhl M-L, et al. Capillary and arteriolar pericytes attract innate leukocytes exiting through venules and 'instruct' them with pattern-recognition and motility programs. Nature Immunology. 2013;14(1):41-51.
30. Yang YL, Andersson P, Hosaka K, Zhang Y, Cao RH, Iwamoto H, et al. The PDGF-BB-SOX7 axis-modulated IL-33 in pericytes and stromal cells promotes metastasis through tumour-associated macrophages. Nature Communications. 2016;7.
31. Yang L, DeBusk LM, Fukuda K, Fingleton B, Green-Jarvis B, Shyr Y, et al. Expansion of myeloid immune suppressor Gr+CD11b+cells in tumor-bearing host directly promotes tumor angiogenesis. Cancer Cell. 2004;6(4):409-21.
32. Zhou Q, Yang D, Ombrello AK, Zavialov AV, Toro C, Zavialov AV, et al. Early-onset stroke and vasculopathy associated with mutations in ADA2. New England Journal of Medicine. 2014;370(10):911-20.
33. Zhu C, van der Weiden MM, Scchetti A, van den Bosch TPP, Chrifi I, Brandt MM, et al. Abstract 2348: Expression of CECR1 by activated M2-type macrophages in glioma. Cancer Research. 2015;75(15 Supplement):2348-.
34. Vignaud JM, Marie B, Klein N, Plenat F, Pech M, Borrelly J, et al. The Role of Platelet-Derived Growth-Factor Production by Tumor-Associated Macrophages in Tumor Stroma Formation in Lung-Cancer. Cancer Research. 1994;54(20):5455-63.
35. Xue Y, Lim S, Yang Y, Wang Z, Jensen LD, Hedlund EM, et al. PDGF-BB modulates hematopoiesis and tumor angiogenesis by inducing erythropoietin production in stromal cells. Nat Med. 2012;18(1):100-10.
36. Sun HQ, Guo DY, Su YP, Yu DM, Wang QL, Wang T, et al. Hyperplasia of Pericytes Is One of the Main Characteristics of Microvascular Architecture in Malignant Glioma. Plos One. 2014;9(12).
37. Ochs K, Sahm F, Opitz CA, Lanz TV, Oezen I, Couraud PO, et al. Immature mesenchymal stem cell-like pericytes as mediators of immunosuppression in human malignant glioma. Journal of Neuroimmunology. 2013;265(1-2):106-16.
38. Zhong X, Liu X, Li Y, Cheng M, Wang W, Tian K, et al. HMGA2 sustains self-renewal and invasiveness of glioma-initiating cells. Oncotarget. 2016.
39. Liu AY, Zheng H, Ouyang G. Periostin, a multifunctional matricellular protein in inflammatory and tumor microenvironments. Matrix Biol. 2014;37:150-6.
40. Park SY, Piao Y, Jeong KJ, Dong J, de Groot JF. Periostin (POSTN) regulates tumor resistance to antiangiogenic therapy in glioma models. Mol Cancer Ther. 2016.
41. Malanchi I, Santamaria-Martinez A, Susanto E, Peng H, Lehr HA, Delaloye JF, et al. Interactions between cancer stem cells and their niche govern metastatic colonization. Nature. 2012;481(7379):85-U95.
42. Erkan M, Kleeff J, Gorbachevski A, Reiser C, Mitkus T, Esposito I, et al. Periostin creates a tumor-supportive microenvironment in the pancreas by sustaining fibrogenic stellate cell activity. Gastroenterology. 2007;132(4):1447-64.
43. Zheng PP, van der Weiden M, Kros JM. Fast tracking of co-localization of multiple markers by using the nanozoomer slide scanner and NDPViewer. Journal of Cellular Physiology. 2014;229(8):967-73.
44. Koh W, Stratman AN, Sacharidou A, Davis GE. In vitro three dimensional collagen matrix models of endothelial lumen formation during vasculogenesis and angiogenesis. Methods Enzymol. 2008;443:83-101.

SUPPLEMENTAL FIGURES

Supplemental Figure 1 Macrophage Stimulated with rhCECR1 promotes angiogenesis in 3D coculture assays

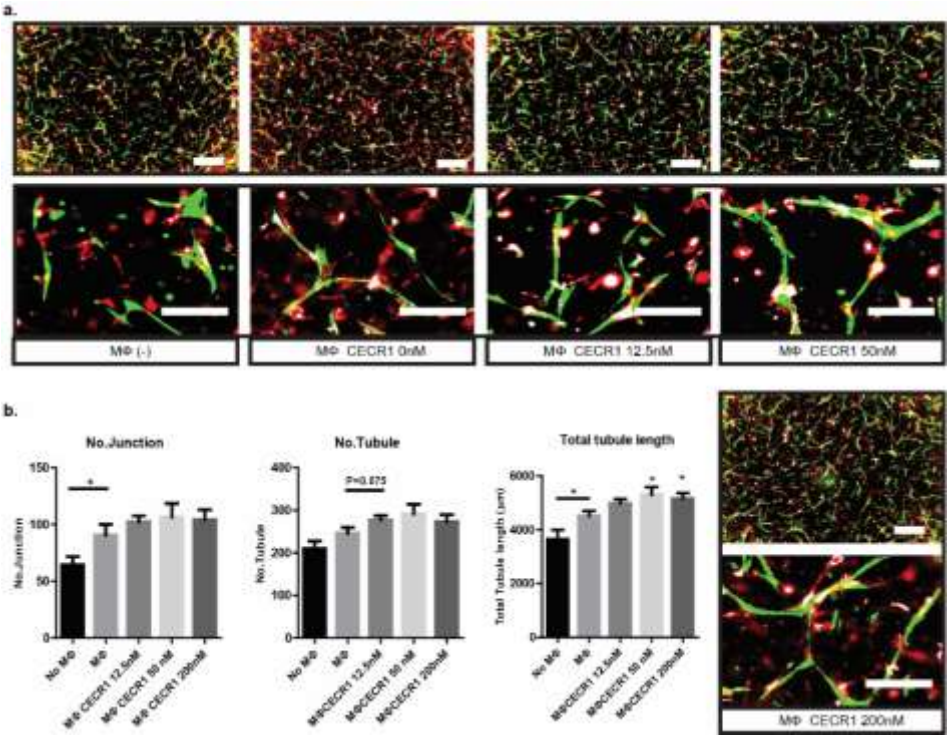

(a) Low and high magnification fluorescent images of neovessel formation by HUVECs (GFP-marked) and human derived pericytes (dsRed-marked) with no macrophage stimulation (no Mϕ), with macrophage stimulation (Mϕ CECR1 0 nM), and with stimulation of macrophages that were exposed to different concentrations of CECR1 during maturation (Mϕ CECR1 12.5, 50 and 200 nM). **(b)** Quantified results of the co-culture experiment. No. of junctions, tubules, and total tubule length data are shown. Represented graphs were taken from at least three experiments. Six wells per condition were conducted in each experiment. * P<0.05. (Scale bar: 100 μm).

Supplemental Figure 2 Stimulation with rhCECR1 promotes angiogenesis in 3D coculture assays

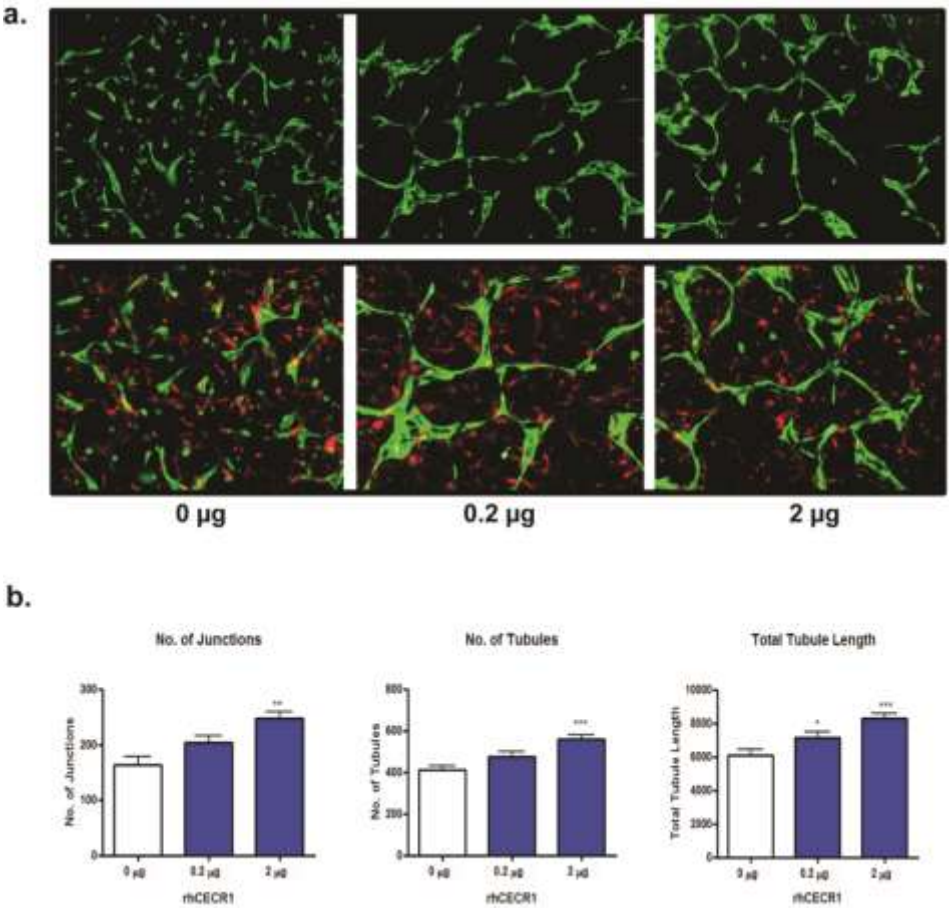

(a) Low and high magnification fluorescent images of neovessel formation by HUVECs (GFP-marked) and human derived pericytes (dsRed-marked) with stimulation of different concentrations of rhCECR1. **(b)** Quantified results of the co-culture experiment. No. of junctions, tubules, and total tubule length data are shown. * P<0.05 ***P<0.005.

Supplemental Figure 3 PDGFB silencing decreases macrophage paracrine activation of angiogenesis in 3D coculture assays

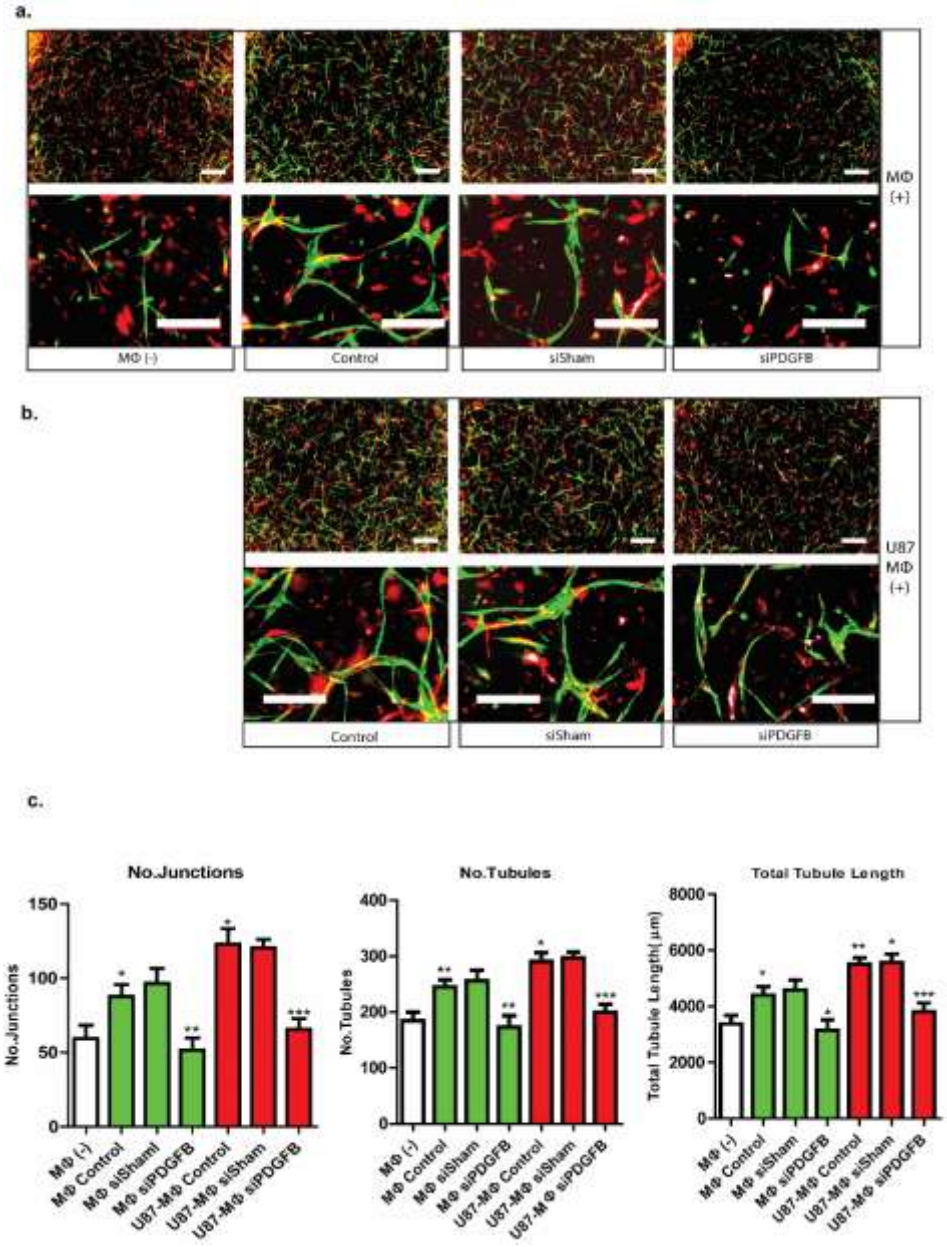

(a) Low and high magnification fluorescent images of neovessel formation by HUVECs (GFP-marked) and human derived pericytes (dsRed-marked) without macrophage stimulation, or with macrophage stimulation (non-treated control, sisham, or siPDGFB treated) that were pre-treated with or without U87 supernatant during differentiation. **(b)** Quantified results of the co-culture experiment from three times. No. of junctions, tubules, and total tubule length data are shown. *P<0.05 **P<0.01 ***P<0.005. (Scale bar: 100 µm).

Supplemental Figure 4 Periostin expression in TCGA human GBM samples correlates with a genetic profile that is associated with angiogenesis and cell migration

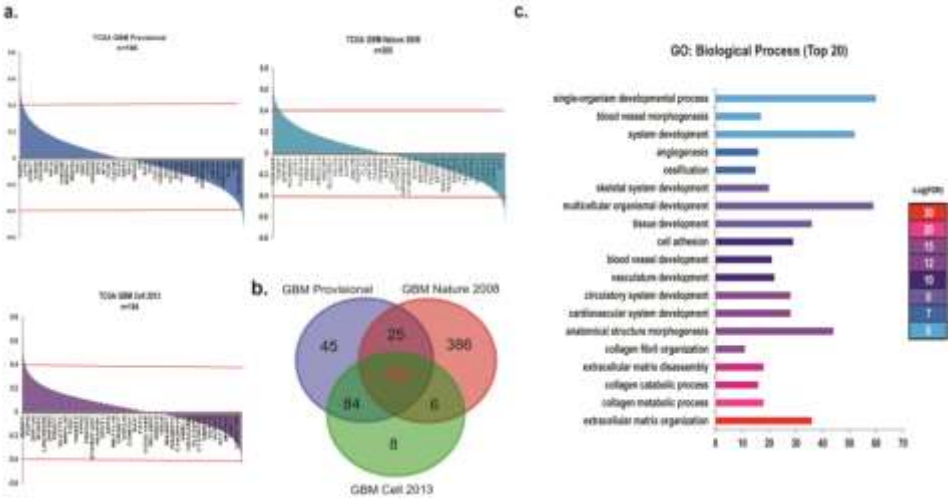

(a) Correlation analysis of periostin mRNA levels with gene sets of three different TCGA human GBM data files. Graphs show r values on y-axis, and individual genes that significantly correlate with periostin on x-axis. **(b)** Venn graph demonstrating the overlap between the genes that significantly correlate with periostin expression in the three data sets. **(c)** Functional annotation of the 139 overlapping genes produced a list of top 20 significant biological processes. GO terms are shown on the y-axis. No. of input genes per GO term are indicated on the x-axis.

Supplemental Figure 5 Proposed working mechanism of CECR1 in the cross-talk between (M2-like) macrophages and pericytes

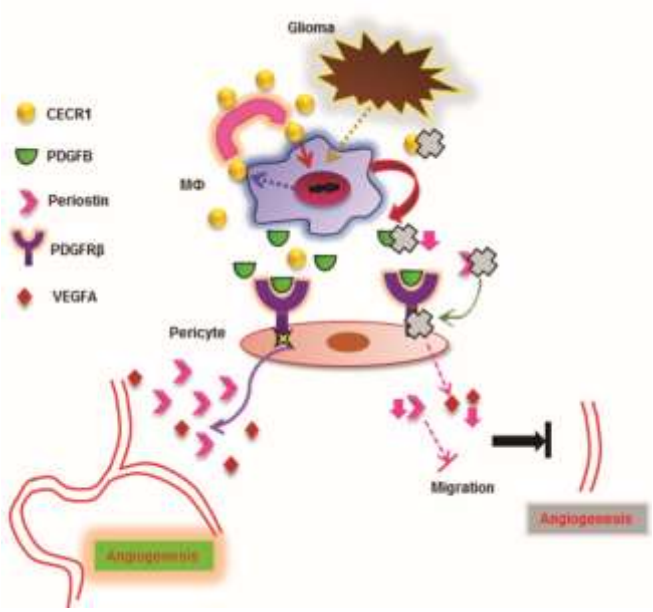

The GBM environment promotes CECR1 production in (M2) TAMs, which enhances PDGFB expression and secretion. PDGFB/PDGFRβ signaling is crucial for the vascular maturation process in angiogenesis, during which newly formed microvessels secrete PDGFB to guide perivasular coverage by pericytes. PDGFB secreted by (M2) GAMs at perivascular locations activate PDGFRβ signaling and promote both pericyte migration, and periostin production in support of angiogenesis. Therapeutic agents (indicated in the diagram as a grey cross) that target CECR1, PDGFB, PDGFRβ, or periostin, could interfere with macrophage-pericyte cross-talk and subsequently counter tumor-angiogenesis.

Supplementary Information accompanies the paper on the Oncogene website (http://www.nature.com/onc)

Chapter 5

Periostin is expressed by pericytes and is crucial for angiogenesis in glioma

Karin Huizer, MD (1); Changbin Zhu, MD (1); Ihsan Chrifi, MSc (2); Bart Krist, BSc (1); Denise Zorgman (1); Marcel van der Weiden (1); Caroline Cheng, PhD (2,3); Johan M. Kros, MD, PhD (1); Dana A. Mustafa, PhD (1).

(Submitted for publication)

ABSTRACT

In a previous study we found specific overexpression of periostin in glioma blood vessels.

Recently, in a murin glioma model periostin expression was linked to glioma stem cells and associated with glioma progression. The aim of this study was to identify the cellular source of periostin expression in human gliomas, its expression levels in the various glioma grades and to study the effect of periostin on glioma angiogenesis. To this aim, we compared human glioma samples of various malignancy grades for the expression of periostin and sought the cellular source of its expression by confocal microscopy using multiple markers and in situ RNA to tissue samples. By silencing POSTN expression in an in vitro model for angiogenesis we studied the effects of periostin on angiogenesis.

We found that the expression of periostin is exclusively by PDGFRbeta positive cells, of which only few cells appeared positive for the glioma stem cell markers SOX-2 and olig 2. Silencing of POSTN in pericytes in the in vitro angiogenesis model resulted in attenuation of the number and length of the tubules formed, and the number of junctions the vessels formed. The results identify the pericytes as the main source of periostin in human glioma, and highlight the importance of periostin for the formation of angiogenesis, thereby proposing periostin as a novel target for developing new anti-angiogenic strategies for glioma.

INTRODUCTION

In order to find new targets for effective anti-angiogenic therapy for gliomas, the identification of molecules that play key roles in neovascularization is crucial. In spite of the fact that gliomas are among the tumors with highest degree of vascularization, anti-angiogenic therapies have not yielded major improvements in clinical outcome [1]. It remains unclear why anti-angiogenic therapies largely fail, and whether the currently used drugs address all players in the complex process of angiogenesis. Notorious changes in protein expression patterns of the vessel walls of incipient gliomas have been recorded [2, 3]. The blood vessels in high-grade gliomas / glioblastomas (GBM) show proliferation of endothelial cells, pericytes and other mural cells, altogether designated as microvascular proliferation (MVP). Because VEGF levels are associated with hypoxia and it is generally assumed that along with tumor progression hypoxia increases, VEGF inhibitors like bevacizumab are only used in patients with high-grade gliomas. Given the notion that shifts in protein expression patterns have been recorded in the vasculature of low-grade gliomas, new targets for anti-angiogenic therapies, targeting early events of angiogenesis in glioma, need to be explored.

In a previous study we identified some proteins that are specifically upregulated in tumor angiogenesis [2]. Among the matricellular proteins αV-integrin and tenascin-C we most prominently identified periostin. Matricellular proteins are expressed during development, tissue repair and cancer and contribute to angiogenesis by making the extracellular matrix permissive for new vascular sprouts [4-10]. In various epithelial tumors increased levels periostin were found [4, 11-14] and a prominent role of periostin at sites of metastasis was reported [15]. Periostin has only recently been associated with glioma invasion and vasculature[2, 16-18]. However, most data were obtained in mice models and data on the expression site of POSTN in human glioma are still largely missing. In addition, the effects of periostin expression on glioma angiogenesis have not been investigated so far.

In the present study we explored the expression of periostin in human glioma samples by immunohistochemical detection of co-expression patterns and in situ RNA detection and found expression of periostin by PDGFRβ+ pericytes, with only limited overlap with SOX-2+/olig-2+ glioma stem cells (GSC). Silencing of the *POSTN* gene in cultured pericytes in the presence of glioma cells, resulted in a reduction of angiogenic capacity, pointing to the importance of periostin for glioma angiogenesis. The results of this work highlight the importance of periostin to glioma angiogenesis, and present a plea for its candidacy as new target for anti-angiogenic therapeutic strategies in gliomas.

MATERIALS AND METHODS

Tissue samples

Tissue samples of 12 GBM, 10 PA, 10 grade II and III astrocytoma were selected. In order to make comparisons with normal brain and non-neoplastic lesions in which angiogenesis takes place, 8 arteriovenous malformations, 5 cavernous hemangiomas, 9 hemangioblastomas and 8 samples of normal brain were included for comparison. The age and gender distributions of the patients from whom the tumors and lesions were used are shown in Table 1.

Table 1 Tissue types, ages and sexes of the patients and relative RNA expression for tenascin-C, periostin and Integrin-αV.

	n (male / female)	Median age (range)	POSTN	TNC	Integrin-αV
Glioblastoma	12 (10/2)	47 (14/58)	Z=-3.0 p=0.003	Z=-3.7 p=0.0002	Z=-3.7 p=0.0002
Pilocytic astrocytoma	10 (3/7)	20 (4-51)	Z=-3.3 p=0.0004	Z=-3.6 p=0.0004	Z=-3.6 p=0.0004
Astrocytoma (WHO grade II/III)	10 (5/5)	44 (32-59)	Z=-0.9 p=0.4	Z=-2.8 p=0.005	Z=-3.1 p=0.002
Arteriovenous malformation	8 (7/1)	41 (11/65)	Z=-2.2 p=0.03	Z=-2.4 p=0.015	Z=-2.8 p=0.004
Cavernous hemangioma	5 (1/4)	22 (7/34)	Z=-2.4 p=0.02	Z=-2.9 p=0.003	Z=-2.9 p=0.003
Hemangioblastoma	9 (5/4)	31 (13/82)	Z=-3.6 p=0.0004	Z=-3.3 p=0.001	Z=-3.1 p=0.002
Control brain	8 (5/3)	48 (28/62)			

TNC = tenascin-C; POSTN = periostin.
The Z-values are calculated by the Mann Whitney U test and are relative to the expressional levels in normal brain.

All patients had given consent for using their biomaterials and the study was approved by the medical ethical committee of the Erasmus Medical Center. Part of each tissue sample was freshly-frozen and stored at -80ºC for RNA isolation while another part was formalin-fixed and embedded in paraffin for immunohistochemistry.

Immunohistochemistry

For immunohistochemistry we used formalin-fixed, paraffin-embedded material corresponding to the same sample used for RNA isolation. After deparaffinization with xylene four adjacent sections for each sample were stained with the following antibodies and dilutions: tenascin-C (Abcam, Cambridge, UK, 1:100), Periostin (Sigma Life Science, HPA012306, 1:50), integrin-αV, and CD31, (DAKO, Denmark, 1:40). Samples were incubated with primary antibodies for 30 minutes at room temperature, and washed with PBS. Next, the samples were incubated with alkaline phosphatase conjugated secondary antibodies for 30 minutes at room temperature. Consequently, the slides were washed

with Tris/HCl buffer, and developed for 30 minutes using New Fuchsin Alkaline Phosphatase Substrate solution. Finally, the slides were rinsed with tapwater, and counterstained with haematoxylin. Immunohistochemical stainings were evaluated and scored by the neuropathologist (JMK).

Triple Labeling Immunofluorescence

Four-µm-thick paraffin sections were cut from formalin-fixed paraffin-imbedded blocks of one GBM and one PA sample. Deparaffinized sections were pretreated for antigen retrieval by microwave in an EDTA-HCl retrieval solution buffer (Klinipath, 43979001, ph 9). Slides were washed in PBS/tween 0.1% and incubated overnight at 4ºC with a mixture of the following primary antibodies: Mouse monoclonal integrin-αV (Santa Cruz sc-9969, 1: 40) and rabbit polyclonal periostin (Atlas antibodies HPA012306, 1:100). Slides were washed twice with PBS/tween 0.1%, and incubated for two hour at room temperature with a mixture of the following two secondary antibodies: goat anti-mouse Cy3 (Biolegend, 405309, 1:200) and donkey anti-rabbit Cy5 (Jackson, 711-175-152, 1:50).

After washing, the slides were incubated for one hour at room temperature with normal mouse serum (Jackson, 015-000-120, 1:20). The purpose of this step was to saturate the open binding sites on the goat anti-mouse secondary antibody with IgG. The slides were incubated for one hour at room temperature with unconjugated Fab goat anti-mouse IgG (H+L) (Jackson, 115-007-003). This step covers the remaining serum-derived mouse IgG binding sites. The slides were washed and incubated overnight at 4ºC with monoclonal primary antibody against tenascin–C (Abcam, Ab 58954, 1: 100). Washed slides were incubated for two hours at room temperature with secondary antibody (goat anti-mouse-FITC conjugated, Biolegend, 405305, 1: 100). The slides were stained for 5 minutes with 0.1% solution of Sudan Black (Sigma, 199.664) in ethanol 70 %. The sudan black step is included to diminish autofluorescence of lipofuscin. Slides were stained with DAPI and mounted with coverslips.

RNA isolation and RT-PCR

For each sample, 10-15 sections of 20 µm thickness were cut by cryostat. Sections were collected in RNase free Eppendorf tubes, snap frozen on dry ice, and stored at -80ºC until RNA isolation. To verify the presence of tumor in all the sections used for RNA isolation, we cut 5 µm sections before and after sampling for RNA isolation and verified content of lesional tissues in H&E stained sections. Total RNA was isolated using RNA-Bee (Campro, Veenendaal, The Netherlands) according to the instructions supplied by the manufacturer. Following isolation, RNA samples were diluted in nuclease-free water, snap frozen on dry ice and subsequently stored at -80ºC. Total RNA quantity was determined by Nanodrop and RNA integrity was checked using gel electrophoresis. To generate cDNA, 1 µg of total RNA was reverse transcribed using the RevertAid cDNA

synthesis kit (Fermentas). cDNA samples were dissolved in 20 µl nuclease-free water, and stored at -20ºC until analysis by RT-PCR.

Samples were analyzed in the Applied Biosystems 7500 Fast Real-Time PCR System.

We used the following commercially available exon-spanning TaqMan Gene Expression Assays (Applied Biosystems): Periostin, exon 3-4 (Hs00170815_m1), Hypoxanthine phosphoribosyltransferase 1 (HPRT1), exon 1-2 (Hs01003267_m1) and beta-Actin, exon 1-1 (Hs99999903_m1). Four µl of each cDNA sample was amplified for 40 rounds, in a reaction volume of 20 µl. Maximal reliable Ct levels were set at 35. For Ct values exceeding 35, the ΔCt levels were replaced by the lowest ΔCt value minus one for each target (corresponding with 50% of the lowest detected level of expression). Since GeNorm and NormFinder analysis recognized HPRT1 as the most stable reference gene among all tissue groups, we used HPRT1 as our reference gene. We quantified the relative expression level for each gene by calculating ΔCt values: ΔCt = Ct (HPRT1) – Ct (target).

Statistics

Using the Mann-Whitney U test in SPSS 17.0.2, ΔCt values were compared between PAs, grade II/III astrocytomas, GBMs, arteriovenous malformations, cavernous hemangiomas, hemangioblastomas and normal brain. All glioma subgroups were compared to each other. Due to multiple testing, P-values < 0.01 were considered statistically significant.

In situ RNA hybridization

In situ hybridization was performed using the RNAscope1 2.0 HD Brown Chromogenic Reagent Kit according to the manufacturer's instructions (Advanced Cell Diagnostics, Hayward, CA). Hs-POSTN probe (Advanced Cell Diagnostics #409181) was used following the manual protocol. Briefly, prepared slides were baked for 1 h at 60°C prior to use. After deparaffinization and hydration, tissues and cells were air-dried and treated with a peroxidase blocker before heating in a target retrieval solution (pretreatment 2 solution as part of the RNAscope1 kit; Advanced Cell Diagnostics #320043) for 20 min at 95–100°C. Protease (pretreatment 3 solution of the RNAscope1 kit; Advanced Cell Diagnostics #320045) was then applied for 30 min at 40°C. Target probes were hybridized for 2 h at 40°C, followed by a series of signal amplification and washing steps. Hybridization signals were detected by chromogenic reactions using DAB chromogen followed by 1:1 (vol/vol)-diluted hematoxylin (Fisher Scientific, Pittsburg, PA) counterstaining.

POSTN in various cell types

The expression of the POSTN gene was measured by RT-PCR in HUVECs (ScienCell-1800), pericytes (ScienCell-1200) and human astrocytes (scienCell-8000). The POSTN

protein expression is measured by Western Blotting in cell lysates of HUVECs, pericytes and astrocytes.

HUVECs and pericytes were co-cultured for 3 days by using DMEM media + SCF, SDF-1α and IL-3 and the protein expression of POSTN is measured in both cell types and in their media. Subsequently, HUVECs and pericytes were co-cultured (DMEM media + SCF, SDF-1α and IL-3) and stimulated by adding conditioned media of glioma cells (U87).

Silencing of POSTN

POSTN in pericytes was silenced by using two different siRNA sequences (Supplemental Figure 1). POSTN was successfully downregulated using siPOSTNs2 (n= 3).

Angiogenesis model

HUVECs were labeled with GFP and pericytes with DsRed. The HUVECs and pericytes were mixed at ratio 5:1 and cultured in medium consisting of DMEM + SCF; SDF-1$^{\alpha}$ and IL-3. To create 3D angiogenesis model, bovine collagen type 1 was mixed with pericytes and added to a 96-well plate. HUVEC were placed on top of the collagen 1. Parameters of angiogenesis (i.e., number and lengths of tubules and number of junctions) were measured up to 5 days as described previously [19]. The experiments were repeated 6 times in 6 wells. The angiogenesis experiments were repeated by using U87 conditioned media.

RESULTS

Immunohistochemistry & RT-PCR

In PA and GBM, expression of periostin was present in the perivascular area of hypertrophic and glomeruloid vessels (Figure 1A). In PA expression was exclusively found around the blood vessels, while in GBM, periostin was also markedly present in areas away from the blood vessels. In grade II/III astrocytomas that have by definition no MVP, little expression around the blood vessels was seen. The

Results of immunohistochemistry corresponded to those of RT-PCR; periostin expression was low in normal brain and in grade II/III astrocytomas, as opposed to the expression in PA, GBM and the vascular malformations (arteriovenous malformations, cavernous hemangiomas) and hemangioblastomas, where periostin was strongly expressed (Figure 1B).

Figure 1

Figure 1A

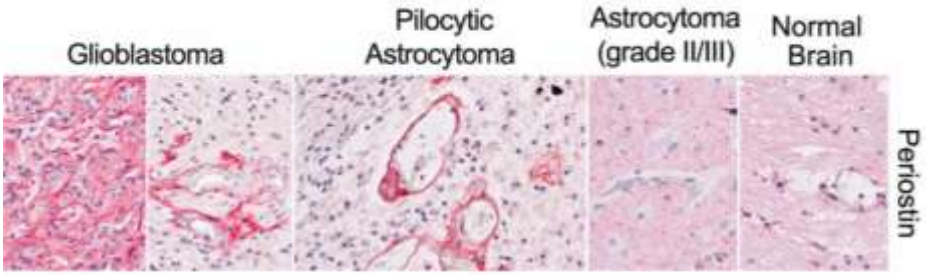

Figure 1B

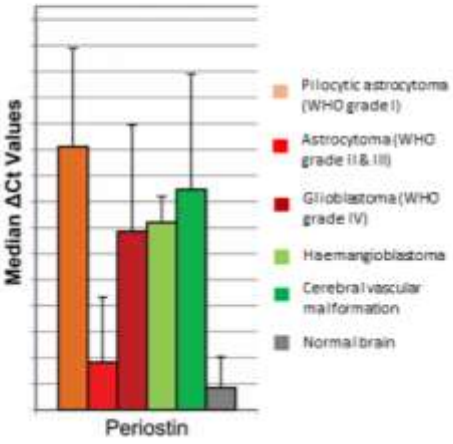

Figure 1A:POSTN is expressed in the perivascular area in both glioblastoma (GBM) and pilocytic astrocytoma (PA). Unlike the expression in PA, in GBM POSTN is also expressed in areas away from the blood vessels. In astrocytoma grade II / III and normal brain samples scarce cells express POSTN. (H&E, x 200). **Figure 1B:** POSTN expression in various types of brain tumors was confirmed by RT-PCR. POSTN is expressed at a high level in GBMs and Pas. In contrast, POSTN was expressed at a low level in astrocytoma grade II /III, and normal brain samples (showing limited or no angiogenesis).

Confocal microscopy to periostin and PDGFRβ expression demonstrated co-localization of these two proteins (Figure 2), indicative of periostin expression by pericytes.

Figure 2

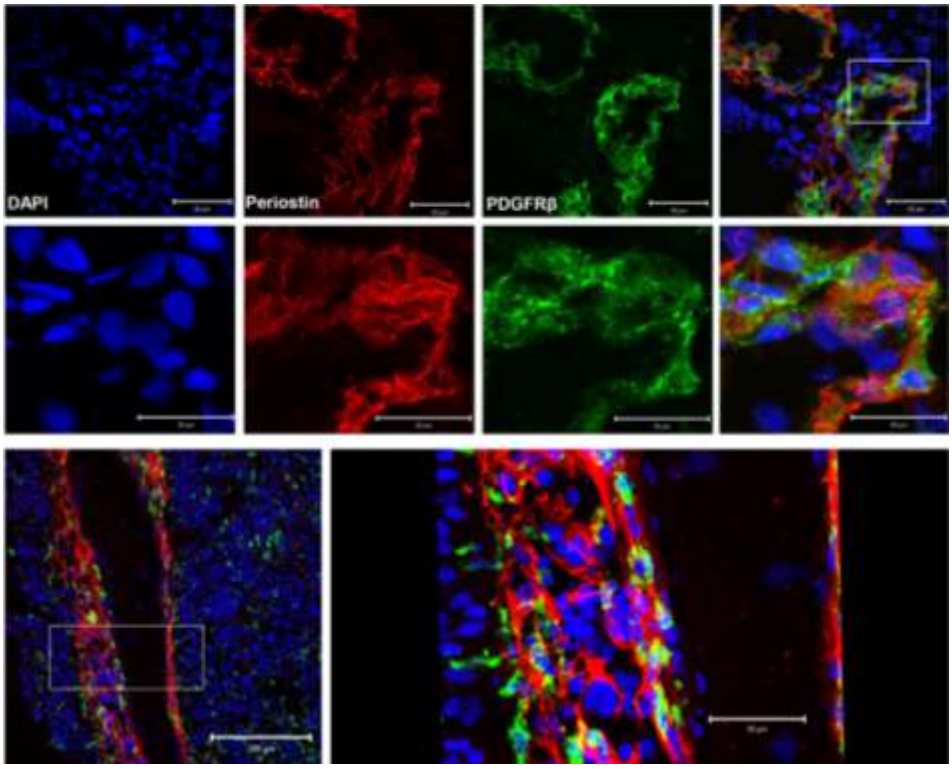

Confocal images of blood vessels in GBMs. PDGFRβ is a marker for (cerebral) pericytes. POSTN is expressed by PDGFRβ^{+} cells. Blue=DAPI (nuclear staining); Red=POSTN; Green= PDGFRβ (pericytes); merged images show that POSTN expression is localized in the pericytes.

Immunohistochemistry to the glioma stem cell markers olig-2 and Sox-2 and periostin showed only few cells positive for periostin and any of the two stem cell markers. (Figure 3).

Figure 3

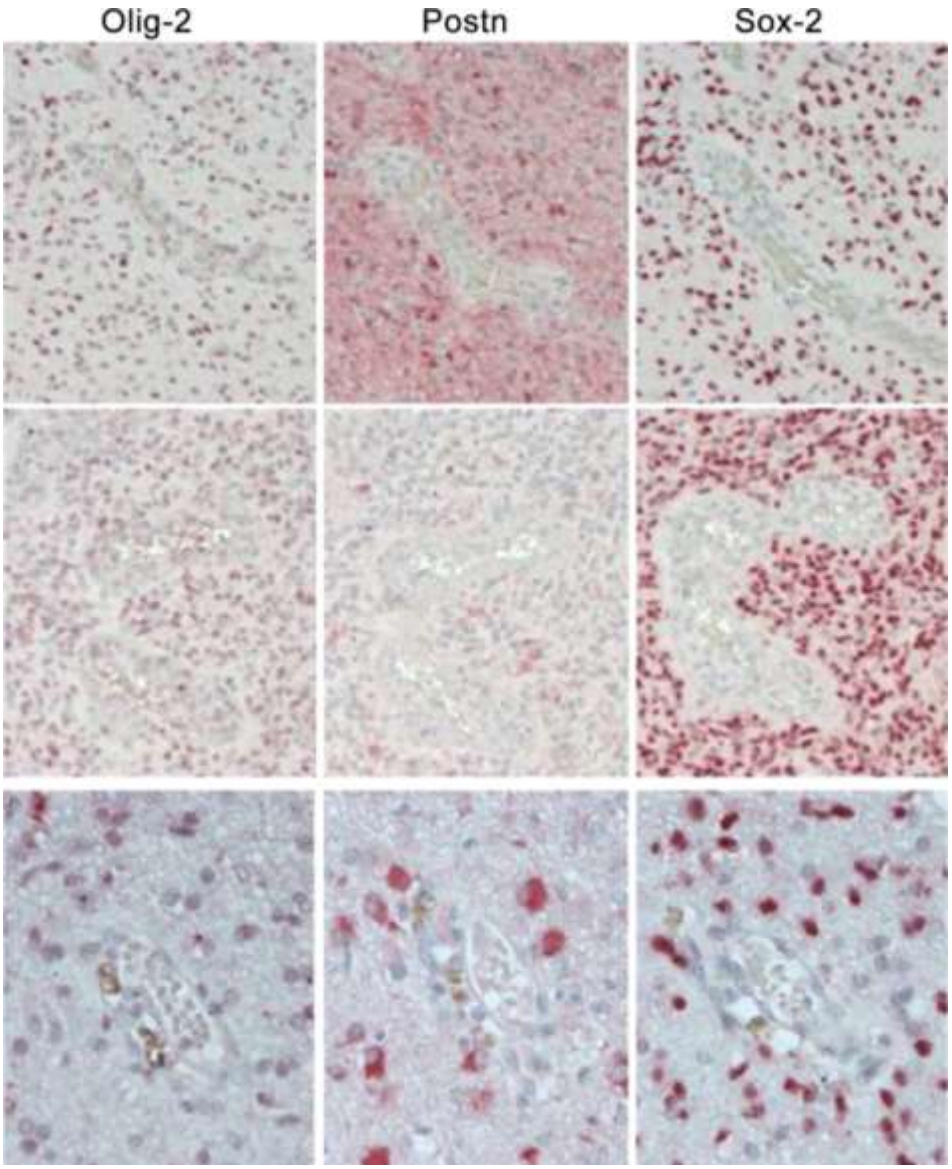

Immunohistochemical staining of GBM samples for the glioma stem cell markers Olig-2 and Sox-2 show that POSTN is not expressed by Olig-2+ / Sox-2+ cells. Very limited $POSTN^{+}$ cells express either oligo-2 or Sox-2, showing that POSTN is not expressed by stem cells in human GBMs.

In situ hybridization RNA

In situ RNA expression of periostin was found in PDGFRβ-positive cells (pericytes, Figure 4A).

Figure 4A

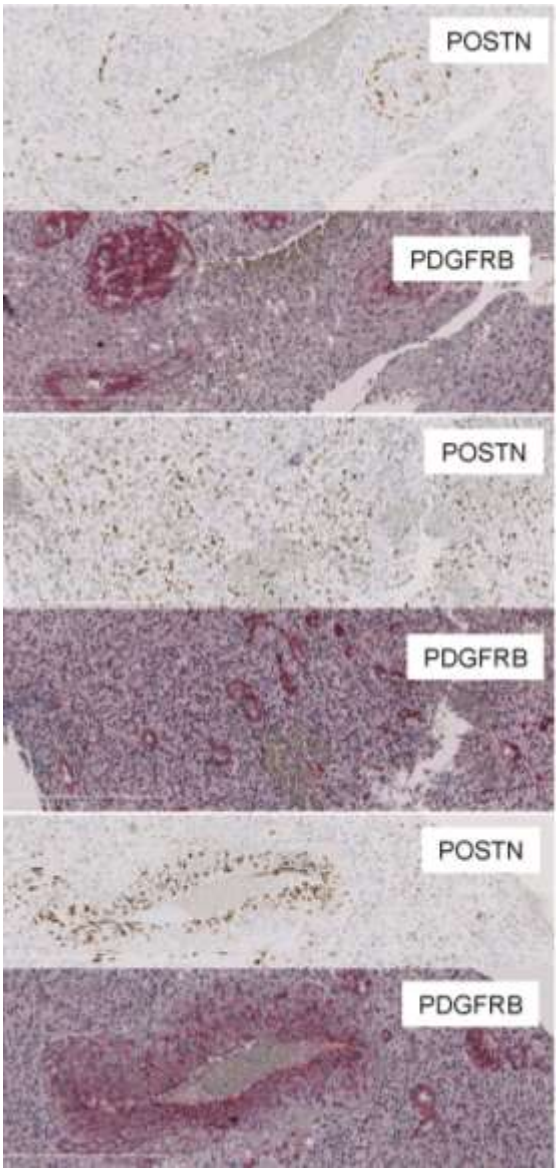

In situ RNA expression of periostin was found in the PDGFRβ^{+} pericytes. Few POSTN^{+} cells were found scattered outside the endothelial layer.

These cells were found scattered outside the endothelial layer and no co-localization of RNA in situ signal with GFAP+ astrocytic cells, or CD31+ endothelial cells was seen (Figure 4B).

Figure 4B

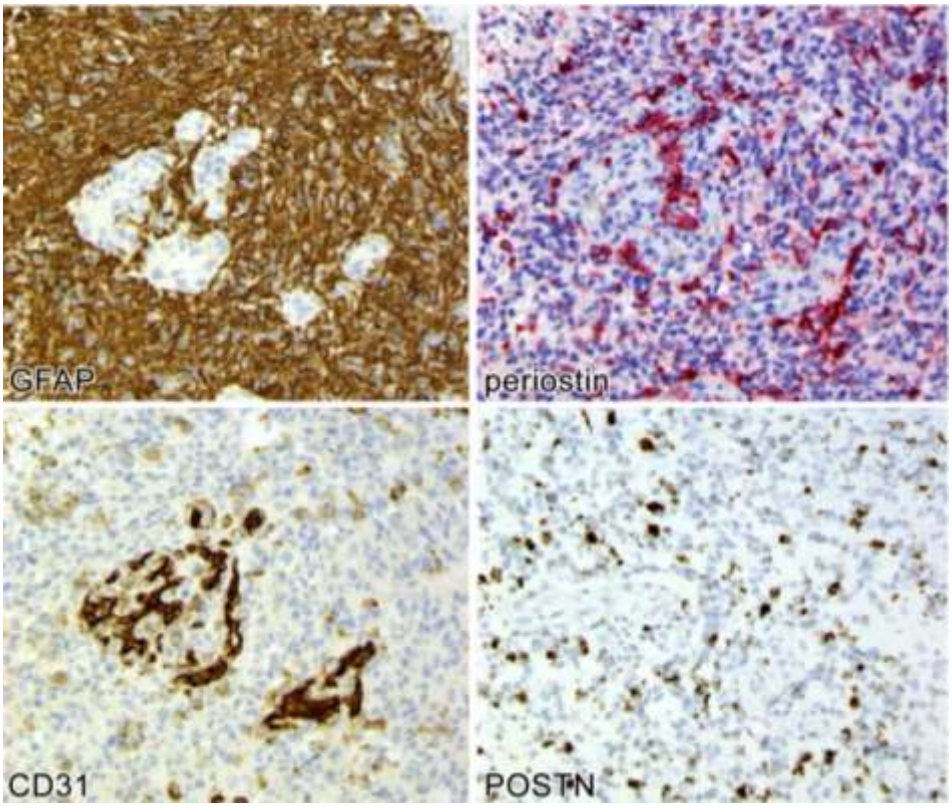

POSTN RNA in situ expression overlaps with the periostin protein (left lower and upper panels) but there is no co-localization with $CD31^{+}$ endothelial cells or GFAF+ astrocytic (tumor) cells (right lower and upper panels).

Pericytes are the main source of POSTN; in vitro results

Measurements of the expression of POSTN by RT-PCR in HUVEC, pericytes and astrocytes revealed that periostin is expressed mainly in pericytes. Based on RT-PCR results and western plot, no periostin expression was detected in HUVECs while pericytes expressed high levels of POSTN. Periostin was expressed in astroctyes but the level of expression was lower than that in pericytes (Figure 5A).

Figure 5

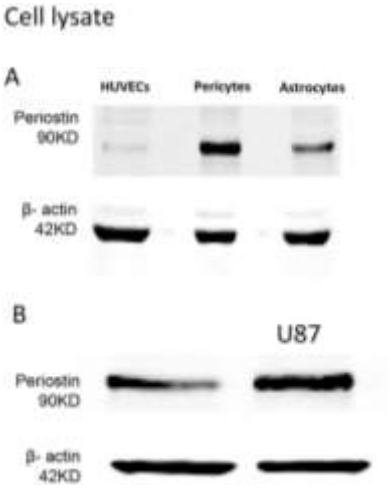

A. Western blot results: HUVECs do not express POSTN at all. The same results are confirmed by IHC and RNA in situ hybridization. β-actin was used as control to normalize POSTN expression.
B. Conditioned media of glioma cells stimulate pericytes to express higher levels of POSTN: the expression of POSTN in pericytes has increased after adding condition media of glioma cells (U87). Conditioned media of glioma cells did not stimulate HUVEC's to express POSTN: the expression of POSTN in HUVEC cells was not affected after adding condition media of glioma cells (U87) (data not shown).

Following co-culturing HUVECs and pericytes *POSTN* gene, and protein expression was low in the HUVECs, while the gene was upregulated in pericytes without protein change. However, following stimulating the co-cultures with condition media of glioma cells (U87), pericytes expressed higher levels of periostin (Figure 5B).

POSTN supports angiogenesis

Because pericytes expressed the highest level of periostin, we proceeded to silence periostin in pericytes. Silencing of POSTN was achieved by two different si RNA sequences. POSTN was successfully downregulated using siPOSTN for both sequences (n=3; mean ± S.E.M.; p , 0.005) (Suppl. Figure 1). The efficient downregulation of POSTN in cell lysates and pericyte-conditioned medium was achieved for sequence #2. Efficient

downregulation of periostin protein by using sequence #1 was only achieved in the conditioned medium, not the cell lysates.

The successful silencing of POSTN in pericytes resulted in significant attenuation of the number and length of the tubules formed, and the number of junctions the vessels formed (Figure 6A and B).

Figure 6A

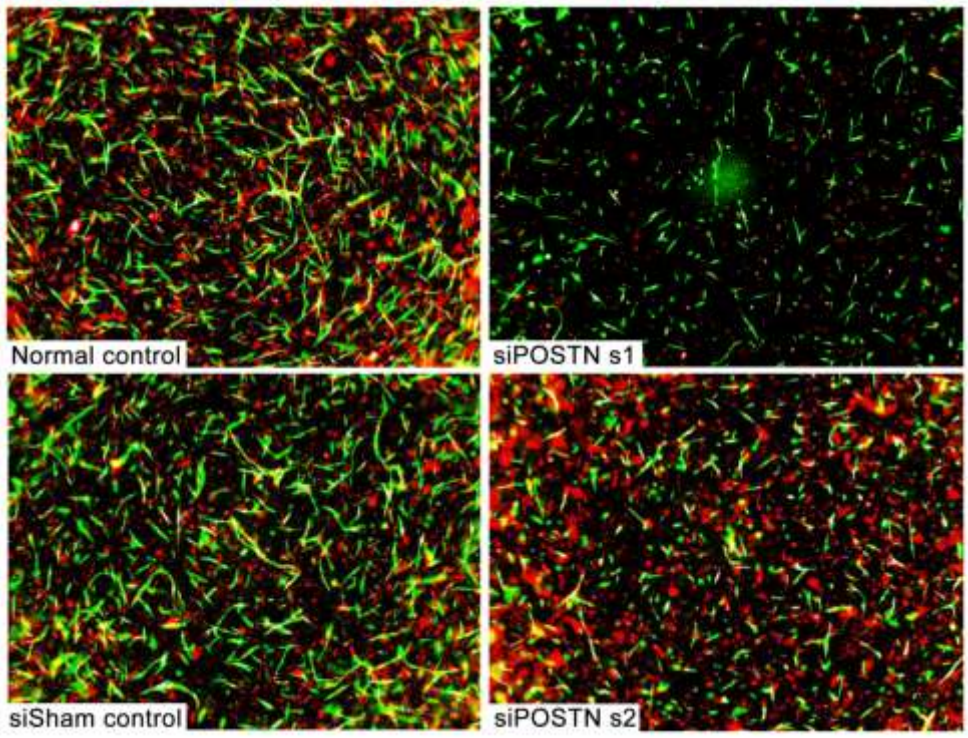

Figure 6B

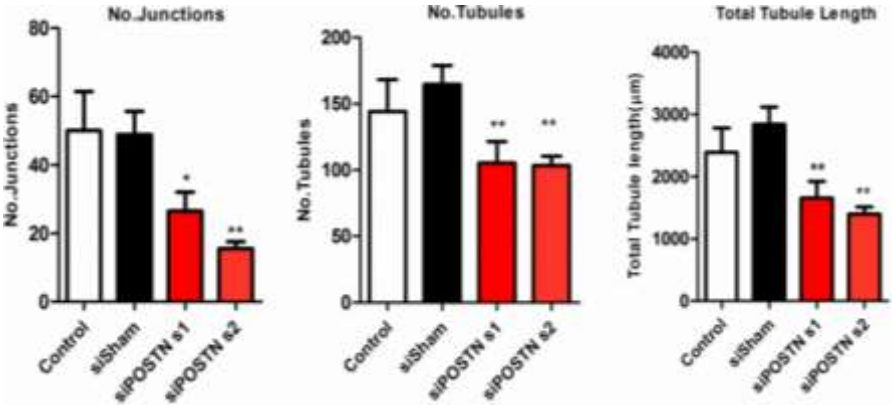

A. Silencing POSTN has a significant effect on the number and lengths of tubules and number of junctions formed in the *In vitro* 3D angiogenesis model. Green=HUVEC; Red=Pericytes; siSham=negative control for silencing; siPOSTN1 &2= Silencing POSTN in pericytes by using 2 different sequences. **B.** Angiogenesis parameters are affected by silencing POSTN: silencing POSTN affected the number of tubule formation and the length of the tubules more significantly than the number of junctions.

DISCUSSION

Periostin is a member of the TGF family of which the expression is induced by TGF-β and BMP-2 [20]. Periostin is a multifunctional matricellular protein that regulates the formation of the peridontal ligaments, the cardiac valves and acts in bone morphogenesis [21]. Further, Periostin interacts with other ECM components like tenascin-C [22] and the bone morphogenic proteins 1/2 (BMP1/2) that promote the remodeling of the extracellular matrix by promoting the secretion of fibronectin and collagen [23,24]. Periostin has been associated with cancers of the GI tract [25-27] and breast cancer. In breast and colon cancer it was shown that the expression of periostin in stromal cells is induced by tumor cells and is associated with cell proliferation, immune evasion, migration and genomic instability and decreases apoptosis of cancer cells [13, 28, 29]. Among other extracellular matrix proteins, periostin also plays a role in regulating the epithelial-mesenchymal transition (EMT) of tumor cells [30]. In breast cancer, periostin is reportedly expressed by tumor-associated fibroblast residing in the microenvironment and enhances the metastatic potential of the tumor cells [31]. Interaction between periostin and Wnt3/4 and LRP5/6 activates canonical Wnt signaling. In breast cancer periostin also promotes the resuscitation and proliferation of perivascular located tumor stem cells [32]. The N-terminal region binds to the integrins αVβ+3,αVβ5, α6β4 through its FAS domain [30] thereby stimulating the migration of tumor associated endothelial cells and tumor cells via the activation of Akt/PKB and Focal Adhesion Kinase(FAK)-mediated signaling pathways [13]. The intracellular domain of pre-NOTCH1 is recognized by periostin causing the activation of the Notch pathway [33]. Loss of Postn in the ErbB2/Neu-driven murin breast tumor model results in reduced activity of the Notch signaling pathway and deceleration of tumor growth [34].

To date, only few studies have focused on the expression of periostin in glial neoplasms [2, 35]. In a study based on data from the cancer genome atlas, upregulation of periostin expression in GBMs was associated with tumor progression and shortened survival rates [36]. Periostin secretion has been associated with human glioma cell invasion, adhesion, migration and stem cell survival, and correlates directly with glioma grade [37]. The expression of periostin in GBM is reversely related to clinical outcome (Disease free survival and overall survival). The association between the expression levels of periostin on the one hand, and glioma grade and patient survival on the other, may well be explained by the increase in angiogenesis during glioma progression. Periostin expression was reportedly found in cells of astrocytic lineage and “vascular ele-

ments" but no double labeling for GFAP or other markers was provided [37]. Although we found expression of periostin in cultured astrocytes we were unable to detect any expression in astrocytic tumor cells in the human glioma samples.

In the present study we demonstrate the specific link between periostin expression and glioma angiogenesis. Periostin has been associated with invasion of glial tumor cells and was not specifically linked to angiogenesis [16, 38]. However, periostin was associated with angiogenesis previously: it promotes angiogenesis in wound healing, vascular heart disease, and also in neoplasia [39-44]. The elevated expression levels are due to hypoxia and VEGF-driven angiogenesis [45-47]. Under hypoxic circumstances periostin promotes the incorporation of tenascin-C into the extracellular matrix serving various reparative processes [48, 49]. In addition, during breast cancer-associated angiogenesis the so-called tip cells (endothelial cells that navigate the branching of newly formed vessels) also transiently express periostin. In the GBMs included in this study we found the expression of periostin concentrated around the blood vessels and variable expression in the neuropil. The marked expression of periostin around vessels suggests that its upregulation is mediated by hypoxia, which is supported by the results of several studies [50, 51]. The extravascular expression of periostin in GBM in the present study is reminiscent of findings in ovarian carcinoma [11, 13, 14, 52], colon cancer [11, 53], pancreas carcinoma [14], breast cancer [28] and neuroblastoma [54]. The expression of periostin in GBM and PA is suggestive of involvement in the formation of vessel hypertrophy underlying vascular dysfunction. The significant difference in the expressional levels of periostin in astrocytomas grades II and III on the one hand, and GBM on the other hand, suggests that periostin plays a specific role in the genesis of vascular hypertrophy.

There is interesting recent data on the expression of periostin in a murin glioma model. It was shown that SOX-2+/Oligo-2+ glioma stem cells express periostin that, by interaction with Integrin αVβ3 recruit peripheral monocytes to the perivascular spaces where these cells subsequently differentiate into M2-like macrophages [55]. In this study we confirm predominant expression around the blood vessels. In addition, we identified the PDGFRβ+ pericytes as the source of periostin production. Although we found overlap of the immunophenotypes of these cells with the glioma stem cell profile (SOX2+/olig2+), the majority of cells producing periostin are not immunopositive for the stem cell profile. Therefore, the data indicate that the situation of periostin expression in mice is only partly recapitulated in man. In previous work [56] we found that TAMs with M2 profiles present in gliomas contribute to glioma angiogenesis by the production of CECR1. The present results obtained in the in vitro angiogenesis model reveals a role of periostin, produced by pericytes (not TAMs), in human glioma angiogenesis. The in vitro experiments show that silencing for periostin in pericytes have a negative effect on the number and length of the vascular tubules and the formation of junctions. Studies in mice have shown that by periostin secretion pro-tumoral macrophages are recruited and that periostin propagates tumor growth by suppressing the anti-tumoral functions

of the T lymphocytes [55]. Taken together, the available data point to cellular and molecular interactions in the perivascular niche that involve GSCs, pericytes, TAMs and other cells, that mediate glioma growth and angiogenesis.

Similar to periostin, integrin-αV is another molecule that not only plays a role in angiogenesis, but also in the proliferation, migration and invasion of the tumor cells [57]. In the central nervous system VEGF triggers the expression of integrin-αV by activated endothelial cells, pericytes and glial cells. The expression of integrin-αVβ3 and integrin-αVβ5 also parallels the progression from low-grade to high-grade tumors [4, 58-60]. Schnell et al. found elevated levels of integrin-αV β3 in GBM but not in low-grade gliomas[58]. Because of their prominent expression in tumor tissue and minimal expression in normal brain, tenascin-C and integrin-αV have served as therapeutic targets in phase I and II trials in GBM patients, in which blocking antibodies and RNAi have yielded modest improvements in survival [4, 61, 62]. Because of the functional connection between tenascin-C and periostin, considering the latter in the development of anti-glioma therapeutic strategies seems legitimate.

REFERENCES

1. Van Meir, E.G., et al., *Exciting new advances in neuro-oncology: the avenue to a cure for malignant glioma.* CA Cancer J Clin, 2010. **60**(3): p. 166-93.
2. Mustafa, D.A., et al., *A proteome comparison between physiological angiogenesis and angiogenesis in glioblastoma.* Mol Cell Proteomics, 2012.
3. Mustafa, D., et al., *Expression sites of colligin 2 in glioma blood vessels.* Brain Pathol, 2010. **20**(1): p. 50-65.
4. Tabatabai, G., et al., *Targeting integrins in malignant glioma.* Target Oncol, 2010. **5**(3): p. 175-81.
5. Llera, A.S., et al., *Matricellular proteins and inflammatory cells: a task force to promote or defeat cancer?* Cytokine Growth Factor Rev, 2010. **21**(1): p. 67-76.
6. Midwood, K.S. and G. Orend, *The role of tenascin-C in tissue injury and tumorigenesis.* J Cell Commun Signal, 2009. **3**(3-4): p. 287-310.
7. Orend, G., *Potential oncogenic action of tenascin-C in tumorigenesis.* Int J Biochem Cell Biol, 2005. **37**(5): p. 1066-83.
8. Hsia, H.C. and J.E. Schwarzbauer, *Meet the tenascins: multifunctional and mysterious.* J Biol Chem, 2005. **280**(29): p. 26641-4.
9. Bornstein, P. and E.H. Sage, *Matricellular proteins: extracellular modulators of cell function.* Curr Opin Cell Biol, 2002. **14**(5): p. 608-16.
10. Matsui, Y., J. Morimoto, and T. Uede, *Role of matricellular proteins in cardiac tissue remodeling after myocardial infarction.* World J Biol Chem, 2010. **1**(5): p. 69-80.
11. Bao, S., et al., *Periostin potently promotes metastatic growth of colon cancer by augmenting cell survival via the Akt/PKB pathway.* Cancer Cell, 2004. **5**(4): p. 329-39.
12. Carnemolla, B., et al., *Identification of a glioblastoma-associated tenascin-C isoform by a high affinity recombinant antibody.* Am J Pathol, 1999. **154**(5): p. 1345-52.
13. Ruan, K., S. Bao, and G. Ouyang, *The multifaceted role of periostin in tumorigenesis.* Cell Mol Life Sci, 2009. **66**(14): p. 2219-30.
14. Baril, P., et al., *Periostin promotes invasiveness and resistance of pancreatic cancer cells to hypoxia-induced cell death: role of the beta4 integrin and the PI3k pathway.* Oncogene, 2007. **26**(14): p. 2082-94.
15. Oskarsson, T. and J. Massague, *Extracellular matrix players in metastatic niches.* EMBO J, 2012. **31**(2): p. 254-6.
16. Broudy, V.C., et al., *Human umbilical vein endothelial cells display high-affinity c-kit receptors and produce a soluble form of the c-kit receptor.* Blood, 1994. **83**(8): p. 2145-52.
17. Lal, A., et al., *A public database for gene expression in human cancers.* Cancer Res, 1999. **59**(21): p. 5403-7.
18. Tso, C.L., et al., *Primary glioblastomas express mesenchymal stem-like properties.* Mol Cancer Res, 2006. **4**(9): p. 607-19.
19. Koh, W., et al., *In vitro three dimensional collagen matrix models of endothelial lumen formation during vasculogenesis and angiogenesis.* Methods Enzymol, 2008. **443**: p. 83-101.
20. Horiuchi, K., et al., *Identification and characterization of a novel protein, periostin, with restricted expression to periosteum and periodontal ligament and increased expression by transforming growth factor beta.* J Bone Miner Res, 1999. **14**(7): p. 1239-49.
21. Conway, S.J., et al., *The role of periostin in tissue remodeling across health and disease.* Cell Mol Life Sci, 2013.
22. Kii, I., et al., *Incorporation of Tenascin-C into the Extracellular Matrix by Periostin Underlies an Extracellular Meshwork Architecture.* Journal of Biological Chemistry, 2010. **285**(3): p. 2028-2039.
23. Hwang, E.Y., et al., *Structural characterization and interaction of periostin and bone morphogenetic protein for regulation of collagen cross-linking.* Biochem Biophys Res Commun, 2014. **449**(4): p. 425-31.
24. Kii, I., T. Nishiyama, and A. Kudo, *Periostin promotes secretion of fibronectin from the endoplasmic reticulum.* Biochem Biophys Res Commun, 2016. **470**(4): p. 888-93.
25. Moniuszko, T., et al., *Role of periostin in esophageal, gastric and colon cancer.* Oncol Lett, 2016. **12**(2): p. 783-787.

26. Xu, X., et al., *Periostin expression in intra-tumoral stromal cells is prognostic and predictive for colorectal carcinoma via creating a cancer-supportive niche*. 2015. 2015.
27. Sato-Matsubara, M. and N. Kawada, *New player in tumor-stromal interaction: Granulin as a novel therapeutic target for pancreatic ductal adenocarcinoma liver metastasis.* Hepatology, 2016: p. n/a-n/a.
28. Contie, S., et al., *Increased expression and serum levels of the stromal cell-secreted protein periostin in breast cancer bone metastases.* Int J Cancer, 2011. **128**(2): p. 352-60.
29. Kikuchi, Y., et al., *Periostin is expressed in pericryptal fibroblasts and cancer-associated fibroblasts in the colon.* J Histochem Cytochem, 2008. **56**(8): p. 753-64.
30. Morra, L. and H. Moch, *Periostin expression and epithelial-mesenchymal transition in cancer: a review and an update.* Virchows Arch, 2011. **459**(5): p. 465-75.
31. Malanchi, I., et al., *Interactions between cancer stem cells and their niche govern metastatic colonization.* Nature, 2012. **481**(7379): p. 85-U95.
32. Ghajar, C.M., et al., *The perivascular niche regulates breast tumour dormancy.* Nat Cell Biol, 2013. **15**(7): p. 807-17.
33. Tanabe, H., et al., *Periostin associates with Notch1 precursor to maintain Notch1 expression under a stress condition in mouse cells.* PLoS One, 2010. **5**(8): p. e12234.
34. Sriram, R., et al., *Loss of periostin/OSF-2 in ErbB2/Neu-driven tumors results in androgen receptor-positive molecular apocrine-like tumors with reduced Notch1 activity.* Breast Cancer Res, 2015. **17**: p. 7.
35. Formolo, C.A., et al., *Secretome signature of invasive glioblastoma multiforme.* J Proteome Res, 2011. **10**(7): p. 3149-59.
36. Zinn, P.O., et al., *Radiogenomic mapping of edema/cellular invasion MRI-phenotypes in glioblastoma multiforme.* PLoS One, 2011. **6**(10): p. e25451.
37. Mikheev, A.M., et al., *Periostin is a novel therapeutic target that predicts and regulates glioma malignancy.* Neuro-Oncology, 2015. **17**(3): p. 372-382.
38. Formolo, C.A., et al., *Secretome Signature of Invasive Glioblastoma Multiforme.* J Proteome Res, 2011.
39. Hill, J.J., et al., *Identification of Vascular Breast Tumor Markers by Laser Capture Microdissection and Label-Free LC-MS.* J Proteome Res, 2011. **10**(5): p. 2479-93.
40. Hakuno, D., et al., *Periostin advances atherosclerotic and rheumatic cardiac valve degeneration by inducing angiogenesis and MMP production in humans and rodents.* J Clin Invest, 2010. **120**(7): p. 2292-306.
41. Zhu, M., et al., *Periostin promotes ovarian cancer angiogenesis and metastasis.* Gynecol Oncol, 2010. **119**(2): p. 337-44.
42. Takanami, I., T. Abiko, and S. Koizumi, *Expression of periostin in patients with non-small cell lung cancer: correlation with angiogenesis and lymphangiogenesis.* Int J Biol Markers, 2008. **23**(3): p. 182-6.
43. Roy, S., et al., *Transcriptome-wide analysis of blood vessels laser captured from human skin and chronic wound-edge tissue.* Proc Natl Acad Sci U S A, 2007. **104**(36): p. 14472-7.
44. Gillan, L., et al., *Periostin secreted by epithelial ovarian carcinoma is a ligand for alpha(V)beta(3) and alpha(V)beta(5) integrins and promotes cell motility.* Cancer Res, 2002. **62**(18): p. 5358-64.
45. Liang, X., et al., *Molecular pathology and CXCR4 expression in surgically excised retinal hemangioblastomas associated with von Hippel-Lindau disease.* Ophthalmology, 2007. **114**(1): p. 147-56.
46. Takagi, Y., et al., *Expression of thioredoxin-1 and hypoxia inducible factor-1alpha in cerebral arteriovenous malformations: Possible role of redox regulatory factor in neoangiogenic property.* Surg Neurol Int, 2011. **2**: p. 61.
47. Zhu, Y., et al., *In vitro characterization of the angiogenic phenotype and genotype of the endothelia derived from sporadic cerebral cavernous malformations.* Neurosurgery, 2011. **69**(3): p. 722-31; discussion 731-2.
48. Kudo, A., *Periostin in fibrillogenesis for tissue regeneration: periostin actions inside and outside the cell.* Cell Mol Life Sci, 2011. **68**(19): p. 3201-7.
49. Kii, I., et al., *Incorporation of tenascin-C into the extracellular matrix by periostin underlies an extracellular meshwork architecture.* J Biol Chem, 2010. **285**(3): p. 2028-39.
50. Shimamura, M., et al., *Role of central nervous system periostin in cerebral ischemia.* Stroke, 2012. **43**(4): p. 1108-14.

51. Ouyang, G., et al., *Upregulated expression of periostin by hypoxia in non-small-cell lung cancer cells promotes cell survival via the Akt/PKB pathway.* Cancer Lett, 2009. **281**(2): p. 213-9.
52. Choi, K.U., et al., *Lysophosphatidic acid-induced expression of periostin in stromal cells: Prognoistic relevance of periostin expression in epithelial ovarian cancer.* Int J Cancer, 2011. **128**(2): p. 332-42.
53. Ben, Q.W., et al., *Circulating levels of periostin may help identify patients with more aggressive colorectal cancer.* Int J Oncol, 2009. **34**(3): p. 821-8.
54. Sasaki, H., et al., *Expression of the periostin mRNA level in neuroblastoma.* J Pediatr Surg, 2002. **37**(9): p. 1293-7.
55. Zhou, W., et al., *Periostin secreted by glioblastoma stem cells recruits M2 tumour-associated macrophages and promotes malignant growth.* Nat Cell Biol, 2015. **17**(2): p. 170-82.
56. Zhu, C., et al., *Activation of CECR1 in M2-like TAMs promotes paracrine stimulation-mediated glial tumor progression.* Neuro Oncol, 2017.
57. Weis, S.M. and D.A. Cheresh, *alphav Integrins in Angiogenesis and Cancer.* Cold Spring Harb Perspect Med, 2011. **1**(1): p. a006478.
58. Schnell, O., et al., *Expression of integrin alphavbeta3 in gliomas correlates with tumor grade and is not restricted to tumor vasculature.* Brain Pathol, 2008. **18**(3): p. 378-86.
59. D'Abaco, G.M. and A.H. Kaye, *Integrins: molecular determinants of glioma invasion.* J Clin Neurosci, 2007. **14**(11): p. 1041-8.
60. Hashimoto, T., et al., *Gene microarray analysis of human brain arteriovenous malformations.* Neurosurgery, 2004. **54**(2): p. 410-23; discussion 423-5.
61. Rolle, K., et al., *Promising human brain tumors therapy with interference RNA intervention (iRNAi).* Cancer Biol Ther, 2010. **9**(5): p. 396-406.
62. Reardon, D.A., M.R. Zalutsky, and D.D. Bigner, *Antitenascin-C monoclonal antibody radioimmunotherapy for malignant glioma patients.* Expert Rev Anticancer Ther, 2007. **7**(5): p. 675-87.

SUPPLEMENTAL FIGURES

Suppl. Figure 1

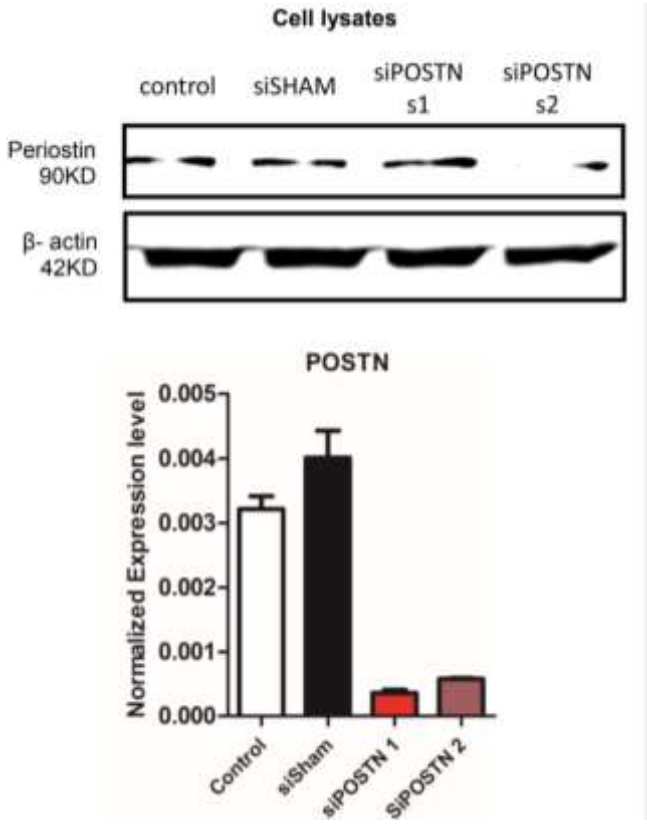

(upper part): RT-PCR results of siPOSTN: The differences of the expression levels of POSTN in the cell lysates indicate successful silencing at the RNA level for both probes used. **(lower part):** Western blotting of the cell lysates for periostin following siPOSTN shows that probe #2 yielded better silencing results than probe #1d.

Suppl. Figure 2

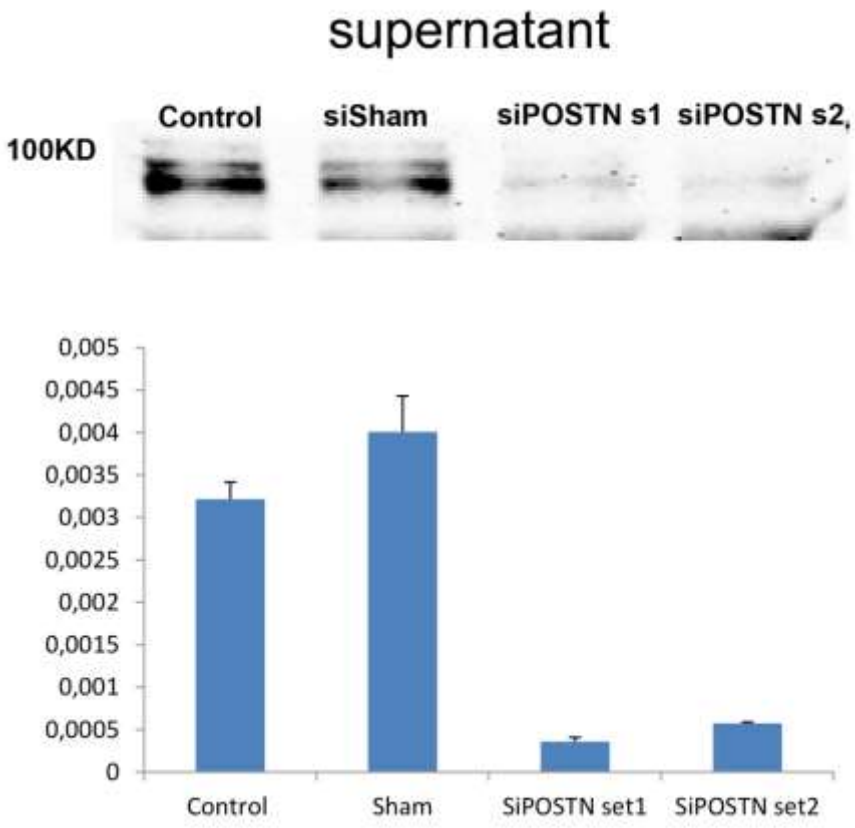

(Upper panel): RT-PCR results of siPOSTN: The differences of the expression levels of the secreted POSTN in the supernatant show a successful silencing at the RNA level for both probes used. **(Lower panel):** Western blotting results of siPOSTN: The secreted protein expressions of POSTN reveal successful silencing using both siPOSTN probes.

Chapter 6

Proteome analysis of the CECR1 mediated response in tumor associated macrophages identifies key pathways and molecules in the immune response regulation of glioma

Changbin Zhu, M.D. M.Sc.; Dana Mustafa, Ph.D; Ihsan Chrifi B.A.Sc., Lennard Dekker, Ph.D.; Pieter J.M. Leenen, Ph.D.; Dirk J. Duncker, M.D., Ph.D.; Theo M. Luider, Ph.D.; Johan M. Kros, M.D., Ph.D.*; Caroline Cheng Ph.D.* (* equal contribution of last authors)

(Submission in prep.)

ABSTRACT

Introduction: Tumor associated macrophages (TAMs) promote tumor development, angiogenesis and distal metastasis. In previous studies, we showed that Eye Syndrome Critical Region Protein 1(CECR1) is expressed by M2-like TAMs in glioma and promotes M2 TAMs differentiation, affecting tumor cell proliferation and migration. Here we investigated the proteomic profile of TAMs expressing CECR1.

Methods: THP-1 macrophages were siRNA silenced for CECR1 *in vitro*, with or without stimulation by glioma (U87) cells. Lysates were analyzed by (nano)LC-MS. Significant altered protein levels were identified ($P<0.05$), followed by pathway annotation (STRING, IPA and Cytoscape).

Results: CECR1 silencing upregulated 67 proteins in THP1-derived macrophages. Pathway annotation mapped this set to 3 major pathways relevant to macrophage functions, including MHCI antigen presentation, phagosome maturation and endocytosis. Stimulation by U87 cells attenuated the changes that were observed on protein and mRNA levels in response to CECR1 silencing. LAT2 was upregulated by CECR1 knockdown in U87 co-cultured macrophages and was associated with a IL-10^{low}, IL-12^{high} M1-like phenotype. CECR1 silencing also downregulated S20 proteasome complex proteins PSMA5, PSMA7, PSMC6 and PSMD8 in the U87 coculture conditions. This protein profile was linked to a low proliferation rate of CECR1-silenced TAMs. Overlap analysis identified S100A9 and PLAU as CECR1-related proteins that were significantly correlated with expression of CECR1 and macrophage lineage markers in three large public GBM datasets.

Conclusion: This study reports the molecular pathways and key molecules that are mediated by CECR1 function in macrophages and TAMs in glioma.

INTRODUCTION

Glial tumors are highly heterogeneous in cell composition and are located in the immune privileged environment of the central nervous system, limiting effective therapies. In glioblastoma multiforme (GBM), mesenchymal cells with macrophage or microglia characteristics can comprise up to 40% of all local cells (REF: PMC4373835). Macrophages are a major component of the innate immune system[1], contributing to early pathogen recognition, removal and presentation[2,3]. Displaying relatively high plasticity, macrophages can adapt to the local microenvironments by differentiating into subphenotypes with various functions[5,6]. In classic immunology, for simplicity of study, phenotypes of macrophages are usually put into the perspective of the M1 and M2 spectrum[7]. In the microenvironment of malignant tumors, recruited monocytes predominantly differentiate into tumor-associated macrophages (TAMs), that typically exhibit an M2-like macrophage phenotype. M2-like TAMs are characterized by higher expression levels of cell surface markers CD163, CD204, CD206, and CSFR1. In addition, M2-like TAMs secrete higher levels of IL-10, CCL18, TGF-β, and COX-2[4]. This paracrine profile mainly induces local immune-suppression by inhibiting infiltration of CD8+ T cells and promoting activation of the regulatory T cells population[11]. TAMs also promote tumor angiogenesis via secretion of pro-angiogenic factors and enzymes like VEGFA, VEGFC, PDGFB, PDGFC, uPA, FGF, Cathepsin and MMPs[12,13]. In breast, prostate, bladder and cervical cancers, the presence of M2-like TAMs tumors is therefore strongly associated with immunosuppressive action and dismal prognosis[8-10]. In glioma a significant higher number of TAMs are observed in high-grade tumors that is associated with increased vascular density of the tumor tissue.

An improved understanding of the molecular regulators of M2-like TAMs will ease the identification of new drug targets in the treatment of GBM and other types of malignant tumors. In previous studies on diffuse gliomas we have examined the function of cat eye syndrome critical region 1 (CECR1), a conserved molecule that is highly expressed in the macrophage lineage[15]. CECR1 reportedly functions as a growth factor and immune regulator through its adenosine deaminase enzymatic activity as well as by direct binding to adenosine receptors in invertebrate and vertebrate[16,17,18]. More specifically, CECR1 binds with adenosine receptors and functions as a growth factor for monocytes and T lymphocytes via autocrine and paracrine stimulation[19]. In monocytes, CECR1 was also shown to promote monocyte differentiation (PMID:20453107). In a recent genetic study, loss-of-function mutations in CECR1 were shown to be associated with a range of vascular and inflammatory phenotypes in patients with syndromic presentations of early-onset stroke, systemic vasculopathy and auto-inflammatory diseases (PMID 24552284). The cytokine profile of patient-derived CECR1 gene deficient macrophages demonstrated a predominant M1-like pro-inflammatory phenotype[20,21]. Our previous findings reported increased expression of CECR1 in TAMs of gliomas, and provided causal evidence that CECR1 is vital for promoting TAM differentiation towards

an M2-like (immune-suppressive) phenotype (REF). Furthermore, we demonstrated that CECR1 functions as an oncogenic molecule that enhances glioma proliferation, migration and angiogenesis via direct crosstalk between TAMs, glial cells and vascular cells.

Although these studies have improved our understanding of CECR1 function in TAMs, the complex intracellular molecular mechanisms in macrophages that are mediated by CECR1 remain to be further elucidated. In this study we aimed to define the function of CECR1 in TAMs by a proteomics approach. We identified key CECR1 regulated molecules and pathways in normal macrophages and TAMs that are activated by glial tumor cells.

MATERIAL AND METHODS

Cell Culture

The human monocytic cell line, THP-1 cells were obtained from the department of Hematology, Erasmus Medical Center, Rotterdam. THP-1 cells were cultured in RPMI-1640 medium supplemented with 10% fetal bovine serum (FBS) and 1% Penicillin/Streptomycin. THP-1 macrophage differentiation was induced by stimulating with PMA (Sigma, Sweden) for 48 hours at the concentration of 100 ng/ml. The human GBM cell line U87 was purchased from ATCC (USA) and maintained in DMEM with 10% FBS and 1% Penicillin/Streptomycin.

siRNA Transfection

A mix of four siRNA sequences that target CECR1 mRNA (5'-GUGCCAAAGGCUUGUCCUA-3',5-CUUCCACGCCGGAGAAACA-3', 5'-GCCCAAAGCUAGUUAGUAC-3', 5'-UCGCAGAAUCCAUCCGAAU-3') and scrambled non-targeting siRNAs (5'-UGGUUUACAUGUCGACUAA-3', 5'-UGGUUUACAUGUUGUGUGA-3', 5'-UGGUUUACAUGUUUUCUGA-3', UGGUUUACAUGUUUUCCUA-3') were obtained from Dharmacon (GE health care, Netherland). THP-1 derived macrophage cultures were transfected after 48 hours of PMA treatment, following the manufacture's protocol (using Dharmacon transfection reagent). Efficiency of CECR1 knockdown was assessed after 24 and 48 hours at transcriptional level and protein level. For co-culture experiments siRNA transfected cells were used 24 hours post transfection.

Co-Culture

100,000 U87 cells were seeded on top of the culture inserts with a pore size of 0.4µm (Fisher Scientific, USA). SiRNA transfected macrophages were seeded into the lower chamber in 6-well plates. Macrophages were co-cultured with U87 cells in ~~serum-free~~

RPMI-1640 medium for 48 hours and 96 hours for RNA and protein isolation respectively. Real-time qPCR and proteomic analysis were performed after 48 hours and 96 hours post co-culturing respectively. Macrophages without U87 cell co-culture were harvested 48 hours and 96 hours post transfection for qPCR and proteomic measurement respectively (Figure 1).

Figure 1 Schematic illustration of study design and work flow

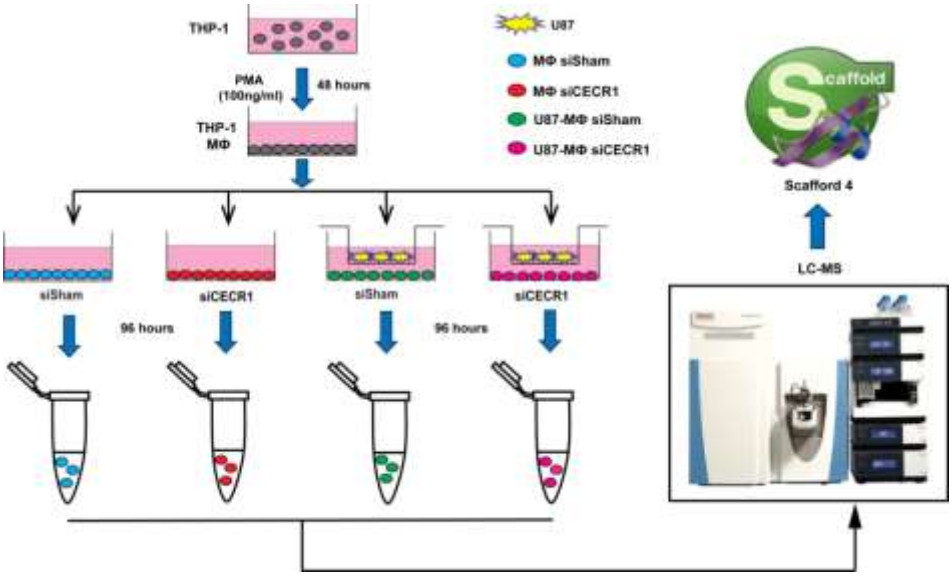

Human monocytic cell line THP-1 cells were differentiated into macrophage by PMA (100ng/ml) for 48 hours followed by siRNA transfection, non-targeted, scramble siSham as transfection control. At the same time, glioblastoma cell line U87 was co-cultured with macrophage with/without CECR1 silencing. After 96 hours' incubation, cell lysates of these macrophages were harvested and analyzed by nano-LC/MS. Raw data was imported into Scafford 4 and further exported into Excel sheet for further analysis.

Proteomics analysis

Macrophage cell pellets were harvested and 150 µl of RapiGest (Waters Corporation, Milford, MA) in 50 mM NH4HCO3 was added to each sample. Samples were sonificated for 4 min at 70% amplitude at a maximum temperature of 25 °C (Branson, Ultrasonic, Danbury, CT). The proteins were reduced with 10 mM dithiothreitol (DTT) at 60°C for 30 min. After the mixture was cooled down to room temperature, it was alkylated in the dark with 50 mM iodoacetamide at ambient temperature for 30 min, and digested overnight with 5 µl trypsin (Promega, Madison, WI). To inactivate trypsin and to degrade the RapiGest, 2 µl of 50% TFA was added and samples were subsequently incubated for 30 minutes at 37°C. Samples were centrifuged at maximum speed for 15 min at 4°C and the supernatants were transferred to LC vials to be measured on the LC-MS.

The digested samples were measured on a nano-LC (Thermo Fisher Scientific, Germering, Germany).

Raw data from proteomics measurements was imported into Scaffold 4 followed by export in Excel sheet format. Total unique peptide count per peptide in each group was compared by student's T-Test. Proteins were considered differentially expressed when $P<0.05$.

RNA isolation and Real time qPCR

Total RNA was isolated from macrophages using RNA isolation kit (bio-line, USA) and reversely synthesized into cDNA using Sensi-fast cDNA synthesis kit (Bio-line, USA) following manufacture's protocol. QPCR was performed by assessment of Syber Green signal using CFX96 Touch™ Real-Time PCR Detection System (Bio-rad, USA). Transcripts of CECR1, S100A9, PLAU, CTSH, HLA-A, HLA-C, ITGB7, WDFY, EVL, SEPT7, IL-10, IL-12p35 were measured and normalized to β-actin (Primers for all targets are shown in Supplementary table 1)

MTT Assay

THP-1 macrophages were transfected with siSham and siCECR1. The following day transfected macrophages were seeded in 96-well plates at a density of 5000 cells/well. Macrophages were treated by U87 derived conditioned medium. Macrophages without U87 conditioned medium treatment were measured at the same day as a reference measurement. Macrophage proliferation was monitored for the next five days using MTT, 3-(4,5-dimethylthiazol-2-yl)-2,5-diphenyltetrazolium bromide (Sigma, Sweden), which was added at a concentration of 0.45 mg/ml to each well. After 4 hours of incubation, the MTT signals were measured by spectrometry at the 570 nm absorbance wave length.

Western Blot

20 µg of total protein was loaded onto a 10% SDS-PAGE gel and blotted to Nitro cellulose membranes followed by incubation with block buffer (Licor Bioscience, USA). Protein levels were assessed by immunoblotting using specific antibodies against LAT2 (Cell Signaling Technology, 1:1000), and β-actin (Abcam, 1:500) as a loading control, followed by incubation with secondary antibodies (IRdye 680 CW, IRDye 800 CW, Licor Bioscience, USA) and detection of signals using the Odyssey imaging system (Licor Bioscience, USA).

Immunofluorescent staining

Macrophages silenced for CECR1 versus sisham-transfected controls were treated with U87 conditioned medium for 48 hours. Macrophages were fixed in 4%PFA for 15 min. Cells were permeabilized followed by a blocking step. Primary antibodies against CECR1(Sigma, 1:200), Ki67(Dako 1:200), and secondary antibodies were applied to detect expression of target proteins. 10 areas were randomly selected and pictures were taken under the confocal microscope (Zeiss, The Netherlands). The number of Ki67 positive cells was counted in each image view.

Bioinformatics

Raw data generated by Scaffold 4 was exported into Excel. Significantly expressed proteins were enriched in biological process pathways and KEGG pathways by STRING database(http://string-db.org/). Proteins that were not significantly changed were imported as background molecules and mapped into canonical pathways together with significantly expressed proteins using Ingenuity Pathway Analysis (Qiagen, USA). Proteins mapped into Canonical Pathways were exported, and networks were generated by STRING online software. Information from each network were exported and visualized using Cytoscape 3.3. Mutual expressed proteins were identified and visualized by Venne Graph (http://bioinformatics.psb.ugent.be/webtools/Venn/). Correlation analysis was performed using the TCGA GBM database via the c-Bioportal provided by the Memorial Sloan-Kettering Cancer Center. Calculated Pearson and Spearman correlation coefficiencies were used to generate Heat maps using Excel.

Statistics

Unique peptides from the proteomic analysis were compared per group in each experiment and analyzed using unpaired two-tailed students' T-Test. Proteins were considered significantly differentially expressed when $P<0.05$. All *in vitro* data were tested using unpaired two-tailed student's T test (Significance levels $P<0.05$). All data are presented in Mean ± S.E.M. unless otherwise stated.

RESULTS

Changes in proteomic profile of THP-1 macrophages in response to CECR1 silencing

For proteomics analysis, CECR1 was silenced in THP-1 macrophages for 96 hours. The efficiency of CECR1 silencing was assessed by immunofluorescence of the CECR1 signal in siCECR1 treated macrophages compared with non-targeting scrambled siRNA (si-sham) transfected control macrophages (Supplementary figure 1). Protein lysates derived from CECR1-silenced versus sisham treated macrophages were analyzed by mass spectrometry (Figure 2a). In total, protein levels of 102 proteins were affected by CECR1 silencing (Supplementary table 2,3). 35 proteins were down-regulated (more enriched in sisham group), and 67 proteins were upregulated in the CECR1-silenced group (more enriched in the siCECR1 group (Figure 2b).

Gene ontology analysis indicated that these 35 down-regulated proteins were enriched in pathways like “protein folding”, “translation”, and “peptide metabolic process” (Figure 2c). The 67 proteins upregulated were enriched in several Gene Ontology and KEGG pathways and cell mechanisms including ”Antigen processing and presentation of exogenous peptide antigen via MHC class I”, “type I interferon signaling pathway” as well as “Phagosome” (Figure 2d, e).

For more in depth analysis, proteins which were not significantly affected by CECR1 silencing were analyzed together with the 67 upregulated proteins, using Ingenuity Pathway Analysis (IPA). Retrieved networks include “MHC I Antigen Presenting”, “Phagosome maturation” and “Caveolin mediated endocytosis”. These networks and detailed information of protein components of each network of are presented in Figure 3a, b, c; Table 1-3. Among the 67 proteins that were upregulated in the CECR1 silenced condition, 15 proteins including HLA-A, B, C, TAPBP, TAP1, ISG15, ELAVL1 and CTSS were predicated to be downstream targets of IFN-γ signaling (Figure 3d). Together these data indicate that CECR1 in normal macrophages are involved in regulating MHCI antigen presentation, phagosome maturation, caveolin mediated endocytosis, and IFNγ regulated signaling.

Table 1. Proteins in MΦ siCECR1 mapped to Antigen Presenting Pathway by IPA

UniProt	Symbol	Entrez Gene Name	Location	Type(s)	Fold Change	P-Value
P30501	HLA-C	major histocompatibility complex. class I. C	Plasma Membrane	other	8	0.001
Q03518	TAP1	major transporter 1. ATP- binding cassette. sub-family B (MDR/TAP)	Cytoplasm	transporter	1.500038989	0.006
P01892	HLA-A	histocompatibility complex. class I. A	Plasma Membrane	other	1.2397077	0.007
Q03519	TAP2	transporter 2. ATP- binding cassette. sub-family B (MDR/TAP)	Cytoplasm	transporter	1.500038989	0.008
P27797	CALR	calreticulin	Cytoplasm	transcription regulator	1.135242102	0.01
O15533	TAPBP	TAP binding protein (tapasin)	Cytoplasm	transporter	1.333298677	0.023
P10319	HLA-B	major histocompatibility complex. class I. B	Plasma Membrane	transmembrane receptor	1.275444392	0.035
P28062	PSMB8	proteasome subunit beta 8	Cytoplasm	peptidase	1.143138335	0.067
P28065	PSMB9	proteasome subunit beta 9	Cytoplasm	peptidase	0.833353207	0.37
P61769	B2M	beta-2- microglobulin	Plasma Membrane	transmembrane receptor	1	0.42
P30101	PDIA3	protein disulfide isomerase family A member 3	Cytoplasm	peptidase	1.07549439	0.43
P28072	PSMB6	proteasome subunit beta 6	Nucleus	peptidase	0.799960128	0.52
P27824	CANX	calnexin	Cytoplasm	other	0.967947027	0.6

Table 2

UniProt	Symbol	Entrez Gene Name	Location	Type(s)	Fold Change	P-Value
P30501	HLA-C	major histocompatibility complex. class I. C	Plasma Membrane	other	8.33	0.001
P54920	NAPA	NSF attachment protein alpha	Cytoplasm	transporter	1.83	0.005
Q03518	TAP1	transporter 1. ATP-binding cassette. sub-family B (MDR/TAP)	Cytoplasm	transporter	1.50	0.006
P01892	HLA-A	major histocompatibility complex. class I. A	Plasma Membrane	other	1.24	0.007
Q13488	TCIRG1	T-cell immune regulator 1. ATPase H+ transporting V0 subunit a3	Plasma Membrane	enzyme	1.33	0.007
P27797	CALR	calreticulin	Cytoplasm	transcription regulator	1.14	0.01
Q06830	PRDX1	peroxiredoxin 1	Cytoplasm	enzyme	0.91	0.029
P46459	NSF	N-ethylmaleimide sensitive factor	Cytoplasm	transporter	1.17	0.031
P10319	HLA-B	major histocompatibility complex. class I. B	Plasma Membrane	transmembrane receptor	1.28	0.035
P51148	RAB5C	RAB5C. member RAS oncogene family	Cytoplasm	enzyme	1.33	0.055
P20645	M6PR	mannose-6-phosphate receptor. cation dependent	Cytoplasm	transporter	2.00	0.089
P11279	LAMP1	lysosomal associated membrane protein 1	Plasma Membrane	other	1.20	0.12
P30041	PRDX6	peroxiredoxin 6	Cytoplasm	enzyme	0.85	0.12
Q71U36	TUBA1A	tubulin alpha 1a	Cytoplasm	other	0.81	0.12
Q93050	ATP6V0A1	ATPase H+ transporting V0 subunit a1	Cytoplasm	transporter	2.64	0.13
P38606	ATP6V1A	ATPase H+ transporting V1 subunit A	Plasma Membrane	transporter	0.85	0.18
Q14204	DYNC1H1	dynein cytoplasmic 1 heavy chain 1	Cytoplasm	peptidase	0.79	0.19
Q13509	TUBB3	tubulin beta 3 class III	Cytoplasm	other	0.95	0.19
Q9UI12	ATP6V1H	ATPase H+ transporting V1 subunit H	Cytoplasm	transporter	0.81	0.23
Q13409	DYNC1I2	dynein cytoplasmic 1 intermediate chain 2	Cytoplasm	other	0.70	0.25
P36543	ATP6V1E1	ATPase H+ transporting V1 subunit E1	Cytoplasm	transporter	1.83	0.28
Q9BUF5	TUBB6	tubulin beta 6 class V	Cytoplasm	other	1.57	0.34
Q15904	ATP6AP1	ATPase H+ transporting accessory protein 1	Cytoplasm	transporter	0.60	0.37

UniProt	Symbol	Entrez Gene Name	Location	Type(s)	Fold Change	P-Value
P63167	DYNLL1	dynein light chain LC8-type 1	Cytoplasm	other	0.50	0.37
P13473	LAMP2	lysosomal associated membrane protein 2	Plasma Membrane	enzyme	0.90	0.37
Q15836	VAMP3	vesicle associated membrane protein 3	Plasma Membrane	other	0.50	0.37
P68371	TUBB4B	tubulin beta 4B class IVb	Cytoplasm	other	0.96	0.41
P61769	B2M	beta-2-microglobulin	Plasma Membrane	transmembrane receptor	1.00	0.42
P21283	ATP6V1C1	ATPase H+ transporting V1 subunit C1	Cytoplasm	transporter	0.86	0.52
Q9BQE3	TUBA1C	tubulin alpha 1c	Cytoplasm	other	0.98	0.52
P07437	TUBB	tubulin beta class I	Cytoplasm	other	0.96	0.59
P27824	CANX	calnexin	Cytoplasm	other	0.97	0.6
P68366	TUBA4A	tubulin alpha 4a	Cytoplasm	other	0.97	0.62
P30044	PRDX5	peroxiredoxin 5	Cytoplasm	enzyme	1.00	0.64
P61421	ATP6V0D1	ATPase H+ transporting V0 subunit d1	Cytoplasm	transporter	1.06	0.74
P51149	RAB7A	RAB7A. member RAS oncogene family	Cytoplasm	enzyme	1.06	0.91
P21281	ATP6V1B2	ATPase H+ transporting V1 subunit B2	Cytoplasm	transporter	1.05	1

Table 3

UniProt	Symbol	Entrez Gene Name	Location	Type(s)	Fold Change	P-Value
P30501	HLA-C	major histocompatibility complex. class I. C	Plasma Membrane	other	8.33	0.001
P26010	ITGB7	integrin subunit beta 7	Plasma Membrane	transmembrane receptor	4.33	0.001
P01892	HLA-A	major histocompatibility complex. class I. A	Plasma Membrane	other	1.24	0.007
P10319	HLA-B	major histocompatibility complex. class I. B	Plasma Membrane	transmembrane receptor	1.28	0.035
P05556	ITGB1	integrin subunit beta 1	Plasma Membrane	transmembrane receptor	1.19	0.05
P51148	RAB5C	RAB5C. member RAS oncogene family	Cytoplasm	enzyme	1.33	0.055
P11215	ITGAM	integrin subunit alpha M	Plasma Membrane	transmembrane receptor	1.29	0.074
P35606	COPB2	coatomer protein complex subunit beta 2	Cytoplasm	transporter	1.50	0.081
P20702	ITGAX	integrin subunit alpha X	Plasma Membrane	transmembrane receptor	1.17	0.1
P53621	COPA	coatomer protein complex subunit alpha	Cytoplasm	transporter	1.25	0.12
P38570	ITGAE	integrin subunit alpha E	Plasma Membrane	other	2.33	0.12
P61923	COPZ1	coatomer protein complex subunit zeta 1	Cytoplasm	transporter	0.43	0.13
O14579	COPE	coatomer protein complex subunit epsilon	Cytoplasm	transporter	0.77	0.19
Q9Y678	COPG1	coatomer protein complex subunit gamma 1	Cytoplasm	transporter	1.00	0.23
P18031	PTPN1	protein tyrosine phosphatase. non-receptor type 1	Cytoplasm	phosphatase	1.18	0.23
O75955	FLOT1	flotillin 1	Plasma Membrane	other	1.43	0.24
P60709	ACTB	actin. beta	Cytoplasm	other	0.96	0.26
P63267	ACTG2	actin. gamma 2. smooth muscle. enteric	Cytoplasm	other	1.03	0.29
P06756	ITGAV	integrin subunit alpha V	Plasma Membrane	ion channel	0.69	0.33
P18084	ITGB5	integrin subunit beta 5	Plasma Membrane	other	0.50	0.33
P50570	DNM2	dynamin 2	Plasma Membrane	enzyme	0.78	0.37
Q14254	FLOT2	flotillin 2	Plasma Membrane	other	1.67	0.37
P61769	B2M	beta-2-microglobulin	Plasma Membrane	transmembrane receptor	1.00	0.42
P08648	ITGA5	integrin subunit alpha 5	Plasma Membrane	transmembrane receptor	1.10	0.47
P48444	ARCN1	archain 1	Cytoplasm	other	0.90	0.61
P53618	COPB1	coatomer protein complex subunit beta 1	Cytoplasm	transporter	1.00	0.64

Figure 2 CECR1 silencing in THP-1 macrophages influenced various functions of macrophages

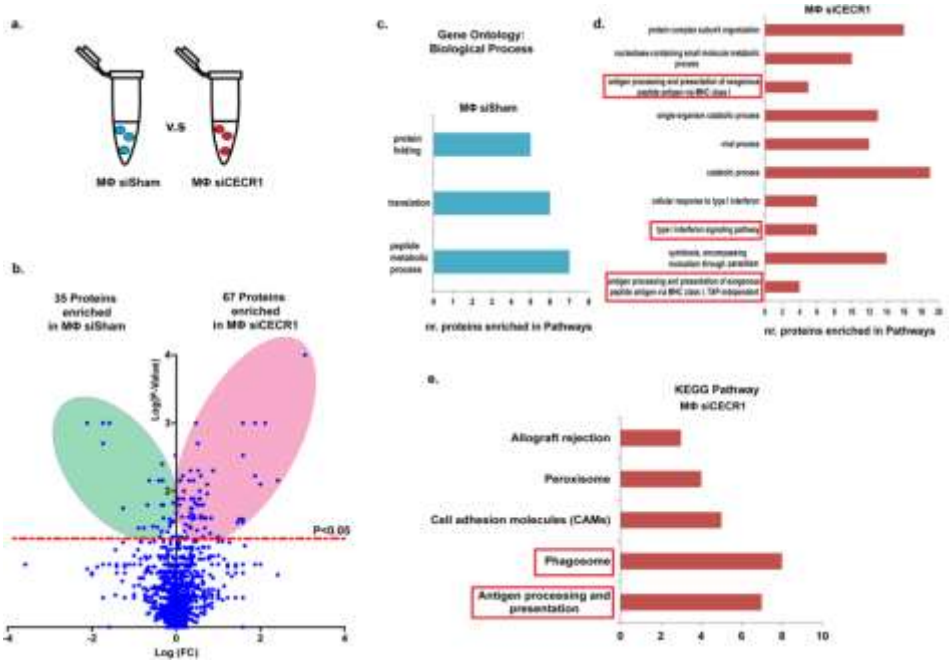

a. Schematic illustration displayed comparison of proteins from macrophage with siSham and siCECR1
b. Volcano blot showing differentially expressed proteins in macrophage with siSham and macrophage with siCECR1. Proteins were considered as differentially expressed when p value<0.05
c. Bar graph displaying the annotation of Gene Ontology with FDR (False Discovery Rate) <0.05 enriched in macrophage with siSham compared with macrophage transfected by siCECR1
d. Bar graph displaying the top 10 annotations of Gene Ontology with FDR (False Discovery Rate) <0.05 enriched in macrophage with siCECR1 compared with macrophage transfected by siSham control.
e. Bar graph showing the result of proteins in macrophage with siCECR1 from top 5 KEGG pathway.

Changes in proteomic profile of U87 stimulated THP-1 macrophages in response to CECR1 silencing

THP-1 macrophages treated with CECR1 silencing were co-cultured with U87 cells to mimic TAMs differentiation conditions and were compared with U87 co-cultured macrophages treated with siSham (Figure 4a). In total, 47 proteins were significantly affected by CECR1 silencing (Figure 4b); 18 proteins were upregulated, and 29 proteins were downregulated by CECR1 silencing in U87 co-cultured THP-1 macrophages (Supplementary table 4,5). Gene ontology analysis could not identify a pathway that was significantly annotated to the 18 upregulated proteins. The majority of pathways that were significantly linked to the 29 downregulated proteins were based on four proteasome proteins, PSMC6, PSMA7, PSMA5, and PSMD8 (Figure 4c, d). The most relevant pathways were all mainly involved in regulation of cell cycle (Figure 4d). In line with these findings, the proliferation rate of U87-stimulated THP-1 macrophage with CECR1 silencing was

lower than U86-stimulated sisham control macrophages, as shown by MTT assay (Figure 4e). In addition, the number of cells positive for Ki67 (a marker for cell proliferation) in U87-stimulated THP-1 macrophages with CECR1 silencing was significantly lower than in siSham-treated control macrophages (Figure 4f, g).

Although these four proteins were involved in antigen presentation, other proteins that are vital for the proteosome step in this pathway such as TAP, TAPBP and HLA-A, B, C are not enriched in CECR1 silenced THP-1 macrophages (Supplementary figure 2), indicating that this process is not affected in by CECR1 under U87 coculture conditions.

Figure 3 CECR1 silencing in THP-1 macrophages enhanced MHC I Antigen Presenting, Phagosome maturation, Caveolin mediated endocytosis and IFN-γ responsive signaling.

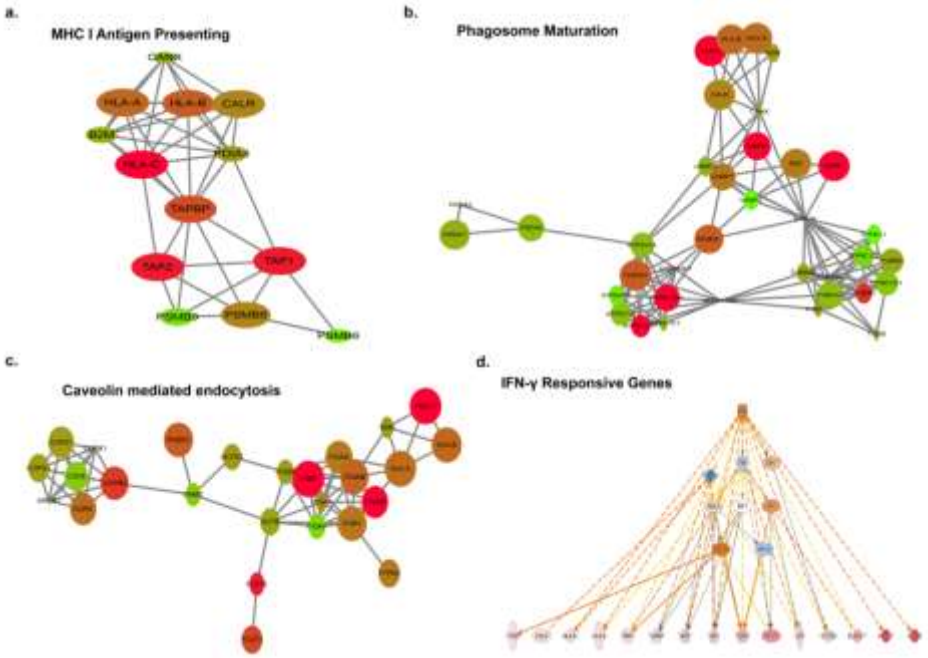

a. Network generated by Cytoscape presenting MHC I antigen presenting pathway from IPA analysis. Nodes with red color indicated proteins significantly enriched in macrophage with siCECR1 ($P<0.05$). Green nodes indicated proteins equally enriched in macrophage with sisham and siCECR1.
b. Network generated by Cytoscape presenting Phagosome maturation pathway from IPA analysis. Nodes with red color indicated proteins significantly enriched in macrophage with siCECR1 ($P<0.05$). Green nodes indicated proteins equally enriched in macrophage with sisham and siCECR1.
c. Network generated by Cytoscape presenting Phagosome maturation pathway from IPA analysis. Nodes with red color indicated proteins significantly enriched in macrophage with siCECR1 ($P<0.05$). Green nodes indicated proteins equally enriched in macrophage with sisham and siCECR1.
d. Upstream prediction of significantly expressed proteins in macrophage with CECR1 silencing from IPA.

Figure 4 CECR1 silencing leads a limited response in U87 co-cultured THP-1 macrophage

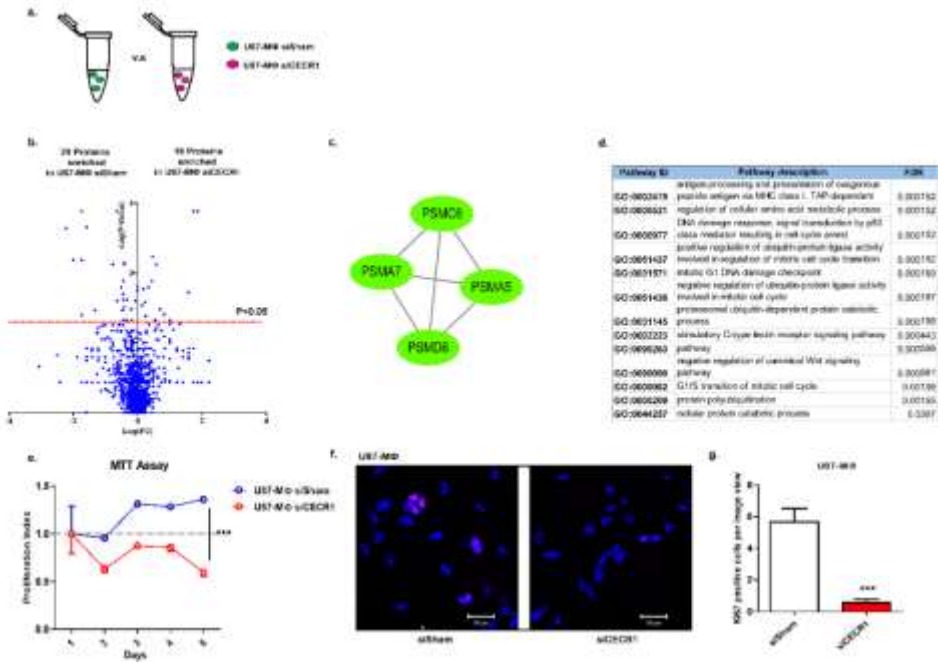

a. Schematic illustration displayed comparison of proteins from U87 co-cultured macrophage with siSham and siCECR1

b. Volcano blot showing differentially expressed proteins in U87 co-cultured macrophage with siSham and macrophage with siCECR1. Proteins were considered as differentially expressed when P value<0.05

c. Network generated by Cytoscape of proteasome proteins PSMC6, PSMA5, PSMA7 and PSMD8. Raw data of network was exported from STRING.

d. Table listing 13 pathways mostly related to proteasome network with FDR<0.05 from Gene Ontology.

e. MTT assay assessing proliferation of U87 co-cultured macrophage for continuous five days. Data were shown as mean± S.E.M. Two-way anova was used to test the difference of U87 co-cultured macrophage with siSham and siCECR1. ***P<0.005

f. Ki67 staining of U87 co-cultured macrophage with siSham and siCECR1. Scale bar: 50μm

g. Quantification of Ki67 positive cells per image view in U87 co-cultured macrophage with siSham and siCECR1. Data were shown as mean± S.E.M. ***P<0.005

Stimulation by U87 cells attenuates the changes that occur at protein and mRNA level in response to CECR1 silencing in THP-1 macrophages.

As only a very limited effect of CECR1 silencing on immune response was observed in CECR1 silenced U87 THP-1 macrophages, a comparison of CECR1 silenced macrophage with/without U87 co-culture was conducted (Figure 5a). 57 proteins were downregulated in U87 co-cultured macrophages with CECR1 silencing compared to macrophages with CECR1 silencing without U87 stimulation (Figure 5b). The annotation of Gene Ontology analysis using the downregulated proteins as input, indicated “endocytosis”,

"phagocytosis", "immune response" as well as "phagolysosome assembly" may be affected (Figure 5c). To assess whether protein levels were downregulated on mRNA level, transcripts of key molecules involved in above pathways like HLA-A, C, ITGB7, EVL, WDFY, SEPT7 were evaluated in macrophages with/without U87 co-culture. CECR1 silencing increased gene expression of these molecules. However, U87 stimulation attenuated this upregulation of target genes in response to CECR1 silencing (Figure 5d). Thus, the changes observed on protein level in response to CECR1 silencing on THP-1 macrophages is regulated on gene expression level, but U87 stimulation diminishes this response.

Figure 5. U87 cells attenuated CECR1 Silencing mediated response in macrophage

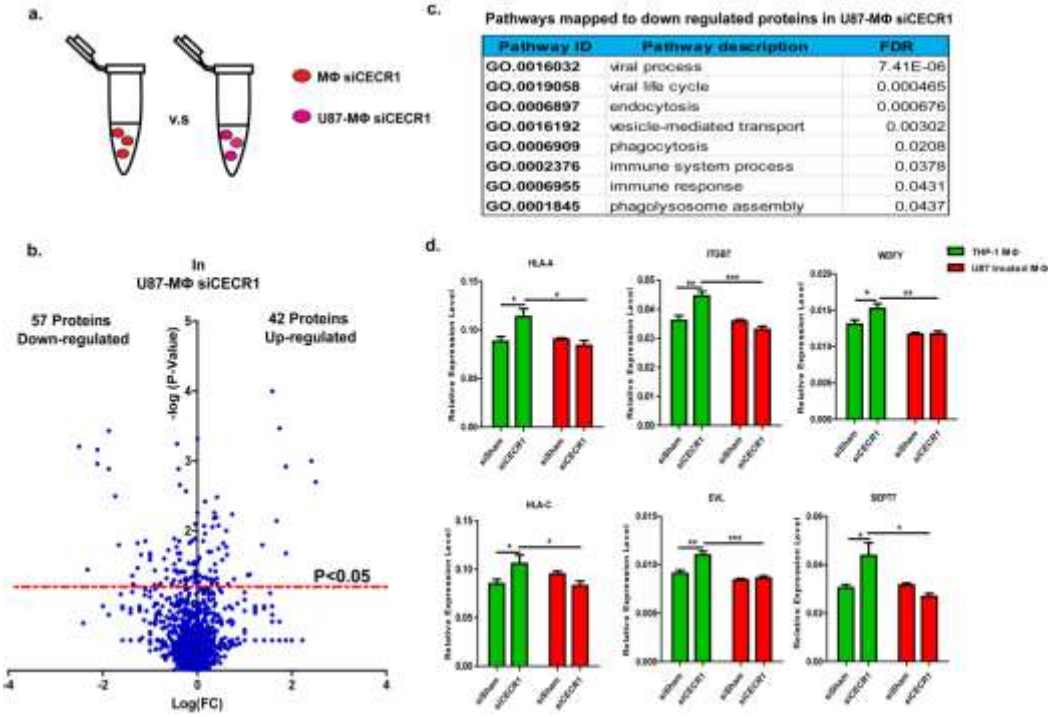

Pathway ID	Pathway description	FDR
GO.0016032	viral process	7.41E-06
GO.0019058	viral life cycle	0.000465
GO.0006897	endocytosis	0.000676
GO.0016192	vesicle-mediated transport	0.00302
GO.0006909	phagocytosis	0.0208
GO.0002376	immune system process	0.0378
GO.0006955	immune response	0.0431
GO.0001845	phagolysosome assembly	0.0437

a. Schematic illustration displayed comparison of proteins from macrophage with siCECR1 with/without U87 co-culture.

b. Volcano blot showing differentially expressed proteins in macrophage with siCECR1 with/without U87 co-culture. Proteins were considered as differentially expressed when P value<0.05

c. Table listing top 10 pathways with FDR<0.05 related to downregulated proteins in U87 co-cultured macrophage with CECR1 knockdown

d. Real time PCR validation of HLA-A, C, ITGB7, WDFY, EVL, SEPT7 in macrophage with siCECR1 knockdown and with/without U87 co-culture. Data were shown as mean± S.E.M. * P<0.05, **P<0.01, ***P<0.005

Overlap analysis identifies S100A9 and PLAU as two CECR1-related proteins that are significantly correlated with expression of CECR1 and macrophage lineage markers in three large public GBM datasets.

As shown in our previous study, CECR1 was highly expressed in macrophages stimulated by U87 cells. Proteins that are enriched in U87 treated macrophages may thus be putatively regulated by CECR1. Next we compared the list of proteins that were upregulated in U87-stimulated THP-1macrophages versus macrophages without U87 treatment (Supplementary table 6) with the list of proteins that were downregulated in THP-1 macrophages with CECR1 silencing compared to sisham treated THP-1 macrophages (Supplementary table 2). This overlap analysis retrieved three common proteins, which are EEF1G, S100A9 and DNAJC10 (Figure 6a). Similarly, the comparison of enriched proteins in U87-stimulated macrophages versus macrophages without U87 treatment (Supplementary table 6) with proteins that were downregulated in U87 co-cultured macrophages with CECR1 silencing versus U87 co-cultured sisham treated macrophages (Supplementary table 5) resulted in 9 common proteins (Figure 6d). QPCR analysis validated the downregulation of S100A9 and PLAU expression in CECR1 silenced macrophage with/without U87 co-culture compared to their related sisham controls. U87 stimulation significantly increased expression of S100A9 and PLAU in macrophages (Figure 6 b, e). Analysis of S100A9 and PLAU in the TCGA GBM database using 3 large public GBM datasets demonstrated that both S100A9 and PLAU expression levels are positively correlated with CECR1 and other monocyte/macrophage lineage markers (Figure 6c, f). Although the overlap analyses indicated that DNAJC10 is the most relevant molecule under regulation of CECR1, the analysis of DNAJC10 using the same public GBM datasets did not show any correlation with CECR1 as well as other markers of monocytes/macrophages (data not shown).

LAT2 was upregulated by CECR1 knockdown in U87 co-cultured macrophages.

Further overlap analysis identified LAT2 as a CECR1-related protein (Figure 7a) via comparison of downregulated proteins in U87-stimulated THP-1 macrophages versus macrophage without U87 treatment (Supplementary table 7) with proteins upregulated in U87 co-cultured macrophages with CECR1 silencing versus sisham treated controls (Supplementary table 4). LAT2 was validated to be upregulated in U87 co-cultured macrophages by CECR1 silencing by western blot analysis (Figure 7b, c). In line with this finding, CECR1-silenced U87 co-cultured macrophages displayed a IL-10 low and IL-12p35 high expression profile, which implied a more pro-inflammatory phenotype (Figure 7d, e).

Figure 6. S100A9, PLAU are two mostly CECR1-related molecules in macrophage

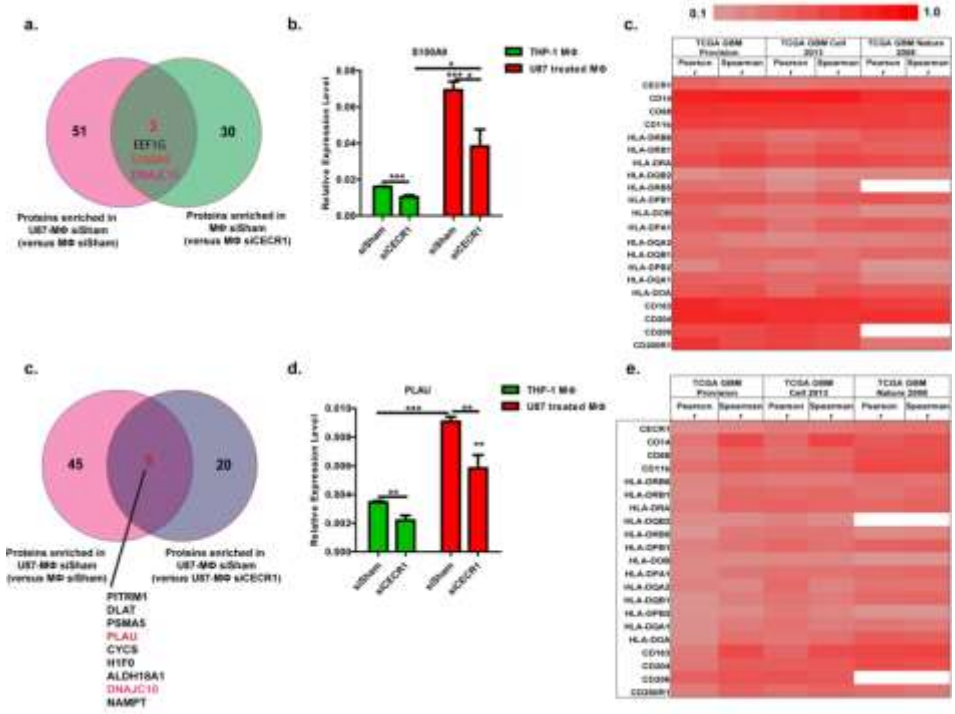

a. Venn graph showing the overlapped proteins from proteins enriched in U87 co-cultured macrophage with siSham(versus macrophage with siSham) and proteins enriched in macrophage with siSham (versus macrophage with siCECR1)

b. Real time PCR validation of S100A9 expression in macrophage with siCECR1 knockdown and with/without U87 co-culture. Data were shown as mean± S.E.M. * P<0.05, ***P<0.005

c. Heat map showing correlation co-efficiency from both pearson and spearman analysis of S100A9 with CECR1 and monocyte/macrophage markers from three TCGA GBM database.

d. Venn graph showing the overlapped proteins from proteins enriched in U87 co-cultured macrophage with siSham (versus macrophage with siSham) and proteins enriched in U87 co-cultured macrophage with siSham (versus macrophage with siCECR1)

e. Real time PCR validation of PLAU expression in macrophage with siCECR1 knockdown and with/without U87 co-culture. Data were shown as mean± S.E.M. ** P<0.01, ***P<0.005

f. Heat map showing correlation co-efficiency from both pearson and spearman analysis of PLAU with CECR1 and monocyte/macrophage markers from three TCGA GBM database.

Figure 7 LAT2 was upregulated by CECR1 knockdown in U87 co-cultured macrophage

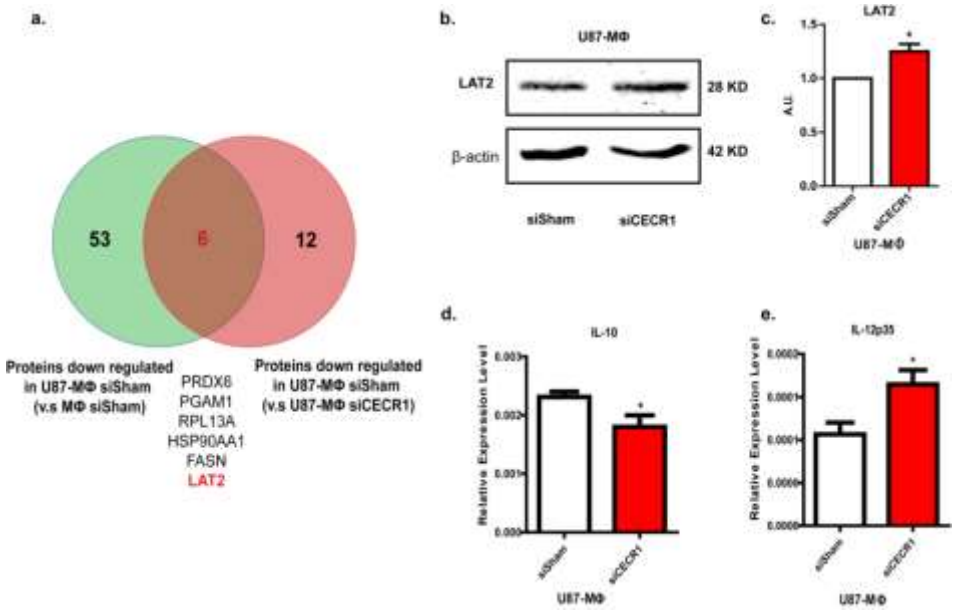

a. Venn graph showing the overlapped proteins from proteins downregulated in U87 co-cultured macrophage with siSham(versus macrophage with siSham) and proteins downregulated in macrophage with siSham (versus macrophage with siCECR1)

b. Western blot analysis of LAT2 expression in U87 co-cultured macrophage with siSham and siCECR1

c. Quantification of LAT2 protein band in U87 co-cultured macrophage with siSham and siCECR1

d. Real time PCR measurement of IL-10 expression in U87 co-cultured macrophage with/without CECR1 silencing. Data were shown as mean± S.E.M. * P<0.05

e. Real time PCR measurement of IL-12p35 expression in U87 co-cultured macrophage with/without CECR1 silencing. Data were shown as mean± S.E.M. * P<0.05

DISCUSSION

Recent studies have highlighted the importance of CECR1 in the regulation of the innate immune response[19]. *In vitro*, monocytes-derived from patients with deleterious CECR1 mutations showed diminished capacity of M2 macrophage differentiation, whereas M1 macrophage differentiation remained unaffected (PMID 24552284). The TAM population in glial tumors exhibits a mainly M2-macrophage like phenotype. We previously reported that CECR1 was strongly expressed in high-grade gliomas by M2-like TAMs. In line with the results of the genetic study, CECR1 proved vital for differentiation of monocytes towards M2-like TAMs in a glial tumor paracrine environment (U87 supernatant stimulation) (REF). CECR1 activity in M2-like TAMs promoted paracrine stimulation of glial tumor cell migration and proliferation (REF). In addition, CECR1 function facilitated paracrine crosstalk of M2-like TAMs with perivascular pericytes, contributing to tumor

angiogenesis (REF). Although these studies provide direct evidence for the significant role of CECR1 in TAM regulation, the molecular mechanisms that drive the CECR1-mediated function of TAMs remain to be elucidated. A genome-wide "omics" approach could help reveal the CECR1 mechanisms. A genome-wide transcriptome dataset of peripheral blood mononuclear cells (PBMCs) derived from patients with CECR1 mutations has been published, showing marked increased expression of neutrophil-associated genes in the disease condition[27]. Another case-report study did not detect upregulation of neutrophil-associated genes in the patient's BPMCs, but demonstrated an increase in IFN-γ response genes[28]. In line with this report, patients with CECR1 genetic mutations that received anti-TNF-α antibody treatment reached complete remission or partially recovered from their autoimmune disease-like symptoms[26]. The latter clearly demonstrates the potential value of in depth analysis of CECR1 mediated mechanisms in identifying new drug targets for therapy development. As most molecular data on CECR1 function in immune cells were obtained from the mixed PBMC population, these findings remain difficult to extrapolate to aid in our understanding of the CECR1 working mechanism of local TAMs in glial tumors. The general working mechanism of CECR1 in monocytes/macrophages also requires further exploration.

In this study we conducted proteomics analysis of siRNA mediated CECR1 silencing in macrophages that were stimulated with or without glial tumor cells (U87) in co-culture. In the absence of U87 stimulation, CECR1 silencing in macrophages showed a protein profile that is related to key mechanisms in macrophage immune response regulation, including "MHC I antigen presenting" and "Phagosome maturation", "Caveolin mediated endocytosis" and "Type I interferon signaling pathway". These pathways are mostly involved in pro-inflammatory responses and anti-pathogen defense, and are more in line with M1-macrophage function. Among these three pathways, "MHC I Antigen Presenting" and "Phagosome maturation" have been reported to be regulated via IFN-γ signaling [29]. IFN-γ has been recognized as the main cytokine that is associated to induction of the M1 response (PMC:3944738). Our data showed upregulation of proteins mapping into interferon responding pathway in response to CECR-1 silencing of macrophages, including ISG15, HLA-A, HLA-B, HLA-C, TAP1, TAP2, TAPBP, and TIMP-1. Furthermore, several proteins that are recently reported to be involved in immune response like WDFY1, a regulator of the Toll-like receptor signaling pathways[30] and SEPT7 involved in phagosome assembly and vesicle transport[29] were also enriched in CECR1-silenced macrophages. WDFY1 is as an adaptor protein anchored on the membrane of early endosomes. It participates in Toll like receptor pathways and activates NF-κB signaling pathway in macrophages, which in turn, activates the transcription of type I interferons as well as other inflammatory factors including key proteins of the M1 macrophage cytokine release repertoire such as TNF-α, IL-6 and CXCL10[30] (PMID:24013843). Moreover, CECR1 silencing in macrophages promotes higher levels of proteins that are associated with the MHC I antigen presenting function. This would trigger imply enhanced CD8+ T cell activation, a feature that is more associated with

M1-macrophages[31]. Thus, in line with present literature and our previous studies, current data shows that CECR1 function in macrophages is indeed important to endorse M2 macrophage function, as made evident by the shift towards a more M1 macrophage-like proteosome profile that is observed in response to CECR1-silencing.

Malignant tumor including glial tumors are known to influence the local immune response including hampering vital macrophage functions like antigen presenting and phagocytosis[33]. In this study, we observed a general inhibitory effect of U87 cell on the CECR1-silencing response in macrophages: Coculture with U87 cells reversed the CECR1-silencing induced pro-inflammatory M1-like protein profile in macrophages. No upregulation of proteins involved in "MHC I antigen presenting" and "Phagosome maturation", "Caveolin mediated endocytosis" and "Type I interferon signaling pathway" was observed. In contrast, CECR1 silencing in macrophages under U87 costimulation mainly downregulated proteins that were part of cell cycle regulation. In line with this proteome profile, CECR1 silenced macrophages with U87 stimulation indeed showed a lower proliferation capacity compared to sisham treated controls. Macrophage proliferation has been reported to be activated by paracrine stimulation of malignant tumor cells, mainly via secretion of various cytokines and growth factors like M-CSF[34'35]. Numerous studies have indicated that reduction of the number of immuno-suppresive (M2) macrophages in tumors could be an effective therapeutic approach[35,36]. Our proteomics analysis revealed downregulation by CECR1 silencing of the proteasome proteins PSMA5, PSMA7, PSMC6 and PSMD8 in the U87 coculture conditions. PSMA5 and PSMA7 are essential subunits of the complete assembly of the 20S proteosome core complex, whereas PSMC6 and PSMD8 are essential subunits of the 19S regulatory particle. Together, 1 20S core and 2 19S regulator particles form the functional 26S proteosome complex (PMC:2902798). The 26S proteasome complex participates in various critical cell pathways including DNA synthesis, repair, transcription, translation and cell signal transduction (PMC:2902798) as well as antigen presentation[37] and regulation of cell cycle transition[38]. Cell proliferation and cell cycle is mainly regulated by 26S proteosomes by targeting p53[39] and inhibitors of cell cycle dependent kinase, like p21[40], p27[41], for ubiquitin-mediated degradation. Inhibition of S26 proteasome activity led to cell cycle arrest and induced apoptosis by increasing levels of p53, p21 and p27[42]. Our findings indicate that CECR1 silencing may contribute to low proliferation rate of TAMs via downregulation of essential protein components of the S26 proteosome complex. Thus, CECR1 depletion may be considered as a novel approach in targeting TAM proliferation in gliomas.

Overlap analysis of our data identified S100A9 and PLAU as two CECR1-related proteins that are significantly correlated with expression of CECR1 and macrophage lineage markers in GBMs. These two molecules were previously shown to be highly expressed in myeloid cells[12,43]. S100A9 was also shown to promote glioma growth and angiogenesis by interaction with the PAGE receptor on the surface of glioma cells[44], a process mediated via activation of MAPK and NF-κB pathways[45]. PLAU is one of the proangiogenic

factors that can be produced TAMs[12]. It was shown to aid the invasion and metastasis of various types of cancer cells via binding to PLAUR, subsequently activating downstream pathways like ERK1/2[46], PI3K/Akt[47]. Moreover, the interaction of PLAU-PLAUR raised plasmin levels, contributing to the activation of matrix metalloproteinases[48].

In U87 co-cultured macrophages CECR1 silencing upregulated protein levels of LAT2. Coincidently, U87 treatment decreased the LAT2 expression in sisham treated macrophages. Previous studies pointed to the immune modulatory function of LAT2 via competing with TREM-2/LAT signaling pathway, which resulted in upregulation of IL-12 and downregulation of IL-10 in LPS stimulated macrophages[49]. Indeed, CECR1-silenced macrophages in U87 coculture conditions displayed an decrease in IL-10/IL-12p35 ratio.

In conclusion, in this study we have identified, for the first time to our knowledge, the molecular pathways and key molecules that are mediated by CECR1 function in macrophages and glial tumor associated macrophages. Our proteome dataset could provide the basis for the development of interesting drug targets for future immunotherapy development in the treatment of malignant (glial) tumors as well as auto immune disease.

REFERENCES

1. Rivera A, Siracusa MC, Yap GS, Gause WC. Innate cell communication kick-starts pathogen-specific immunity. *Nat Immunol.* 2016; 17(4):356-363.
2. Erwig LP, Gow NA. Interactions of fungal pathogens with phagocytes. *Nature reviews. Microbiology.* 2016; 14(3):163-176.
3. Flannagan RS, Heit B, Heinrichs DE. Antimicrobial Mechanisms of Macrophages and the Immune Evasion Strategies of Staphylococcus aureus. *Pathogens.* 2015; 4(4):826-868.
4. Li W, Graeber MB. The molecular profile of microglia under the influence of glioma. *Neuro Oncol.* 2012; 14(8):958-978.
5. Hambardzumyan D, Gutmann DH, Kettenmann H. The role of microglia and macrophages in glioma maintenance and progression. *Nature Neuroscience.* 2016; 19(1):20-27.
6. Xue J, Schmidt SV, Sander J, et al. Transcriptome-based network analysis reveals a spectrum model of human macrophage activation. *Immunity.* 2014; 40(2):274-288.
7. Martinez FO, Gordon S. The M1 and M2 paradigm of macrophage activation: time for reassessment. *F1000Prime Rep.* 2014; 6:13.
8. Iglesia MD, Parker JS, Hoadley KA, Serody JS, Perou CM, Vincent BG. Genomic Analysis of Immune Cell Infiltrates Across 11 Tumor Types. *J Natl Cancer Inst.* 2016; 108(11).
9. Prosniak M, Harshyne LA, Andrews DW, et al. Glioma grade is associated with the accumulation and activity of cells bearing M2 monocyte markers. *Clin Cancer Res.* 2013; 19(14):3776-3786.
10. Komohara Y, Ohnishi K, Kuratsu J, Takeya M. Possible involvement of the M2 anti-inflammatory macrophage phenotype in growth of human gliomas. *J Pathol.* 2008; 216(1):15-24.
11. Cekanaviciute E, Fathali N, Doyle KP, Williams AM, Han J, Buckwalter MS. Astrocytic transforming growth factor-beta signaling reduces subacute neuroinflammation after stroke in mice. *Glia.* 2014; 62(8):1227-1240.
12. Murdoch C, Muthana M, Coffelt SB, Lewis CE. The role of myeloid cells in the promotion of tumour angiogenesis. *Nat Rev Cancer.* 2008; 8(8):618-631.
13. Riabov V, Gudima A, Wang N, Mickley A, Orekhov A, Kzhyshkowska J. Role of tumor associated macrophages in tumor angiogenesis and lymphangiogenesis. *Front Physiol.* 2014; 5:75.
14. Zhu C, van der Weiden MM, Scchetti A, et al. Abstract 2348: Expression of CECR1 by activated M2-type macrophages in glioma. *Cancer Research.* 2015; 75(15 Supplement):2348-2348.
15. Conlon BA, Law WR. Macrophages are a source of extracellular adenosine deaminase-2 during inflammatory responses. *Clin Exp Immunol.* 2004; 138(1):14-20.
16. Zavialov AV, Engstrom A. Human ADA2 belongs to a new family of growth factors with adenosine deaminase activity. *Biochem J.* 2005; 391(Pt 1):51-57.
17. Novakova M, Dolezal T. Expression of Drosophila adenosine deaminase in immune cells during inflammatory response. *PLoS One.* 2011; 6(3):e17741.
18. Footz TK, Brinkman-Mills P, Banting GS, et al. Analysis of the cat eye syndrome critical region in humans and the region of conserved synteny in mice: a search for candidate genes at or near the human chromosome 22 pericentromere. *Genome Research.* 2001; 11(6):1053-1070.
19. Zavialov AV, Gracia E, Glaichenhaus N, Franco R, Zavialov AV, Lauvau G. Human adenosine deaminase 2 induces differentiation of monocytes into macrophages and stimulates proliferation of T helper cells and macrophages. *J Leukoc Biol.* 2010; 88(2):279-290.
20. Zhou Q, Yang D, Ombrello AK, et al. Early-onset stroke and vasculopathy associated with mutations in ADA2. *New England Journal of Medicine.* 2014; 370(10):911-920.
21. Navon Elkan P, Pierce SB, Segel R, et al. Mutant adenosine deaminase 2 in a polyarteritis nodosa vasculopathy. *New England Journal of Medicine.* 2014; 370(10):921-931.
22. Mondal Bama C, Mukherjee T, Mandal L, et al. Interaction between Differentiating Cell- and Niche-Derived Signals in Hematopoietic Progenitor Maintenance. *Cell.* 2011; 147(7):1589-1600.

23. Stoffels M, Kastner DL. Old Dogs, New Tricks: Monogenic Autoinflammatory Disease Unleashed. *Annual review of genomics and human genetics.* 2016; 17:245-272.
24. Sims JS, Grinshpun B, Feng Y, et al. Diversity and divergence of the glioma-infiltrating T-cell receptor repertoire. *Proc Natl Acad Sci U S A.* 2016; 113(25):E3529-3537.
25. Schepp J, Bulashevska A, Mannhardt-Laakmann W, et al. Deficiency of Adenosine Deaminase 2 Causes Antibody Deficiency. *J Clin Immunol.* 2016; 36(3):179-186.
26. Nanthapisal S, Murphy C, Omoyinmi E, et al. Deficiency of Adenosine Deaminase Type 2: A Description of Phenotype and Genotype in Fifteen Cases. *Arthritis Rheumatol.* 2016; 68(9):2314-2322.
27. Belot A, Wassmer E, Twilt M, et al. Mutations in CECR1 associated with a neutrophil signature in peripheral blood. *Pediatr Rheumatol Online J.* 2014; 12:44.
28. Uettwiller F, Sarrabay G, Rodero MP, et al. ADA2 deficiency: case report of a new phenotype and novel mutation in two sisters. *RMD open.* 2016; 2(1):e000236.
29. Trost M, English L, Lemieux S, Courcelles M, Desjardins M, Thibault P. The phagosomal proteome in interferon-gamma-activated macrophages. *Immunity.* 2009; 30(1):143-154.
30. Hu YH, Zhang Y, Jiang LQ, et al. WDFY1 mediates TLR3/4 signaling by recruiting TRIF. *EMBO Rep.* 2015; 16(4):447-455.
31. Smyth LA, Lechler RI, Lombardi G. Continuous Acquisition of MHC:Peptide Complexes by Recipient Cells Contributes to the Generation of Anti-Graft CD8+ T Cell Immunity. *Am J Transplant.* 2016.
32. Kaneda MM, Messer KS, Ralainirina N, et al. PI3Kγ is a molecular switch that controls immune suppression. *Nature.* 2016; advance online publication.
33. Noy R, Pollard JW. Tumor-associated macrophages: from mechanisms to therapy. *Immunity.* 2014; 41(1):49-61.
34. Jackaman C, Yeoh TL, Acuil ML, Gardner JK, Nelson DJ. Murine mesothelioma induces locally-proliferating IL-10+TNF-α+CD206−CX3CR1+ M3 macrophages that can be selectively depleted by chemotherapy or immunotherapy. *OncoImmunology.* 2016; 5(6):e1173299.
35. Quail DF, Bowman RL, Akkari L, et al. The tumor microenvironment underlies acquired resistance to CSF-1R inhibition in gliomas. *Science.* 2016; 352(6288):aad3018.
36. Pyonteck SM, Akkari L, Schuhmacher AJ, et al. CSF-1R inhibition alters macrophage polarization and blocks glioma progression. *Nat Med.* 2013; 19(10):1264-1272.
37. Livneh I, Cohen-Kaplan V, Cohen-Rosenzweig C, Avni N, Ciechanover A. The life cycle of the 26S proteasome: from birth, through regulation and function, and onto its death. *Cell Res.* 2016; 26(8):869-885.
38. Guo X, Dixon JE. The 26S proteasome: A cell cycle regulator regulated by cell cycle. *Cell Cycle.* 2016; 15(7):875-876.
39. Asher G, Shaul Y. p53 Proteasomal Degradation: Poly-Ubiquitination is Not the Whole Story. *Cell Cycle.* 2005; 4(8):1015-1018.
40. Jin Y, Zeng SX, Sun X-X, et al. MDMX Promotes Proteasomal Turnover of p21 at G1 and Early S Phases Independently of, but in Cooperation with, MDM2. *Molecular and Cellular Biology.* 2008; 28(4):1218-1229.
41. Munoz U, Bartolome F, Bermejo F, Martin-Requero A. Enhanced proteasome-dependent degradation of the CDK inhibitor p27(kip1) in immortalized lymphocytes from Alzheimer's dementia patients. *Neurobiology of aging.* 2008; 29(10):1474-1484.
42. Suh KS, Tanaka T, Sarojini S, et al. The role of the ubiquitin proteasome system in lymphoma. *Crit Rev Oncol Hematol.* 2013; 87(3):306-322.
43. Lim SY, Yuzhalin AE, Gordon-Weeks AN, Muschel RJ. Tumor-infiltrating monocytes/macrophages promote tumor invasion and migration by upregulating S100A8 and S100A9 expression in cancer cells. *Oncogene.* 2016.
44. Chen X, Zhang L, Zhang IY, et al. RAGE expression in tumor-associated macrophages promotes angiogenesis in glioma. *Cancer Res.* 2014; 74(24):7285-7297.
45. Cheng S, Zhang X, Huang N, Qiu Q, Jin Y, Jiang D. Down-regulation of S100A9 inhibits osteosarcoma cell growth through inactivating MAPK and NF-κB signaling pathways. *BMC Cancer.* 2016; 16(1):1-12.

46. Aguirre-Ghiso JA, Liu D, Mignatti A, Kovalski K, Ossowski L. Urokinase Receptor and Fibronectin Regulate the ERKMAPK to p38MAPK Activity Ratios That Determine Carcinoma Cell Proliferation or Dormancy In Vivo. *Molecular Biology of the Cell.* 2001; 12(4):863-879.
47. Wang S, Jiang L, Han Y, et al. *Urokinase-type plasminogen activator receptor promotes proliferation and invasion with reduced cisplatin sensitivity in malignant mesothelioma*2016.
48. Carmeliet P, Moons L, Lijnen R, et al. Urokinase-generated plasmin activates matrix metalloproteinases during aneurysm formation. *Nat Genet.* 1997; 17(4):439-444.
49. Whittaker GC, Orr SJ, Quigley L, et al. The Linker for Activation of B Cells (LAB)/Non-T Cell Activation Linker (NTAL) Regulates Triggering Receptor Expressed on Myeloid Cells (TREM)-2 Signaling and Macrophage Inflammatory Responses Independently of the Linker for Activation of T Cells. *Journal of Biological Chemistry.* 2010; 285(5):2976-2985.

SUPPLEMENTARY DATA

Supplementary Figure 1

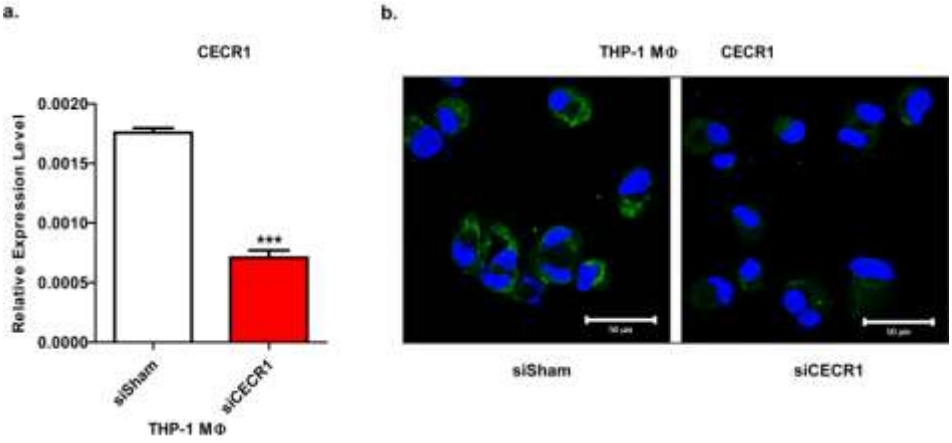

(A) Transcript of CECR1 was assessed by real time qPCR. Data were shown as Mean ± SEM. *** P<0.005 based on student's T-test. N=3

(B) Representative figure of CECR1 immunostaining of macrophages with siSham and siCECR1 transfection. Experiments were repeated three times with similar read out. Scale bar: 50µm

Supplementary Figure 2

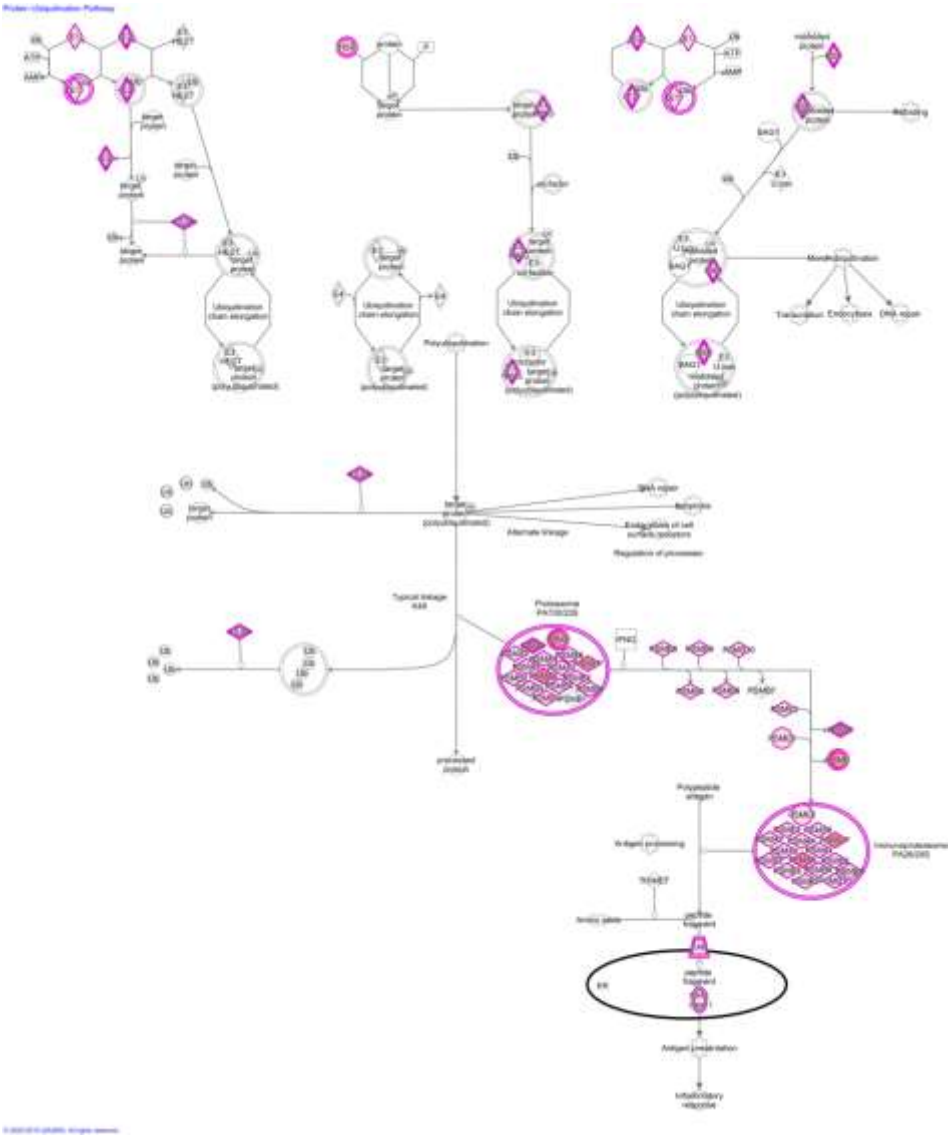

Schematic diagram of IPA data showing involvement of PSMA5, 7, PSMC6, PSMD8 in S20 proteasome complex related pathways.

Supplementary table 1: Sequence of Primers for Real time qPCR

Primers	Oligo Sequence (5'-3')
CECR1 Forward	TGGCGTTAAGCTGCCTTACT
CECR1 Reverse	GCTACAGGGTGGTTCCTCAA
S100A9 Forward	TCCTCGGCTTTGACAGAGTG
S100A9 Reverse	TGCCCCAGCTTCACAGAGTA
CTSH Forward	CCTGTGAAAAATCAGGGTGCCT
CTSH Reverse	TGAAGACAACTGAGGCTGCAA
PLAU Forward	CCCAGGAAATGGGACAGGG
PLAU Reverse	ACAGTTCGCCTGTTCGTATCT
HLA-A Forward	CGACGCCGCGAGCCAGA
HLA-A Reverse	GCGATGTAATCCTTGCCGTCGTAG
HLA-C Forward	GGAGACACAGAAGTACAAGCG
HLA-C Reverse	CGTCGTAGGCGTACTGGTCATA
ITGB7 Forward	GAGGAAGGACTGCTCTGCAC
ITGB7 Reverse	ACCATGCCCGAGATCCCAAG
WDFY Forward	ACGGATATTTGTGGGCCAGG
WDFY Reverse	CGGTTCTGATGAGCTGGGTA
EVL Forward	AGGGTCTGTGGTCCTCTGAT
EVL Reverse	GCAGATACTCTGTTCACTTGTGG
SEPT7 Forward	CACGCTTATGGTAGTGGGTGA
SEPT7 Reverse	TGAGCAGCAACTGAACACCA
IL-10 Forward	GGCACCCAGTCTGAGAACAG
IL-10 Reverse	TGGCAACCCAGGTAACCCTTA
IL-12p35 Forward	GCTCCAGAAGGCCAGACAAA
IL-12p35 Reverse	GCCAGGCAACTCCCATTAGT
β-actin Forward	TCCCTGGAGAAGAGCTACGA
β-actin Reverse	AGCACTGTGTTGGCGTACAG

Supplementary Table 2

UniProt	Symbol	Entrez Gene Name	Location	Type(s)	Fold Change	P-value
O43312	MTSS1	metastasis suppressor 1	Cytoplasm	transporter	4.33	0.001
Q8IXB1	DNAJC10	DnaJ heat shock protein family (Hsp40) member C10	Cytoplasm	enzyme	3.33	0.002
Q8NE86	MCU	mitochondrial calcium uniporter	Cytoplasm	enzyme	3.33	0.002
P62899	RPL31	ribosomal protein L31	Cytoplasm	enzyme	3.33	0.002
P63313	TMSB10	thymosin beta 10	Cytoplasm	phosphatase	3.33	0.001
Q99471	PFDN5	prefoldin subunit 5	Nucleus	enzyme	3.00	0.001
Q9UBQ0	VPS29	VPS29 retromer complex	Cytoplasm	other	3.00	0.001
P06702	S100A9	S100 calcium binding protein A9	Cytoplasm	enzyme	2.40	0.018
P62333	PSMC6	proteasome 26S subunit. ATPase 6	Nucleus	kinase	1.86	0.035
Q9BUJ2	HNRNPUL1	heterogeneous nuclear ribonucleoprotein U like 1	Nucleus	kinase	1.70	0.035
Q14643	ITPR1	inositol 1.4.5-trisphosphate receptor type 1	Cytoplasm	other	1.60	0.016
P09668	CTSH	cathepsin H	Cytoplasm	other	1.56	0.007
Q92974	ARHGEF2	Rho/Rac guanine nucleotide exchange factor 2	Cytoplasm	enzyme	1.47	0.033
P14868	DARS	aspartyl-tRNA synthetase	Cytoplasm	other	1.36	0.034
Q15019	SEPT2	septin 2	Cytoplasm	enzyme	1.33	0.007
Q9NSD9	FARSB	phenylalanyl-tRNA synthetase beta subunit	Cytoplasm	enzyme	1.30	0.047
Q9UHB9	SRP68	signal recognition particle 68	Nucleus	other	1.30	0.047
P27348	YWHAQ	tyrosine 3- monooxygenase/ tryptophan 5- monooxygenase activation protein theta	Cytoplasm	other	1.28	0.039
P34910	EVI2B	ecotropic viral integration site 2B	Plasma Membrane	enzyme	1.27	0.016
Q92598	HSPH1	heat shock protein family H (Hsp110) member 1	Cytoplasm	enzyme	1.26	0.004
P09661	SNRPA1	small nuclear ribonucleoprotein polypeptide A'	Nucleus	other	1.25	0.007
P52815	MRPL12	mitochondrial ribosomal protein L12	Cytoplasm	enzyme	1.24	0.016
O43399	TPD52L2	tumor protein D52 like 2	Cytoplasm	other	1.23	0.025

UniProt	Symbol	Entrez Gene Name	Location	Type(s)	Fold Change	P-value
Q14697	GANAB	glucosidase II alpha subunit	Cytoplasm	transcription regulator	1.14	0.04
P08559	PDHA1	pyruvate dehydrogenase (lipoamide) alpha 1	Cytoplasm	phosphatase	1.11	0.026
P49368	CCT3	chaperonin containing TCP1 subunit 3	Cytoplasm	transcription regulator	1.11	0.033
P07339	CTSD	cathepsin D	Cytoplasm	peptidase	1.11	0.05
Q06830	PRDX1	peroxiredoxin 1	Cytoplasm	other	1.10	0.029
Q8TCT9	HM13	histocompatibility (minor) 13	Cytoplasm	other	1.06	0.047
P26641	EEF1G	eukaryotic translation elongation factor 1 gamma	Cytoplasm	enzyme	1.05	0.015
Q07020	RPL18	ribosomal protein L18	Cytoplasm	enzyme	1.05	0.047
P07355	ANXA2	annexin A2	Plasma Membrane	transporter	1.05	0.028
P14618	PKM	pyruvate kinase. muscle	Cytoplasm	transporter	1.01	0.003

Supplementary Table 3

Uniprot	Symbol	Entrez Gene Name	Location	Type(s)	Fold Change	P-value
P30501	HLA-C	major histocompatibility complex. class I. C	Plasma Membrane	enzyme	8.33	0.001
Q16181	SEPT7	septin 7	Cytoplasm	transporter	5.33	0.007
P26010	ITGB7	integrin subunit beta 7	Plasma Membrane	transporter	4.33	0.001
P05161	ISG15	ISG15 ubiquitin-like modifier	Extracellular Space	enzyme	4.00	0.008
Q9UI08	EVL	Enah/Vasp-like	Plasma Membrane	enzyme	3.67	0.001
Q96C23	GALM	galactose mutarotase (aldose 1-epimerase)	Cytoplasm	enzyme	3.67	0.001
Q53H82	LACTB2	lactamase beta 2	Cytoplasm	enzyme	3.67	0.006
Q8IWB7	WDFY1	WD repeat and FYVE domain containing 1	Cytoplasm	other	3.67	0.001
P00390	GSR	glutathione reductase	Cytoplasm	transcription regulator	3.00	0.029
Q96N66	MBOAT7	membrane bound O-acyltransferase domain containing 7	Plasma Membrane	other	3.00	0.001
Q9NX40	OCIAD1	OCIA domain containing 1	Cytoplasm	other	3.00	0.003
Q13596	SNX1	sorting nexin 1	Cytoplasm	enzyme	3.00	0.026
Q0VD83	APOBR	apolipoprotein B receptor	Plasma Membrane	enzyme	2.83	0.026
Q8TCS8	PNPT1	polyribonucleotide nucleotidyltransferase 1	Cytoplasm	other	2.75	0.029
Q92804	TAF15	TATA-box binding protein associated factor 15	Nucleus	transcription regulator	2.00	0.047
P54920	NAPA	NSF attachment protein alpha	Cytoplasm	peptidase	1.83	0.005
Q15717	ELAVL1	ELAV like RNA binding protein 1	Cytoplasm	other	1.78	0.025
P43304	GPD2	glycerol-3-phosphate dehydrogenase 2	Cytoplasm	other	1.75	0.042
P01137	TGFB1	transforming growth factor beta 1	Extracellular Space	translation regulator	1.67	0.008
Q9NYU2	UGGT1	UDP-glucose glycoprotein glucosyltransferase 1	Cytoplasm	translation regulator	1.67	0.011
Q8NBQ5	HSD17B11	hydroxysteroid (17-beta) dehydrogenase 11	Cytoplasm	other	1.64	0.025
P29218	IMPA1	inositol monophosphatase 1	Cytoplasm	translation regulator	1.60	0.035
Q02543	RPL18A	ribosomal protein L18a	Cytoplasm	enzyme	1.58	0.025
Q00688	FKBP3	FK506 binding protein 3	Nucleus	other	1.56	0.016

Uniprot	Symbol	Entrez Gene Name	Location	Type(s)	Fold Change	P-value
Q02978	SLC25A11	solute carrier family 25 member 11	Cytoplasm	enzyme	1.56	0.047
O95466	FMNL1	formin like 1	Cytoplasm	cytokine	1.50	0.025
Q9UGP8	SEC63	SEC63 homolog. protein translocation regulator	Cytoplasm	enzyme	1.50	0.023
Q03518	TAP1	transporter 1. ATP-binding cassette. sub-family B (MDR/TAP)	Cytoplasm	other	1.50	0.006
P11413	G6PD	glucose-6-phosphate dehydrogenase	Cytoplasm	transmembrane receptor	1.48	0.013
P16435	POR	cytochrome p450 oxidoreductase	Cytoplasm	transmembrane receptor	1.48	0.01
Q9P2E9	RRBP1	ribosome binding protein 1	Cytoplasm	enzyme	1.46	0.016
P14854	COX6B1	cytochrome c oxidase subunit 6B1	Cytoplasm	enzyme	1.45	0.013
Q03519	TAP2	transporter 2. ATP-binding cassette. sub-family B (MDR/TAP)	Cytoplasm	other	1.44	0.005
P04040	CAT	catalase	Cytoplasm	enzyme	1.43	0.002
P62280	RPS11	ribosomal protein S11	Cytoplasm	other	1.42	0.016
P62820	RAB1A	RAB1A. member RAS oncogene family	Cytoplasm	enzyme	1.41	0.038
O14950	MYL12B	myosin light chain 12B	Cytoplasm	enzyme	1.38	0.001
Q9Y3Z3	SAMHD1	SAM domain and HD domain 1	Nucleus	enzyme	1.36	0.015
P27105	STOM	stomatin	Plasma Membrane	enzyme	1.36	0.025
P07305	H1F0	H1 histone family member 0	Nucleus	enzyme	1.33	0.013
O15533	TAPBP	TAP binding protein (tapasin)	Cytoplasm	kinase	1.33	0.023
Q13488	TCIRG1	T-cell immune regulator 1. ATPase H+ transporting V0 subunit a3	Plasma Membrane	kinase	1.33	0.007
O75947	ATP5H	ATP synthase. H+ transporting. mitochondrial Fo complex subunit D	Cytoplasm	peptidase	1.31	0.026
P25774	CTSS	cathepsin S	Cytoplasm	enzyme	1.30	0.025
P07737	PFN1	profilin 1	Cytoplasm	other	1.30	0.018
P31948	STIP1	stress induced phosphoprotein 1	Cytoplasm	ion channel	1.28	0.013
P23786	CPT2	carnitine palmitoyltransferase 2	Cytoplasm	enzyme	1.28	0.021
P10319	HLA-B	major histocompatibility complex. class I. B	Plasma Membrane	transmembrane receptor	1.28	0.035
P13804	ETFA	electron transfer flavoprotein alpha subunit	Cytoplasm	enzyme	1.27	0.018

Uniprot	Symbol	Entrez Gene Name	Location	Type(s)	Fold Change	P-value
O75874	IDH1	isocitrate dehydrogenase (NADP(+)) 1. cytosolic	Cytoplasm	transcription regulator	1.26	0.005
P22307	SCP2	sterol carrier protein 2	Cytoplasm	transmembrane receptor	1.25	0.033
P01892	HLA-A	major histocompatibility complex. class I. A	Plasma Membrane	ion channel	1.24	0.007
Q99536	VAT1	vesicle amine transport 1	Plasma Membrane	transporter	1.23	0.024
P05556	ITGB1	integrin subunit beta 1	Plasma Membrane	other	1.19	0.05
Q9NX63	CHCHD3	coiled-coil-helix-coiled-coil-helix domain containing 3	Cytoplasm	enzyme	1.19	0.047
P46459	NSF	N-ethylmaleimide sensitive factor	Cytoplasm	enzyme	1.17	0.031
Q99623	PHB2	prohibitin 2	Cytoplasm	other	1.15	0.039
P27797	CALR	calreticulin	Cytoplasm	other	1.14	0.01
P55265	ADAR	adenosine deaminase. RNA-specific	Nucleus	peptidase	1.13	0.013
Q15942	ZYX	zyxin	Plasma Membrane	enzyme	1.12	0.006
P12109	COL6A1	collagen type VI alpha 1	Extracellular Space	peptidase	1.10	0.047
Q02878	RPL6	ribosomal protein L6	Nucleus	other	1.10	0.024
P10599	TXN	thioredoxin	Cytoplasm	other	1.07	0.007
P07910	HNRNPC	heterogeneous nuclear ribonucleoprotein C (C1/C2)	Nucleus	other	1.06	0.007
P28799	GRN	granulin	Extracellular Space	other	1.06	0.016
Q15067	ACOX1	acyl-CoA oxidase 1. palmitoyl	Cytoplasm	other	1.05	0.047
P01033	TIMP1	TIMP metallopeptidase inhibitor 1	Extracellular Space	other	1.05	0.013

Supplementary Table 4

Uniprot	Symbol	Entrez Gene Name	Location	Type(s)	Fold Change	P-Value
P49757	NUMB	NUMB endocytic adaptor protein	Plasma Membrane	other	3.665474579	0.001
Q13231	CHIT1	chitinase 1	Extracellular Space	enzyme	3.333412829	0.001
P01137	TGFB1	transforming growth factor beta 1	Extracellular Space	growth factor	3.000077979	0.019
Q16181	SEPT7	septin 7	Cytoplasm	other	2.500124605	0.038
Q9GZY6	LAT2	linker for activation of T-cells family member 2	Plasma Membrane	other	2	0.047
P40429	RPL13A	ribosomal protein L13a	Cytoplasm	other	1.777685362	0.039
P30041	PRDX6	peroxiredoxin 6	Cytoplasm	enzyme	1.624504793	0.033
P50281	MMP14	matrix metallopeptidase 14	Extracellular Space	peptidase	1.500038989	0.007
P30520	ADSS	adenylosuccinate synthase	Cytoplasm	enzyme	1.461044379	0.047
P49327	FASN	fatty acid synthase	Cytoplasm	enzyme	1.382232207	0.006
Q9BV40	VAMP8	vesicle associated membrane protein 8	Plasma Membrane	transporter	1.363202607	0.013
P08559	PDHA1	pyruvate dehydrogenase (lipoamide) alpha 1	Cytoplasm	enzyme	1.278099363	0.047
Q07955	SRSF1	serine/arginine-rich splicing factor 1	Nucleus	other	1.266634254	0.016
P26038	MSN	moesin	Plasma Membrane	other	1.20664392	0.038
O00567	NOP56	NOP56 ribonucleoprotein	Nucleus	other	1.17609125	0.026
P18669	PGAM1	phosphoglycerate mutase 1	Cytoplasm	phosphatase	1.135242102	0.016
P07900	HSP90AA1	heat shock protein 90kDa alpha family class A member 1	Cytoplasm	enzyme	1.100378609	0.023
P62937	PPIA	peptidylprolyl isomerase A	Cytoplasm	enzyme	1.060687741	0.001

Supplementary Table 5

Uniprot	Symbol	Entrez Gene Name	Location	Type(s)	Fold Change	P-Value
Q0VD83	APOBR	apolipoprotein B receptor	Plasma Membrane	transmembrane receptor	0.21	0.002
O94874	UFL1	UFM1 specific ligase 1	Cytoplasm	other	0.25	0.006
Q8N1F7	NUP93	nucleoporin 93kDa	Nucleus	other	0.30	0.001
Q99685	MGLL	monoglyceride lipase	Plasma Membrane	enzyme	0.30	0.001
P48556	PSMD8	proteasome 26S subunit. non-ATPase 8	Cytoplasm	other	0.30	0.006
P00749	PLAU	plasminogen activator. urokinase	Extracellular Space	peptidase	0.30	0.04
P54886	ALDH18A1	aldehyde dehydrogenase 18 family member A1	Cytoplasm	kinase	0.33	0.002
Q14011	CIRBP	cold inducible RNA binding protein	Nucleus	translation regulator	0.33	0.002
P53634	CTSC	cathepsin C	Cytoplasm	peptidase	0.33	0.002
Q8IXB1	DNAJC10	DnaJ heat shock protein family (Hsp40) member C10	Cytoplasm	enzyme	0.40	0.034
P62979	RPS27A	ribosomal protein S27a	Cytoplasm	other	0.47	0.049
P28066	PSMA5	proteasome subunit alpha 5	Cytoplasm	peptidase	0.59	0.007
Q96JJ7	TMX3	thioredoxin related transmembrane protein 3	Cytoplasm	enzyme	0.64	0.001
Q5JRX3	PITRM1	pitrilysin metallopeptidase 1	Cytoplasm	peptidase	0.65	0.025
O94925	GLS	glutaminase	Cytoplasm	enzyme	0.70	0.016
O96008	TOMM40	translocase of outer mitochondrial membrane 40	Cytoplasm	ion channel	0.72	0.034
P23284	PPIB	peptidylprolyl isomerase B	Cytoplasm	enzyme	0.73	0.02
Q00341	HDLBP	high density lipoprotein binding protein	Nucleus	transporter	0.74	0.024
P07305	H1F0	H1 histone family member 0	Nucleus	other	0.74	0.025
P00491	PNP	purine nucleoside phosphorylase	Nucleus	enzyme	0.74	0.047
P62333	PSMC6	proteasome 26S subunit. ATPase 6	Nucleus	peptidase	0.75	0.007
O14818	PSMA7	proteasome subunit alpha 7	Cytoplasm	peptidase	0.75	0.007
P43490	NAMPT	nicotinamide phosphoribosyltransferase	Extracellular Space	cytokine	0.75	0.031
P10515	DLAT	dihydrolipoamide S-acetyltransferase	Cytoplasm	enzyme	0.79	0.047

P99999	CYCS	cytochrome c. somatic	Cytoplasm	transporter	0.80	0.024
O95571	ETHE1	ETHE1. persulfide dioxygenase	Cytoplasm	enzyme	0.87	0.033
Q15942	ZYX	zyxin	Plasma Membrane	other	0.88	0.047
P61019	RAB2A	RAB2A. member RAS oncogene family	Cytoplasm	enzyme	0.92	0.026
P62277	RPS13	ribosomal protein S13	Cytoplasm	other	0.95	0.025

Supplementary Table 6

UniProt	Symbol	Entrez Gene Name	Location	Type(s)	Fold Change	P-Value
P01584	IL1B	interleukin 1 beta	Extracellular Space	cytokine	7.00	0.002
O75431	MTX2	metaxin 2	Cytoplasm	transporter	4.33	0.008
Q9Y2J2	EPB41L3	erythrocyte membrane protein band 4.1 like 3	Plasma Membrane	other	3.50	0.009
Q9ULC5	ACSL5	acyl-CoA synthetase long-chain family member 5	Cytoplasm	enzyme	3.33	0.001
P17813	ENG	endoglin	Plasma Membrane	transmembrane receptor	3.33	0.002
P00749	PLAU	plasminogen activator. urokinase	Extracellular Space	peptidase	3.33	0.04
P00390	GSR	glutathione reductase	Cytoplasm	enzyme	3.20	0.008
P28074	PSMB5	proteasome subunit beta 5	Cytoplasm	peptidase	3.00	0.002
P54886	ALDH18A1	aldehyde dehydrogenase 18 family member A1	Cytoplasm	kinase	3.00	0.002
P06280	GLA	galactosidase alpha	Cytoplasm	enzyme	3.00	0.006
P49006	MARCKSL1	MARCKS-like 1	Cytoplasm	other	3.00	0.029
Q9HCC0	MCCC2	methylcrotonoyl-CoA carboxylase 2	Cytoplasm	enzyme	2.60	0.033
Q9UNM6	PSMD13	proteasome 26S subunit. non-ATPase 13	Cytoplasm	peptidase	2.43	0.006
P20340	RAB6A	RAB6A. member RAS oncogene family	Cytoplasm	enzyme	2.17	0.024
Q9Y230	RUVBL2	RuvB like AAA ATPase 2	Nucleus	transcription regulator	1.88	0.019
Q13148	TARDBP	TAR DNA binding protein	Nucleus	transcription regulator	1.88	0.047
P35914	HMGCL	3-hydroxymethyl-3-methylglutaryl-CoA lyase	Cytoplasm	enzyme	1.86	0.039
P05109	S100A8	S100 calcium binding protein A8	Cytoplasm	other	1.78	0.006
P18031	PTPN1	protein tyrosine phosphatase. non-receptor type 1	Cytoplasm	phosphatase	1.73	0.05
P07305	H1F0	H1 histone family member 0	Nucleus	other	1.58	0.016
Q02543	RPL18A	ribosomal protein L18a	Cytoplasm	other	1.58	0.016
P06702	S100A9	S100 calcium binding protein A9	Cytoplasm	other	1.58	0.039
P62269	RPS18	ribosomal protein S18	Cytoplasm	other	1.56	0.05
O75533	SF3B1	splicing factor 3b subunit 1	Nucleus	other	1.54	0.009

UniProt	Symbol	Entrez Gene Name	Location	Type(s)	Fold Change	P-Value
Q8IXB1	DNAJC10	DnaJ heat shock protein family (Hsp40) member C10	Cytoplasm	enzyme	1.50	0.013
Q5JRX3	PITRM1	pitrilysin metallopeptidase 1	Cytoplasm	peptidase	1.48	0.039
P10515	DLAT	dihydrolipoamide S-acetyltransferase	Cytoplasm	enzyme	1.46	0.013
P14854	COX6B1	cytochrome c oxidase subunit 6B1	Cytoplasm	enzyme	1.45	0.013
Q9P2E9	RRBP1	ribosome binding protein 1	Cytoplasm	other	1.43	0.009
P62820	RAB1A	RAB1A. member RAS oncogene family	Cytoplasm	enzyme	1.41	0.001
P49748	ACADVL	acyl-CoA dehydrogenase. very long chain	Cytoplasm	enzyme	1.41	0.034
P48163	ME1	malic enzyme 1	Cytoplasm	enzyme	1.40	0.007
Q7Z7H5	TMED4	transmembrane p24 trafficking protein 4	Cytoplasm	transporter	1.40	0.047
P51148	RAB5C	RAB5C. member RAS oncogene family	Cytoplasm	enzyme	1.38	0.019
P23786	CPT2	carnitine palmitoyltransferase 2	Cytoplasm	enzyme	1.34	0.003
Q15067	ACOX1	acyl-CoA oxidase 1. palmitoyl	Cytoplasm	enzyme	1.33	0.013
P54920	NAPA	NSF attachment protein alpha	Cytoplasm	transporter	1.33	0.035
P28066	PSMA5	proteasome subunit alpha 5	Cytoplasm	peptidase	1.31	0.024
P43490	NAMPT	nicotinamide phosphoribosyltransferase	Extracellular Space	cytokine	1.29	0.003
P13804	ETFA	electron transfer flavoprotein alpha subunit	Cytoplasm	transporter	1.24	0.003
P11387	TOP1	topoisomerase (DNA) I	Nucleus	enzyme	1.24	0.017
P52272	HNRNPM	heterogeneous nuclear ribonucleoprotein M	Nucleus	other	1.20	0.034
P07602	PSAP	prosaposin	Extracellular Space	other	1.13	0.006
P25774	CTSS	cathepsin S	Cytoplasm	peptidase	1.13	0.007
P0DMV8	HSPA1A/HSPA1B	heat shock protein family A (Hsp70) member 1A	Cytoplasm	enzyme	1.13	0.047
P07910	HNRNPC	heterogeneous nuclear ribonucleoprotein C (C1/C2)	Nucleus	other	1.12	0
P99999	CYCS	cytochrome c. somatic	Cytoplasm	transporter	1.11	0.024
P27797	CALR	calreticulin	Cytoplasm	transcription regulator	1.10	0.049
Q99536	VAT1	vesicle amine transport 1	Plasma Membrane	transporter	1.09	0.013

UniProt	Symbol	Entrez Gene Name	Location	Type(s)	Fold Change	P-Value
Q68CZ2	TNS3	tensin 3	Plasma Membrane	phosphatase	1.07	0.03
Q9Y6N5	SQRDL	sulfide quinone reductase-like (yeast)	Cytoplasm	enzyme	1.05	0.038
P62937	PPIA	peptidylprolyl isomerase A	Cytoplasm	enzyme	1.03	0.007
P26641	EEF1G	eukaryotic translation elongation factor 1 gamma	Cytoplasm	translation regulator	1.02	0.019
P06576	ATP5B	ATP synthase. H+ transporting. mitochondrial F1 complex. beta polypeptide	Cytoplasm	transporter	1.01	0.005

Supplementary Table 7

UniProt	Symbol	Entrez Gene Name	Location	Type(s)	Fold Change	P-Value
P60709	ACTB	actin. beta	Cytoplasm	other	0.99	0.039
P06733	ENO1	enolase 1	Cytoplasm	enzyme	0.99	0.032
P49368	CCT3	chaperonin containing TCP1 subunit 3	Cytoplasm	other	0.97	0.024
Q9Y490	TLN1	talin 1	Plasma Membrane	other	0.97	0.026
P04075	ALDOA	aldolase. fructose-bisphosphate A	Cytoplasm	enzyme	0.97	0.043
P07437	TUBB	tubulin beta class I	Cytoplasm	other	0.96	0.03
P07355	ANXA2	annexin A2	Plasma Membrane	other	0.94	0.033
Q15365	PCBP1	poly(rC) binding protein 1	Nucleus	translation regulator	0.94	0.046
P40121	CAPG	capping actin protein. gelsolin like	Nucleus	other	0.91	0.002
Q06830	PRDX1	peroxiredoxin 1	Cytoplasm	enzyme	0.91	0.034
Q06323	PSME1	proteasome activator subunit 1	Cytoplasm	other	0.90	0.013
Q9BQE3	TUBA1C	tubulin alpha 1c	Cytoplasm	other	0.90	0.003
P18669	PGAM1	phosphoglycerate mutase 1	Cytoplasm	phosphatase	0.88	0.043
P07900	HSP90AA1	heat shock protein 90kDa alpha family class A member 1	Cytoplasm	enzyme	0.88	0.027
P27348	YWHAQ	tyrosine 3-monooxygenase/tryptophan 5-monooxygenase activation protein theta	Cytoplasm	other	0.86	0.003
P52907	CAPZA1	capping actin protein of muscle Z-line alpha subunit 1	Cytoplasm	other	0.86	0.013
Q99798	ACO2	aconitase 2	Cytoplasm	enzyme	0.85	0.016
P18621	RPL17	ribosomal protein L17	Cytoplasm	other	0.84	0.024
P20702	ITGAX	integrin subunit alpha X	Plasma Membrane	transmembrane receptor	0.83	0.015
P09211	GSTP1	glutathione S-transferase pi 1	Cytoplasm	enzyme	0.82	0.008
P54136	RARS	arginyl-tRNA synthetase	Cytoplasm	enzyme	0.82	0.016
Q32P28	P3H1	prolyl 3-hydroxylase 1	Nucleus	enzyme	0.81	0.047
P68104	EEF1A1	eukaryotic translation elongation factor 1 alpha 1	Cytoplasm	translation regulator	0.79	0.036

UniProt	Symbol	Entrez Gene Name	Location	Type(s)	Fold Change	P-Value
Q92598	HSPH1	heat shock protein family H (Hsp110) member 1	Cytoplasm	other	0.78	0.044
O43312	MTSS1	metastasis suppressor 1	Cytoplasm	other	0.77	0.047
Q9UI12	ATP6V1H	ATPase H+ transporting V1 subunit H	Cytoplasm	transporter	0.75	0.016
Q16831	UPP1	uridine phosphorylase 1	Cytoplasm	enzyme	0.73	0.05
Q9UQ80	PA2G4	proliferation-associated 2G4	Nucleus	transcription regulator	0.72	0.001
P30153	PPP2R1A	protein phosphatase 2 regulatory subunit A. alpha	Cytoplasm	phosphatase	0.71	0.033
Q96KP4	CNDP2	CNDP dipeptidase 2 (metallopeptidase M20 family)	Cytoplasm	peptidase	0.71	0.014
P63313	TMSB10/TMSB4X	thymosin beta 10	Cytoplasm	other	0.70	0.035
P15311	EZR	ezrin	Plasma Membrane	other	0.69	0.021
O14579	COPE	coatomer protein complex subunit epsilon	Cytoplasm	transporter	0.69	0.025
Q15185	PTGES3	prostaglandin E synthase 3	Cytoplasm	enzyme	0.65	0.023
P40429	RPL13A	ribosomal protein L13a	Cytoplasm	other	0.64	0.026
P31146	CORO1A	coronin 1A	Cytoplasm	other	0.64	0.007
Q8NCW5	NAXE	NAD(P)HX epimerase	Extracellular Space	enzyme	0.63	0.008
Q15019	SEPT2	septin 2	Cytoplasm	enzyme	0.63	0.039
P30041	PRDX6	peroxiredoxin 6	Cytoplasm	enzyme	0.62	0.034
P49327	FASN	fatty acid synthase	Cytoplasm	enzyme	0.60	0.009
O60749	SNX2	sorting nexin 2	Cytoplasm	transporter	0.54	0.012
P12955	PEPD	peptidase D	Cytoplasm	peptidase	0.54	0.033
Q14318	FKBP8	FK506 binding protein 8	Cytoplasm	other	0.50	0.047
Q9GZY6	LAT2	linker for activation of T-cells family member 2	Plasma Membrane	other	0.47	0.034
P14174	MIF	macrophage migration inhibitory factor (glycosylation-inhibiting factor)	Extracellular Space	cytokine	0.45	0.023
P17858	PFKL	phosphofructokinase. liver type	Cytoplasm	kinase	0.34	0.02
Q9UL25	RAB21	RAB21. member RAS oncogene family	Cytoplasm	enzyme	0.33	0.001

UniProt	Symbol	Entrez Gene Name	Location	Type(s)	Fold Change	P-Value
Q14012	CAMK1	calcium/calmodulin dependent protein kinase I	Cytoplasm	kinase	0.33	0.002
Q9HB71	CACYBP	calcyclin binding protein	Nucleus	other	0.30	0.002
Q06210	GFPT1	glutamine--fructose-6-phosphate transaminase 1	Cytoplasm	enzyme	0.30	0.002
P62899	RPL31	ribosomal protein L31	Cytoplasm	other	0.30	0.002
P13473	LAMP2	lysosomal associated membrane protein 2	Plasma Membrane	enzyme	0.30	0.002
Q14257	RCN2	reticulocalbin 2	Cytoplasm	other	0.30	0.002
O95352	ATG7	autophagy related 7	Cytoplasm	enzyme	0.30	0.002
P21291	CSRP1	cysteine and glycine rich protein 1	Nucleus	other	0.27	0.001
P16949	STMN1	stathmin 1	Cytoplasm	other	0.23	0.001
Q13177	PAK2	p21 protein (Cdc42/Rac)-activated kinase 2	Cytoplasm	kinase	0.23	0.007
P13798	APEH	acylaminoacyl-peptide hydrolase	Cytoplasm	peptidase	0.23	0.014
P98171	ARHGAP4	Rho GTPase activating protein 4	Cytoplasm	other	0.20	0.001

Chapter 7
Expression of P2RY12 in microglia in astrocytomas relates to M1/M2 status

Chapter 7

Expression site of P2RY12 in residential microglial cells in astrocytomas correlates with M1 and M2 marker expression and tumor grade.

Changbin Zhu, MD, MSc.; Johan M. Kros MD, PhD.; Marcel van der Weiden, MSc.; PingPin Zheng, MD, PhD; Caroline Cheng, PhD.*; Dana A. Mustafa, PhD.* (* equal contribution of last authors)

(Acta Neuropathol Comm. 2017, 10;5(1) ahead of print)

ABSTRACT

The role of resident microglial cells in the pathogenesis and progression of glial tumors is still obscure mainly due to a lack of specific markers. Recently P2RY12, a P2 purinergic receptor, was introduced as a specific marker for microglial cells under normal and pathologic conditions. Here we analyzed the expression of P2RY12 in astrocytomas of various malignancy grades in relation to markers for M1 and M2 macrophage activation profiles by using two web-based glioma datasets and confocal immunohistochemistry to 28 astrocytoma samples grades II-IV. In the gliomas, P2RY12 immunoreactivity delineated CD68 negative cells with otherwise microglial features from CD68 positive tumor associated macrophages (TAMs). The presence of P2RY12 positive cells correlated positively with overall survival. P2RY12 mRNA levels and membrane-bound localization of P2RY12 were inversely correlated with increasing malignancy grade, and the expression site of P2RY12 shifted from cytoplasmic in low-grade gliomas, to nuclear in high-grade tumors. The cytoplasmic expression of P2RY12 was associated with the expression of M1 markers, characteristic of the pro-inflammatory macrophage response. In contrast, the nuclear localization of P2RY12 was predominant in the higher graded tumors and associated with the expression of the M2 marker CD163.

We conclude that P2RY12 is a specific marker for resident microglia in glioma and its expression and localization correspond to tumor grade and predominant stage of M1/M2 immune response.

INTRODUCTION

Microglial cells are brain-specific tissue resident macrophages that are directly derived from yolk-sac erythromyeloid precursor cells (EMP) during embryonic development (1). As major contributors to the immune status of the central nervous system (CNS) microglial cells scan the CNS for cellular debris by continuously protract and retract their cell processes (2). The microglial survey mediates the immune response, supports the homeostasis of the neurons and, in collaboration with astrocytes, maintains the integrity of the blood-brain barrier (BBB) (3-5). Microglial cells become activated by a large variety of pathogenic situations. Upon activation, the cells take on an amoeboid shape and initiate the paracrine recruitment of blood-derived macrophages into the altered brain parenchyma, initiating an inflammatory response (6, 7). Microglia serves additional, only partly known, roles in repair processes following the acute stage of tissue damage (8, 9). Recent studies addressing the phenotypic adaptations of peripheral macrophages in cancer have shown that tumor associated macrophages (TAMs), similar to the M1 and M2 activation states of macrophages, display particular marker profiles of pro- and anti-oncogenic action (10, 11). TAMs with anti-tumor action share characteristics with M1 macrophages; are capable of antigen presentation and paracrine signaling to promote inflammation, thereby hampering tumor growth and prolonging patient survival (12, 13). These cells are referred to as M1-like cells. In contrast, TAMs that promote tumor progression are associated with an immunosuppressive response; contribute to tumor angiogenesis and proliferation, and are associated with poor clinical outcomes (14-16) and these cells are referred to as M2-like cells. In general, TAMs are more similar to M2 - than M1 macrophages (17).

Recent reports have pointed to the heterogeneity of microglial cells (16). In glioblastoma, microglia displays a pro-oncogenic phenotype resembling that of M2-like macrophages, because the cells are in a microenvironment rich in glioma (stem) cell derived factors like TGF-β1, MCP-1, PGE-2, and soluble colony stimulating factors (18). There is data showing that resident microglia in glioblastomas plays a role in tumor progression and invasion by the release of cytokines and proteases (19-21). However, the mechanism of microglial activation and the contribution of microglia to tumor progression are largely unknown. In order to obtain insight in the specific action of residential microglial cells in gliomas, proper discrimination of these cells from TAMs is necessary. So far, specific markers for residential microglial cells that delineate these cells from other recruited cells of monocyte lineage, are lacking. As a matter of fact, TAMs share many markers with microglial cells. The microglial marker Iba-1 is co-expressed with CD45 and is therefore, not discriminative between residential microglia and monocytic cells that migrated into the brain (22). In the brains of patients who suffered from Alzheimer disease (AD) the markers CD45 and Iba-1 were used in combination with P2RY12 to separate macrophages from microglia (22). Considering the growing interest in understanding the role of microglial cells in gliomas, specific markers for the identification of resident microglia in the context of primary brain tumors are urgently needed.

Recently, the Purinergic Receptor P2Y12 (P2RY12) was proposed as a specific marker for healthy rodent CNS microglial cells, discriminating these cells from other types of tissue resident macrophages or blood-derived monocytes (23). P2RY12 was claimed as a specific marker for microglial cells in human brains (24-26). P2RY12 belongs to the family of P2 purinergic receptors, consisting of seven transmembrane G protein coupled receptors (GPCRs) that contribute to ATP-and ADP-mediated cell migration *in vitro* (27). P2RY12 is expressed in activated platelets and notoriously, in microglial cells (28). P2RY12 deficiency in P2RY12 knockdown mice significantly compromised microglial chemotaxis and extension of microglial foot processes in response to CNS injury (29, 30). In this study, we scrutinized P2RY12 as a marker for microglial cells in glial tumors. We also investigated the relation between the expression of P2RY12 and that of pro- or anti-inflammatory markers; the expression sites in the microglial cells and the relation with tumor progression.

MATERIAL AND METHODS

Patient samples

All patient samples were obtained from the Archives of the Department of Pathology, Erasmus Medical Center, Rotterdam, with approval of medical ethical committee of the Erasmus Medical Center. Twenty-eight glioma samples (11 astrocytomas WHO grade II (A II), 7 anaplastic astrocytomas (WHO grade III; AA) and 10 glioblastomas (GBMs) were collected and all diagnoses were confirmed by a certified pathologist (JMK). The mean ages ± standard deviations and the male/female ratio are summarized in (Table 1). Four autopsy brains of patients who did not have brain tumors were used as a control. Post-mortem times of the control cases were 8 hours or less.

Table 1. summary of the patients used for immunohistochemistry

	Astrocytoma grade II (AII)	Anaplastic Astrocytoma (AA)	Glioblastoma (GBM)	Control (autopsy brains)
Mean age ± st. dev.	42 ± 12.8	40 ± 12.8	45 ± 14.9	58 ± 13.3
Male/Female	4/7	4/3	7/3	2/2

Immunostaining

Adjacent sections of 5µm thickness from Formalin Fixed Paraffin Embedded (FFPE) samples were used for immunohistochemical analysis. The sections were incubated with antibodies against P2RY12 (1:100; Sigma, Sweden); CD68 (1:800; Dako, Denmark) GFAP (1:200; Dako, Denmark); CD45 (1:100; Dako, Denmark) and CD163 (1:400; Abd Serotec, USA). The staining procedure and scanning of the stained sections were per-

formed according to the protocol described previously (31). For double labeling, Alexa Fluor 488 and 555-conjugated secondary antibodies (1:200, Thermo Fisher Scientific, The Netherlands) were used for detection. For triple staining, Goat anti-Mouse F(ab)2 fragment (Jackson ImmunoResearch, WestGrove, PA, USA) was used to block background epitopes and Alexa Fluor 647-conjugated secondary antibody (Thermo Fisher Scientific, The Netherlands) was used for detection. The fluorescent labeled samples were analyzed by using the confocal microscope LSM 700 (Zeiss, The Netherlands). Signal positive areas and staining intensity were quantified using the Image J program to five high power field (40x) areas of each immunostained slide.

Public database

The transcription level of P2RY12 was assessed in human gliomas of various WHO grades, using 2 different datasets derived from the public NCBI GEO database (GDS 4467 Gene ID 64805 and GDS1816 Gene ID 64805). In addition, transcriptional data of P2ry12 in a murine glioma model were obtained from the GEO database (GSE 86573) (32). RNA-sequencing data of P2RY12 combined with clinical data were obtained from two TCGA glioblastoma databases (Provisional: 166 GBM patients (33). In addition, information on IDH1 mutation as well as MGMT methylation status were also obtained from the TCGA GBM database (Cell, 2013). The R program and CGDS-R package provided by the cBioPortal for cancer genomics from Memorial Sloan-Kettering Cancer Center was used to download and process data.

To study the relation between P2RY12 mRNA expression levels and markers for microglia identification, a mutual exclusivity analysis was performed as described previously (34, 35). The GBM TCGA dataset (GBM, provisional) and a low-grade glioma TCGA dataset were selected for analysis using the cBioPortal websource (Supplementary Table 1). High P2RY12 expression was defined by a Z score ≥ 2. Z score = (individual P2RY12 value – mean P2RY12 value) / std. dev. of the whole sample set. A log Odd Ratio (OR) >0 indicates a trend of co-occurrence in expression of P2RY12 with the listed genes and log (OR) <0 indicates a trend of mutual exclusivity in expression pattern.

Statistics

The results of immunostaining and the data from public database were analyzed by the Mann-Whitney U test ($P<0.05$ was considered significant). Survival analysis was performed using the Log-rank test ($P<0.05$ was considered significant). All data and graphs were analyzed and made by using Graph pad Prism 5.0.

RESULTS

Reduction of membrane P2RY12 signal correlates with glioma grade.

The analysis of the public databases revealed that P2RY12 is mainly expressed in A II, while less in AA and GBM (Figure 1a). The results of immunostaining for P2RY12 are shown in Figure 1b. P2RY12 positive cells in autopsy brains and A II presented the typical ramified morphology with extended processes. In contrast, in AA a mixture of both ramified and amoeboid P2RY12 positive cells were noticed. In the GBMs the P2RY12 staining was less on the cell membranes while the signal was mainly visible in the nuclei ($P2RY12^{nuclei+}$). Quantitative analysis of the percentage of P2RY12 positive areas per image view revealed a significant smaller number of P2RY12 positive cells in the AA and GBM as compared to A II (Figure 1b, c). Double staining of P2RY12 with the pan- macrophage marker CD68 revealed a large population of CD68 negative, P2RY12 positive cells ($CD68^{-}$ $P2RY12^{+}$) distinct from TAMs ($CD68^{+}$ $P2RY12^{-}$) in all glioma samples (Figure 1e). The population of $P2RY12^{+}$ cells did not overlap with the population of GFAP positive tumor cells or reactive astrocytes (Figure 1f). In autopsy brain, A II and AA, the $CD68^{+}$ TAMs generally had round cell bodies and were located around the blood vessels. In GBM, $CD68^{+}$ TAMs were not only located around the blood vessels (Figure 1e, white arrows), but were spatially mixed with the $P2RY12^{nuclei+}$ cells.

Figure 1 Legends to Figure 1. Reduced P2RY12 expression and nucleus translocation in microglia/macrophages correlated with glioma progression.

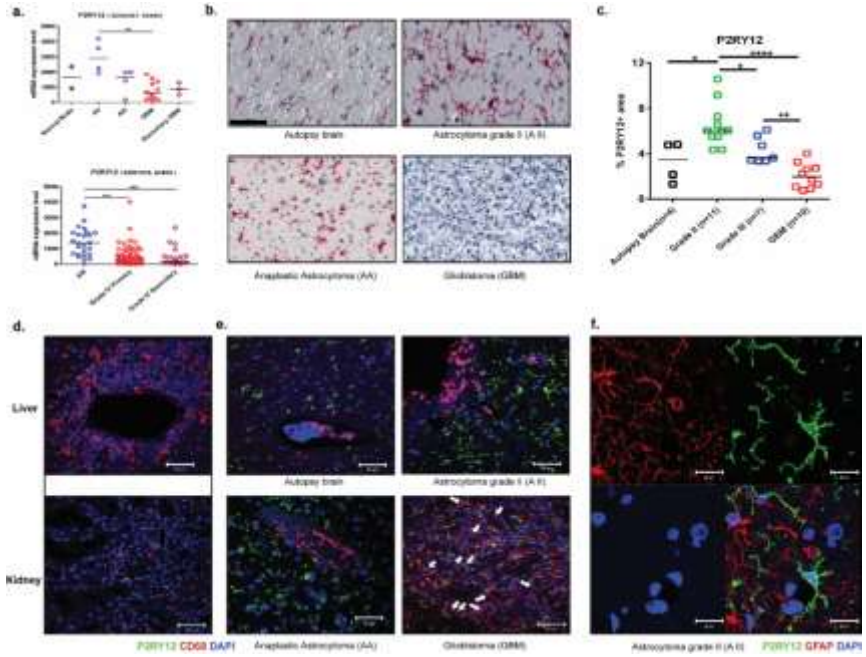

a: Analysis of GEO databases reveals decrease of P2RY12 mRNA expression with progression of glioma. Results are shown in the median values of P2RY12 mRNA levels. ** P<0.01; ***P<0.005. A II: Astrocytoma WHO grade II, AA: Anaplastic Astrocytoma (WHO grade III), GBM: Glioblastoma. **b:** Immunohistochemical staining for P2RY12 in normal brain and different grades of glioma. Representative pictures were selected from each group. Cells with the P2RY12 signal localized mainly in the cytoplasm display the classic ramified microglial morphology in autopsy brain, A II and AA. Cells with nuclear location of P2RY12 are mainly observed in GBM samples (scale bar: 100 µm). **c:** Quantification of percentages of P2RY12 positive areas per image field in autopsy brain, A II and GBM. Mean values of each group are indicated. * P<0.05, ** P<0.01 ****P<0.001. **d:** Confocal images showing CD68 and P2RY12 staining in tissue samples of liver and kidney (scale bar: 50 µm).**e:** Confocal images showing the spatial relation between CD68 and P2RY12 positive cells in autopsy brain, A II, AA and GBM (scale bar: 50 µm). **f:** Confocal images showing no overlap between GFAP and P2RY12 staining in astrocytoma grade II (scale bar: 20 µm).

P2RY12$^{nuclei+}$ cells are not of myeloid origin, but represent resident microglia.

Higher numbers of CD45 positive cells were observed in AA and GBM than in A II. The CD45+ cells were mostly present around the blood vessels (Figure 2a, A II versus AA versus GBM). Double staining for CD45 and P2RY12 did not reveal double-stained cells, indicating that the P2RY12 positive cells are not derived from myeloid lineage (Figure 2a). CD45 positive cells were observed in higher graded tumors, prominently around blood vessels (Figure 2a, A II versus AA versus GBM). To further evaluate the identity of CD68^{+}P2RY12$^{nuclei+}$ cells double immunostaining for CD45 and CD68 (Figure 2b and e) and triple immunostaining for CD68, CD45 and P2RY12 was carried out. Two large cell populations were observed, namely CD68^{+}CD45^{+}P2RY12^{-} and CD68^{+}CD45^{-}P2RY12$^{nuclei+}$ cells, the former to be interpreted as monocytes/macrophages, and the latter as the resident microglial population (Figure 2c, d, f, g).

In the GEO dataset GSE 86573 generated from a murine glioma model the expression of P2ry12 by microglia (MG) was significantly higher than that by bone marrow-derived macrophages (BMDM) (Supplementary Figure 1).

Cytoplasmic or nuclear distribution of P2RY12 in microglia relates to the functional marker profiles.

The results of immunostaining for the M2 markers CD163, CD204 and P2RY12 showed that cytoplasmic P2RY12 expression did not overlap with CD163 and CD204 positivity (Figure 3a1-3, d1-3). In contrast, cells with nuclear located P2RY12 showed distinct overlap with CD163 and CD204 (Figure 3c1-3, f1-3). Confocal analysis revealed that cells with a low CD163 signal show ramified cell processes and higher P2RY12 signals. Cells with a high CD163 signal are either negative for P2RY12, or display nuclear localization of P2RY12 (Figure 4a and b, cyan and white arrows). Triple labeling for CD45, CD163 and P2RY12 differentiated between two cell populations: CD163^{+} P2RY12$^{nuclei+}$ cells devoid of CD45 signals and CD163^{+} CD45^{+} P2RY12^{+} cells (Figure 4c and d).

Figure 2.

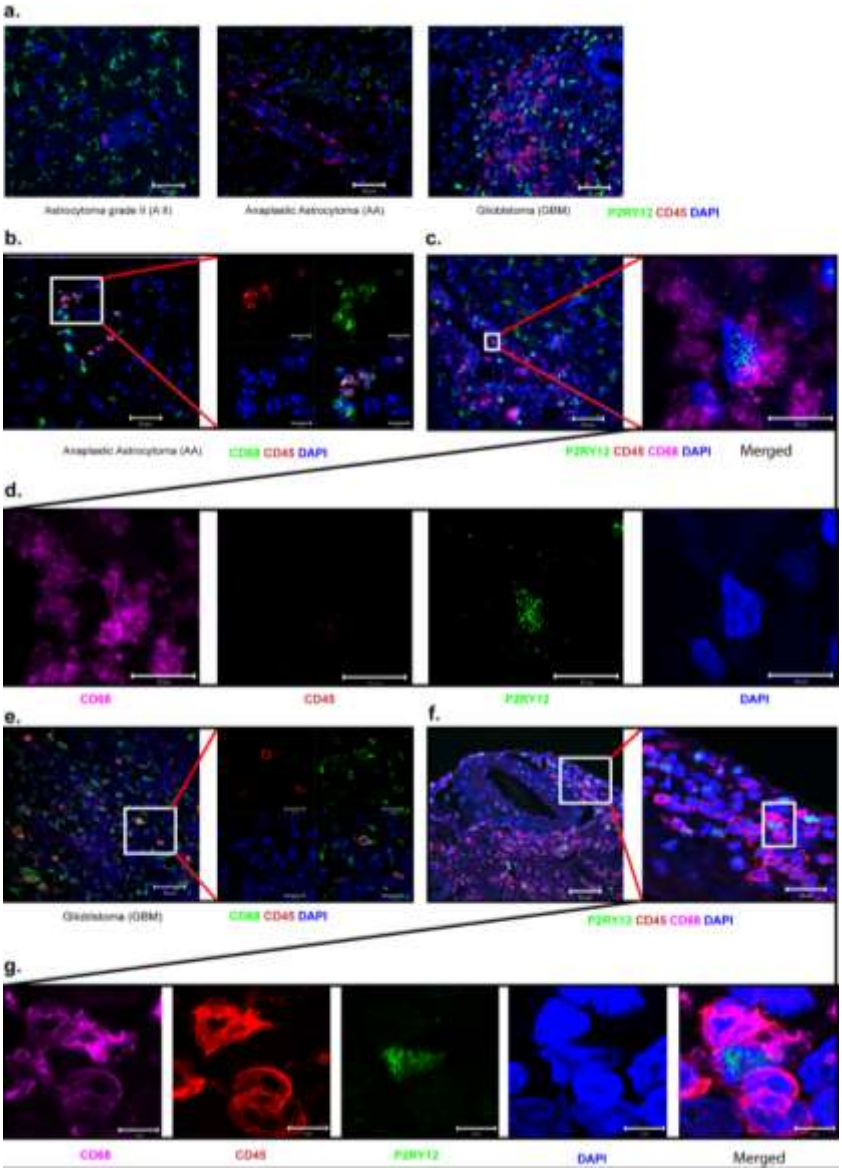

a: Cells in high grade glioma expressing P2RY12 in the nuclei are not recruited cells of myeloid origin, but resident microglia. **b:** Confocal images showing CD68 and CD45 signals in AA (scale bars: left image; 50 µm, right panel; 20 µm). **c:** Confocal images of triple staining for CD68, P2RY12 and CD45 in AA. Left image: Merged overview of triple staining (scale bar: 50 µm). Right image: Merged high magnification of a P2RY12 positive cell (scale bar: 10 µm). **d:** Panel of single channel images of a P2RY12 positive cell in AA (scale bar: 10 µm). **e:** Confocal images showing CD68 and CD45 staining in GBM (scale bar: left image; 50 µm, right panel; 20 µm). **f:** Confocal images showing triple staining for CD68, P2RY12 and CD45 in GBM. Left panel: Merged overview of triple staining (scale bar: 50 µm). Right panel: Merged higher magnification view of P2RY12 positive cells (scale bar: 10 µm). **g:** Panel of high magnification single channel images of P2RY12 positive cells in GBM (scale bar: 10 µm).

Figure 3 Cytoplasmatic and nuclear distribution of P2RY12 in microglia is correlated with M2-like activation in high grade glioma.

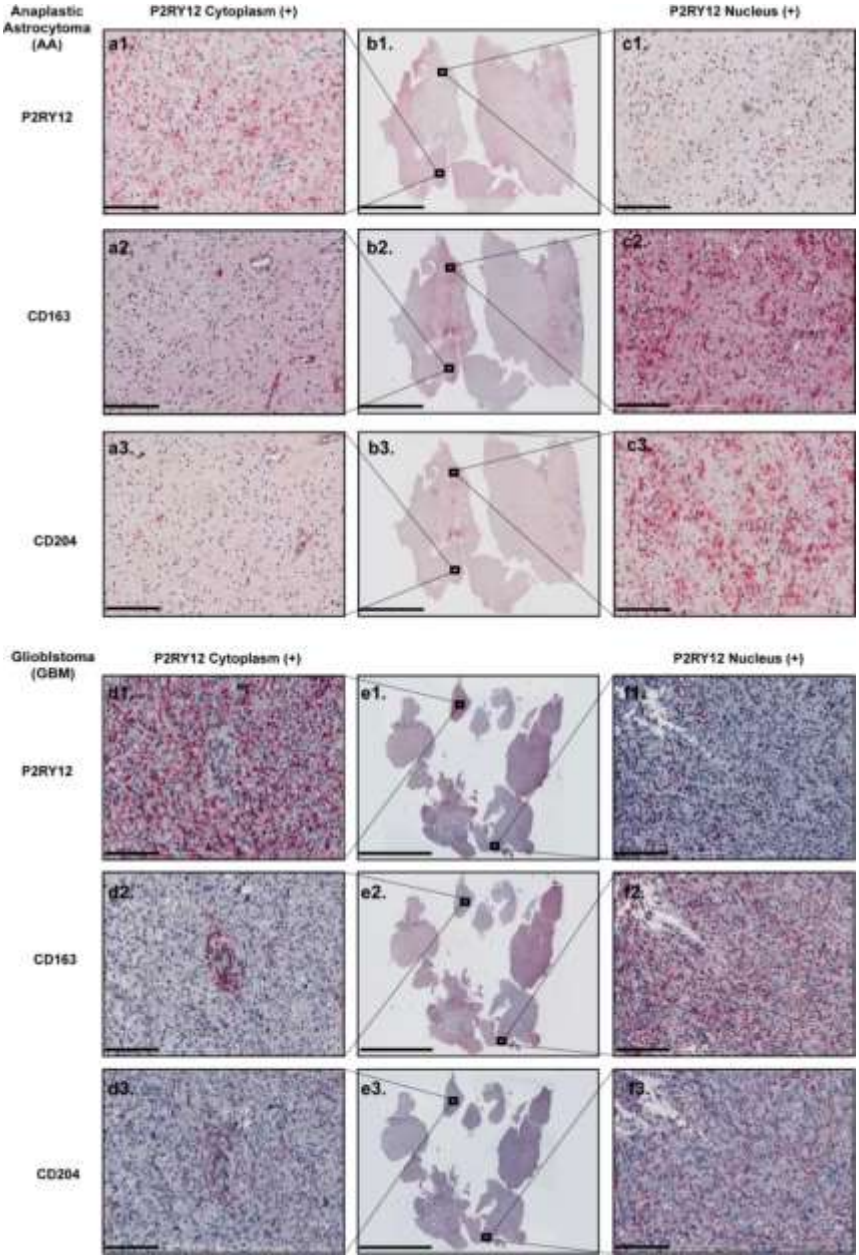

a1-a3: Co-expression of cytoplasmic P2RY12 with CD163 and CD204 in AA (scale bar: 200 µm). **b1-b3:** Overview of AA tissue samples (scale bar: 10mm). **c1-c3:** Co-expression of nuclear P2RY12 with CD163 and CD204 in AA (scale bar: 200 µm). **d1-d3:** Co-expression of cytoplasmic P2RY12 with CD163 and CD204 in GBM (scale bar: 200 µm). **e1-e3:** Overview of GBM tissue samples (scale bar: 10mm). **f1-f3:** Co-expression of nuclear P2RY12 with CD163 and CD204 in GBM (scale bar: 200 µm).

Figure 4 Confocal analysis of co-localization of P2RY12, CD163 and CD45 in GBM.

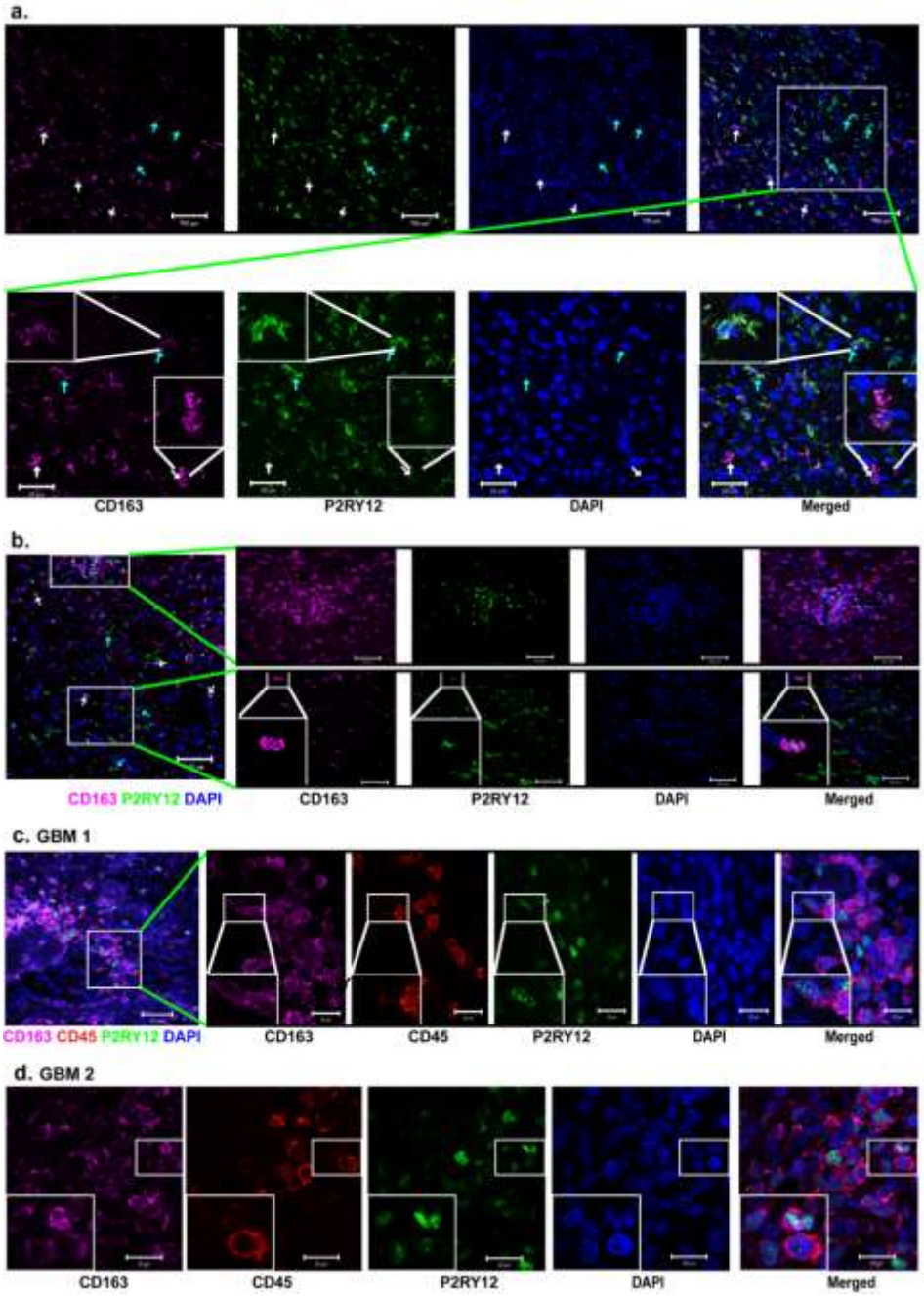

a: Upper row: overview of immunostaining for P2RY12 and CD163 in a representative GBM. White arrows indicate nuclear P2RY12 signal in cells with high CD163 signal; Cyan arrows indicate cytoplasmic P2RY12 signal in cells with low CD163 signal (scale bar:100 µm). Lower row: selected view of P2RY12 and CD163 staining in

glioblastoma. White arrows indicate cells with weak P2RY12 and high CD163 signal (scale bar: 50 µm). Inserts: details of cells with low CD163 and strong cytoplasmic P2RY12 signals, and cells with strong CD163 and weak P2RY12 signals. **b:** Overview with two inserts. Upper panel: area with cells with nuclear P2RY12 signal with strong CD163 expression (scale bar: 50 µm). Lower panel: area with cytoplasmic P2RY12 signals and weak CD163 expression (scale bar: 50 µm). White arrows: nuclear P2RY12 expression with strong CD163 signals. **c:** Overview: triple staining for CD163, P2RY12 and CD45 in GBM (scale bar: 50 µm). Inserts (scale bar: 20 µm): Cells with high CD163 and nuclear P2RY12 signals did not overlap with CD45. **d:** Confocal images showing triple staining for CD163, P2RY12 and CD45 in GBM (scale bar: 20 µm). Cells with high CD163 and nuclear P2RY12 signal did not overlap with CD45.

High expression levels of P2RY12 are associated with favorable clinical outcomes.

P2RY12 RNA expression data was obtained from two TCGA glioma databases. From the glioma database (33), 151 patients were collected for analysis (Table 2). Twenty-one tumors with at least 1-fold increase of P2RY12 expression were defined as the "P2RY12 high" group, while the tumors expressing P2RY12 al lower levels than 1-fold increase were defined as the "P2RY12-low" group. Patients with tumors of the P2RY12-high group had longer overall survival times (P=0.03), but not a longer disease free survival than those in the P2RY12-low group (Figure 5a). In the glioma provisional database from TCGA the P2RY12-high group showed a trend of longer disease free survival (P=0.0608) as well as a significant increase in overall survival time (P=0.0446) (Supplementary Figure 1a and b, upper and lower graph). Univariate analysis by the Log-rank test revealed that patients in the P2RY12-high group have lower hazard ratios for disease recurrence (HR=0.445, P=0.0187) than patients in the P2RY12 low group. Similarly, the P2RY12-high group has a lower hazard ratio for overall survival versus the P2RY12-low group (HR=0.4598, P=0.04) (Supplementary Figure 1c). The data show that P2RY12 up-regulation positively correlates with prognosis and overall survival of GBM patients. The expressional levels of P2RY12 are significantly higher in gliomas with the IDH1 (R132H) mutation as compared to the IDH wt gliomas (Supplementary Figure 3a). There is, however, no effect of P2RY12 expression on overall survival when the population was stratified for IDH1 mutation status (Supplementary Figures 3b and c). There were no expressional differences of P2RY12 between gliomas with or without MGMT promoter methylation (Supplementary Figure 4a). The expression of P2RY12 did not affect the overall survival of the patients when stratified for MGMT promoter methylation status (Supplementary Figures 4b and c).

Table 2. Summary of patients' information from TCGA GBM database

TCGA GBM Database n=151			
P2RY12		High (n=21)	Low (n=130)
RNA level ± S.D	(RNA Seq V2 RSEM)	3263±722.6	499.5±580.1
ge (year) ± S.D.		55.1±15.1	61.5±12.4
Gender	Male	17(21)	79(130)
	Female	4(21)	51(130)
DH1 mutation	WT	17(21)	127(130)
	Mutant	4(21)	3(130)
Subtype	Neural	7(21)	19(130)
	Pro-Neural	1(21)	27(130)
	Classical	4(21)	35(130)
	Mesenchymal	5(21)	44(130)
	G-CIMP	4(21)	4(130)
	N/A	0	1(130)
Therapy	TMZ Chemoradiation, TMZ Chemo	9(21)	55(130)
	Standard Radiation, TMZ Chemo	3(21)	21(130)
	Nonstandard Radiation, TMZ Chemo	2(21)	11(130)
	Standard Radiation, Alkylating Chemo	1(21)	
	Unspecified Radiation	6(21)	17(130)
	Alkylating Chemo		1(130)

Figure 5 Analysis of TCGA datasets: High expression levels of P2RY12 in GBM patients predict a favorable outcome.

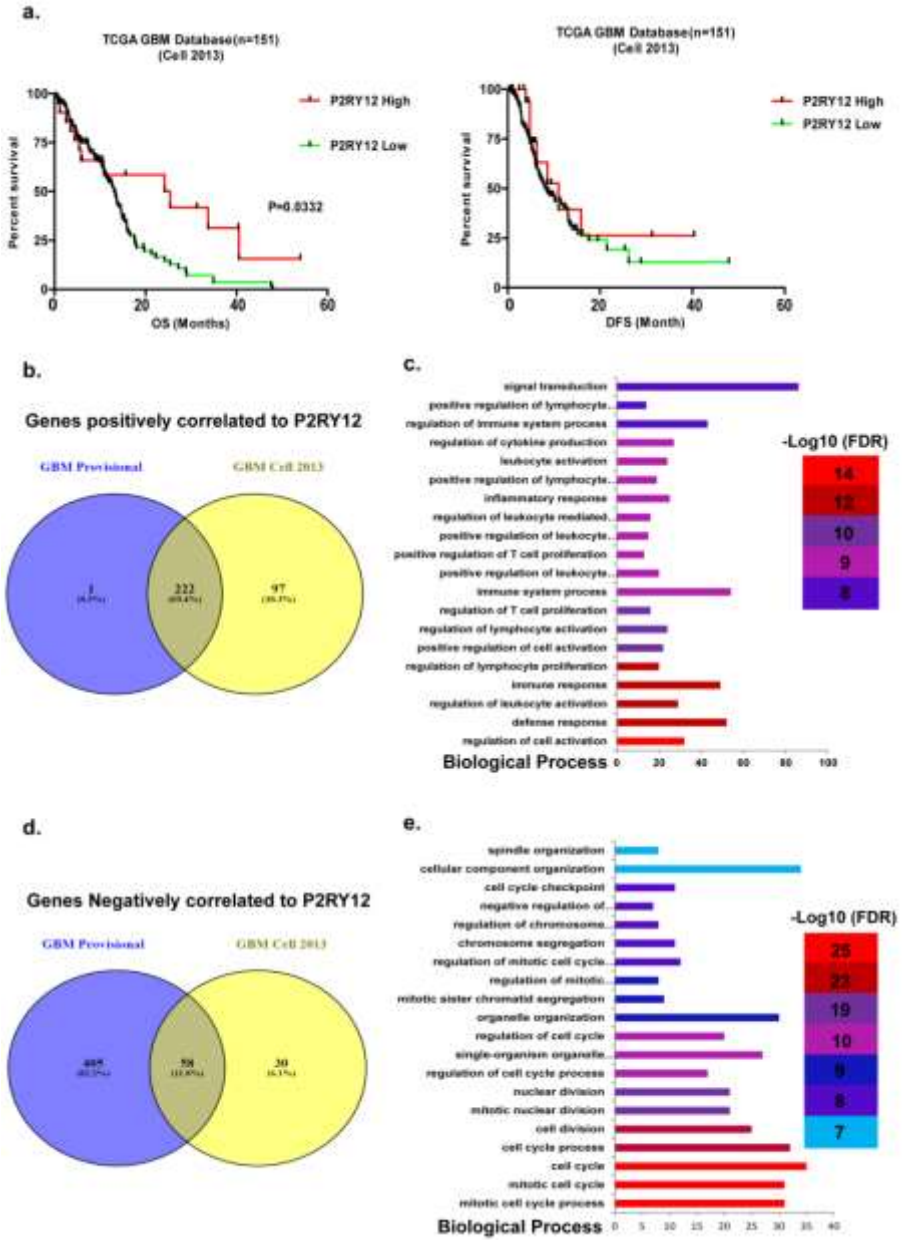

a: Kaplan-Meier curves showing disease free survival and overall survival curves of patients with different P2RY12 expression levels. **b:** Overlap of the genes found in the two datasets that positively correlate with P2RY12 expression. **c:** Top 20 most significant biological processes resulting from functional annotation of the 222 overlapping genes. The GO terms are shown on the y-axis. The numbers of input genes per GO term are indicated on the x-axis. **d:** Overlap of the genes found in the two datasets that negatively correlate with

P2RY12 expression. **e:** Top 20 most significant biological processes resulting from functional annotation of the 58 overlapping genes. The GO terms are shown on the y-axis. The numbers of input genes per GO term are indicated on the x-axis.

P2RY12 expression correlates with microglia/macrophage function.

P2RY12 had a significant likelihood for co-occurrence with the microglia markers Iba-1 and CX3CR1 in GBM, and CX3CR1, CD11b in low grade glioma. Likewise, IRF8, a transcription factor for the function and development of microglia cells (36, 37) is expressed simultaneous with P2RY12 in both GBM and low grade gliomas. Due to the limited number of samples in the high P2RY12 expression group, the p-values of associations with log(OR) <-3 remain non-significant, despite a high probability and tendency for mutual exclusion.

The associations between P2RY12 and other markers are listed in the Supplementary Table. Genes positively (Spearman r ≥0.5) or negatively (Spearman r≤-0.3) correlated with P2RY12 from the two TCGA GBM database were selected for pathway enrichment analysis (Figure 5b, d). Pathway analysis from Gene Ontology based on 222 P2RY12 positively correlating genes included the regulation of immune response including defense response, leukocyte activation, T cell activation (Figure 5c). Pathway analysis on 58 P2RY12 negatively correlating genes mainly included cell cycle regulation and cell proliferation (Figure 5e). The findings indicate that P2RY12 expression is positively correlated with markers commonly used for microglia in the CNS and positive immune response, but is inversely associated with markers for peripheral recruited macrophages, M2-like microglia/macrophage activation and cell proliferation.

DISCUSSION

In the present study, we found that resident microglial cells in gliomas specifically express P2RY12 and that the expression distinguishes microglia from other monocytes and macrophages. This finding in human gliomas corroborates the data we generated from the murine gliomas represented in the GEO database. The analysis of the public glioma datasets and the multi-labeling experiments of the glioma biopsy specimens confirmed that P2RY12 mRNA and protein expression is confined to resident microglial cells. In addition, P2RY12 expression is associated with tumor grade: the expression is less in AA and GBM, as compared to A II. However, the expression of P2RY12 is not an independent prognosticator in gliomas; when strong prognostic factors as IDH mutational status or methylation status of MGMT are taken into consideration, no additional effects of the expression are found. The expression of P2RY12 appeared to be higher in the IDH mutated tumors, which is in line with the association of IDH mutation and better prognosis on the one hand, and the pro-inflammatory status on the other. Remarkably, with

increasing malignancy grade there is a shift from cytoplasmic to nuclear expression, and in the high-grade tumors the nuclear expression of P2RY12 coincides with that of the M2 markers CD163 and CD204 (Figure 1a and c, Figure 4). We also observed that in the high-grade gliomas the P2RY12 positive microglial cells have taken an amoeboid phenotype (Figure 1b).

Upon pathologic stimuli, resting microglia adopt a highly dynamic phenotype referred to as "ramified microglia", with an extensive motile set of foot processes that continuously survey the local environment to recognize and eliminate pathogens (25). Loss of microglial expression of P2RY12 in knockout mice resulted in impaired polarization, migration and extension of microglial processes towards extracellular nucleotides released from damaged cells, indicating that P2RY12 is required to guide microglial chemotaxis (29). Further studies revealed that a raise of local extracellular ATP/ADP levels at the site of CNS injury activates Gi/o-coupled P2RY12, followed by PI3K and PLC signaling-mediated migration of microglial cells towards the chemotactic source (27). Exogenous stimuli like lipopolysaccharides (LPS) can cause a dramatic reduction of the P2RY12 expression in microglia cells *in vitro* accompanied by the retraction of microglial processes and metamorphosis into an amoeboid shape (29). These phenomena indicate a function of P2RY12 in the activation of immune regulation during inflammation.

The environmental changes taking place under various pathological conditions cause ATP/ADP leaks that are noticed by the P2RY12 receptors of microglia and lead to changes affecting the cell processes and motility of the cells (38). High concentrations of purinergic nucleotides and nucleosides such as adenosine and ATP were shown to work in synergy with LPS activation of microglial cells, promoting chemo repulsion away from the ATP source, a process that is associated with increased local adenosine A2A receptor signaling (38, 39). The expression of the adenosine A2A receptor increases significantly in response to LPS, while P2RY12 expression decreased by LPS, indicating that the shift from a ramified towards an amoeboid phenotype depends on the balance between P2RY12 and A2A receptor signaling, respectively (38). More studies are required to elucidate the exact regulatory mechanism of microglia immune-activation by these two significant signaling pathways.

In this study we observed nuclear localization of P2RY12 in microglial cells in the high-grade tumors, while in the lower graded astrocytomas P2RY12 was expressed in the cytoplasm. G protein-coupled receptors (GPCRs), such as P2RY12 and its family members are considered as cell surface bound mediators of intracellular signaling. From *in vitro* and *in vivo* studies, it is known that some receptors have a nuclear localization. These receptors include the receptors for apelin, angiotensin II AT1, parathyroid hormone, glutamate mGluR5, endothelin ETA and ETB, and the prostaglandins EP1, EP3, and EP4 (40). The mechanism and functional implications of nuclear translocation remains obscure. It has been suggested that nuclear import is programmed by the DNA sequence of the receptors. Nuclear GPCRs complex proteins such as heterotrimeric G proteins, phospholipase A2, and phospholipase C seem to remain active in intracellular

signaling, similar to the activation of nuclear endothelin and prostaglandin receptors that were proven to increase nuclear Ca^{2+}concentrations (40). However, the functional implications of nuclear localization of the P2RY12 receptor and its association with advanced tumor grade needs to be further unraveled.

CONCLUSION

The expression site of P2RY12 matches astrocytoma grade, and also reflects the activation status of microglia cells in the tumors. Because of its association with the stage of immune response, P2RY12 may become an interesting drug target for future immune-modulation based therapy for the patients suffering from these tumors.

REFERENCES

1. Lavin Y, Mortha A, Rahman A, Merad M. Regulation of macrophage development and function in peripheral tissues. Nat Rev Immunol. 2015;15(12):731-44.
2. Nayak D, Roth TL, McGavern DB. Microglia development and function. Annu Rev Immunol. 2014;32:367-402.
3. Lou N, Takano T, Pei Y, Xavier AL, Goldman SA, Nedergaard M. Purinergic receptor P2RY12-dependent microglial closure of the injured blood-brain barrier. Proc Natl Acad Sci U S A. 2016;113(4):1074-9.
4. Parkhurst CN, Gan WB. Microglia dynamics and function in the CNS. Curr Opin Neurobiol. 2010;20(5):595-600.
5. Tremblay ME, Stevens B, Sierra A, Wake H, Bessis A, Nimmerjahn A. The role of microglia in the healthy brain. J Neurosci. 2011;31(45):16064-9.
6. Block ML, Zecca L, Hong JS. Microglia-mediated neurotoxicity: uncovering the molecular mechanisms. Nat Rev Neurosci. 2007;8(1):57-69.
7. Hanisch UK. Microglia as a source and target of cytokines. Glia. 2002;40(2):140-55.
8. Lalancette-Hebert M, Gowing G, Simard A, Weng YC, Kriz J. Selective ablation of proliferating microglial cells exacerbates ischemic injury in the brain. J Neurosci. 2007;27(10):2596-605.
9. Neumann J, Gunzer M, Gutzeit HO, Ullrich O, Reymann KG, Dinkel K. Microglia provide neuroprotection after ischemia. FASEB J. 2006;20(6):714-6.
10. Martinez FO, Gordon S. The M1 and M2 paradigm of macrophage activation: time for reassessment. F1000Prime Rep. 2014;6:13.
11. Ostuni R, Kratochvill F, Murray PJ, Natoli G. Macrophages and cancer: from mechanisms to therapeutic implications. Trends Immunol. 2015;36(4):229-39.
12. Noy R, Pollard JW. Tumor-associated macrophages: from mechanisms to therapy. Immunity. 2014;41(1):49-61.
13. Zhang M, He Y, Sun X, Li Q, Wang W, Zhao A, et al. A high M1/M2 ratio of tumor-associated macrophages is associated with extended survival in ovarian cancer patients. J Ovarian Res. 2014;7:19.
14. Komohara Y, Ohnishi K, Kuratsu J, Takeya M. Possible involvement of the M2 anti-inflammatory macrophage phenotype in growth of human gliomas. J Pathol. 2008;216(1):15-24.
15. Prosniak M, Harshyne LA, Andrews DW, Kenyon LC, Bedelbaeva K, Apanasovich TV, et al. Glioma grade is associated with the accumulation and activity of cells bearing M2 monocyte markers. Clin Cancer Res. 2013;19(14):3776-86.
16. Hambardzumyan D, Gutmann DH, Kettenmann H. The role of microglia and macrophages in glioma maintenance and progression. Nature Neuroscience. 2016;19(1):20-7.
17. Szulzewsky F, Arora S, de Witte L, Ulas T, Markovic D, Schultze JL, et al. Human glioblastoma-associated microglia/monocytes express a distinct RNA profile compared to human control and murine samples. Glia. 2016;64(8):1416-36.
18. Li W, Graeber MB. The molecular profile of microglia under the influence of glioma. Neuro Oncol. 2012;14(8):958-78.
19. Markovic DS, Glass R, Synowitz M, Rooijen N, Kettenmann H. Microglia stimulate the invasiveness of glioma cells by increasing the activity of metalloprotease-2. J Neuropathol Exp Neurol. 2005;64(9):754-62.
20. Sliwa M, Markovic D, Gabrusiewicz K, Synowitz M, Glass R, Zawadzka M, et al. The invasion promoting effect of microglia on glioblastoma cells is inhibited by cyclosporin A. Brain. 2007;130:476-89.
21. Watters JJ, Schartner JM, Badie B. Microglia function in brain tumors. J Neurosci Res. 2005;81(3):447-55.
22. Jay TR, Miller CM, Cheng PJ, Graham LC, Bemiller S, Broihier ML, et al. TREM2 deficiency eliminates TREM2+ inflammatory macrophages and ameliorates pathology in Alzheimer's disease mouse models. J Exp Med. 2015;212(3):287-95.
23. Butovsky O, Jedrychowski MP, Moore CS, Cialic R, Lanser AJ, Gabriely G, et al. Identification of a unique TGF-beta-dependent molecular and functional signature in microglia. Nat Neurosci. 2014;17(1):131-43.

24. Bennett ML, Bennett FC, Liddelow SA, Ajami B, Zamanian JL, Fernhoff NB, et al. New tools for studying microglia in the mouse and human CNS. Proc Natl Acad Sci U S A. 2016.
25. Butowski N, Colman H, De Groot JF, Omuro AM, Nayak L, Wen PY, et al. Orally administered colony stimulating factor 1 receptor inhibitor PLX3397 in recurrent glioblastoma: an Ivy Foundation Early Phase Clinical Trials Consortium phase II study. Neuro-Oncology. 2015.
26. Sasaki Y, Hoshi M, Akazawa C, Nakamura Y, Tsuzuki H, Inoue K, et al. Selective expression of Gi/o-coupled ATP receptor P2Y12 in microglia in rat brain. Glia. 2003;44(3):242-50.
27. Cattaneo M. P2Y12 receptors: structure and function. J Thromb Haemost. 2015;13 Suppl 1:S10-6.
28. Lecchi A, Razzari C, Paoletta S, Dupuis A, Nakamura L, Ohlmann P, et al. Identification of a new dysfunctional platelet P2Y12 receptor variant associated with bleeding diathesis. Blood. 2015;125(6):1006-13.
29. Haynes SE, Hollopeter G, Yang G, Kurpius D, Dailey ME, Gan WB, et al. The P2Y12 receptor regulates microglial activation by extracellular nucleotides. Nat Neurosci. 2006;9(12):1512-9.
30. Ohsawa K, Irino Y, Sanagi T, Nakamura Y, Suzuki E, Inoue K, et al. P2Y12 receptor-mediated integrin-beta1 activation regulates microglial process extension induced by ATP. Glia. 2010;58(7):790-801.
31. Zheng PP, van der Weiden M, Kros JM. Fast tracking of co-localization of multiple markers by using the nanozoomer slide scanner and NDPViewer. Journal of Cellular Physiology. 2014;229(8):967-73.
32. Bowman RL, Klemm F, Akkari L, Pyonteck SM, Sevenich L, Quail DF, et al. Macrophage Ontogeny Underlies Differences in Tumor-Specific Education in Brain Malignancies. Cell Rep. 2016;17(9):2445-59.
33. Brennan CW, Verhaak RG, McKenna A, Campos B, Noushmehr H, Salama SR, et al. The somatic genomic landscape of glioblastoma. Cell. 2013;155(2):462-77.
34. Ciriello G, Cerami E, Sander C, Schultz N. Mutual exclusivity analysis identifies oncogenic network modules. Genome Research. 2012;22(2):398-406.
35. Gao JJ, Aksoy BA, Dogrusoz U, Dresdner G, Gross B, Sumer SO, et al. Integrative Analysis of Complex Cancer Genomics and Clinical Profiles Using the cBioPortal. Sci Signal. 2013;6(269).
36. Kierdorf K, Erny D, Goldmann T, Sander V, Schulz C, Perdiguero EG, et al. Microglia emerge from erythromyeloid precursors via Pu.1- and Irf8-dependent pathways. Nat Neurosci. 2013;16(3):273-80.
37. Kierdorf K, Prinz M. Factors regulating microglia activation. Front Cell Neurosci. 2013;7:44.
38. Koizumi S, Ohsawa K, Inoue K, Kohsaka S. Purinergic receptors in microglia: Functional modal shifts of microglia mediated by P2 and P1 receptors. Glia. 2013;61(1):47-54.
39. Orr AG, Orr AL, Li XJ, Gross RE, Traynelis SF. Adenosine A(2A) receptor mediates microglial process retraction. Nat Neurosci. 2009;12(7):872-8.
40. Lee DK, Lanca AJ, Cheng R, Nguyen T, Ji XD, Gobeil F, Jr., et al. Agonist-independent nuclear localization of the Apelin, angiotensin AT1, and bradykinin B2 receptors. J Biol Chem. 2004;279(9):7901-8.

SUPPLEMENTARY DATA

Supplementary Figure 2. High expression levels of P2RY12 in GBM patients predict a favorable outcome based on analysis of TCGA GBM database provisional

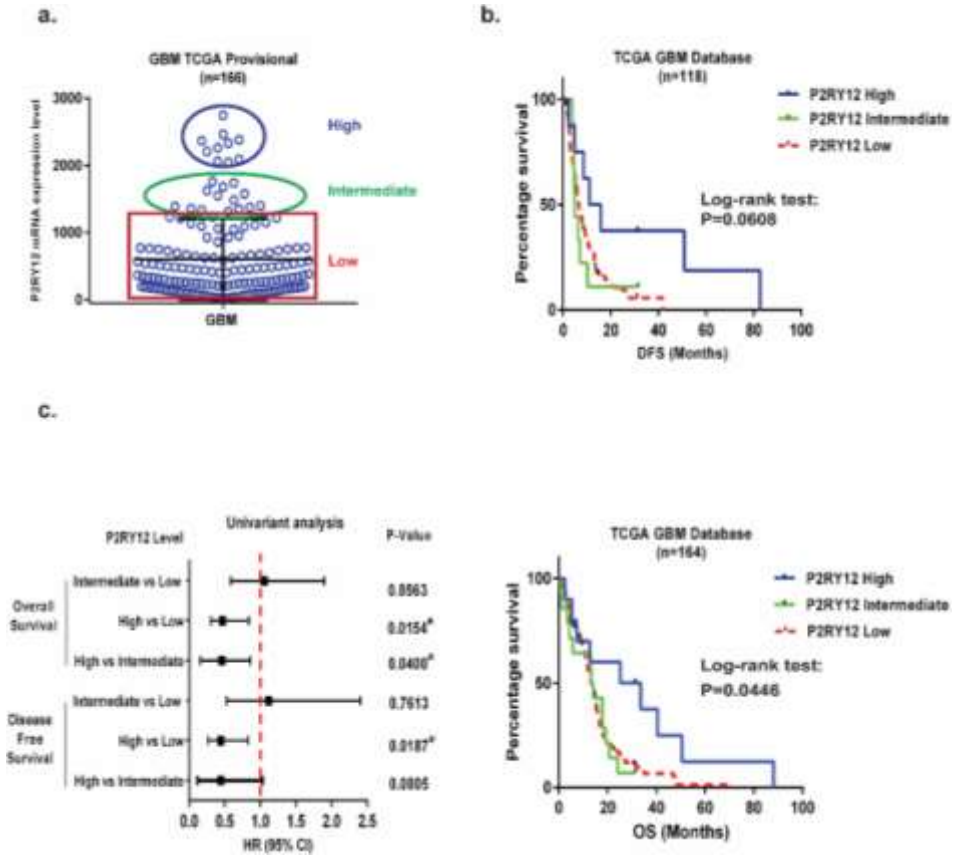

a: Overview of P2RY12 expression level of 166 GBM patient samples in TCGA GBM provisional database. **b:** Kaplan-Meier graphs showing disease free survival and overall survival in patients with different P2RY12 expression levels. **c:** Graphs showing hazard ratios (HR) with 95% confidential interval (CI) of disease free survival (left) and overall survival (right) in different groups of patients.

Supplementary Figure 3. High expression of P2RY12 did not predict overall survival in GBM patients either with IDH1 WT (Wild Type) or mutant statue

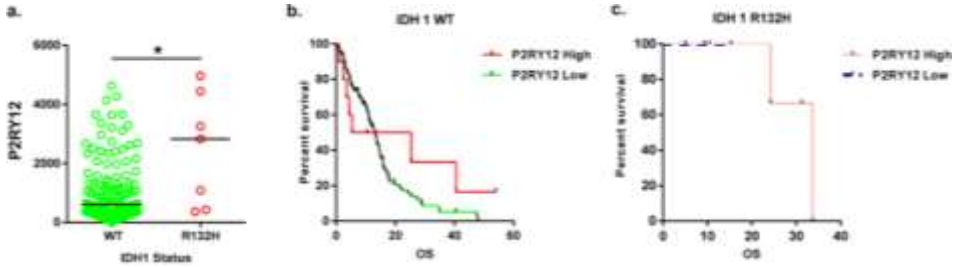

a. Analysis of TCGA GBM database (Cell, 2013) reveals increased P2RY12 mRNA expression in patients with IDH1 mutation(R132H). Results are shown in the median values of P2RY12 mRNA levels. * P<0.05. WT: Wild type. **b.** Kaplan-Meier graph showing overall survival in IDH1 wild type patients with different P2RY12 expression levels **c.** Kaplan-Meier graph showing overall survival in IDH1 mutant (R132H) patients with different P2RY12 expression levels.

Supplementary Figure 4. High expression of P2RY12 did not correlate with overall survival of GBM patients with either MGMT unmenthylation or MGMT methylation status

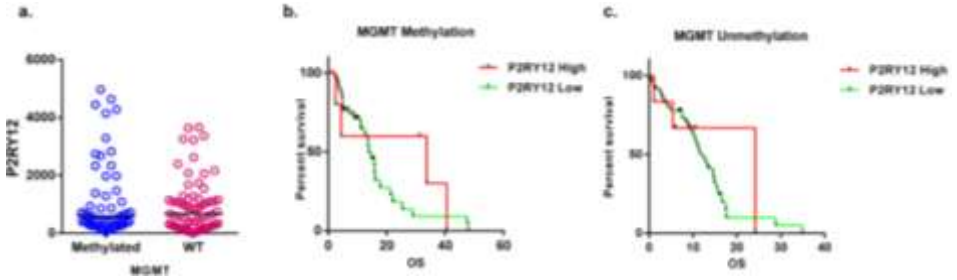

a. Analysis of TCGA GBM database (Cell, 2013) reveals stable expression of P2RY12 mRNA in patients with/without MGMT methylation. Results are shown in the median values of P2RY12 mRNA levels. **b.** Kaplan-Meier graph showing overall survival in MGMT-methylated patients with different P2RY12 expression levels **c.** Kaplan-Meier graph showing overall survival in MGMT unmethylated patients with different P2RY12 expression levels.

Supplementary Table 1. Summary of mutual exclusivity analysis from two TCGA glioma database

Mutual Exclusivity to P2RY12 Expression		TCGA GBM provisional database(RNA-Seq) n=196 Upregulation: Z12			TCGA Low grade glioma provisional database(RNA-Seq) n=530 Upregulation: Z12		
	Genes	Log (OR)	P-Value	Association	Log (OR)	P-Value	Association
Microglia/Macrophage markers	AIF1 (Iba-1)	1.83	0.055	Co-occurrence	1.1	0.11	NS
	CX3CR1	2.56	0.0078	Co-occurrence	3.25	<0.001	Co-occurrence
	IRF8	3.44	<0.001	Co-occurrence	2.08	<0.001	Co-occurrence
	ITGAM (CD11b)	0.861	0.861	NS	1.81	0.01	Co-occurrence
Recruited myeloid cell markers	PTPRC (CD45)	>3	0.89	Mutual exclusivity	1.1	0.11	NS
	CCR2	<-3	0.8	Mutual exclusivity	0.85	0.25	NS
	ITGAX (CD11c)	1.671	0.094	NS	>-3	0.28	Mutual exclusivity
Activated phenotype markers	CD163	>-3	0.83	Mutual exclusivity	>-3	0.5	Mutual exclusivity
	MSR1 (CD204)	<-3	0.6	Mutual exclusivity	0.055	0.63	NS
	MRC1	<-3	0.6	Mutual exclusivity	>-3	0.5	Mutual exclusivity
	IRF4	<-3	0.68	Mutual exclusivity	>-3	0.91	Mutual exclusivity
	STAT1	1.95	0.026	Co-occurrence	0.059	0.429	NS
	STAT3	>-3	0.685	Mutual exclusivity	-0.136	0.685	Mutual exclusivity
	STAT6	<-3	0.528	Mutual exclusivity	0.071	0.43	NS
	NOS-3	<-3	0.68	Mutual exclusivity	>-3	0.96	Mutual exclusivity
Secreted factors	IL10	0.48	0.51	NS	1.15	0.097	NS
	IL6	<-3	0.68	Mutual exclusivity	-0.37	0.53	Mutual exclusivity
	IL8	<-3	0.25	Mutual exclusivity	>-3	0.87	Mutual exclusivity
	IL10	<-3	0.64	Mutual exclusivity	0.5	0.48	NS
	CXCL8	<-3	0.56	Mutual exclusivity	>-3	0.91	Mutual exclusivity
	CXCL9	<-3	0.56	Mutual exclusivity	0.88	0.27	NS
	CXCL10	<-3	0.56	Mutual exclusivity	>-3	0.45	Mutual exclusivity
	CCL2	<-3	0.6	Mutual exclusivity	>-3	0.54	Mutual exclusivity
	CCL5	<-3	0.6	Mutual exclusivity	0.11	0.811	NS
	CCL17	<-3	0.999	Mutual exclusivity	>-3	0.91	Mutual exclusivity
	CCL18	<-3	0.83	Mutual exclusivity	>-3	0.83	Mutual exclusivity
	CCL22	<-3	0.85	Mutual exclusivity	>-3	0.91	Mutual exclusivity
	TNF-α	1.87	0.09	NS	1.41	0.08	NS
	IFN-γ	<-3	0.76	Mutual exclusivity	0.1	1.91	NS

TCGA GBM provisional database and low grade glioma database were analyzed from cBioPortal. P2RY12 upregulation was defined by Z score. Z score=(Individual P2RY12 value-mean value)/Standard deviation of whole sample set. Odd ratio(OR) represents the co-occurrence of P2RY12 with listed molecules in the supplementary table. The significance was examed by fisher's test. Log(OR)>0, with P<0.05 indicates a trend of co-occurrence. Log(OR)<0 indicated the trend of mutual exclusivity.

Chapter 8
General Discussion

Chapter 8

General Discussion

CECR1 is a highly conserved protein that reportedly regulates embryo and larva development in both vertebrates and invertebrate with adenosine deaminase activity [1-4]. Studies in both drosophila [5] and humans [6] point to a putative role of CECR1 in regulating immune functions through mediating the proliferation of monocytes, lymphocytes and the differentiation of monocytes into macrophages. CECR1 loss of functions mutations in patients result in clinical manifestations related to hyper reactivity of the immune system [4, 7-9]. The candidate effector cell for CECR1 expression is the monocyte/macrophage. So far, most studies on the functions of CECR1 have only associated CECR1 with inflammation in general, without further specification of the immune response, especially in relation to cancer. The investigations reported in this thesis link CECR1 expression in glioma to tumor associated macrophages (TAMs).

In **Chapter 3** the expression of CECR1 by pro-M2 macrophages was demonstrated by using various immunohistochemical lineage markers and cytokines. In skin biopsies of patients with CECR1 mutations overproduction of TNF-α was found together with over-expression of IL-1β and iNOS [9]. In adenoid cystic carcinoma of salivary glands the promotor of CECR1 appears to be hypo-methylated [10], indicative of over-transcription of CECR1 during carcinogenesis. Furthermore, high levels of CECR1 were detected in the serum of patients with breast cancer [11]. These findings are in line with the hypo-methylated state of CECR1 and the over-expression of CECR1 in glioma and are illustrative of the association between CECR1 and tumorigenesis. Starting from the idea that M2-like macrophages promote carcinogenesis, we showed that the expression of CECR1 is increased in M2-like macrophages in glioblastoma. Furthermore, the contribution of CECR1 in M2-like polarization of CECR1 producing macrophages was confirmed by either CECR1 depletion or CECR1 overexpression. We showed that CECR1 is a tumor-promoting molecule that is mainly expressed and released by macrophages in glioma. The direct pro-tumoral effect of CECR1 is accompanied by M2 polarization of these cells. The paracrine effects of CECR1 include cell proliferation, migration and upregulation of the intracellular MAPK pathway in glioma cells. The direct effector molecules regulated by CECR1 remain unknown so far. It is very likely that CECR1 mediated expression of cytokines in TAMs stimulate these intracellular signalling pathways in glioma cells (**Chapter 3)**. For example: the immune modulating molecule IL-10 is not only involved in mediating an immune suppressive microenvironment but also plays a role in enhancing the progression of cancer cells via STAT3 activation in cancer cells [12]. CCL18, which takes part in tumor progression including adherence to the extracellular matrix, migration, invasion and tumor angiogenesis, activates the intracellular PLCγ1, PKCζ, and Ca^{2+} pathways through interaction with its receptor PITPNM3 [13]. It may well activate focal adhesion kinase (FAK)-triggered clustering of integrin β1 [13]. CXCL12, a classic pro-tumoral molecule, that interacts with CXCR4 and regulates multiple biological functions in cancer development including thee MAPK pathway [14].

In order to obtain a complete picture of the CECR1-mediatated response in macrophages, a proteome analysis-based analysis was applied (**Chapter 6**). Surprisingly, CECR1

expression appeared to be negatively related to proteins involved in the innate immune response including phagocytosis, phagosome maturation, antigen presentation and the type I interferon signalling pathway. Among these pathways, antigen presentation and processes related to phagocytosis, are tightly regulated by IFN-γ. Two studies from patients bearing CECR1 mutations reported an increased expression of IFN-γ induced genes in peripheral monocyte [15] and a neutrophil-derived gene signature [16]. In our dataset the up-regulation of several proteins in response to CECR1 silencing in macrophages downstream of IFN-γ were predicted by Ingenuity Pathway Analysis (Chapter 6). The suppression of CECR1 expression in macrophages significantly increases the expression of MHC-I molecules like HLA-A, B, C. Furthermore, several phagosome proteins such as TAPBP, TAP1, TAP2 are upregulated upon CECR1 depletion. Macrophages function as antigen presenting cells when stimulated by exogenous pathogens or endogenous debris. The antigen peptides processed by phagocytosis are presented by either MHC II molecules to $CD4^+$ T cells or MHC I molecules to $CD8^+$ T cells. Taken together, suppression of CECR1 enhances the phagocytosis ability and the IFN-γ mediated MHC I antigen presentation to $CD8^+$ T cells [17]. These data are promising for the development of immune therapies for gliomas. Both in vitro studies focusing on deciphering the mechanisms and assessing the pre-clinical therapeutic effect are required to further develop these ideas. Unfortunately, the majority of secreted factors are missing from the proteome analysis because cell lysates were used. Analysis of the TCGA GBM database revealed that, among other monocyte/macrophage markers, S100A9 and PLAU positively correlated with the expression of CECR1. S100A9 and PLAU have been found in myeloid cells, and S100A9 was shown to promote glioma growth and angiogenesis by interaction with its receptor RAGE on the surface of tumor cells [18]. S100A9 was proven to trigger activation of MAPK and NF-κB pathways [19], promoting tumor growth and angiogenesis [20]. PLAU was one of the proangiogenic factors produced by tumor associated macrophages [21]. PLAU aids in the invasion and metastasis of various tumor types via binding to PLAUR, activating downstream pathways like ERK1/2 [22], PI3K/Akt signaling transduction [23]. Another interesting finding following CECR1 knockdown was the identification of LAT2. This protein was upregulated in CECR1 knockdown macrophages co-cultured with U87, and down-regulated in pure U87 co-cultured macrophage. The function of LAT2 is to mediate the response of B cells and monocytes / macrophages [24]. The expression of LAT2 appeared to be increased in matured macrophages, but decreased in monocyte [25]. The function of LAT2 includes mediation of the B cell response and affects monocytes /macrophages [24]. LAT2 knockout macrophages and dendritic cells lose the ability to produce pro-inflammatory cytokines like IL-12, IFN-γ and IL-23 [25, 26]. In our own dataset, in macrophages under U87-coculture conditions, CECR1 knockdown not only increased the LAT2 expression, but also increased the IL-12 transcriptional level, while decreasing the IL-10 level. The data in Chapter 3 on the cytokines profile under CECR1 depletion and CECR1 treatment shows a similar trend of cytokine expression. Taken together, the data indicates that CECR1

depletion may function through LAT2 regulating expression and secretion of pro-inflammatory factors by macrophages, thereby promoting anti-tumoral immunity in glioma.

Angiogenesis is a prominent feature of glioblastoma [27] and is regulated by tumor-associated macrophages [28]. The matricellular protein periostin was shown to serve as a potent chemoattractant for TAMs [29]. In this thesis, we discovered that the source of periostin is not glioma initiating cells or glioma stem cells, but mainly pericytes. Only part of the PDGFB+ pericytes appeared also OLIG2+/SOX2+. We screened various pro-angiogenic molecules such as VEGFA, Angiopoietin1, 2, IL-8, VWF as well as PDGFB in macrophages with CECR1 silencing and those cells being treated by CECR1 protein. Only PDGFB was significantly influenced by CECR1 in macrophages (Chapter 4). Pericytes exclusively express the PDGFB receptor, PDGFRB. CECR1 mutations cause vascular instability [30], thus presenting a possible link between CECR1 and pericyte function. The findings prompted us to focus on the cross-talk between macrophage and pericytes, not endothelial cells. The PDGFB-PDGFRβ axis in pericytes takes part in various aspects of biological functions including cell proliferation, migration, secretion of cytokines and growth factors [31]. We confirmed that the pro-angiogenic action of periostin is under the control of macrophages through paracrine interactions involving PDGFB-PDGFRβ. Periostin appears to serve as a terminal effector molecule for the upstream CECR1 signal from macrophages. Periostin affects migration and the pro-angiogenesis action of the pericytes. The studies described in Chapter 4 reveal the positive feedback between tumor associated macrophage infiltration and pericyte functions in angiogenesis. Infiltrated macrophages secreted higher levels of CECR1 in the tumor microenvironment, leading to more PDGFB secretion from macrophages via autocrine activation. This PDGFB trigger causes the secretion of periostin into extracellular matrix by pericytes. Periostin seems to have many more functions, since it enhances the monocyte/macrophage infiltration, increases the production of VEGFA and other pro-angiogenic molecules, and influences the migration by regulating focal adhesion molecules. Consequently, the CECR1-PDGFB-PDGFRB-Periostin mediated cross talk between pericytes and macrophages accelerates the neo-vascularization and tumor associated macrophage infiltration in GBM.

Microglia and macrophages coexist in the neuropil and perivascular areas of glioma [28]. Mature microglia and infiltrated macrophages share many cell markers [32]. However, these cell types do differ in their immune modulatory actions. In Chapter 3 we showed that CECR1 is expressed by microglia and / or macrophages and additional immunophenotypical characterization is necessary to distinguish between the two cell types. As shown by Butovsky et al, P2RY12 is uniquely expressed by microglia but not by peripheral macrophages [33] and we were able to also make a distinction between these cell types in the context of glioma by using anti-P2RY12 antibody. In Chapter 7 we noticed P2RY12 expression in glioma. Remarkably, in high-grade glioma (glioblastoma,

GBM) P2RY12 showed nuclear localization. In autopsy brains and in grade II astrocytomas P2RY12 specifically stained microglia. Interestingly, in anaplastic astrocytoma P2RY12 was seen in the cytoplasm and the nuclei of the microglial cells. Cells with either P2RY12 cytoplasm and nuclear localization also expressed the pan-macrophage marker CD68. To confirm the origin of P2RY12 positive cells, CD45 was applied. CD45 positive cells were negative for P2RY12 suggestive of the non-myeloid origin of the cells. In the grade III astrocytomas and glioblastomas the cells with P2RY12 nuclear translocation were also immunopositive for the markers of M2 microglia/macrophages such as CD163 and CD204. Therefore, downregulation and nuclear translocation of P2RY12 seems to be a feature of microglial cells with a M2 phenotype in high grade glioma.

Previous studies have suggested that microglial cells, representing the initial responsive innate immune cells, form the initial host immune response against the glial tumor cells. The immune-profile of microglia in low-grade glioma resembles that of the M1 state, i.e., pro-inflammation and equipped for antigen presentation [34, 35]. Along with tumor progression peripheral monocytes are increasingly recruited to become glioma associated macrophages by the interference of various factors derived from the glioma cells and due to the hypoxic microenvironment. The shift in intracellular P2RY12 expression site during the progression from low- to high-grade glioma may be related to the distribution of microglia and macrophages in the tumors. Based on the TCGA GBM and low-grade glioma database, particular sets of genes correlate with P2RY12 expression and reflect an immune and pro-inflammatory response. In parallel, other sets of genes that negatively correlate with P2RY12 expression are related to the cell cycle and pathways operating during cell proliferation, corroborating data in the literature on P2RY12[36]. P2RY12 expression status is associated with tumor grade and also with immune status of the tumor, and with overall survival time. The development of strategies to manipulate the P2RY12 positive cells may become important to future therapeutic strategies for glioma.

PERSPECTIVES:

Better understanding the biology of CECR1 in glioma associated microglia/macrophage benefits future clinical care

Only recently the adenosine deaminase activity of CECR1 was recognized [11, 37-41], and the expression and function of CECR1 in monocyte/macrophages and its immune modulatory roles in various inflammatory diseases from both human and porcine were reported [4, 6-9, 30, 42-44]. In auto-immune diseases, the loss of function mutation of CECR1 leads to a hyper-reactive immune response characterized by augmented TNF-α and IL-β levels [30], upregulated neutrophil gene signatures [16] and upregulation of interferon stimulating genes [15]. Due to the over-reactivated systemic inflammation,

patients with CECR1 mutations may present with immune cell infiltrations and instable vascular architecture [30]. Elevated CECR1 levels are found in breast cancers [11] and also in glial tumors as described in this thesis. CECR1 overexpression leads to immune suppression and a tumor promoting profile of macrophages. Overexpressed or down-regulated CECR1 influences vascular formation by mediating the migration and pro-angiogenic properties of pericytes that contribute to the integrity of endothelial cells and vessel maturations. The proteomic data suggests that CECR1 silenced macrophages activate CD8+ T cells by stimulation of the antigen presenting pathways. It would be interesting if this *in sillico* prediction could be validated *in vivo* and eventually translated into clinical practice. The inhibition of CECR1 expression in macrophages seems to be promising for the development of new therapies like immunotherapy or anti-vascular therapy by targeting CECR1 in glioma associated macrophages.

The siRNA mediated CECR1 knockdown could not be maintained for long. However, the effects of siRNA in gene silencing were confirmed at both transcriptional and protein level, and the high rate of off-target effects of siRNA could be ignored. The effects of CECR1 depletion in macrophages could be enhanced if CECR1 could be totally removed from the genome by either Cre-Loxp or CRISPR-Cas9 system. Previous work pointed out that CECR1 is a vital mediator in maintaining survival of monocyte and macrophages and M2 macrophages in particular. It would be interesting to design inducible CECR1 knockout monocyte cell lines (THP-1, U937) or monocyte-specific inducible CECR1 knockout zebrafish, to study the effects of elimination of CECR1 in a longer time frame.

A glioma Patient-derived Tumor Xenograft (PTX) model could be applied to conduct *in vivo* investigation of the contribution of CECR1 in the gliomagenesis. It would enable the exploration of the contribution of CECR1 in the various steps associated with glioma associated macrophages (GAMs) including ontogeny, macrophage differentiation and the preclinical value of CECR1 depletion *in vitro*, *ex-vivo* and *in vivo*. Moreover, further experiments could also be carried out to study the restored anti-tumor innate immune response by total depletion of CECR1 in glioma associated macrophages *in vivo*.

A limitation of the proteomics measurements of the macrophage lysates is the fact that the majority of secreted factors which may exist in the supernatant of culture medium are missed. It would be interesting to harvest proteins in the culture medium followed by mass spectrometry for identifying the secreted cytokines under CECR1 regulation. Another drawback of the current studies is that we were unable to explore the effects of CECR1 at the transcriptional level. We only rendered data of the downstream effects of CECR1 at the proteomic level. The data was quite limited due to the insufficient harvested protein samples. A whole transcriptome RNA-sequencing approach would be beneficial to future studies on the functions of CECR1.

Exploring the mechanisms by which CECR1 mediates macrophages and related inflammatory responses to promote tumor progression as well as angiogenesis in more detail is necessary. There are 3 aspects of the downstream targets of CECR1 in macro-

phages: a) Increasing the IFN-γ induced antigen presentation followed by CD8+T cells activation, b) Suppressing the expression of S100A9 and PLAU attenuating the various intracellular signalling pathways including the MAPK pathway in both glioma and vascular cells, c) Upregulating of LAT2 expression in macrophage enhancing the pro-inflammatory factors secretion. We hypothesize that CECR1 regulates the expression of LAT2 that subsequently triggers pro-inflammatory cytokines secretion. Among these cytokines, IFN-γ may be candidate activator on MHC I antigen presentation process in macrophage and on CD8+ T cells.

LAT2, as a lipid raft adaptor protein, was proved to interact with GRB2, activating downstream PI3K [45]. Phosphorylation of PI3K transduces the signal to AKT followed by mediating nuclear localization of NF-κB[46] as well as NF-ATc[47] which aid the transcription of pro-inflammatory factors. Intracellular β-catenin would be phosphorylated as well, but labeled β-catenin would be further degraded rather than entering into nucleus recruiting TCF4 [48]. Therefore, validating the CECR1-LAT2 axis may provide a better explanation of how CECR1 depletion mediates the immune function of macrophages. Whether the LAT2 signaling pathway is also related to the expression of S100A9 as well as PLAU needs further investigation.

As a growth factor like molecule, CECR1 was shown to anchor on the surface of immune cells including monocytes, macrophages and T cells. In recent studies on CECR1 a diagram of CECR1 mediated immune regulation was made [49]. CECR1 interacts with several molecules of different types of immune cells like CD16+ non-classical monocytes, neutrophils, regulatory T cells, and B cells that do not express CD26, a nature receptor of ADA1. The focus is on CECR1 function in tumor-associated macrophages and the proteins putatively recognizing and interacting with CECR1in macrophages and tumor associated macrophages. How do they contribute to mediate CECR1 functions? Is there any link to the established downstream molecule like LAT2 expression? Are there other binding proteins and related mechanisms active in the CECR1 mediating immune modulation and survival of other immune cells besides CD39 on the surface of T regulatory cells? Are there adenosine receptors on macrophages and T lymphocytes, and are there other binding proteins and related mechanisms on CECR1 mediating immune modulation and survival of other immune cells? These questions can be answered by analysing whole tissue lysates and subsequent protein pull down. Such proteomic analysis will give indications on potential partner molecules of CECR1 which subsequently should be validated by IHC or IF. Thus, applying immunoprecipitation combining with mass spectrometry would be the next step to get in depth ideas about potential partner proteins of CECR1 in tumor associated macrophages and in other types of immune cells. Deciphering the details on the CECR1-mediated macrophage response and the contribution of CECR1 in tumor immune microenvironment is most challenging. It should be kept in mind that microglia and monocyte-derived macrophages stem from two different precursor cells[28]. Because of the different lineages the effects of CECR1 expression may be different. Isolating microglia as well as tumor associated macrophages from

the same glioma patient followed by CECR1 knockdown and full transcriptome RNA-sequencing may be an appropriate approach to capture possible differences.

In conclusion, the studies carried out in this thesis are pioneers to scientific work focusing on CECR1 in tumor associated macrophage especially in glioblastoma. There are still many unclear aspects waiting for further in depth and dedicated investigation. From the studies it may be concluded that CECR1 as a promising therapeutic target for cancer immunotherapy.

REFERENCE

1. Zuberova, M., et al., Increased extracellular adenosine in Drosophila that are deficient in adenosine deaminase activates a release of energy stores leading to wasting and death. Disease Models & Mechanisms, 2010. **3**(11-12): p. 773-784.
2. Iijima, R., et al., The extracellular adenosine deaminase growth factor, ADGF/CECR1, plays a role in Xenopus embryogenesis via the adenosine/P1 receptor. J Biol Chem, 2008. **283**(4): p. 2255-64.
3. Riazi, A.M., G. Van Arsdell, and M. Buchwald, Transgenic expression of CECR1 adenosine deaminase in mice results in abnormal development of heart and kidney. Transgenic Res, 2005. **14**(3): p. 333-6.
4. Caorsi, R., et al., Monogenic polyarteritis: the lesson of ADA2 deficiency. Pediatr Rheumatol Online J, 2016. **14**(1): p. 51.
5. Novakova, M. and T. Dolezal, Expression of Drosophila adenosine deaminase in immune cells during inflammatory response. PLoS One, 2011. **6**(3): p. e17741.
6. Zavialov, A.V., et al., Human adenosine deaminase 2 induces differentiation of monocytes into macrophages and stimulates proliferation of T helper cells and macrophages. J Leukoc Biol, 2010. **88**(2): p. 279-90.
7. Schepp, J., et al., Deficiency of Adenosine Deaminase 2 Causes Antibody Deficiency. J Clin Immunol, 2016. **36**(3): p. 179-86.
8. Nanthapisal, S., et al., Deficiency of Adenosine Deaminase Type 2: A Description of Phenotype and Genotype in Fifteen Cases. Arthritis Rheumatol, 2016. **68**(9): p. 2314-22.
9. Navon Elkan, P., et al., Mutant adenosine deaminase 2 in a polyarteritis nodosa vasculopathy. N Engl J Med, 2014. **370**(10): p. 921-31.
10. Shao, C., et al., Integrated, genome-wide screening for hypomethylated oncogenes in salivary gland adenoid cystic carcinoma. Clin Cancer Res, 2011. **17**(13): p. 4320-30.
11. Aghaei, M., et al., Adenosine deaminase activity in the serum and malignant tumors of breast cancer: the assessment of isoenzyme ADA1 and ADA2 activities. Clin Biochem, 2005. **38**(10): p. 887-91.
12. Khare, V., et al., IL10R2 Overexpression Promotes IL22/STAT3 Signaling in Colorectal Carcinogenesis. Cancer Immunol Res, 2015. **3**(11): p. 1227-35.
13. Chen, J., et al., CCL18 from tumor-associated macrophages promotes breast cancer metastasis via PITPNM3. Cancer cell, 2011. **19**(4): p. 541-55.
14. Sun, X., et al., CXCL12/CXCR4/CXCR7 Chemokine Axis and Cancer Progression. Cancer metastasis reviews, 2010. **29**(4): p. 709-722.
15. Uettwiller, F., et al., ADA2 deficiency: case report of a new phenotype and novel mutation in two sisters. RMD Open, 2016. **2**(1): p. e000236.
16. Belot, A., et al., Mutations in CECR1 associated with a neutrophil signature in peripheral blood. Pediatr Rheumatol Online J, 2014. **12**: p. 44.
17. Zhou, F., Molecular mechanisms of IFN-gamma to up-regulate MHC class I antigen processing and presentation. Int Rev Immunol, 2009. **28**(3-4): p. 239-60.
18. Yin, C., et al., RAGE-binding S100A8/A9 promotes the migration and invasion of human breast cancer cells through actin polymerization and epithelial–mesenchymal transition. Breast Cancer Research and Treatment, 2013. **142**(2): p. 297-309.
19. Xu, X., et al., S100A9 promotes human lung fibroblast cells activation through receptor for advanced glycation end-product-mediated extracellular-regulated kinase 1/2, mitogen-activated protein-kinase and nuclear factor-κB-dependent pathways. Clinical & Experimental Immunology, 2013. **173**(3): p. 523-535.
20. Mikheev, A.M., et al., Periostin is a novel therapeutic target that predicts and regulates glioma malignancy. Neuro-Oncology, 2015. **17**(3): p. 372-382.
21. Murdoch, C., et al., The role of myeloid cells in the promotion of tumour angiogenesis. Nature Reviews Cancer, 2008. **8**(8): p. 618-631.

22. Khoi, P.N., et al., Cadmium induces urokinase-type plasminogen activator receptor expression and the cell invasiveness of human gastric cancer cells via the ERK-1/2, NF-kappaB, and AP-1 signaling pathways. Int J Oncol, 2014. **45**(4): p. 1760-8.
23. Wang, S., et al., Urokinase-type plasminogen activator receptor promotes proliferation and invasion with reduced cisplatin sensitivity in malignant mesothelioma. Oncotarget, 2016.
24. Janssen, E., et al., LAB: a new membrane-associated adaptor molecule in B cell activation. Nat Immunol, 2003. **4**(2): p. 117-23.
25. Whittaker, G.C., et al., The Linker for Activation of B Cells (LAB)/Non-T Cell Activation Linker (NTAL) Regulates Triggering Receptor Expressed on Myeloid Cells (TREM)-2 Signaling and Macrophage Inflammatory Responses Independently of the Linker for Activation of T Cells. Journal of Biological Chemistry, 2010. **285**(5): p. 2976-2985.
26. Orr, S.J., et al., LAB/NTAL Facilitates Fungal/PAMP-induced IL-12 and IFN-γ Production by Repressing β-Catenin Activation in Dendritic Cells. PLOS Pathogens, 2013. **9**(5): p. e1003357.
27. Vartanian, A., et al., GBM's multifaceted landscape: highlighting regional and microenvironmental heterogeneity. Neuro Oncol, 2014. **16**(9): p. 1167-75.
28. Hambardzumyan, D., D.H. Gutmann, and H. Kettenmann, The role of microglia and macrophages in glioma maintenance and progression. Nature Neuroscience, 2016. **19**(1): p. 20-27.
29. Zhou, W., et al., Periostin secreted by glioblastoma stem cells recruits M2 tumour-associated macrophages and promotes malignant growth. Nat Cell Biol, 2015. **17**(2): p. 170-82.
30. Zhou, Q., et al., Early-onset stroke and vasculopathy associated with mutations in ADA2. N Engl J Med, 2014. **370**(10): p. 911-20.
31. Sweeney, M.D., S. Ayyadurai, and B.V. Zlokovic, Pericytes of the neurovascular unit: key functions and signaling pathways. Nat Neurosci, 2016. **19**(6): p. 771-83.
32. Lavin, Y., et al., Regulation of macrophage development and function in peripheral tissues. Nat Rev Immunol, 2015. **15**(12): p. 731-44.
33. Butovsky, O., et al., Identification of a unique TGF-beta-dependent molecular and functional signature in microglia. Nat Neurosci, 2014. **17**(1): p. 131-43.
34. Michelson, N., et al., Exploring the role of inflammation in the malignant transformation of low-grade gliomas. J Neuroimmunol, 2016. **297**: p. 132-40.
35. Tran, C.T., et al., Differential expression of MHC class II molecules by microglia and neoplastic astroglia: relevance for the escape of astrocytoma cells from immune surveillance. Neuropathol Appl Neurobiol, 1998. **24**(4): p. 293-301.
36. Szulzewsky, F., et al., Human glioblastoma-associated microglia/monocytes express a distinct RNA profile compared to human control and murine samples. Glia, 2016. **64**(8): p. 1416-36.
37. Zavialov, A.V. and A. Engstrom, Human ADA2 belongs to a new family of growth factors with adenosine deaminase activity. Biochem J, 2005. **391**(Pt 1): p. 51-7.
38. Dolezal, T., et al., A role for adenosine deaminase in Drosophila larval development. PLoS Biol, 2005. **3**(7): p. e201.
39. Conlon, B.A. and W.R. Law, Macrophages are a source of extracellular adenosine deaminase-2 during inflammatory responses. Clin Exp Immunol, 2004. **138**(1): p. 14-20.
40. Yoneyama, Y., et al., Serum adenosine deaminase activity in women with pre-eclampsia. Gynecol Obstet Invest, 2002. **54**(3): p. 164-7.
41. Footz, T.K., et al., Analysis of the cat eye syndrome critical region in humans and the region of conserved synteny in mice: a search for candidate genes at or near the human chromosome 22 pericentromere. Genome Res, 2001. **11**(6): p. 1053-70.
42. Sims, J.S., et al., Diversity and divergence of the glioma-infiltrating T-cell receptor repertoire. Proc Natl Acad Sci U S A, 2016. **113**(25): p. E3529-37.
43. Fulzele, S., et al., MicroRNA-146b-3p regulates retinal inflammation by suppressing adenosine deaminase-2 in diabetes. Biomed Res Int, 2015. **2015**: p. 846501.
44. Elsherbiny, N.M., et al., Potential roles of adenosine deaminase-2 in diabetic retinopathy. Biochem Biophys Res Commun, 2013. **436**(3): p. 355-61.

45. Ferreira, G.A., et al., LAT2, a Lipid Raft Protein That Participates in AKT Phosphorylation in Mantle Cell Lymphoma, Is a Target for Perifosine Chemotherapy. Blood, 2014. **124**(21): p. 923-923.
46. Sun, Z.-J., et al., Activation of PI3K/Akt/IKK-α/NF-κB signaling pathway is required for the apoptosis-evasion in human salivary adenoid cystic carcinoma: its inhibition by quercetin. Apoptosis, 2010. **15**(7): p. 850-863.
47. Zanoni, I. and F. Granucci, Regulation and dysregulation of innate immunity by NFAT signaling downstream of pattern recognition receptors (PRRs). Eur J Immunol, 2012. **42**(8): p. 1924-31.
48. Manicassamy, S., et al., Activation of β-Catenin in Dendritic Cells Regulates Immunity Versus Tolerance in the Intestine. Science, 2010. **329**(5993): p. 849-853.
49. Kaljas, Y., et al., Human adenosine deaminases ADA1 and ADA2 bind to different subsets of immune cells. Cell Mol Life Sci, 2016.

Summary

The complex tumor microenvironment of glioma, constituting various cell population, supports the progression, resistance and recurrence of tumors. Among these types of cells, resident microglia and macrophages contribute almost 30-50% of tumor tissues depending on individuals. Latest studies defined these cells as glioma supporting cells by supporting growth of glioma cells and developing GBM angiogenesis. Thus, exploring novel molecular targets and their functions in glioma microglia/macrophage would definitely be urgent and useful in benefiting future clinical practice

In this thesis, the ontogeny of macrophage and its contribution on glial tumor development and angiogenesis was systematically reviewed to get an overall picture of the importance of macrophage in malignant cancers (Chapter 1, 2). As a novel discovered molecule, CECR1 was first of our knowledge reported in microglia/macrophage in glioma. CECR1 was displayed as a M2-like macrophage-specific oncogenic protein affecting MAPK pathway in glioma cells (Chapter 3).

Abundant angiogenesis is highly characteristic for gliomas. CECR1 not only mediates the biological behavior of glial tumor cells, it also enhanced the angiogenesis process under the influence of GBM cells. The proangiogenic property was tightly linked to M2-like phenotype. PDGF-B, as a M2-macrophage expressing molecule, was a promising downstream target of CECR1. It serves as a "bridge" integrating the functions of macrophage with pericyte. Moreover, it transduced the signal from CECR1 to pericyte activating periostin expression through PDGFB-PDGFRB axis (Chapter 4). As a predefined proangiogenic extracellular matrix component, periostin, was further proved to be expressed by pericyte and reactive astrocytes, other than glioma initiating cells, resulting a regulatory role in angiogenesis (Chapter 5).In order to validate and expand the knowledge on CECR1 mediated response in macrophage, proteomic analysis was applied. CECR1 in macrophage negatively regulated innate immune response. However, as glioma cells applied to culture system, CECR1 mainly regulated survival and proliferation of macrophage, other than regulating immune response (Chapter 6). Microglia belongs to monocyte/phagocytosis system. It shares most of macrophage markers, which makes it difficult to distinguish from myeloid originated macrophage in GBM. P2RY12, as a microglia specific receptor, was surprisingly found translocated to nucleus in M2-like microglia cells with a dramatic expression level. By utilizing TCGA database, P2RY12 is related to activated immune response and pro-inflammatory signalling, while it reverse-

ly correlated to cell proliferation and cell cycle transition (Chapter 7). Thus, P2RY12 potentially serves as a microglia-specific tumor suppressor molecule.

Samenvatting

Macrofagen en microglia maken tot 50% van de celpopulatie van gliomen uit, en zijn betrokken bij de tumor progressie, therapie resistentie en tumor recidieven na therapie. Recente studies beschrijven niet alleen betrokkenheid van deze cellen bij tumorgroei, maar ook specifiek bij tumor angiogenese. De functies van deze cellen, en de daaraan ten grondslag liggende moleculaire paden, zijn derhalve belangrijk voor nieuwe inzichten in de tumor genese en het ontwikkelen van nieuwe therapieën (Hoofdstukken 1 en 2).

In dit proefschrift worden de macrofagen die in gliomen voorkomen onder de loep genomen en hun belang voor de tumor biologie in kaart gebracht (Hoofdstukken 1 en 2). Het CECR1 molecuul werd recentelijk met angiogenese in verband gebracht en in dit proefschrift wordt CECR1 expressie door macrofagen en microgliale cellen in gliomen verder uitgewerkt. Het blijkt dat CECR1 tot expressie komt in de context van het M2-macrofagen profiel en dat CECR1 invloed heeft op de MAPK pathway (Hoofdstuk 3). Tevens blijkt dat CECR1 onder invloed van de gliale tumorcellen, angiogenese in gliomen bevordert (Hoofdstuk 4). CECR1 afkomstig uit de M2-macrofagen medieert de productie van periostine door pericyten via paracrine effecten van PDGFB-PDGFRβ signaling, waardoor tumor angiogenesis wordt gestimuleerd (Hoofdstuk 5). Door middel van proteoom studies werd het negatieve effect van de expressie van CECR1 op de immuunrespons aangetoond (Hoofdstuk 6). Om microgliale cellen te onderscheiden van andere macrofagen (die bijvoorbeeld CECR1 tot expressie kunnen brengen) werd in Hoofdstuk 7 de waarde van de microglia-specifieke receptor P2RY12 aangetoond.

Acknowledgments

After all the scientific work now it is time to sincerely thank all of you, my parents, my promotor, co-promotors, colleagues and friends. Without your support, it could be hardly imagined how can I eventually wrote this thesis.

Firstly, I would like to thank my parents. Because of your understanding and your support, I can dedicate myself into these four years' academic life and enjoy these four years of different life style in Netherlands. Though, the Chinese tradition makes it difficult, now I would like to speak loudly: I love you!

Sincerely, I would like to thank my promotor, Prof. Kros and my co-promotors, Dr. Caroline Cheng and Dr. Dana. Mustafa.

Dear Max, as I always call you, first of all, I really appreciated that you gave me this opportunity coming to the Netherlands. I still remembered, almost five years ago, you solved all the problems I during the Ph.D. application, At the beginning of my Ph.D. period, there were quite some strange and new ideas raised by me. As a sophisticated researcher and guider in academic world, you always teach me how to focus the current topic, or in your word, learn how to walk. Your word, don't run before you can walk, always recalling in my mind. But, when you saw the solid and interesting preliminary data on CECR1, you gave me the opportunity trying this new project, CECR1 project. Without your support, I cannot make this project into real papers and eventually into the whole thesis of my Ph.D. Moreover, I sincerely thank you for all of your effort on revising my manuscripts and the whole thesis and adapting those ones into simple but precise academic paper work.

Dear Caroline, thanks for your kind supervision in these four years. From my first year, when I was still master student doing internship in your lab, every you arranged work discussion every week talking about the data last week and planned the work for this week. At that time, I was not that accustomed, and felt a bit push of you. At that time, every week discussion let me feel really nervous. However, gradually, I started thinking and planning by myself, doing my own work independently. Our work discussion became once every 2-3 weeks. But I really enjoy the time discussing projects and science with you. You are always helpful to be the first quality control of each of my paper. By the way, I really appreciated you always protected me from all the complains of other lab colleagues. As the trouble maker in your lab, sincerely thanks for your kindness letting me finish all the work there but not just kicking me out of the place.

Dear Dana, always thanks for your kindness. You are a nice and decent lady who can consider every detail aspect not only in science but also in daily life. Thanks for providing me useful information on both of research and life. Thanks for your understanding so that I can focus myself on this CECR1 project.

I would like to thank Chinese Scholar Ship Council (CSC) for granting me learning and staying in Netherlands for four years. Hope this ambitious project of our motherland,

will definitely bring the prosperity and strength to China in the near future. Many thanks to Mr. Mu Tian, though he did not work for EUCC anymore, for coordinating all the affairs during my application. Here, I also would like to thank Shanghai Jiao Tong University School of Medicine. It is the place where I touched and stepped into the paradise of medicine. It also provided me the opportunity knowing Erasmus Medical Center. Eventually, due to the collaboration ship between two medical institutes, I can have this chance.

Before my Ph.D. period, firstly I was enrolled in master of science program, molecular medicine. Many thanks to Professor Anton Grootegoed, director of that school, and Benno and Marjolein for all the work you made taking care of us, master students. I would like to thank all my peer classmates in Molmed master program. It was really great experience to know all of you guys.

I would like to thank all the people that helped me so much during my stay in Netherlands. Prof. Duncker, thanks to give me the chance always staying in the MCL lab finishing all the lab work in this thesis. Really enjoy talking to you. Dr. Leenen, or like I always called you, Pieter, you always provide constructive ideas and critical comments on my manuscripts which really improved the quality of those ones. Pingpin, thanks for all the talks after working hours, these talks with your wisdom taught me a lot and inspired me so much. Marcel, thanks for all of your dedicated contribution on the histology work. Without you, all the beautiful IHC artwork would never be on the paper. Andrea, thanks for the flow cytometry support. Karin, thanks for sharing real Dutch knowledge and helped me to fuse into Dutch life style. And really thanks to contact and arrange blood samples with blood bank for my study.

Ihsan, my friend, it is my pleasure to collaborate with you to finish our CECR1 angiogenesis paper. Thanks a lot for your effort and dedication to that work. Ang really thanks for your effort on all the revision work when I was in China. Marteen, my fiiend, also may call you little Noortij's father, always remembered your fancy voice when you were singing in the lab following the music from radio. Thanks to provide me a lot help in the lab. By the way, it was really enjoyable to discuss with your guys about the projects, ideas and detail techniques in the lab or around the coffee corner, in the cell culture room, in the office, sometimes in the little dark microscope room. Christ, my friend, thanks a lot for bringing the reagents from Utrecht and carrying me to Utrecht for collecting some of the blood samples. Merle, very nice to know you, and really thanks your qPCR work for PDGFB. This work really helped me to construct all the story on CECR1 angiogenesis paper. Yanti, Marejon, Anushika, Lau, Esther, thanks to all of your for supporting me in the lab and guide me how to maintain a lab well.

时光荏苒，在荷兰四年的时光转眼间到了尽头。很感谢在这段青春的岁月里遇见了你们，我的小伙伴们。海波、超哥、舟桥、宝月、潇磊、刘凡、温蓓、毛庆皓、余诺、晨光、高文、高雅、黄玲、同伟、于雪、若愚、展明、莹莹、恒宇小朋

友、陈思、丹莉、婉璐、国影、唐颖、文世、洪波、跃邦、党文、李杉、栗梦、陈侃、静静、秋实、奎奎、恒哥、凯音、张凯、罗南、平臻、吴斌、小俊、芙蓉、刘学、小鲁、孙伟、超平、马华、文浩、瑶瑶、小璐、晓哥、世豪、海燕、晓娜、天时、蔡蕊、唐江涛、武永康、若昊、克若、维希、佳波、元杰、励勤、浩波、孙崇、刘垚、张倩、刘玥、黄莹莹、甫雨、万亿、龚勋、刘娟、源远、书佳、雁彬、涡蜗、小月、陆莲、裴炜、杨帆、丛明曦、嘉乐、包包、卜妍、许馨、麦伦、周围、萌萌、黄若桐、腾飞、蒲霞、小白、洁婷、小楠、大喜、勇哥、豆豆。无论是一次次的聚餐聊天，饮酒谈心还是那一次次彻夜的狼人大战还是阿瓦隆的声嘶力竭，亦或是一次次的结伴出行，挖蚝捉蟹，烧烤小炒，大快朵颐，每一段，每一次都是那么记忆犹新。笔至此处，不由心至荷兰。正是有了你们，我可以这样说，我的青春已无悔！多么想再一次和各位杀一局，玩一场。

当然还得感谢这些年中遇到的各位，王程程、赵辰、陈秀、孙雯、李尤。感谢你们在不同的时间段使我快速成长了起来，也祝你们在各自的人生轨迹中各自安好。

感谢交大医学院07临床医学八年制的同学弟兄们，陆冰、老五、张胤、万润、毛毛、庄淳、拓彬、瓜姐、阿彭、丁杰、丁莹、蔡昱。这么多年的同学情谊并未因我出国而减退。在国内还要请各位老师多多指教啦。在也衷心希望我们的傅炜同学不惧病魔，快快康复。

也要感谢在这半年中一起度过实习岁月的小朋友们。12级八年制法语班的苗苗、晨宝、岳岳、依明、晨怡、大白、露克。12级临床五年制一大班的东东、博文、萍儿、婧雯、安妮还有山崎。相处时日不多，但你们洋溢的青春气息感染了我这个老年人，谢谢你们对我这个老学长的帮助，也珍惜与你们在一起一段段欢声笑语的实习生活。

在这里，也要感谢上海交通大学基础医学院高级实验师程枫老师，许伟榕老师。感谢二位老师在八年制本科阶段RBL（Research Based Learning）项目中给予的指导，也正是因为有了这份机会，开启了我对科研的兴趣。应该说没有二位的启蒙，也许现在还不会pipet。

感谢仁济妇产科狄文主任，同济大学附属第一妇幼保健院万小平主任，分别在大二，大五的时候分别强调了科学研究在医生成长中的重要性。也因此引导了我对科学研究的定位及建立了我对追求科学研究道路坚定的信心。

感谢新华医院小儿神经外科马杰教授，儿外科王俊主任接收我进入小儿外科团队从事小儿神经外科方向的工作。特别感谢新华小儿神经外科李奇峰医生，赵阳医生，张晨冉医生，王保城医生等在刚回国进入临床各方面工作提供的帮助和建议。

Curriculum Vitae

Changbin Zhu was born in Shanghai, China on June 23, 1989. In 2007, after graduating from the prestigious Da Tong high school in Shanghai he started his medical education (8 year program) at the Jiao Tong University School of Medicine (SJTUSM) in Shanghai. In 2009 he began his first research program studying CCR5 in gastric and colorectal carcinoma under the supervision of Prof. Feng Chen and Prof. Jun Mei at the SJTUSM. In 2010 this project was nominated as the Top 100 innovation projects for undergraduates in Shanghai. Subsequently he started laboratory work in Prof. Jianhua Wang's lab where he worked on the chemokine receptor CXCR7 in prostate cancer. During this time Dr. Zhu donated hematopoietic stem cells to a patient with leukemia as one of the volunteers at EXPO 2010 in Shanghai – a deed that was awarded "The excellent volunteer in the year of 2010". In 2011 dr. Zhu was selected by the University of Michigan as the only exchange student involved in a laboratory internship. In 2012 he did 6 months' clinical rotation in Shanghai Ruijin Hospital and Shanghai Xinhua hospital.

Dr. Zhu started the 4-years PhD program supported by the China Scholarship Council (CSC) at the Erasmus Medical Center, Rotterdam, The Netherlands on a project submitted by Dr. D. Mustafa. In the first two years, he followed the Master of Science molecular medicine program, and obtained the M.Sc. degree in the September, 2014. The Ph.D. project on the influences of the immune system on glioma angiogenesis was based on a collaboration between the Departments of Pathology (Dr. D. Mustafa, Prof. J.M. Kros) and Experimental Cardiology (Dr. C. Cheng, Prof. D.J. Duncker). In this project Dr. Zhu proposed and proved the pro-tumoral, pro-angiogenic and anti-inflammatory functions of newly discovered protein CECR1 in the context of human glioblastoma, one of the most aggressive brain tumors with dismal prognosis. The results may well initiate new therapeutic approaches for glial tumors. From September 2016 Dr. Zhu returned to Shanghai to continue his medical training and specialization in pediatric neurosurgery under the guidance of Prof. Jie Ma in the Department of Pediatric Neurosurgery, Shanghai Xinhua Hospital.

PhD Portfolio

Name: Changbin Zhu
Ph.D. period: August 2012 – September 2016
Department: Pathology
Research school: Molecular Medicine
Promotor: Prof. dr. Johan M. Kros
Co-promotores: Dr. Dana Mustafa; Dr. Caroline Cheng

PHD TRAINING

In-Depth Courses	Year
Molecular and Cellular Biology A	2012-2013
Contemporary research topics	2012-2013
Written and Oral presentation of Research	2012-2013
Survival Analysis	2012
Molecular and Cellular Biology B	2013
Evolution and Development	2013
The Biology of Disease	2013
Biomedical Research Techniques	2013
Workshop on Photoshop and Illustrator CS6 for PhD-students and other researchers	2013
The Basic Introduction Course on SPSS	2013
The Advances in Comparative Pathology: The Central Nervous System	2014
Scientific English Writing	2014
The course on R	2016
Research Integrity	2016

Presentations	
Presentation at the JNI scientific meeting	2014
Presentation at the Neuro-Oncology Laboratory meeting	2014
Presentation at the JNI scientific meeting	2015
Presentation at the Neuro-Oncology Laboratory meeting	2015

International Conferences

CGC.nl meeting Translational cancer genomics, Amsterdam, NL	2013
AACR Annual Meeting, Philadelphia, U.S.A.	2015

Seminars, Symposiums and Scientific meetings

Daniel den Hoed Cancer Hospital Day	2012-2015
Molecular Medicine Day	2014-2015
JNI Scientific Meeting	2012-2016
Neuro-oncology laboratory meeting	2014-2015

Publication List

1. **Zhu C**, Mustafa D, Zheng PP, van der Weiden M, Sacchetti A, Brandt M, Chrifi I, Tempel D, Leenen PJ, Duncker DJ, Cheng C[*], Kros JM[*]. Activation of CECR1 in M2-like TAMs promotes paracrine stimulation-mediated glial tumor progression. Neuro Oncol. 2017 Jan 3. pii: now251. doi: 10.1093/neuonc/now251. [Epub ahead of print], impact factor (IF) 7.4

2. **Zhu C**, Kros JM, van der Weiden M, Zheng P, Cheng C[*], Mustafa DA[*]. Expression site of P2RY12 in residential microglial cells in astrocytomas correlates with M1 and M2 marker expression and tumor grade. Acta Neuropathol Commun. 2017 Jan 10;5(1):4. doi: 10.1186/s40478-016-0405-5, impact factor (IF) to be determined

3. **Zhu C**[#], Chrifi I[#], Mustafa D, Zheng PP, van der Weiden M , Leenen PJ, Duncker DJ, Kros JM[*], Cheng C[*]. CECR1-mediated crosstalk between macrophages and vascular mural cells promotes neo-vascularization in malignant glioma. (Accepted for publication, Oncogene, 2017), impact factor (IF) 7.9

4. **Zhu C**, Kros JM, Cheng C[*], Mustafa DA[*]. The contribution of "Tumor-Associated Macrophages" in tumor neo-angiogenesis and implications for anti-angiogenic strategies. (Accepted for publication, Neuro Oncology, 2017), impact factor (IF) 7.4

5. **Zhu C**, Mustafa D, Leenen PJ, Duncker DJ, Kros JM[*], Cheng C[*]. Proteome analysis of the CECR1 mediated response in macrophages and tumor associated macrophages identify key pathways and molecules in immune response regulation of glial tumors. (Submitted for publication).

6. Huizer K[#], Zhu C[#], Chrifi I, Krist B, Zorgman D, van der Weiden M, Cheng C, Kros JM, Mustafa DA. Periostin is expressed by pericytes and is crucial for angiogenesis in glioma. (Submitted for publication).

7. **Zhu C**, Jiang Z, Cheng F, Qian G, Research Progress of chemokine receptor CCR5, Journal of Shanghai Jiao Tong University (Medical Science). Vol.32 No.6 Jun.2012:809-814, impact factor (IF) to be determined.

8. Liu W, Yuan S, Wei F, Yang J, Zhang Z, **Zhu C**, Ma J, Reliability and Validity of the Chinese Version Appropriateness Evaluation Protocol. PLoS One. 2015 Aug 25;10(8):e0136498. doi: 10.1371/journal.pone.0136498, impact factor (IF) 3.5

9. Chrifi I, Louzao-Martinez L, Brandt M, van Dijk CGM, Burgisser P, **Zhu C**, Kros JM, Duncker DJ, Cheng C. CMTM3 mediates angiogenesis by regulating cell surface availability of Ve-cadherin in endothelial adherens junctions. Arteriosclerosis, Thrombosis, and Vascular Biology, in press, impact factor (IF) 6.0

#: These authors contributed equally as first authors.

***** : These authors contributed equally as corresponding authors.